

ESNR 2019



EUROPEAN SOCIETY OF NEURORADIOLOGY
Diagnostic and Interventional
42nd ANNUAL MEETING
26th Advanced Course in Diagnostic Neuroradiology
11th Advanced Course in Interventional Neuroradiology
September 18th – 22nd 2019
Oslo, Norway
Conference Venue: Radisson Blu Plaza Hotel Oslo

PRESIDENT

Paulina Due - Tønnessen, MD PhD

SCIENTIFIC COMMITTEE

Paulina Due - Tønnessen

Marion Smits

Tarek Yousry

Naci Koçer

Bernhard Schuknecht

Pia Maly Sundgren

Luigi Manfre

Pedro Vilela

LOCAL ORGANIZING COMMITTEE

Paulina Due – Tønnessen

Mona Beyer

Geir Ringstad

Andrés Server Alonso

Kyrre E. Emblem

Atle Bjørnerud

Bård Nedregaard

Pål Bache Marthinsen

ESNR PRESIDENTIAL ADDRESS

A warm welcome to the 42nd Annual Meeting of the European Society of Neuroradiology (ESNR). On this 50th birthday of our Society it is a pleasure to host you in Oslo, voted by Lonely Planet as one of the ten best cities in the world to visit.

The ESNR's Scientific Program Committee, chaired by Congress President Paulina Due-Tønnessen, has made an exquisite program for you to attend. As last year we start with offering a pre-course on 'ASL in clinical practice' on Wednesday afternoon. On Thursday, the 26th advanced course in diagnostic neuroradiology on 'Adult and Pediatric Inflammatory and Demyelinating CNS Diseases' and the 11th advanced course in interventional neuroradiology on 'Stroke' will refresh your knowledge on the newest guidelines and state-of-the-art imaging and will teach you all you need to know to be up-to-date in these topics. The Annual Meeting starts on Friday and will offer a perfect mix of cutting edge neuroradiology, including artificial intelligence, MR-elastography and the glymphatic system, refresher topics and scientific oral and poster presentations. Exciting joint sessions with our sister societies ASNR, ASPNR and ESHNR and a session in cooperation with the Spanish Society of Neuroradiology will broaden your view.

During the Annual Meeting we will celebrate Prof. Vic Haughton and Prof. Turgut Tali as Honorary Members for their outstanding contributions to neuroradiology during their long and successful professional careers.

But ESNR's Annual Meeting is not about science only. It is also the perfect occasion and location to network, meet old friends and colleagues and make new ones. Our invited faculty will give you the opportunity to talk and discuss science with the brightest minds in neuroradiology. Enjoy Oslo's innovative architecture, unmissable museums, cool bars, bistros and cafés. Allow me to share one personal tip: take a boat across the bay to the Frammuseum. There you will relive the voyages of Norwegian explorer Roald Amundsen, the first man to reach the South Pole. His ship, the Fram is on prominent display in the museum.

Prof. Johan Van Goethem,
ESNR President

WELCOME ADDRESS**ESNR annual meeting and advanced course 2019: Northern enlightening**

Dear friends and colleagues,

In this 50th year anniversary of the ESNR, it is my great honour and pleasure to welcome you all to the 42nd ESNR Annual Meeting, 26th advanced course in diagnostic neuroradiology and 11th advanced course in interventional neuroradiology, on behalf of the scientific and local organizing committees. The meeting will take place from 18-22 September in Oslo, Norway, starting with a pre- course on Wednesday afternoon.

Meet with your friends and colleagues to be enlightened by the latest updates on hot topics and new imaging techniques within **artificial intelligence, MRI elastography and the glymphatic system**, as well as a broad range of scientific and educational sessions covering subjects spanning from **Advanced Courses in Stroke Update and Adult and pediatric inflammatory and demyelinating disorders** to **Educational Sessions** with topics within **head/neck, spine, CNS tumours, dementia and epilepsy**, and more. Also this year we will have a pre- course on a very hot topic, **ASL in clinical practice: what, when and how**.

The congress venue is in downtown Oslo at the Oslo Plaza Hotel, next to the Central Train Station and with all facilities within short walking distance, including many hotels and restaurants. This is also near to the magnificent City Hall (home of the annual Nobel Peace Prize ceremony), where the welcome reception will take place on Thursday evening. Oslo is a small capital, and in the vibrating city center, you will at the same time be a short walk from boats bringing you out on the beautiful Oslo fjord, or a subway trip away from beautiful hills and forests surrounding the city. Oslo was recently named by The New York Times as one of the “places to go in 2018”.

We hope you will learn something new in the field of Neuroradiology and meet old friends and make new ones, enjoying our great city and country. We warmly welcome you to Oslo, Norway, and are looking forward to see you!

Dr. Paulina Due – Tønnessen

Congress President, 42nd ESNR Annual Meeting

**The European Society of Neuroradiology – Diagnostic and Interventional
Executive Committee**

President	Johan Van Goethem
Vice – President	Pia Maly Sundgren
Secretary General	Andrea Rossi
Treasurer	Cem Calli
Chairperson of the Subspecialty Committee Diagnostic Neuroradiology	Tarek Yousry
Chairperson of the Subspecialty Committee Head and Neck Neuroradiology	Bernhard Schuknecht
Chairperson of the Subspecialty Committee Interventional Neuroradiology	Naci Koçer
Chairperson of the Subspecialty Committee Pediatric Neuroradiology	Pia Maly Sundgren
Chairperson of the Subspecialty Committee Spine Neuroradiology	Luigi Manfre
Secretary of the Institutional Council	Pedro Vilela

Institutional Council

Australia / NZ	C. Mandel	Latvia	G. Krumina
Austria	H. Deutschmann	Netherlands	M. Smits
Belgium	C. Mabilia	Norway	P. Due-Tønnessen
Bosnia Herzegovina	Z. Merhemic		
Brazil	R. Hoffmann Nunes	Poland	A. Majos
Bulgaria	D. Zlatareva	Portugal	R. Manaças
Croatia	M. Špero	Serbia	T. Stosic-Opincal
Denmark	E. Cortsen	Slovenia	K. Surlan Popovic
Finland	R. Vanninen	South Africa	L. Janse van Rensburg
France	F. Cotton	Spain	A. Ramos
Germany	H. Urbach	Sweden	R. Siemund
Greece	E. Kapsalaki		
Gulf	A. Own	Switzerland	K. O. Lövblad
Hungary	L. Kozák	Turkey	I. Saatçi
Ireland	S. Looby	United Kingdom	K. Lobotesis
Italy	C. Gaudino		

Institutional Members

Australian and New Zealand Society of Neuroradiology	Latvian Society of Neuroradiology
Austrian Society of Neuroradiology	Neuroradiology Section of the Association of Radiology of Bosnia & Herzegovina
Belgian Society of Neuroradiology	Neuroradiology Section of the Croatian Society of Radiology
Brazilian Society of Neuroradiology	Neuroradiology Subgroup of the Radiological Society of South Africa
British Society of Neuroradiologists	Norwegian Society of Neuroradiology
Bulgarian Society of Neuroradiology & Head and Neck Radiology	Polish Medical Society of Radiology - neuroradiology section
Danish Society of Neuroradiology	Portuguese Society of Neuroradiology
Dutch Society of Neuroradiology	Serbian Society of Neuroradiology
Finnish Society of Neuroradiology	Slovenian Section of Neuroradiology
French Society of Neuroradiology	Spanish Society of Neuroradiology
German Society of Neuroradiology	Swedish Society of Neuroradiology
Greek Society of Neuroradiology	Swiss Society of Neuroradiology
Gulf Neuroradiology Society	Turkish Society of Neuroradiology
Hungarian Society of Neuroradiology	
Irish Society of Neuroradiology	
Italian Society of Neuroradiology	

Committees of the ESNR

Diagnostic Neuroradiology

Tarek Yousry (**Chair**)
 Marion Smits
 Nuria Bargallo Alabart
 Meike Vernooij

Head and Neck Neuroradiology

Bernhard Schuknecht (**Chair**)
 Sotirios Bisdas
 Katarina Surlan Popovic

Interventional Neuroradiology

Naci Koçer (**Chair**)
 Jens Fiehler
 Laurent Pierot
 Işıl Saatci

Pediatric Neuroradiology

Pia Maly Sundgren (**Chair**)
 Maria Argyropoulou
 Bård Nedregaard

Spine Neuroradiology

Luigi Manfre (**Chair**)
 Adrian Kastler
 Reuben Grech
 Hosam Alqatami
 Alexander Loizides

Rules

Philippe Demaerel (**Chair**)
 Andrea Rossi
 Marek Sasiadiek
 Dojan Stojanov

Scientific Programme

Paulina Due – Tønnessen (**Chair**)
 Marion Smits
 Tarek Yousry
 Naci Koçer
 Bernhard Schuknecht
 Pia Maly Sundgren
 Luigi Manfre
 Pedro Vilela

Membership

Cem Calli (**Chair**)
 Paulina Due – Tønnessen
 Zulejha Merhemic

Social Media

Gennaro D'Anna (**Chair**)
 Efrosini Papadaki
 Julia Fruehwald-Pallamar
 Yelda Ozsunar Dayanir
 Chiara Gaudino
 Johan Van Goethem
 Luc van den Hauwe
 Rudiger Von Kummer

ESONR

Majda M. Thurnher (**Chair**)
 Johan Van Goethem
 Luigi Manfre
 Naci Koçer
 Pia Maly Sundgren
 Bernhard Schuknecht
 Tarek A. Yousry
 E. Turgut Tali

Founding Members

P. Amundsen
 P. Andersen
 H. Backmund
 K. Bergström
 V. Bernasconi
 A.S. Bligh
 G. Bonte
 J. Bories
 G. Bradac
 J.P. Braun
 P. Buffard
 J.W.D. Bull
 E.H. Burrows
 A. Calabrò
 R. Chrzanowski
 G. Cornélis
 S. Cronqvist
 K. Decker
 P. Dettori
 R. Djindjian
 A. Donaldson
 G. du Boulay
 J. Duquesnel
 Ph. Engel
 L. Escudero
 H. Fischgold
 T. Greitz

G. Gryspeerdt
 H. Hacker, Germany
 D.T. Hawkins
 R. Hoare
 P. Huber
 H.H. Jacobsen
 J. Jeanmart
 J. Jirout
 E.M. Klausberger
 J. Legré
 B. Liliequist
 E. Lindgren
 G. Lombardi
 J. Metzger
 P. Moxon
 D. Müller
 R. Oberson
 A. Passerini
 L. Penning
 J. Petrov
 L. Picard
 P. Potthoff
 L. Psenner
 R. Reid
 J. Roulleau
 M. Roth
 G. Ruggiero
 G. Salamon
 W. Shepherd
 J. Simon
 F. Smaltino
 J. Solé-Llenas
 A. Tänzer
 A. Thibaut
 H. Vogelsang
 A. Wackenheim
 S. Wende
 G. Westberg
 I. Wickholm
 O. Wiedermann
 G.B. Ziedses des Plantes

THE ESNR AWARDS: THE EUROPEAN NEURORADIOLOGY AWARDS IN DIAGNOSTIC AND INTERVENTIONAL NEURORADIOLOGY

History

In 2008, the Executive Committee of the ESNR decided to introduce two new scientific prizes for young neuroradiologists. The new prizes were created in honour of the Pioneers and Past Presidents of European Neuroradiology, and are awarded for the best papers in diagnostic and interventional neuroradiology.

In 2012, the Executive Committee of ESNR decided to give the name of one of the Pioneers of the society and the name of one of its Past Presidents in an order as “ESNR Awards in Honor of”, and to present their short CV and pictures at the Awards Ceremony during the ESNR Annual Congress or during the Symposium Neuroradiologicum.

Among those awards, the proposal of Springer to institute the “ESNR-Springer Award” was also accepted. The prize money of € 1000 will be awarded by Springer to the first-named author (ESNR Member) of the most cited article of the latest impact factor (current year: IF previous years, e.g.: 2016: IF 2015) together with a free registration to the ESNR Annual Meeting of the current year. The Article will be highlighted on the journal webpage (Springer.com)

Rules of participation

Article 1: The two prizes reward the achievements of young scientists, under the age of 40 years on the day of application, working in the field of neuroradiology in a European centre and having been accepted as Full, Associate, Junior, or Institutional Member of the ESNR.

Article 2: The prizes, each to the amount of € 4000, are awarded every year at the Awards Ceremony during the annual congress of the ESNR, or during the Symposium Neuroradiologicum when the ESNR Annual Congress does not take place. The Awards Ceremony is a respected event during each congress; other simultaneous ESNR sessions are not allowed, and the ceremony may not be split in two or more parts. The Award Ceremony is conducted by the Chair of the Awards Committee, who also introduces the awardees and presents the prizes together with the ESNR President.

Article 3: The candidate must be the first author of an original work in the fields of research in neuroradiology: diagnostic or interventional neuroradiology. Applications can be placed for a scientific work that was:

- a. published online or in print in a peer-reviewed scientific journal listed in SCI within the last 12 months before the date of submission, or
- b. submitted, still unpublished, accepted or not yet accepted.

The candidate must not have received any other prize for the same work, and must not have received the ESNR award of the same category previously.

Article 4: All submissions must be **in English** and should include:

- application letter indicating the title of the scientific paper upon which the application is based, and reporting its status if not yet published;
- the scientific paper (unpublished or to be submitted);
- the full Curriculum Vitae and a photo of the candidate.

These documents must be exclusively submitted, as electronic attachments, via e-mail to the address indicated below. Please note that each submitted article and its relevant images should be included in a separate attachment.

By submitting the work the author agrees, if declared the winner, to present the work at the next ESNR Annual Congress or Symposium Neuroradiologicum. Should the winner be unable to participate because of proven urgent reasons, the presentation can be made by a co-author of the same paper. If no presentation is made, the prize money will not be awarded. Payment of the prize money is made after the relevant ESNR Annual Congress or Symposium Neuroradiologicum has taken place.

Article 5: A single author can apply for more than one prize with scientific papers on clearly different topics as confirmed by the Awards Committee.

Article 6: Authors are requested to indicate to which of the two awards categories each scientific paper is addressed. If the Awards Committee considers another category to be more appropriate, the submission may be re-classified.

Article 7: A Scientific Jury will assess and rate the submitted papers. The Jury is composed of the members of the Awards Committee, plus four internationally known specialists in neuroradiology, who will rate each application independently from each other. If the rating does not give clear results, the prize-winners will be identified by consensus of all jury members.

The members of the Scientific Jury should declare not to have a conflict of interests. In case of conflict of interests, the juror is excluded from the Scientific Jury for the current year and specific prize category, and is replaced by another juror of equal scientific standing.

The Chair of the Awards Committee shall be invited as a Faculty member to the ESNR Annual Meeting or Symposium Neuroradiologicum where the award ceremony takes place.

Article 9: The ESNR will advertise the prizes by a dedicated newsletter and in the society website, as of January 1st each year. The deadline for applications is set at March 1st each year. The Award Committee will designate the laureates after receiving the evaluations of the jurors, as a rule by May 1st. Should the Award Committee decide that, in any category, no submission meets sufficient quality requirements, no prize will be awarded in that category.

Article 10: All candidates will be notified in writing of the result of their application. The laureates will be invited to give a six-minute oral presentation at the Award Ceremony during the ESNR Annual Congress, or Symposium Neuroradiologicum when the ESNR Annual Congress does not take place. The congress registration fee of the laureates is waived; the travel expenses will be reimbursed.

The names of the laureates, as well as the titles and abstracts of their scientific works, will be placed on the ESNR website and published in the society pages of *Neuroradiology*. In case the winning paper is still unpublished, the authors agree that "*Neuroradiology*", the official ESNR journal, shall have the right of publication after peer-review.

Article 11: All possible questions and issues regarding the awarding of the Prizes shall be dealt with at the discretion of the Awards Committee and the ESNR Executive Committee. The decision of the ESNR Executive Committee is final.

Article 12: Candidacy implies full acceptance of the rules.

Please send your submissions to the attention of the
ESNR Secretary General
Email: info@esnr.org

The object of the email should read: ESNR award submission.

THE DEADLINE FOR RECEIPT OF SUBMISSIONS IS MARCH 1ST

ESNR Annual Congress, Advanced Course in Diagnostic Neuroradiology and Advanced Course in Interventional Neuroradiology of the ESNR

The European Society of Neuroradiology holds each year a scientific congress at a place and date designated by the Executive Committee. On the day before the congress, Advanced Courses in Diagnostic Neuroradiology and Interventional Neuroradiology are organized in parallel sessions. The business meeting (General Assembly) of the Society is held in conjunction with this annual scientific congress.

Since its creation in 1969, the ESNR has organized 42 annual congresses. This year the 26th Advanced Course in Diagnostic Neuroradiology and the 11th Advanced Course in Interventional Neuroradiology will be held on the day before the congress. In recognition of the importance of the Symposium Neuroradiologicum, which is held every four years, no scientific congress of the ESNR is held when the Symposium takes place in Europe.

Future Annual Meetings

43rd Congress

1st – 4th October 2020
Lisbon, Portugal
President: Pedro Vilela

44th Congress

October 2021
Geneva, Switzerland
President: Karl Lovblad

The European Course in Neuroradiology

The European Course in Neuroradiology has been a story of success ever since the first course in Toulouse in 1984. More than 1000 young neuro-radiologists have completed the cycle of three courses over the past 21 years. The ECNR was conceived as a means to create a common and shared culture, common meeting points and a common standard of knowledge. The form that was adopted and used for the coming 6 cycles, each consisting of three courses, included the major bodies of knowledge as described by the headlines; intracranial nervous system, the spine and spinal cord and the base of the skull, maxillofacial and head and neck neuroradiology.

European School of Neuroradiology (ESONR) - the new concept

The ESONR - European School of Neuroradiology - is the most important and complete training programme organized by the ESNR - European Society of Neuroradiology within the main frame, and in partnership with, the ESOR - European School of Radiology. The purpose of this training and education program is based on the vision of what the ESNR considers the range of competences and skills that are the basis of a high qualified neuroradiological activity. The program is designed to offer a pathway to reach such professional and cultural levels. The final points will be the examinations to be certificated at the different levels and in the different branches of this discipline.

Courses are organized at 3 different levels: 1st Level: **ESOR - Galen Foundation Courses in Neuroradiology**, 2nd level: **ECNR - Course in Neuroradiology, Diagnostic and Interventional** and finally 3rd level: **ESNR Advanced Courses of Higher Qualification in Interventional Endovascular Neuroradiology, Interventional Spine Neuroradiology, Advanced Diagnostic Neuroradiology and Paediatric Neuroradiology**.

ECNR - European Course in Diagnostic and Interventional Neuroradiology

The ECNR is the fundamental Neuroradiology course aimed at neuro-radiologists, established or in training. It is based on cycles of four courses (modules), each lasting five days, dedicated to diagnostic and interventional neuroradiology. The full cycle is considered complete after the attendee has participated in all four modules, which can be done in a single cycle or in different cycles.

The scientific content of the course is determined by the ESONR Committee of the European Society of Neuroradiology, taking into account international standards and guidelines for training in diagnostic and interventional neuroradiology. The participating educators will be internationally renowned European experts, to be selected on the basis of their

scientific background and educational skills to ensure high- quality lectures and interactive case discussions.

The following topics have been chosen, each to be covered in five full days of lectures and workshops:

- Anatomy, congenital malformations and genetics.
- Trauma, Infection, Inflammation and Degenerative Disease
- Tumours of the Brain and Spinal Canal
- Vascular Disease of the Brain and Spinal Canal

Seventh Cycle - Scientific Director: Guido Wilms (Leuven)

First Module: Embryology, Anatomy, Malformations - Crieff, October 4 – 11, 2002 –Local Director:Wendy J. Taylor

Second Module: Tumours of the CNS - Riga, April 11 - 18, 2003 – Local Director: Cosma Andreula

Third Module: Vascular Disease of the CNS - Malta, October, 24 - 30, 2003 - Local Director: Athanassios Gouliamos

Fourth Module: Trauma and Degenerative Disease of the CNS - Riga, April 23-27, 2004 -Local Director: Johan Van Goethem

Eighth Cycle -Scientific Director: Ernst-Wilhelm Radü (Basel)

First Module: Embryology/Anatomy/Malformations/Genetics - Basel, October 22-26, 2004

Second Module: Tumors of the CNS - Basel, March 18-22, 2005

Third Module: Vascular Diseases of the CNS - Basel, October 21-25, 2005

Fourth Module: Trauma/Degenerative Diseases of the CNS - Basel, March 10-14, 2006

Ninth Cycle - Scientific Director: Ernst-Wilhelm Radü (Basel)

First Module: Embryology/Anatomy/Malformations/Genetics - Basel, October 20 - 24, 2006

Second Module: Tumours of the CNS - Basel, March 23 - 27, 2007

Third Module: Vascular Diseases of the CNS - Basel, November 2 - 6, 2007

Fourth Module: Trauma/Degenerative Diseases of the CNS - Basel, April 11 - 15, 2008

Tenth Cycle - Scientific Directors: Massimo Gallucci (L'Aquila), AlexRovira (Barcelona)

First Module: Embryology/Anatomy/Malformations/Genetics - Tarragona, October 10 – 14, 2008

Second Module: Tumors and Tumor-like Vascular Lesions- Rome, March 20 – 24, 2009

Third Module: Vascular Diseases - Tarragona, October 9-13, 2009

Fourth Module: Trauma/Degenerative/Metabolic/Inflammatory Diseases - Rome, March 19-23, 2010

Eleventh Cycle - Scientific Directors: Massimo Gallucci (L'Aquila), Alex Rovira (Barcelona)

First Module: Embryology/Anatomy/Malformations/Genetics - Tarragona, November 5-9, 2010

Second Module: Tumors and Tumor-like Vascular Lesions- Rome, March 25-29, 2011

Third Module: Vascular Diseases - Tarragona, October 28 - November 1, 2011

Fourth Module: Trauma/Degenerative/Metabolic/Inflammatory Diseases - Milano, April 12-16, 2012

Twelfth Cycle - Scientific Directors: Athanasios Gouliamos (Athens), E. Turgut Tali (Ankara)

First Module: Embryology/Anatomy/Development and Malformations of the CNS - Antalya, November 1-6, 2012

Second Module: CNS Tumors - Athens, April 8 – 13, 2013

Third Module: Vascular Diseases - Antalya, November 3-7, 2013

Fourth Module: Trauma/Degenerative/Metabolic/Inflammatory Diseases - Athens, April6-10, 2014

Thirteenth Cycle - Scientific Directors: Athanasios Gouliamos (Athens), E. Turgut Tali (Ankara)

First Module: Embryology/Anatomy/Development and Malformations of the CNS - Antalya, November 9-13, 2014

Second Module: CNS Tumors - Rhodes, April 14-18, 2015

Third Module: Vascular Diseases - Izmir, November, 2015

Fourth Module: Trauma/Degenerative/Metabolic/Inflammatory Diseases - Rhodes, April, 2016

Fourteenth Cycle - Scientific Directors: Majda M. Thurnher (Vienna), Johan Van Goethem (Antwerp)

First Module: Embryology/Anatomy/Development and Malformations of the CNS - Dubrovnik, October 16-20, 2016

Second Module: CNS Tumors - Antwerp, May 7-11, 2017

Third Module: Vascular Diseases - Dubrovnik, October 22-26, 2017

Fourth Module: Trauma, Infection and Degenerative Disease - Antwerp, May 6-10, 2018

Fifteenth Cycle - Scientific Directors: Majda M. Thurnher (Vienna), Johan Van Goethem (Antwerp)

First Module: Anatomy and Embryology - Dubrovnik, October 21-25, 2018

Second Module: CNS Tumors - Antwerp, April 29-May 3, 2019

Third Module: Vascular and Traumatic Diseases – Rovinj, 13 – 17 October 2019

Neuroradiology

Neuroradiology, published by Springer Verlag, was founded as the official organ of the European Society of Neuroradiology in 1970. Since 2010 on, the Austrian Society of Neuroradiology, the Belgian Society of Neuroradiology, the British Society of Neuroradiologists, the Bulgarian Association of Radiology, the Czech Neuroradiological Society, the Dutch Society of Neuroradiology, the Finnish Society of Neuroradiology, the German Society of Neuroradiology, the Latvian Society of Neuroradiology, the Norwegian Society of Neuroradiology, the Neuroradiological Section of the Hellenic Radiological Society, the Neuroradiological Section of the Polish Radiological Society, the Portugese Society of Neuroradiology, the Romanian Society of Magnetic Resonance in Medicine, the Spanish Society of Neuroradiology, the Swedish Society of Neuroradiology and the Swiss Society of Neuroradiology decided to choose neuroradiology as their (in some cases second) official Journal. Submissions of articles can be done via the website: <http://www.editorialmanager.com/nrad>

NEURORADIOLOGY
EDITORIAL BOARD 2019

Editor-in-Chief

R. von Kummer, Dresden

Managing Editor

L. Babinec, Seattle

*Diagnostic Neuroradiology***F. Barkhof, Amsterdam (Section Editor)**

O. Abe, Tokyo
 J.R. Bapuraj, Ann Arbor
 S. Bisdas, Tübingen
 F. Bonneville, Toulouse
 B. Brea-Álvarez*, Madrid
 M.A. Brockmann, Mainz
 E. Gizewski, Innsbruck
 R. Gupta, Haryana
 H.S. Kim, Seoul
 K. Kudo, Sapporo
 W. Küker, Oxford
 D.S. Liebeskind, Los Angeles
 J. Linn, Dresden
 M. Maeda, Tsu
 F. Meijer, Nijmegen
 C. Oppenheim, Paris
 T. Struffert, Erlangen
 E. T. Tali, Ankara
 M. Thumher, Vienna
 H. Urbach, Freiburg
 P. Valsasina, Milan
 Y. Watanabe, Osaka
 M. Wattjes, Hannover
 G. Wilms, Leuven
 M. Wintermark, Stanford
 T. Yoshiura, Kagoshima

*Advanced Imaging***S. Haller, Geneva (Section Editor)**

C. Benjamin, New Haven
 A. Choe, Baltimore
 P. Dupont, Leuven
 Y. Liu, Beijing
 K. Lövblad, Geneva
 J. Wardlaw, Edinburgh

*Head- Neck- ENT Radiology***J. Casselman, Brugge (Section Editor)**

T. Beale, London
 B. De Foer, Wilrijk
 N. Hosten, Greifswald
 C. Kenis, Heusden-Zolder
 M. Lell, Nuernberg
 A. Rovira Cañellas, Barcelona
 B. Schuknecht, Zurich
 D. Vanneste, Geel

*Interventional Neuroradiology***I. Saatci, Ankara (Section Editor)**

I. Wanke, Hirslanden (Deputy Editor)
 J.-H. Buhk, Hamburg
 S. Cekirge, Ankara
 R. Chapot, Essen
 F. Clarençon, Paris
 M. Forsting, Essen
 G. Gál, Odense
 J. Gerber, Dresden
 M. Goyal, Calgary
 H. Henkes, Stuttgart
 O. Jansen*, Kiel
 A. Krajina, Hradec Králové
 T. Krings, Toronto
 W. Kurre, Passau
 S. Meckel, Freiburg
 D. Meila, Hannover
 J. Mocco, New York
 M.A. Möhlenbruch, Heidelberg
 L. Pierot, Reims
 D.C. Suh, Seoul
 B. Tomandl, Göppingen
 B. Turowski, Düsseldorf
 W. van Zwam, Maastricht
 A. Wakhloo, Burlington
 W. Weber, Bochum

*Paediatric Neuroradiology***A. Rossi, Genoa (Section Editor)**

M. Argyropoulou, Ioannina
 K. Chong, London

F. D'Arco, London
 B. Ertl-Wagner, Toronto
 C. Hoffmann, Tel Hashomer
 P.-L. Khong, Hong Kong
 A. McKinney, Minneapolis
 Z. Patay, Memphis
 A. Righini, Milan
 B.P. Soares, Burlington
 P.C. Sundgren, Lund

*Spinal Neuroradiology***M. Muto, Naples (Section Editor)**

A. Brook, Bronx
 A. Cianfoni, Lugano
 J. Go, Los Angeles
 Z. Kulcsár, Zurich
 M.-A. Weber, Rostock

*Japan***T. Hirai, Miyazaki (Section Editor, Diagnostic)****H. Kiyosue, Oita (Section Editor, Interventional)***Statistical Consultants*

J. Birks, Oxford
 E. Bluhmki, Biberach a.d. Riß
 P. Dupont, Leuven

ESNR

G. D'Anna, Monza

*Affiliated National Society delegate

SCIENTIFIC PROGRAM**WEDNESDAY 18th September 2019 - PRE-COURSE**

13:30 - 17:00	ASL in clinical practice: what, when and how?
13:30 - 14:00	Technical aspects and pitfalls for interpretation <i>Henk-Jan Mutsaerts</i>
14:00 - 14:30	ASL for paediatric Neuroradiology <i>Domenico Tortora</i>
14:30 - 15:00	ASL for neurovascular disease <i>Magdalena Sokolska</i>
15:00 - 15:30	Coffee Break
15:30 - 16:00	ASL for neuro-oncology <i>Marion Smits</i>
16:00 - 16:30	ASL for dementia <i>TBC</i>
16:30 - 17:00	Panel discussion/Q&A with ASL users/experts and audience on the topic 'how do we get ASL in the clinic?' Moderator: <i>Marion Smits</i> Panelists: <i>Henk-Jan Mutsaerts, Domenico Tortora, Magdalena Sokolska</i>

THURSDAY 19th September 2019 – Meeting room 1**26th ADVANCED COURSE IN DIAGNOSTIC NEURORADIOLOGY****ADULT AND PEDIATRIC INFLAMMATORY AND DEMYELINATING CNS DISEASES****08:00 - 10:00****Multiple Sclerosis I****Moderators:****Alex Rovira / Meike Vernooij (NL)**

08:00 - 08:20

MS diagnostic criteria: what is new? do we need them?

TBC

08:20 - 08:40

Pediatric MS: different from the adult form

Mona Beyer / NO

08:40 - 09:00

Primary progressive MS: the forgotten MS phenotype

TBC

09:00 - 09:20

Treatment options in MS: what the neuroradiologists need to know?

Hanne Harbo / NO

09:20 - 09:40

MRI in monitoring and predicting treatment response in MS

Jerome Hodel / FR

09:40 - 10:00

Discussion

10:00 - 10:30**Coffee Break****10:30 - 12:00****Multiple Sclerosis II****Moderators:****Frederik Barkhof / Hanne Harbo**

10:30 - 10:50

Atrophy in MS: can we use this measure in clinical practice

Alex Rovira / SP

10:50 - 11:10

New diagnostic MRI signs on the horizon

Jerome Hodel / FR

11:10 - 11:30

Chronic inflammation in MS: a new aspect of an old story

Jens Wuerfel / CH

11:30 - 11:50

MRI in safety monitoring in MS treated patients

Tarek Yousry / UK

12:00 - 12:50**Industry Sponsored Symposium****13:00 - 13:30****Keynote Lecture – Wim van Zwam****13:30 - 15:30****NMOSD and ADEM****Moderators:****Andres Server Alonso / Maria Argyropoulou (Gr)**

13:30 - 14:00

MRI features of autoimmune encephalitis

Philippe Demaerel / BE

14:00 - 14:30

NMOSD in adults: Imaging findings

Majda Thurnher / AT

14:30 - 15:00

MOG-associated pediatric CNS demyelination: Imaging findings and differential diagnosis

Andres Server Alonso / NO

15:00 - 15:30

Differential diagnosis in pediatric inflammatory demyelinating disorders

Nadine Girard (Fr)

15:30 - 16:00**Coffee Break****16:00 - 17:30****Future****Moderators:****Tarek Yousry / Mona Beyer**

16:00 - 16:20

Novel non-radiological biomarkers: complementary or competitive with MRI?

Bruno Stankoff / FR

16:20 - 16:40

PET in demyelinating diseases: clinical or only a research tool?

Bruno Stankoff / FR

16:40 - 17:00

Ultra-high field MRI in MS

Jens Wuerfel / CH

17:00 - 17:20

Machine learning and artificial intelligence in MS

Frederik Barkhof / NL

THURSDAY 19th September 2019 – Meeting room 2**11th ADVANCED COURSE IN INTERVENTIONAL NEURORADIOLOGY STROKE UPDATE****08:00 - 10:00****Treatment strategies in the light of recent studies****Moderators:**

08:00 – 08:30

Guidelines for thrombectomy in Europe

TBC

08:30 - 09:00

Speed up in the hospital

Marios Psychogios / DE

09:00 – 09:30

Is there an optimal service structure

Marielle Ernst / DE

09:30 - 10:00

Expectations for the future?

TBC

10:00 - 10:30**Coffee Break****10:30 - 12:00****Pathology and physiology in stroke****Moderators:**

10:30 - 10:55

Penumbra et al. revisited

Pasquale Mordasini / CH

10:55 - 11:20

Beyond TICI: Anatomy of stroke

Omer Eker / FR

11:20 - 11:45

TBC

12:00 - 12:50**Industry Sponsored Symposium (in meeting room 1)****13:00 - 13:30****Keynote Lecture (in meeting room 1)****13:30 – 14:30****Imaging for patient selection****Moderators:****Søren Jacob Bakke, Oslo/ Kathinka Kurz, Stavanger**

13:30- 13:50

NE-CT and CTA is enough

Oivind Gjertsen / NO

13:50 - 14:10

When using MRI?

Bjørn Tennøe / NO

14:10 - 14:30

eASPECTS vs. visual rating

Christian Herweh / DE

14:30 – 15:30**Imaging for patient selection**

14:30 - 15:00

Stroke mimics

TBC

15:00 - 15:30

Venous stroke

Pedro Vilela / PT

15:30 - 16:00**Coffee Break****16:00 - 17:30****Technical improvements in acute stroke treatment****Moderators:**

16:00- 16:30

Acronyms: is SAVE really EPIC?

TBC

16:30 - 17:00

Current role of primary aspiration

Peter Schramm / DE

17:00 - 17:30

How do we know what really works?

Pasquale Mordasini / CH

FRIDAY 20th September 2019 – Meeting room 1

08:00 - 08:25	Interactive Cases Diagnostic Erik Magnus, Berntsen Trondheim, NO	
08:30 - 10:00	Brain Tumor	
<i>Moderators:</i>	<i>John Hald, Oslo/ Ana Ramos ES</i>	
08:30 - 08:50	Imaging genomics of glioma	Marion Smits / NL
08:50 - 09:10	Imaging glioma microenvironment: histopathology meets radiology (Rad-Path)	TBC
09:10 - 09:30	Imaging criteria in Neuro-oncology	Pia Sundgren / SE
09:30 - 09:50	Posttreatment evaluation of brain tumors in an evolving therapeutic landscape	TBC
09:50 - 10:00	Discussions	
10:00 - 10:30	Coffee Break	
10:30 - 12:00	Opening Ceremony, Honorary Members and Awards Ceremony	
12:10 - 13:00	Industry Sponsored Symposium	
13:10 - 13:40	Keynote Lecture: Malformations of cortical development: raising awareness, improving detection, and understanding pathomechanisms - Andrea Rossi	
13:45 - 15:15	SCIENTIFIC SESSION - Vascular Intervention	
13:45 - 13:53	2 – O8 Feasibility and efficacy of flow diversion in aneurysm management of small caliber cerebral arteries: long term results of a single center experience with fred jr- <u>ALBERALAR N.D.</u>	
13:53 - 14:01	2 – O4 Complications in posterior circulation mechanical thrombectomy, a retrospective review - <u>DE MIQUEL M.A.</u>	
14:01 - 14:09	2 – O5 Cumulative incidence of restenosis in the endovascular treatment of extra cranial carotid artery stenosis: meta-analysis - <u>CLAVEL P.</u>	
14:09 - 14:17	2 – O3 Stasis index from quantitative hemodynamic assessment as a predictor of brain arteriovenous malformation obliteration after gamma knife surgery - <u>HU Y.</u>	
14:17 - 14:25	2 – O1 Emergency eversion carotid endarterectomy in thrombectomy stroke patients - <u>NIKOUBASHMAN O.</u>	
14:25 - 14:33	2 – O2 Hemorrhage rate and its risk factors in thrombectomy patients receiving emergency carotid artery stenting - <u>NIKOUBASHMAN O.</u>	
14:33 - 14:41	5 – O4 Spinal cord infarction, many more - <u>PENDHARKAR H.</u>	
14:41 - 14:48	2 – O7 6 to 24 hours endovascular thrombectomy for large intracranial vessel occlusion without perfusion ct patient selection: single center experience - <u>ALEXANDRE A.</u>	
14:48 - 14:56	3 – O4 Exercise-induced fluctuation in cerebral blood flow among patients with main arterial occlusions implies a mechanism for cerebral autoregulation: a pet study - <u>HIURA M.</u>	
15:20 - 15:50	ESNR meets Spain	
15:50 - 16:15	Coffee Break	
16:15 - 17:30	EBNR Diploma Ceremony	

FRIDAY 20th September 2019 – Meeting room 2

08:00 - 10:00	Neuroradiology educational session Head & Neck	
	<i>Moderators: Leon van Rensburg (SA)</i>	
08:00 - 08:30	Visual impairment	Bernhard Schuknecht / CH
08:30 - 09:00	Double vision	Teresa Nunes / PT
09:00 - 09:30	Hearing impairment and/or vertigo	Steve Connor / UK
09:30 - 10:00	Pulsatile tinnitus	Katarina Surjan Popovic / SI
10:00 - 10:30	Coffee Break	
10:30 - 12:00	Opening Ceremony, Honorary Members and Awards Ceremony (in meeting room 1)	
12:10 - 13:00	Industry Sponsored Symposium (in meeting room 1)	
13:10 - 13:40	Keynote Lecture (in meeting room 1)	
13:45 - 15:15	SCIENTIFIC SESSIONS - Neurodegeneration/ hydrocephalus	
13:45 - 13:53	2 – O6 Treatment of essential tremor (et) and parkinson disease (pd) tremor with mrgfus: preliminary long-term results and evaluation of imaging findings predictive value - <u>BRUNO F.</u>	

13:53 - 14:01	1 – O39 Automated MRI hippocampal subfield measurement in mild cognitive impairment in an amyloid project. <u>CHAWALPARIT O.</u>
14:01 - 14:09	1 – O44 Supra- and infratentorial atrophy following clinically isolated syndromes: a 30-year follow-up study <u>HAIDER L.</u>
14:09 - 14:17	1 – O19 Age- and gender effects on brainstem MR-planimetry - <u>MANGESIUS S.</u>
14:17 - 14:25	1 – O15 Brain changes induced by electroconvulsive therapy - <u>OLTEDAL L.</u>
14:25 - 14:33	1 – O20 MRI-compatible pneumatic stimulator for sensorimotor mapping in patients with brain tumours – <u>LOLLI V.</u>
14:33 - 14:41	1 – O12 Clinical evaluation of quantitative atrophy reports for mri interpretation in dementia: a multi-rater, proof-of-concept study - <u>PEMBERTON H.</u>
14:41 - 14:48	1 – O1 Iron accumulation in deep gray matter is associated with apoe4 gene status in cognitively impaired subjects: a quantitative susceptibility mapping study - <u>YIM Y.</u>
14:48 - 14:56	1 – O26 Agreement between CT and MRI in patients with normal pressure hydrocephalus - <u>KOCKUM K.</u>
14:56 - 15:04	1 - O23 Added value of an automatic registration and subtraction tool for monitoring patients with normal-pressure hydrocephalus - <u>KUCHCINSKI G.</u>
15:04 - 15:12	3 – O3 Visualisation of the intrapetrous facial nerve canal on black bone imaging and a comparison with pre and post gadolinium 3D space sequences - <u>KAFIABADI S.</u>
15:20 - 15:50	ESNR meets Spain (in meeting room 1)
15:50 - 16:15	Coffee Break
16:15 - 17:30	EBNR Diploma Ceremony (in meeting room 1)

FRIDAY 20th September 2019 – Meeting room 3

08:00 - 08:25	Interactive cases	Pediatric
	<i>Bård Nedregard</i>	
08:30 - 10:00	Advanced techniques to provide flow control in curative endovascular AVM and DAVF treatment	
	<i>Moderators: Isabel Wanke/CH</i>	
08:30 - 08:50	Advanced transvenous intranidal flow control technique in curative pial AVM treatment	<i>Suzana Saleme</i>
08:50 - 09:10	Advanced multiplug arterial intranidal flow control technique in curative pial AVM treatment	<i>Saruhan Cekirge / TR</i>
09:10 - 09:30	Advanced arterial and intrasinus flow control approaches in curative DAVF treatment	<i>Rene Chapot / DE</i>
09:30 - 09:50	Curative transvenous DAVF treatment: when and why?	<i>Vitor Mendez Pereira / CA</i>
09:50 - 10:00	Discussion	
10:00 - 10:30	Coffee Break	
10:30 - 12:00	Opening Ceremony, Honorary Members and Awards Ceremony (in meeting room 1)	
12:10 - 13:00	Industry Sponsored Symposium (in meeting room 1)	
13:10 - 13:40	Keynote Lecture (in meeting room 1)	
13:45 - 15:15	SCIENTIFIC SESSIONS – SPINE	
13:45 - 13:53	5 - O12 CT-guided transfacet pedicle screw fixation in lumbar microinstability syndrome: a novel approach - <u>DE VIVO A.E.</u>	
13:53 - 14:01	5 - O11 Intra-osseous basivertebral nerve radiofrequency ablation (bnra) for the treatment of chronic vertebrogenic low back pain - <u>DE VIVO A.E.</u>	
14:01 - 14:09	5 – O2 Gadolinium-enhanced magnetic resonance imaging findings in cervical spondylotic myelopathy - <u>AUGER C.</u>	
14:09 - 14:17	5 – O9 Assessing symptom relief following vertebroplasty in multiple myeloma - <u>CONNOLLY D.</u>	
14:17 - 14:25	5 – O8 Multi-time point fdg-18 pet/mr imaging of spinal cord lesions of unknown etiology - <u>GULE-MONROE M.</u>	
14:25 - 14:33	5 – O7 Statistical parametric mapping of regional bone density at the thoracolumbar spine for opportunistic osteoporosis screening - <u>LÖFFLER M.</u>	
14:33 - 14:41	5 – O6 Magnetic resonance spectroscopy: optimization and clinical application of cervical cord single voxel acquisition at 3 tesla - <u>MANSOUR M.</u>	
14:41 - 14:48	5 – O5 Extramedullary spinal tumors: report of a series cases and imaging findings with pathologic confirmation - <u>MARIC D.</u>	
14:48 - 14:56	5 – O1 Acquired spondylolysis and spondylolisthesis after post-decompression surgery of lumbar spine without fusion - <u>YOO J.H.</u>	
14:56 - 15:04	5 - O10 Cervical spine fracture patterns predict dissection of vertebral artery after blunt injury - <u>KOSTIC J.</u>	

15:04 - 15:12	5 – O3 The potential role of intervertebral lumbar disc fa (fractional anisotropy) map in diffusion tensor imaging (DTI) to select patients suffering from low back pain and who may benefit from intradiscal oxygen-ozone injection - <u>PERRI M.</u>
15:20 - 15:50	ESNR meets Spain (in meeting room 1)
15:50 - 16:15	Coffee Break
16:15 – 17:30	EBNR Diploma Ceremony (in meeting room 1)

FRIDAY 20th September 2019 – Meeting room 4

13:45 - 15:15	SCIENTIFIC SESSIONS – BRAIN TUMOUR
13:45 - 13:53	1 – O41 ASL-perfusion in predicting of brain glioma malignancy and idh1 status - <u>BATALOVA.</u>
13:53 - 14:01	1 – O40 A comparison of microstructural diffusion MRI techniques for the in-vivo assessment of glioma grading - <u>CARLETTI F.</u>
14:01 - 14:09	1 – O27 Assessing the optimal fdg pet imaging time point in glioblastoma - <u>JOHNSON J.</u>
14:09 - 14:17	1 – O22 Prediction of prognosis in patients with newly diagnosed glioblastoma using pre-treatment intra- and peritumoral restriction spectrum imaging - <u>LATYSHEVA A.</u>
14:17 - 14:25	1 – O18 Clinical MR imaging for who grade II/III glioma molecular subtyping: diffusion, age and morphology evaluation system - <u>MAYNARD J.</u>
14:25 - 14:33	1 – O17 MRI assessed responses in tumor and whole brain to srs alone or combined with immunotherapy in patients with brain metastases - <u>NILSEN L.B.</u>
14:33 - 14:41	1 – O16 Endogenous chemical exchange saturation transfer (cest) MR imaging for the diagnosis and therapy response assessment of brain tumors: a systematic review – <u>THUST S.</u>
14:41 - 14:48	1 – O4 Diffusion-weighted MR imaging characteristics of h3 k27m histone-mutant diffuse midline glioma in teenagers and adults - <u>THUST S.</u>
14:48 - 14:56	1 – O3 3d 1h MR-spectroscopy in determining the degree of anaplasia of glial tumours <u>TYURINA A.</u>
14:56 - 15:04	1 – O13 Correlates of intra-operative speech arrest on functional magnetic resonance imaging: tumoral invasion and language plasticity - <u>PASQUINI L.</u>
15:04 - 15:12	1 – O21 Magnetic resonance diffusion-tensor imaging metrics in high grade gliomas: correlation with idh1 gene status in who 2016 era – <u>AGNELLO A.</u>

SATURDAY 21st September 2019 – Meeting room 1 -

08:00 - 08:25	Interactive Cases	Interventional
	<i>TBC</i>	
08:30 – 10:00	What is new on the horizon: MR elastography and mechanics of the Tissue microenvironment	
	Moderator: Kyrre Emblem	
08:30 – 08:50	MR Elastography of the human brain	<i>Ralph Sinkus / UK</i>
08:50 – 09:10	Tracking changes in brain plasticity over time	<i>Martin Reuter / DE</i>
09:10 – 09:30	Mapping tissue heterogeneity with MRI, from bench to bedside	<i>James O'Connor / UK</i>
09:30 – 09:50	Imaging Perfusion Restrictions from Extracellular Solid Stress	<i>Kyrre E. Emblem / NO</i>
09:50 – 10:00	Discussion	
10:00 - 10:30	Coffee Break	
10:30 - 12:00	ESNR General Assembly	
12:10 - 13:00	Industry Sponsored Symposium	
13:15 - 13:45	Keynote Lecture	
13:45 – 15:15	ASNR – ESNR Joint Session	
13:45 – 14:05	Are there enough Interventional Neuroradiologists to treat Stroke? US and European perspective. <i>Josh Hirsch (US) / TBC</i>	
14:05 – 14:25	Data review: The case grows stronger for interventional treatment of stroke. <i>Reade DeLeacy (US)</i>	
14:25 – 14:45	Endovascular thrombectomy beyond the 6 hour time window; how selective should we be? <i>Wim van Zwam (Netherlands)</i>	
14:45 – 15:05	Can AI help in diagnosing stroke and predicting stroke outcome? <i>Antonin Krajina (Czech Republic)</i>	
15:05 – 15:10	Discussions	
15:15 – 16:45	SCIENTIFIC SESSIONS - MS/Epilepsia/tumour	

15:15 - 15:23	1 – O45 The diagnostic value of susceptibility-weighted imaging in multiple sclerosis: the central vein sign and iron rings are specific markers of multiple sclerosis lesions – <u>ROVIRA A.</u>	
15:23 - 15:31	1 – O38 Machine learning approach to texture analysis parameters can predict clinical disability in multiple sclerosis patients - <u>COCOZZA S.</u>	
15:31 - 15:39	1 – O36 Prediction of long-term disability in multiple sclerosis: a role for linear measures of brain atrophy? - <u>DI STASI M.</u>	
15:39 - 15:47	1 – O9 3D t1 black-blood MRI for the detection of acute optic neuritis - <u>RIEDERER I.</u>	
15:47 - 15:55	1 – O5 Accuracy of multiple sclerosis brain volumes in real world magnetic resonance images – <u>SMEETS D.</u>	
15:55 - 16:03	1 – O32 Contribution of MRI voxel-based morphometry in the diagnosis of focal cortical dysplasias - <u>GONZÁLEZ-ORTIZ S.</u>	
16:03 - 16:11	1 – O34 Comparison of ASL perfusion and SPECT examination in laterisation of seizure focus in patients with intractable temporal lobe epilepsy - <u>GARG A.</u>	
16:11 - 16:19	1 – O31 Clinical evaluation of quantitative reports for MRI assessment of suspected medial temporal sclerosis (mts) - <u>GOODKIN O.</u>	
16:19 - 16:27	1 – O7 Correlation between presurgical motor tract diffusion tensor imaging, fiber tractography data and intraoperative evoked potentials during brain tumor surgery - <u>SÁNCHEZ J.J.</u>	
16:27 - 16:35	1 – O6 Diagnostic accuracy of MRI on follow-up imaging of patients with leptomeningeal seeding from non-small cell lung cancer: comparison of contrast-enhanced 3D t1 mprage and contrast-enhanced 2D axial t2 flair - <u>SEONG M.</u>	
16:35 - 16:43	3 – O2 Microstructural changes in CST on contralateral sides of high grade gliomas - <u>POGOSBEKIAN E.</u>	
16:45 - 17:15	Coffee Break	
17:15 – 18:45	Infection	
	Moderators: Clive Sperry, Zulejha Merhemic	
17:15 - 17:40	Brain and spinal infections in children	Tracy Kilborn / SA
17:40 - 18:05	Brain and spine infections in adults	Turgut Tali / TR
18:05 - 18:30	Infection in immunocomprised patients	Majda Thurnher / AT
18:30 – 18:45	Discussion	

SATURDAY 22nd September 2018 – Meeting room 2

08:00 - 08:25	Interactive Cases	Spine
	<i>Luc van der Hauwe (BE)</i>	
08:30 – 10:00	Cutting the edge of Spine Interventional Neuroradiology	
	Moderators: Luigi Manfre, John Go	
08:30 – 08:50	Economics and policy of Interventional radiology	Joshua Hirsch / US
08:50 – 09:10	Vertebral restoration and stabilization : is it possible?	Andrea Brook / US
09:10 – 09:30	Percutaneous treatments of primary spine tumors	Mario Muto / IT
09:30 – 09:50	Spinal canal stenosis and Instability: what we can do	Luigi Manfrè / IT
09:50 – 10:00	Discussions	
10:00 - 10:30	Coffee Break	
10:30 - 12:00	ESNR General Assembly (in meeting room 1)	
12:10 - 13:00	Industry Sponsored Symposium (in meeting room 1)	
13:15 - 13:45	Keynote lecture (in meeting room 1)	
13:45 - 15:15	ESNR/ASPNR Joint Session: What is new pediatric brain tumors	
	Moderators: Bård Nedregard / Laurence Eckel	
13:45 – 14:05	Medulloblastoma revisited	Pia Sundgren / SE
14:05 – 14:25	Brain tumors in fetuses and neonates: strange things do happen	Andrea Rossi / IT
14:25 – 14:45	Diffuse midline glioma – update	Tina Young Poussaint / US
14:45 – 15:05	Surveillance imaging of pediatric brain tumors: when & how	Arastoo Vossough / US
15:05 – 15:10	Discussion	
15:15 – 16:45	SCIENTIFIC SESSIONS - Pediatric neuroradiology	
15:15 - 15:23	4 – O12 Surveillance imaging of low-grade astrocytomas in children: can we reduce follow-up and the use of contrast agents? - <u>CAMPION T.</u>	
15:23 - 15:31	4 – O11 Muscle- MRI pattern of progression in spinal muscular atrophy patients - <u>CRISTIANO L.</u>	
15:31 - 15:39	4 – O10 Hypothalamic malformations in patients with x-linked deafness and incomplete partition type 3 - <u>D'ARCO F.</u>	
15:39 - 15:47	4 – O9 CT findings before and after secondary bone grafting in cleft lip and palate patients: our experience in 120 patients - <u>GÓMEZ-CHIARI M.</u>	

15:47 - 15:55	4 – O8 Accelerated brain aging in premature-born adults - <u>HEDDERICH D.</u>
15:55 - 16:03	4 – O7 Prediction of neurodevelopmental outcome in very preterm infants with cerebral mr spectroscopy and dti using feed-forward neural networks - <u>JANJIC T.</u>
16:03 - 16:11	4 – O6 Magnetic resonance spectroscopic imaging in non-neoplastic paediatric intracranial lesions - <u>NARAYANA VAMYANMANE D.K.</u>
16:11 - 16:19	4 – O5 Practical clinical use of magnetic resonance perfusion imaging for the treatment of pediatric patients with moyamoya disease - <u>NARIAI T.</u>
16:19 - 16:27	4 – O4 Gadolinium retention in pediatric brain: hyperintensity in nucleus dentatus and globus pallidus; when it appears? - <u>PITURA R.</u>
16:27 - 16:35	4 – O3 Investigating the myelination in children using quantitative t2 mapping - <u>PORTO L.</u>
16:35 - 16:43	4 – O2 Magnetic resonance imaging (mri) protocol for craniofacial pathologies, replacing ionising radiation-based computed tomography - <u>TAN A.P.</u>
16:43 - 16:51	4 - O1 Bilateral orbital granulocytic sarcoma in acute myeloid leukemia presenting with proptosis - <u>YAPICI UGURLAR O.</u>
16:45 - 17:15	Coffee Break
17:15 – 18:45	"Big is beautiful" consequences of big data analysis on neuroradiology
	Moderators: Mona Beyer, Atle Bjørnerud
17:15 – 17:40	What have we learnt from really big data in different brain disorders
17:40 – 18:05	Deep learning and other techniques for analyzing Big Data
18:05 – 18:30	Harmonization of data from different sources
18:30 – 18:45	Discussion

Paul S Thompson / US
 Jorge Cardoso / UK
 Paul S Thompson / US

SATURDAY 21st September 2019 – Meeting room 3

08:30 - 10:00 Endovascular treatment of giant aneurysms: advances and still existing difficulties

Moderators: Terje Nome/Gyula Gal

08:30 - 08:55	How to manage giant aneurysms in acute setting
08:55 - 09:20	The impact of flow diverters in endovascular giant aneurysms treatment with still existing problems and how to solve them
09:20 - 09:45	Giant partially clotted vertebrobasilar fusiform arteriosclerotic aneurysms: Is there really role of any treatment
09:45 - 10:00	Discussion

Salvatore Mangiafico / IT
 Naci Kocer / TR

Vitor Mendes Pereira / CA

10:00 - 10:30 Coffee Break

10:30 - 12:00 ESNR General Assembly (in meeting room 1)

12:10 - 13:00 Industry Sponsored Symposium (in meeting room 1)

13:15 - 13:45 Keynote Lecture (in meeting room 1)

13:45 - 15:15 Endovascular treatment of ruptured aneurysms in acute setting: current trends/discussions

Moderators: Øivind Gjertsen/Pedro Vilela

13:45 – 14:05	The current role of intrasaccular flow disruptor-web device in ruptured wide necked aneurysms
	TBC

14:05 – 14:25	How to manage stents or flow diverters in acute ruptured wide necked aneurysms: why and when
---------------	--

Vincent Costalat / FR

14:25 – 14:45	What would be the role of intra or extra saccular bifurcation devices in ruptured wide necked aneurysms
---------------	---

Gyula Gal / SE

14:45 – 15:05	Should “good old balloon remodelling” still be as a mainstay treatment in ruptured wide necked aneurysms?
---------------	---

Civan Islak /TR

15:05 – 15:10 Discussion

15:15 – 16:45 SCIENTIFIC SESSIONS - Diagnostic Neuroradiology

15:15 - 15:23	1 - O42 An observational study to evaluate the management of patients with chronic headache with referral from primary care to direct access to magnetic resonance imaging (MRI) compared to neurology services - <u>ASIF M.</u>
15:23 - 15:31	1 – O28 Comparison of CNR of antidrive-3D-tse black-blood imaging combined with imside taken in clinical cases in our hospital <u>HIRAKA T.</u>
15:31 - 15:39	1 - O24 TMS - EEG and resting-state fMRI accuracy comparison in differentiation of chronic disorders of consciousness - <u>KREMNEVA E.</u>
15:39 - 15:47	1 – O14 Integrity of the cortico-striatal pathway in fabry disease investigated via diffusion MRI connectometry analysis - <u>PAOLELLA C.</u>
15:47 - 15:55	1 – O8 MRI findings of symptomatic vs. asymptomatic trigeminal neurovascular contact in trigeminal neuralgia - <u>SAKINIS T.</u>
15:55 - 16:03	1 – O2 comparative analysis of diffusion metrics obtained using DTI and DKI techniques in the brains of individuals with HIV-1 clade-C infection - <u>VYAS S.</u>

16:03 - 16:11	1 – O43 Dose finding study of gadopiclesol, a new macrocyclic gadolinium-based contrast agent (GBCA), in MRI of central nervous system - <u>ANZALONE N.</u>	
16:11 - 16:19	3 – O5 CT texture analysis for differentiation of pleomorphic adenoma and warthin tumour in salivary gland - <u>HAN M.</u>	
16:19 - 16:27	3 – O1 Comparison between contrast-enhanced proset 3D-TL-turbo field echo (TFE) and contrast enhanced 3D- flair vista for diagnosing bell's palsy - <u>RHIM J.H.</u>	
16:45 - 17:15	Coffee Break	
17:15 – 18:45	Flow remodelling concept in bifurcations: a technical and conceptual advance in endovascular aneurysm treatment	
	Moderators: Bård Nedregard	
17:15 - 17:35	Flow redirection in side branch aneurysms integrated to the aneurysm sac: "the flow remodelling concept" in endovascular treatment	<i>Lauren Spelle / FR</i>
17:35- 17:55	A new aneurysm occlusion classification with the implication of flow remodelling concept	<i>Isil Saatci / TR</i>
17:55 - 18:15	Extrasaccular flow remodelling in endovascular treatment of mca bifurcation and acom aneurysms: long term results	<i>Suzana Saleme</i>
18:15 – 18:35	Intrasaccular flow remodelling with intrasaccular flow disruptors: what are the long-term results and their implications with special emphasis on so- called web remnants	<i>TBC</i>
18:35 – 18:45	Discussions	

SATURDAY 21st September 2019 – Meeting room 4

13:45 - 15:15	The Glymphatic system and Brain Lymphatic Drainage	
	Moderators: Jeffrey Iliff USA/ Geir Ringstad, Oslo, Norway	
13:45 – 14:10	A brain-wide perivascular pathway for CSF-ISF exchange	<i>Jeffrey Iliff / US</i>
14:10 – 14:35	True CNS lymphatic vessels and their role in neurodegeneration	<i>Antoine Louveau / US</i>
14:35 – 15:00	MRI of the human glymphatic system: relevance to neurological disease	<i>Geir Ringstad / NO</i>
15:00 – 15:15	Discussions	
15:15 – 16:45	SCIENTIFIC SESSIONS – Diagnostic Vascular	
15:15 - 15:23	1 – O37 Assessment of dural sinus thrombosis by means of density values: a tool for the emergency radiologist – <u>DELLE PIANE F.</u>	
15:23 - 15:31	1 – O33 Cervico-cranial arterial dissections -clinical and neuroradiology correlations - <u>GEORGIEVSKI-BRKIC B.</u>	
15:31 - 15:39	1 – O35 Vessel wall enhancement of intracranial aneurysms on high resolution MRI: a rupture sign? the Icarus study - <u>GRAMEGNA L.</u>	
15:39 - 15:47	1 – O30 Acute symptomatic lacunar ischemic stroke as first presentation of small vessel disease: how common is it? - <u>GUARNERA A.</u>	
15:47 - 15:55	1 – O29 Clinical usefulness of deep learning based automated detection algorithm in the intracranial haemorrhage - <u>HAHM M.H.</u>	
15:55 - 16:03	1 – O25 Ambulatory blood pressure monitoring and DTI-based microstructural changes in patients with hypertension-related cerebral small vessel disease – <u>KREMNEVA E.</u>	
16:03 - 16:11	1 – O11 Potential of diffusion tensor imaging in the evaluation of neuropsychological disorders secondary to aneurysmal rupture of the anterior complex: preliminary insights from the acom protocol - <u>PREMAT K.</u>	
16:11 - 16:19	1 – O10 Aneurysmal velocity reduction assessment after flow diversion using 4D-pcmri: a prospective study on 23 patients - <u>REYMOND P.</u>	
16:45 - 17:15	Coffee Break	
17:15 – 18:45	Tricks and treats about neonatal imaging	
	Moderators: Chen Hoffmann, Nadine Girard	
17:15 - 17:35	Safety, speed & comfort: how I scan my neonates	<i>Andrea Righini / IT</i>
17:35- 17:55	All things vascular: more than just HIE	<i>Kshitij Mankad / UK</i>
17:55 - 18:15	Infections: on the rise again	<i>Elida Vazquez Mendez/ES</i>
18:15 – 18:35	The preterm brain: a different world	<i>Domenico Tortora / IT</i>
18:35 – 18:45	Discussions	

SUNDAY 22nd September 2019 – Meeting room 1

08:30 - 08:55	Interactive cases	
	Cases we would like to read again: interesting cases reviewed with the benefit of hindsight	
	<i>Pål Bache Marthinsen / NO</i>	
09:00 - 10:30	Prognostication of hypoxic ischemic injury of the brain after cardiac arrest	

	Moderators: Sumeet Kumar	
09:00 - 09:25	The Norwegian Cardiac-Respiratory Arrest Study: Neuro-prognostic markers	<i>Nakstad Rostrup / NO</i>
09:25 - 09:50	Neuroimaging in cardiac arrest: Findings in relation to neurological outcome	<i>Kathinka Kurz / NO</i>
09:50 - 10:15	Imaging of brain death: imaging spectrum, protocols and guidelines	<i>B.K.Velthuis / NL</i>
10:15 - 10:30	Discussions	
10:30 - 11:00	Coffee Break	
11:00 - 12:40	Demens	
	Moderators: Marit Herder, Tromsø , NO /Sven Haller/CH	
11:00 - 11:25	Alzheimers disease –from visual rating scales to automatic measurements in dementia evaluation	<i>Eric Westman / SE</i>
11:25 - 11:50	Differential diagnosis in the dementia rounds	<i>Torsten Danfors and David Fallmar / SE</i>
11:50 - 12:15	Vascular disease and dementia	<i>Meike Vernooij / NL</i>
12:15 - 12:40	Discussions	
12:40 - 13:00	Closing Ceremony	

SUNDAY 22nd September 2019 – Meeting Room 2

08:30 - 08:55	Interactive cases	(Meeting Room 1)	
09:00 - 10:30	Joint session ESNR – ESHNR		
	Skullbase		
	Moderators: Bernhard Schuknecht/		
09:00 - 09:20	Anatomy and variants necessary to know		<i>Tim Beale / UK</i>
09:20 - 09:40	The anterior skull base		<i>Alex Borges / PT</i>
09:40 - 10:00	Sella		<i>Fabrice Bonneville / FR</i>
10:00 - 10:20	Foramen jugulare		<i>Sotirios Bisdas / UK</i>
10:20 - 10:30	Discussions		
10:30 - 11:00	Coffee Break		
11:30 - 12:40	Spine		
	Moderators: Luigi Manfre		
11:00 - 11:25	Imaging in Low Back Pain: what can we do better?		<i>Johan Van Goethem / BE</i>
11:25 - 11:50	Spectral CT/Dual Energy CT		<i>Linda Jacobi Postma / NL</i>
11:50 - 12:15	Imaging for Interventional complications		<i>Bassem Georgy / US</i>
12:15 - 12:40	Image guided diagnosis and management of spinal CSF leaks		<i>Michele H. Johnson / US</i>
12:40 - 13:00	Closing Ceremony (in meeting room 1)		

SUNDAY 22nd September 2019 – Meeting room 3

09:00 - 10:30	My complications in interventional neuroradiology	
	Moderators:	
09:00 - 09:20	Stroke	<i>Terje Nome / NO</i>
09:20 - 09:40	AVM	<i>Salvatore Mangiafico / IT</i>
09:40 - 10:00	Aneurysm	<i>Mats Cronqvist / SE</i>
10:00 - 10:20	Dural AVF	<i>Christian Herweh / DE</i>
10:20 - 10:30	Discussions	
10:30 - 11:00	Coffee Break	
11:00 - 12:40	How to manage extra cranial arterial lesions	
	Moderators:	
11:00 - 11:20	Elective carotis stenting: Technical and philosophical challenges	<i>Omer Eker / TR</i>
11:20 - 11:40	Extracranial vertebral artery revascularization: When, How and Results	<i>Christian Herweh / DE</i>
11:40 - 12:00	Supraaortic vessel dissections and their management	<i>Luisa Biscoito / PT</i>
12:00 - 12:20	Supraaortic revascularization: How to manage tandem or multiple lesions	<i>Kamil Zelenak / SK</i>
12:20 - 12:40	Discussions	
12:40 - 13:00	Closing Ceremony (in meeting room 1)	

ORAL PRESENTATIONS

1. DIAGNOSTIC - BRAIN

1-O1

IRON ACCUMULATION IN DEEP GRAY MATTER IS ASSOCIATED WITH APOE4 GENE STATUS IN COGNITIVELY IMPAIRED SUBJECTS: A QUANTITATIVE SUSCEPTIBILITY MAPPING STUDY

Y. YIM¹, W. Moon², Y. Moon³, S. Han³

¹ Kangwon National University Hospital, Department of Radiology, Chuncheon, SOUTH KOREA, ² Konkuk University Medical Center, Department of Radiology, Seoul, SOUTH KOREA, ³ Konkuk University Medical Center, Department of Neurology, Seoul, SOUTH KOREA

Introduction

Increasing evidence suggests that there is brain iron overload in various neurodegenerative diseases. APOE gene, an important genetic risk factor of Alzheimer's disease, recently revealed relationship with ferritin level. We assessed the relation between APOE status and iron accumulation of deep gray matter in cognitive impaired subjects using quantitative susceptibility mapping (QSM).

Methods

We retrospectively enrolled total 106 cognitively impaired patients with known APOE genotype (26 Alzheimer dementia, 60 mild cognitive impairment, 26 subjective cognitive impairment) who underwent 3T magnetic resonance imaging (MRI) between January 2013 and December 2015. There were 33 patients (age 71.5 ± 9.2) with APOE4 positive (APOE4 +) and 73 patients (age 69.9 ± 7.8) with APOE4 negative (APOE4 -). Reference-normalized QSM was generated by STI suite and in-house software. Regions of interest (ROI) analysis of QSM was done for the deep gray matters: globus pallidus, putamen, caudate nucleus, and pulvinar nucleus of the thalamus. Comparisons of clinicodemographic features and susceptibility values as an iron marker were evaluated by student t-test and chi-square test.

Result

Age, sex, education and known dementia risk factors (hypertension, diabetes, dyslipidemia, smoking, and cardiovascular disease) did not differ between APOE+ and APOE- groups. APOE+ patients had mildly lower MMSE score (21.5 ± 5.4 vs 25.2 ± 4.3) and worse CDR (CDR-SOB) as compared to APOE- patients ($p < 0.001$).

Overall, APOE4+ group shows higher susceptibility values than APOE4- group with significant differences in left putamen (132.73 ± 45.15 ppb vs. 115.19 ± 50.96 ppb, $p = 0.05$), left globus pallidus (206.99 ± 61.24 ppb vs. 176.26 ± 69.64 ppb, $p = 0.002$) and right globus pallidus (215.65 ± 65.39 ppb vs. 180.05 ± 67.33 ppb, $p = 0.001$).

Discussion & Conclusion

In cognitively impaired subjects, presence of APOE4 genotype was associated with higher susceptibility change in deep gray matter, representing higher iron accumulation. Our finding supports the possible link between APOE gene status and brain iron homeostasis in various stage of cognitive impaired subjects.

1-O2

COMPARATIVE ANALYSIS OF DIFFUSION METRICS OBTAINED USING DTI AND DKI TECHNIQUES IN THE BRAINS OF INDIVIDUALS WITH HIV-1 CLADE-C INFECTION

S. VYAS¹, T. Salan², P. Singh¹, M. Kumar², V. Govind²

¹ Postgraduate Institute of Medical Education and Research, Chandigarh, INDIA, ² University of Miami, Miami, USA

Introduction

Long-term HIV infection damages the brain causing cognitive deficiencies and dementia. Diffusion tensor imaging (DTI) can evaluate the integrity of brain tissue structures. However the DTI model assumes Gaussian distribution for the displacement of water molecules. In complex structures, diffusions deviate substantially from a Gaussian form. Diffusional kurtosis imaging (DKI) is an extension to DTI that quantifies the degree of non-Gaussianity, and investigates abnormalities in tissues where DTI is less applicable. In this study, we compared DTI and DKI to examine how long term infection with HIV affects the brain.

Methods

We acquired whole-brain diffusion-weighted (DW) MRI from 50 individuals (25 HIV+ Clade-C Infection, 25 controls) with a 3T-MRI scanner, and collect 9 b0 and 60 DW-images using 30 gradient directions with dual-shell acquisition ($b = 1000/2000$ s/mm²). The data is pre-processed for head motion and eddy-current distortions using FSL. DTI and DKI fitting is performed using the Dipy library to generate DTI maps (FA, MD, AD, RD), and DKI maps such as kurtosis FA (kFA), and mean, axial, and radial kurtosis (MK, AK, RK). We performed an atlas-based analysis using the JHU-MNI-SS-BPM-type2 atlas, and obtain DTI/DKI metrics from 189 anatomical regions of interest (ROI). We applied an F-test ($p < 0.05$; corrected for 189 comparisons using false discovery rate) to find statistically significant differences between control and HIV+ populations for the generated metrics at each ROI.

Result

Only kurtosis metrics revealed high statistically significant differences between the two groups. We observed an increase in MK, AK, and RK in several ROIs (figures 1-3). These changes occur throughout the brain in regions corresponding to the occipital gyrus, temporal gyrus, cingulate

gyrus, and pre-frontal gyrus. Only in the mammillary body and cerebral peduncle we see decrease in MK and RK.

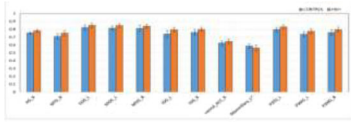


Figure 1: Regions with significant changes in MK between control and HIV populations.

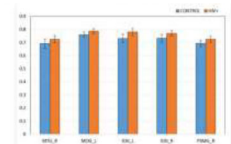


Figure 2: Regions with significant changes in AK between control and HIV populations.



Figure 3: Regions with significant changes in RK between control and HIV populations.

Discussion & Conclusion

The lack of significant changes in DTI metrics suggests minimal disruption to structural integrity in HIV population. However the increase in diffusional kurtosis corresponds to an increase in diffusional heterogeneity. This may be influenced by factors other than structure, such as the concentration of macromolecules, boundary lesions, and irregularly oriented diffusion barriers.

1-O3

3D 1H MR-SPECTROSCOPY IN DETERMINING THE DEGREE OF ANAPLASIA OF GLIAL TUMOURS

A. Tyurina¹, I. Pronin¹, L. Fadeeva¹, V. Kornienko¹

¹ National Medical Research Center of Neurosurgery, Moscow, RUSSIA,

² National Medical Research Center of Neurosurgery, Moscow, RUSSIA,

³ National Medical Research Center of Neurosurgery, Moscow, RUSSIA,

⁴ National Medical Research Center of Neurosurgery, Moscow, RUSSIA

Introduction

Study of 3D proton MR spectroscopy informativity in the diagnosis of glial brain tumors. 20 healthy volunteers, 47 patients with low-grade glioma's and 50 patients with high-grade glioma's. Metabolites which we rely on in our study are: Choline, Creatine, N-Acetylaspartate.

Methods

3D 1H MR-Spectroscopy: MR-scanner 3.0 T, HOS PROBE 3D, FOV = 8 x 8 x 8, TE 144, TA 8.36 min. Postprocessing – ReadyView(SAGE). Stat.Analysis – STATISTICA, R.

Result

In control group of 20 healthy volunteers, we measured the metabolite ratio in whole brain matter. White matter: Cho/NAA – 0.47±0.12, Cho/Cr – 1.19±0.23, NAA/Cr – 2.56±0.55.

Gray matter: Cho/NAA – 0.52±0.14, Cho/Cr – 0.89±0.26, NAA/Cr – 1.73±0.31.

It turned out that between the gray and the white matter of the brain there are statistically significant differences.

As a result of our study, the values of the ratio indices of the main metabolites in glial tumors of various malignancy degrees were obtained.

In low-grade glioma's we measured the metabolite ratio Cho/NAA - 1.6±0.7, Cho/Cr - 2.3±1.2, NAA/Cr - 1.3±0.5

In high-grade glioma's we measured the metabolite ratio Cho/NAA - 2.06±0.76, Cho/Cr - 2.78±0.85, NAA/Cr - 1.33±0.31.

We found significant differences in low-grade and high-grade gliomas (p < 0.001), while high-grade gliomas (Grade IV) showed the highest Cho/NAA values.

Discussion & Conclusion

3D MRSI method has proved informative among patients with glial brain tumors of low and high malignancy grade. This is a method that allows us to get non-invasively information about metabolic changes in the brain tissue.

The 3D proton MR spectroscopy method has high sensitivity (76.5% (Cho / Cr), 82.4% (NAA / Cr)) and specificity (72.3% (Cho / Cr), 82.4% (NAA / Cr)) in the differential diagnosis of low and high malignancy grade tumors.

The thresholds for Cho / Cr and NAA / Cr were 3.01 and 1.2, respectively. AUC > 0.77 using metabolite ratios. There is a clear correlation between Cho / NAA, NAA / Cr and the degree of tumor malignancy: Cho / Cr and Cho / NAA ratios measured in the tumor significantly linearly correlate with the degree of malignancy of the tumor and are 0.680 and 0.734, respectively.

1-O4

DIFFUSION-WEIGHTED MR IMAGING CHARACTERISTICS OF H3 K27M HISTONE-MUTANT DIFFUSE MIDLINE GLIOMA IN TEENAGERS AND ADULTS

S. THUST¹, C. Micallef^{1,2}, S. Okuchi^{1,2}, S. Brandner³, A. Kumar³, K. Mankad⁴, S. Wastling^{1,2}, L. Mancini^{1,2}, R. Jager^{1,2}, A. Shankar⁵

¹ Neuroradiological Academic Unit, Department of Brain, Repair and Rehabilitation, UCL Institute of Neurology, London, UNITED KINGDOM, ² Lysholm Department of Neuroradiology, National Hospital for Neurology and Neurosurgery, London, UNITED KINGDOM, ³ Department of Neurodegenerative Disease, UCL Institute of Neurology and Division of Neuropathology, National Hospital, London, UNITED KINGDOM, ⁴ Department of Radiology, Great Ormond Street Hospital for Children, London, UNITED KINGDOM, ⁵ Teenage and Young Persons Cancer Unit, Department of Paediatric Oncology, University College London Hospitals, London, UNITED KINGDOM

Introduction

Histone H3 K27M-mutant diffuse midline gliomas are highly malignant brain tumours with a mean survival in the region of 9 months. They are diverse in morphology with no distinctive imaging feature reported to date. Reduced diffusivity is a well-known characteristic of cellular gliomas and an adverse poor prognostic predictor in diffuse pontine gliomas, described prior to discovery of molecular tumour subtypes. We present quantitative diffusion-weighted MR imaging data in a H3 K27M-mutant teenage and adult glioma cohort from a quaternary referral centre.

Methods

15 untreated H3 K27M-mutant gliomas (median patient age 19, range 14–64) were analysed. Morphological characteristics including tumour epicentre(s), T2/FLAIR and Gadolinium enhancement patterns, calcification, haemorrhage and cyst formation were documented. Apparent diffusion coefficient (ADC) values (ADC_{min}, ADC_{mean} and ratios to normal appearing white matter (NAWM)) were calculated for each tumour.

Result

Conventional and diffusion imaging features varied between individuals and within tumours. Solid tumour ADC_{min} values were commonly low with a mean of 84.22 mm²/s (48.38 to 110.87 mm²/s). For largest cross-section ADC_{mean} (excluding necrosis) a mean value of 112.09 mm²/s (85.81 to 147.84 mm²/s) was observed. ADC_{min}/NAWM ratio values demonstrated a mean of 1.097 (0.82 to 1.43), and ADC_{mean}/NAWM ratio values showed a mean of 1.47 (1.14 to 2.05).

Discussion & Conclusion

H3 K27M-mutant glioma exhibits variable signal characteristics. Low ADC values appear to be a common, non-invasively quantifiable feature of this tumour type, which could support its identification on imaging.

1-05

ACCURACY OF MULTIPLE SCLEROSIS BRAIN VOLUMES IN REAL WORLD MAGNETIC RESONANCE IMAGES

D.M. SIMA¹, M.I. Ferraz Meyer¹, A. Ribbens¹, W. Van Hecke¹, D. Smeets¹

¹ Icometrix, Leuven, BELGIUM

Introduction

Volumetric analysis of brain images is valuable for following-up multiple sclerosis (MS) patients. However, a large proportion of 2D magnetic resonance images (MRI) is discarded in research and clinical practice as being incompatible with newer and better volumetric acquisitions. We assess reliability of brain volumes obtained from low resolution MRIs with icobrain and we identify the main reasons for potential suboptimal segmentation.

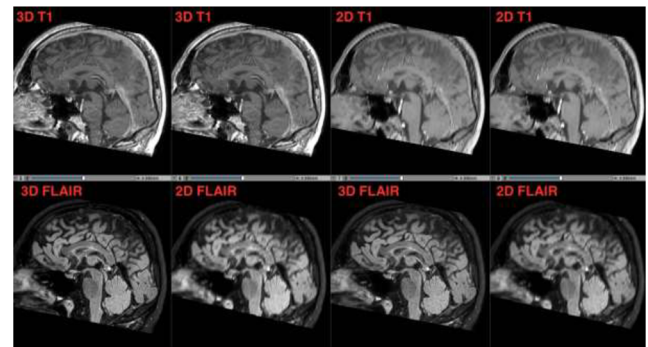
Methods

MRI acquisitions from 305 MS patients were processed with icobrain, a software that computes volumes of brain structures from T1w and FLAIR

images. For each patient, the acquisition session included 3DT1, 3DFLAIR, as well as 2DT1w and 2DFLAIR (slice thickness 0.5–8mm). All 3D and 2D T1/FLAIR combinations were used to obtain four icobrain results per patient. Brain volumes from the 3DT1/3DFLAIR combination were considered ground truth for the 2D results.

62 other MS patients participated in scan-rescan experiments, where 3DT1 and 3DFLAIR images were acquired with repetition. These images were used to determine the 3D test-retest error distribution for whole brain, gray matter, and lateral ventricles volumes.

We analysed the influence of slice thickness on brain volumes and computed the proportion of 2D results being as accurate as those obtained with 3D images. We also included other factors (image contrast, size of field-of-view, etc) in a correlation analysis to establish if they are responsible for volume variability.



Result

Ninety percent of absolute brain volume differences between test and retest based on 3D data were below 21ml for whole brain, 18ml for gray matter and 2ml for ventricles. When using at least one 2D image (T1 or FLAIR), the differences between obtained volumes and ground truth (from 3D images) were equally good in 97% 3DT1/2DFLAIR images, 36% 2DT1/3DFLAIR images, and 32% 2DT1/2DFLAIR images.

Correlations were observed between all brain volume errors and T1 image contrast (Spearman rho: -0.4–0.5, p<0.001) as well as T1 slice thickness (Spearman rho: 0.6–0.8, p<0.001).

Discussion & Conclusion

Brain volumetry based on 2D MR images can be considered very reliable in 32–97% of cases and should not be discarded, but 3D sequences are still recommended for volumetric brain analyses.

1-06

DIAGNOSTIC ACCURACY OF MRI ON FOLLOW-UP IMAGING OF PATIENTS WITH LEPTOMENINGEAL SEEDING FROM NON-SMALL CELL LUNG CANCER: COMPARISON OF CONTRAST-ENHANCED 3D T1 MPRAGE AND CONTRAST-ENHANCED 2D AXIAL T2 FLAIR

M. SEONG¹, S. Park², S.T. Kim¹, M.J. Ahn²

¹ Department of Radiology, Samsung Medical Center, Sungkyunkwan University School of Medicine, Seoul, SOUTH KOREA, ² Div. of

Hematology-Oncology, Department of Medicine, Samsung Medical Center, Sungkyunkwan University School of Medicine, Seoul, SOUTH KOREA

Introduction

Imaging stands on an important part in the diagnosis and treatment response evaluation of leptomeningeal metastasis (LM) along with cerebrospinal fluid (CSF) analysis and neurologic physical exam. Which MRI sequence is most accurate in diagnosis of LM is still controversial. In our institution, both CE 3D T1 MPRAGE and postcontrast 2D T2 fluid attenuated inversion recovery (FLAIR) image are routinely obtained for evaluation of tumorous condition of brain. We tested the diagnostic accuracy of each sequence to evaluate LM on initial and follow-up images in patients with non-small cell lung cancer (NSCLC).

Methods

35 patients with positive CSF cytology were enrolled and the initial and follow-up imaging (162 scans) were retrospectively reviewed by a neuroradiologist blind to the CSF cytology. The diagnostic accuracy of 3D CE T1WI and 2D CE FLAIR was evaluated using CSF cytology as a gold standard. The CSF cytology used was performed within one week before or after MRI scan.

The treatment response was evaluated on MRI at the time of negative or positive conversion of CSF cytology. Treatment response was evaluated as CR, PR, SD, PD, or NE (CR: complete remission; PR: partial remission, definite improvement on MRI; SD: stable disease, minimal change on MRI; PD: progressive disease, definite aggravation on MRI; NE: Not evaluable).

Result

Each patient had MRI scans from once to nine times. The sensitivity, specificity, positive predictive value, negative predictive value, and accuracy of CE 3D T1 and CE FLAIR alone or combined are described in Table 1.

There were 25 events of CSF negative conversion and 13 events of CSF positive conversion. The response evaluation on MRI at the time of CSF cytology conversion is described in Table 2.

Table 1. Diagnostic performance of CE 3D T1 MPRAGE and CE 2D FLAIR, alone or combined

(%)	Sensitivity	Specificity	Positive predictive value	Negative predictive value	Accuracy
3D T1 MPRAGE	55.9	60	75.6	38.0	57.1
2D FLAIR (including suspicious findings)	55.4	58	74.7	36.7	56.2
2D FLAIR (definite findings only)	42.0	70	75.8	35	50.6
3D T1 MPRAGE positive AND 2D FLAIR positive	38.7	82.4	82.7	38.2	52.5
3D T1 MPRAGE positive OR 2D FLAIR positive	73.0	35.3	71.1	37.5	61.1

Table 2. Response evaluation on MRI at the time of CSF cytology negative/positive conversion

(%)		CR	PR	SD	PD	NE
CSF negative conversion	2D FLAIR	40	32	8	0	20
	3D T1 MPRAGE	56	28	8	0	8
CSF positive conversion	2D FLAIR	62	8	8	0	23
	3D T1 MPRAGE	54	38	8	0	0

Discussion & Conclusion

CE T1 MPRAGE and CE FLAIR showed comparable diagnostic performance. When combine these two sequences, sensitivity, specificity, positive predictive value, and accuracy were better than when evaluated with either T1 MPRAGE or FLAIR sequence alone. The response evaluation depending on the MRI had little correlation with CSF negative/positive conversion.

We evaluated MRI of relatively homogeneous patient group composed of NSCLC and included their follow-up MRI scans, which distinguish our study from preceding studies.

1-O7

CORRELATION BETWEEN PRESURGICAL MOTOR TRACT DIFFUSION TENSOR IMAGING , FIBER TRACTOGRAPHY DATA AND INTRAOPERATIVE EVOKED POTENTIALS DURING BRAIN TUMOR SURGERY

J.J. Sánchez ¹, A. Pons ¹, J.L. Sanmillan ², C. Majós ¹, C. Aguilera ¹, A. Torres ², G. Plans ², M. Fernández ², M. Cos ¹, P. Puyalto ³, P. Naval ¹, A. Camins ¹, L. Aja ¹, P. Mora ¹

¹ Hospital de Bellvitge.Institut de Diagnòstic Per la Imatge, Barcelona, SPAIN, ² Hospital de Bellvitge. Neurosurgery Department, Barcelona, SPAIN, ³ Universitat Internacional de Catalunya, Barcelona, SPAIN

Introduction

Diffusion tensor imaging (DTI) and fiber tractography has been used to study the afferent and efferent tracts within the brainstem and brain parenchyma. Presurgical imaging identification of the motor tract combined with structural magnetic resonance images (MR) has proven useful in tumor delimitation during brain tumor surgery.

Methods

A prospective observational study was performed. 1.5 T MR were performed before and after surgery where pyramidal tract were localized. Central sulcus was identified intraoperately and confirmed by motor evoked potentials (MEP’s) by cortical high-frequency stimulation (250Hz). For continuous monitoring of cortical MEP’s, an electric intensity was used to yield a stable fixed waveform for each patient, with eight-point electromyogram (EMG). Data obtained from cortical MEP and the distance between the pyramidal tract and surgical site at pre and postoperative MRI were collected and minimum distance between the resection cavity-pyramidal tract and removal rate by comparing pre and postoperative MR images were measured and analyzed using regression and ANOVA correlation analysis. The p-value was considered as p <0.05.

Result

MR tractography was performed in 44 patients (16 women, 28 men) aged 28-78. The distance between the resection cavity and the motor tract in tractographic sequences postoperatively were 2.5 to 23.7 mm. The results were correlated with data obtained from cortical evoked potentials monitored during surgery. There was a significant linear correlation of 1.08 by

applying a regression test between distance and stimulus intensity ($R^2 = 0.8202$, $P < 0.001$).

Discussion & Conclusion

The identification by DTI of the corticospinal tract prior to brain tumor surgery allows the neurosurgeon an accurate planning of the maximum tumor removal with motor tract preservation. Fiber tractography based on DTI is a reliable and accurate method to evaluate the exact location of pyramidal tract. There is a correlation of the electrophysiological analysis and DTI in the study of the pyramidal tract and so we confirmed the usefulness of the tractography in brain tumor surgery, as favors the preservation of motor function in the procedure.

1-O8

MRI FINDINGS OF SYMPTOMATIC VS. ASYMPTOMATIC TRIGEMINAL NEUROVASCULAR CONTACT IN TRIGEMINAL NEURALGIA

*T. Sakinis*¹, G.A. Ringstad¹, J.O. Ringsby², P.K. Eide², H. Slettebø²

¹ Oslo University Hospital - Rikshospitalet, Department of Radiology, Oslo, NORWAY, ² Oslo University Hospital - Rikshospitalet, Department of Neurosurgery, Oslo, NORWAY

Introduction

Neurovascular contact (NVC) is considered the most frequent cause of trigeminal neuralgia (TN). In literature, the reported prevalence of NVC in normal population varies widely. Recent research has implicated that NVC is common within the population, but is more frequent and pronounced on the symptomatic side of patients suffering from TN. We aimed to assess whether MRI findings of NVC in symptomatic vs. asymptomatic trigeminal nerves are different.

Methods

We collected preoperative MRI studies from patients with TN who had been treated with microvascular decompression (MVD) surgery at our center since 2005. Only studies deemed to be of good quality with thin slices and heavily T2-weighted images were included. We obtained ethical committee approval and informed consent from 102 patients operated with MVD and 24 controls operated for hemifacial spasms, as they had performed similar imaging studies. Assessment of NVC on both sides was performed by a radiologist blinded to clinical data. Both venous and arterial NVCs were registered as well as presence of atrophy. NVC was categorized as severe when it resulted in nerve impression or -dislocation.

Each trigeminal nerve was grouped into one of two categories: "Symptomatic Nerves" (SN) and "Asymptomatic Nerves" (AN), respectively. SN group included 103 nerves (102 TN patients, of whom one had bilateral symptoms). AN group included 149 nerves (101 asymptomatic sides of TN patients and 24*2 nerves

from the control group). Difference between groups was measured using a Two Proportion Z-test.

Result

Any type of NVC was found in 94% (96/103) of SN and 77% (114/149) of AN ($p < 0.001$). Atrophy, or possible atrophy, was seen in 34% (35/103) of SN and 1% (1/149) of AN ($p < 0.001$). Severe NVCs were seen in 49% (50/103) of SN and 13% (19/149) of AN ($p < 0.001$). In all 126 patients, only four did not have NVC on either trigeminal nerve. Three of these were from the control group.

Discussion & Conclusion

NVC seen on MRI is more common in symptomatic than asymptomatic trigeminal nerves, but highly prevalent in both (94% and 77% respectively). Severe NVC, and particularly trigeminal nerve atrophy, are more common in symptomatic than asymptomatic trigeminal nerves.

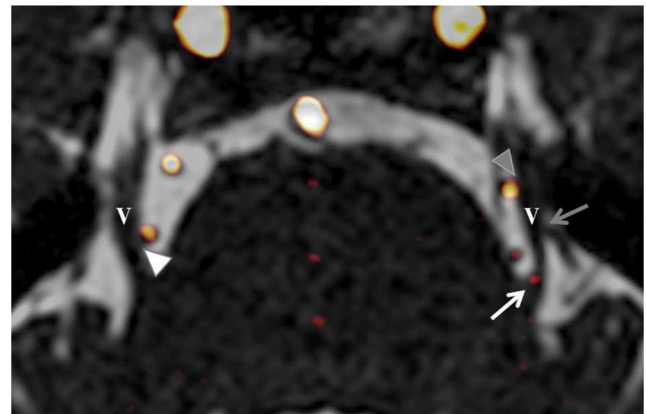


Figure 1. Patient with left-sided trigeminal neuralgia. Fusion of T2 CISS and time-of-flight. Both trigeminal nerves are annotated with "V". There is severe arterial NVC with dislocation (white arrow) and atrophy of the symptomatic left trigeminal nerve. Severe arterial NVC with impression is seen on the asymptomatic right nerve (white arrowhead). Non-severe arterial and venous NVCs are noted on the left side (grey arrowhead and -arrow, respectively).

1-O9

3D T1 BLACK-BLOOD MRI FOR THE DETECTION OF ACUTE OPTIC NEURITIS

*I. RIEDERER*¹, N. Sollmann¹, M. Mühlau^{2,3}, C. Zimmer¹, J.S. Kirschke¹

¹ Department of Neuroradiology, Klinikum rechts der Isar, Technical University of Munich, Munich, GERMANY, ² Department of Neurology, Klinikum rechts der Isar, Technical University of Munich, Munich, GERMANY, ³ TUM-NIC, TUM Neuroimaging Center, Klinikum rechts der Isar, Technical University of Munich, Munich, GERMANY

Introduction

Standard MRI for optic neuritis (ON) includes dedicated contrast-enhanced, fat-suppressed (ce, fs) T1-weighted (w) sequences. Recent 3D T1-w TSE black-blood (BB) sequences improved the detection rate of

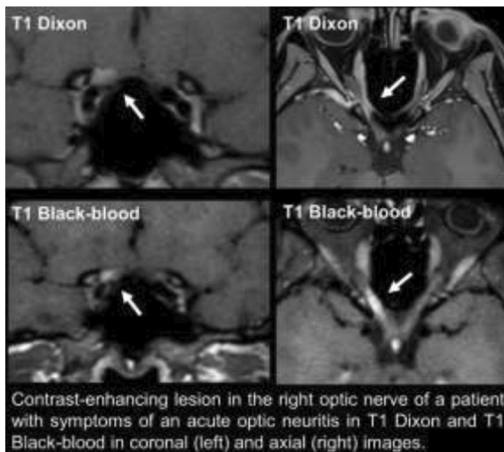
contrast-enhancing brain lesions compared to conventional T1-w MP-RAGE; however, this was not assessed for the optical nerve yet. We compared ce 3D T1 BB images with dedicated ce, fs T1-w images in patients with acute ON.

Methods

MRI data (3T) of 29 patients with symptoms of acute ON was analysed retrospectively, including whole brain 3D T1-w TSE BB, 3D T1-w MP-RAGE, and dedicated fs orbital sequences (3D T1-w Dixon or coronal orientated 2D T1-w TSE Dixon sequence). Contrast-to-noise ratios (CNR) were calculated in contrast-enhancing lesions. Furthermore, images were assessed by two readers regarding overall image quality, artifacts and diagnostic confidence with regard to ON on a 5-point-scale and with regard to the presence of contrast enhancement on a 3-point-scale.

Result

Final diagnosis of unilateral acute ON was set by the treating neurologists in 20 patients. 16 of these 20 patients showed contrast-enhancing lesions; in the 9 patients without ON none optic nerve showed contrast-enhancement. None of the contrast-enhancements in the standard T1 images was missed in T1-w TSE BB images, but six contrast-enhancing lesions were missed by one of the readers in MP-RAGE. CNR was significantly higher ($p < 0.05$) in T1 BB (13.0 ± 7.0) compared to MP-RAGE (8.2 ± 8.3) and T1 Dixon (8.3 ± 5.0). Overall image quality was rated higher in T1-w TSE BB (4.1 ± 0.6) and T1 Dixon (4.1 ± 0.7) compared to MP-RAGE (2.7 ± 0.5 , $p < 0.05$), also with higher diagnostic confidence in T1-w TSE BB (4.4 ± 0.7) and T1 Dixon (4.1 ± 0.7) compared to MP-RAGE (2.6 ± 0.7 , $p < 0.05$).



Discussion & Conclusion

Whole brain ce 3D T1-w TSE BB images showed similar high qualitative and quantitative characteristics as dedicated T1-w Dixon images and outperformed MP-RAGE images regarding ON. Thus, if ce 3D T1-w TSE BB images are acquired to better detect ce brain lesions in MS, additional dedicated orbital sequences may not be needed any longer.

1-O10

ANEURYSMAL VELOCITY REDUCTION ASSESSMENT AFTER FLOW DIVERSION USING 4D-PCMRI: A PROSPECTIVE STUDY ON 23 PATIENTS

*P. Raymond*¹, O. Brina^{1,3}, P. Bouillot², A.S. Luthman¹, C. Santarosa¹, M. Farhat⁴, K. Lovblad¹, P. Machi¹, B. Delattre³, V. Pereira^{1,5,6}, M.I. Vargas¹

¹ Division of Neuroradiology, Diagnostic Department, Geneva University Hospitals, Geneva, SWITZERLAND, ² Department of Quantum Matter Physics, University of Geneva, Geneva, SWITZERLAND, ³ Division of Radiology, Diagnostic Department, Geneva University Hospitals, Geneva, SWITZERLAND, ⁴ Laboratory for Hydraulic Machines, Ecole Polytechnique Fédérale de Lausanne, Lausanne, SWITZERLAND, ⁵ Division of Neuroradiology, Department of Medical Imaging, Toronto Western Hospital, University Health Network, Toronto, CANADA, ⁶ Division of Neurosurgery, Department of Surgery, Toronto Western Hospital, University Health Network, Toronto, CANADA

Introduction

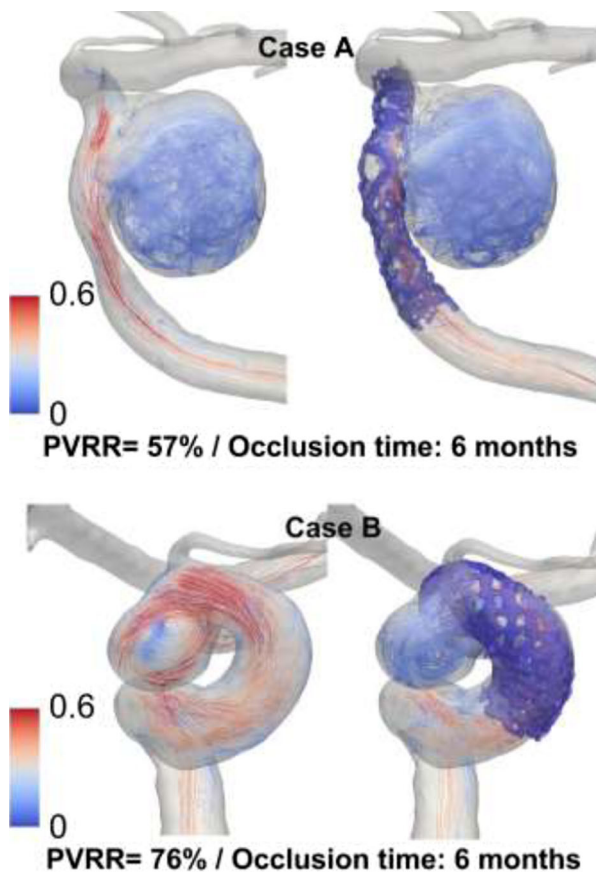
4D phase contrast MRI (4D PCMRI) is the only in-vivo method to measure and to visualize 3D velocity fields. Few studies applied this technique to intracranial flow measurements and even less for evaluating low porosity flow diverter stents (FDSs), broadly used for the endo-vascular treatment of wide neck intracranial aneurysms (IA). Amongst the various parameters influencing the IA thrombosis, the FDS induced flow reduction is assumed to have a leading role, even though its actual impact remains unclear. In the present study, we aimed to clarify this relationship by measuring quantitatively intra-aneurysmal flow changes using 4D PCMRI.

Methods

We acquired prospectively pre- and post-stent implantation 4D PCMRI data on a consecutive series of patients treated with FDS. We developed a post-processing pipeline to extract consistently the IA velocities from the parent vessel. We assessed IA flow changes with the proportional velocity reduction ratio (PVRR) taking into account the parent vessel flow rates for intra-patient normalization. Statistical differences were assessed between PVRR and occlusion times (6, 12 months and no thrombosis at 12 months).

Result

We were able to quantify and observed a velocity reduction with 4D-PCMRI after FDS on all of the 23 patients, The PVRR was gradually lower from 6 to 12 months thrombosis and no thrombosis groups, which is consistent with a diminished flow reduction for delayed occlusions ($p = 0.08$). No specific flow patterns were associated with occlusion times.



Discussion & Conclusion

4D-PCMRI is a non-invasive method to quantify velocities inside IA before and after FDS. A promising trend was found between the IA occlusion time and PVRR. The small differences between the three occlusion groups put in perspective the role of the flow reduction, one of the driving parameter among others, like neck endothelialisation, in the long-term occlusion as shown in recent studies. Moreover in-vivo and in-vitro studies are necessary for a comprehensive understanding of flow diversion treatment response.

1-O11

POTENTIAL OF DIFFUSION TENSOR IMAGING IN THE EVALUATION OF NEUROPSYCHOLOGICAL DISORDERS SECONDARY TO ANEURYSMAL RUPTURE OF THE ANTERIOR COMPLEX: PRELIMINARY INSIGHTS FROM THE ACOM PROTOCOL

*K. Premat*¹, *C. Azuar*², *E. Shotar*¹, *S. Lenck*¹, *N. Sourour*¹, *V. Degos*³, *D. Galanaud*¹, *D. Dormont*¹, *F. Clarencon*¹

¹ La Pitié-Salpêtrière Hospital - Neuroradiology, Paris, FRANCE, ² La Pitié-Salpêtrière Hospital - Neurology, Paris, FRANCE, ³ La Pitié-Salpêtrière Hospital - Neuro-intensive Care, Paris, FRANCE

Introduction

Evaluate the potential of Diffusion Tensor MRI (DTI) in assessing neuropsychological disorders 6 months after the rupture of anterior

communicating aneurysms, in a population with normal morphological MRI

Methods

The protocol is divided in 3 parts: 1) Constitution of the incident population (ACOM group) by excluding patients with abnormal imaging after independent assessment by 2 neuroradiologists. 2) Case-control study comparing DTI voxel-wise parameters between the ACOM group and a control population. Results were considered significant when $p < 1.10^{-4}$ 3) Correlational study between DTI parameters and neuropsychological tests.

Result

After independent reviewing, 12 patients (mean age: 53.2 years ± 10.4) were included in the ACOM group: 75% had at least one disabled cognitive domain and 55% had depression. They were compared to 24 control subjects (mean age: 37.0 years ± 11.1). Although no difference in volumetry were retrieved, significant differences in DTI parameters of global white matter were noted (FA: 0.915 $[\pm 0.05]$ vs 0.943 $[\pm 0.03]$, MD: 1.057 $[\pm 0.06]$ vs 1.013 $[\pm 0.03]$) and in frontal white matter tracts (SFOF, IFOF and ACR). Neuropsychological tests that were correlated to DTI parameters were BREF, Hayling's tests, WCST and TMT.

Discussion & Conclusion

Neuropsychological disorders are under-estimated in this population and appear secondary to diffuse axonal injuries that seem predominant in frontal areas, close to the site of rupture

1-O12

CLINICAL EVALUATION OF QUANTITATIVE ATROPHY REPORTS FOR MRI INTERPRETATION IN DEMENTIA: A MULTI-RATER, PROOF-OF-CONCEPT STUDY

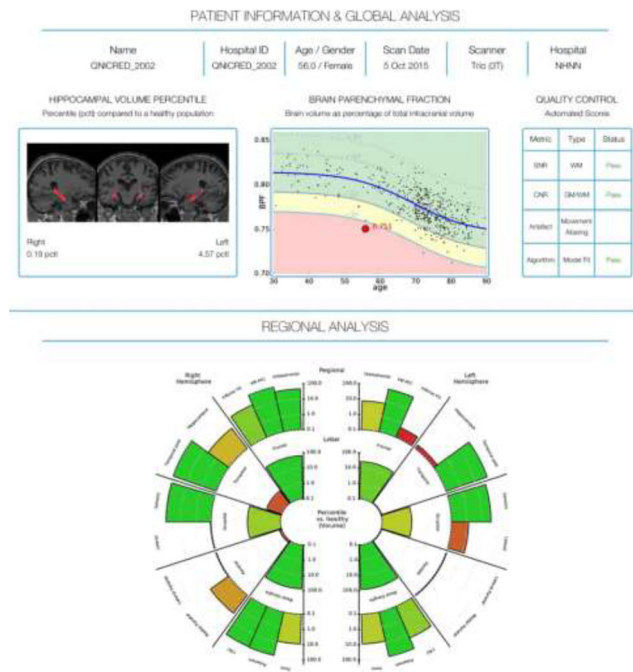
*H. Pemberton*¹, *O. Goodkin*¹, *F. Prados*^{1,2}, *R. Das*¹, *S. Vos*¹, *J. Moggridge*^{1,3}, *W. Coath*¹, *E. Gordon*¹, *A. Schmitt*^{1,3}, *R. Barrett*⁴, *H. Whiteley-Jones*⁴, *C. Burd*⁵, *M. Wattjes*⁶, *S. Haller*⁷, *M. Vernooij*⁸, *L. Harper*¹, *N. Fox*¹, *S. Bisdas*^{1,3}, *M. White*¹, *S. Ourselin*⁹, *T. Yousry*^{1,3}, *M. Cardoso*⁹, *F. Barkhof*^{1,3,10}

¹ University College London, London, UNITED KINGDOM, ² Universitat Oberta de Catalunya, Barcelona, SPAIN, ³ UCLH NHS foundation Trust, London, UNITED KINGDOM, ⁴ Brighton and Sussex University Hospitals, Brighton, UNITED KINGDOM, ⁵ Guys and St Thomas NHS Foundation Trust, London, UNITED KINGDOM, ⁶ Hannover Medical School, Hannover, GERMANY, ⁷ Uppsala University, Uppsala, SWEDEN, ⁸ Erasmus MC University Medical Center, Rotterdam, THE NETHERLANDS, ⁹ Kings College London, London, UNITED KINGDOM, ¹⁰ VU University Medical Center, Amsterdam, THE NETHERLANDS

Introduction

Neuroradiological assessment for dementia is currently subjective, relying on visual interpretation of structural MRI. Early dementia diagnosis is challenging, since atrophy patterns in disease and healthy ageing can be

similar. We examined whether providing a graphical representation of quantitative global and subcortical brain volumes improves diagnostic accuracy and confidence in dementia radiology reporting compared with visual assessment alone.



Methods

Our forced-choice proof-of-concept multi-rater study used MRI from participants whose disease status was determined by clinical examination and cerebrospinal fluid biomarkers (16 AD, 14 FTD, 15 controls; age range 52–81). We used geodesic information flows to automatically quantify volumetric data for each subject. Graphical reports were presented to raters with brain parenchymal fraction plotted against normative dementia-free population data ($n=461$, age range 30–90), and a ‘bullseye’ representation of grey matter volume percentiles split by brain lobe and relevant sub-regions. Nine raters with varying radiological experience (3 each of: consultants; registrars; ‘non-clinical image analysts’) assessed each case twice (with and without the report) in randomised order via a web-based platform. Raters were blinded to clinical and demographic information except age and gender. Scans were classified ‘normal’ or ‘abnormal’; if ‘abnormal’ subsequent choices were ‘AD’ or ‘FTD’. Both decisions were rated against a five-point confidence scale.

Result

The predominant effect of the report was improved diagnostic sensitivity for detecting abnormality ($p=0.015^*$, d effect size=1.03), with no change in specificity. We found no significant effect of the report on overall confidence levels ($p=0.11$, $d=0.59$) or diagnostic accuracy ($p=0.15$, $d=0.53$). However, consultants’ diagnostic accuracy increased when using the report ($p=0.02^*$, $d=4$). Overall, raters’ diagnostic agreement (Cohen’s Kappa) with the ‘gold standard’ was not significantly affected by the report, but the consultant group alone showed significantly increased agreement (0.41 - 0.55, $p=0.04^*$).

Discussion & Conclusion

Quantitative atrophy reports referencing single-subject results to normative data alongside routine visual assessment may improve diagnostic sensitivity within a routine clinical workflow. Sample sizes were low in this initial study, but effect sizes across measures were moderate-to-large in favour of a beneficial report effect. Further validation in larger samples is encouraged.

1-O13

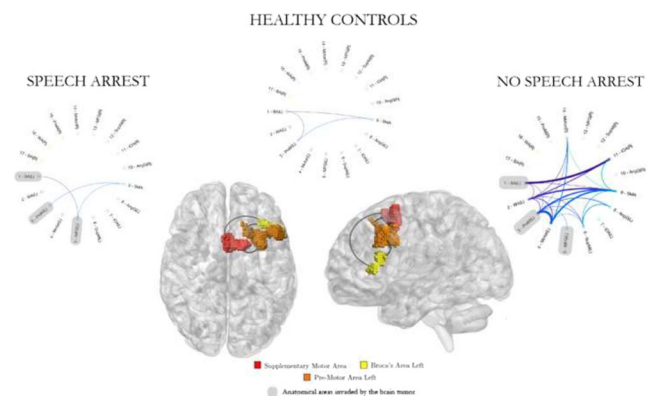
CORRELATES OF INTRA-OPERATIVE SPEECH ARREST ON FUNCTIONAL MAGNETIC RESONANCE IMAGING: TUMORAL INVASION AND LANGUAGE PLASTICITY

L. Pasquini¹, G. Del Ferraro⁴, M. Gene³, K. Peck³, M. Jenabi³, H. Makse⁴, A. Holodny³

¹ Sant'Andrea Hospital, La Sapienza University, Rome, ITALY, ² Bambino Gesù Children's Hospital, Rome, ITALY, ³ Memorial Sloan Kettering Cancer Center, New York, USA, ⁴ City College of New York, New York, USA

Introduction

Reorganization of language may represent an adaptive mechanism of the brain to pathologic processes, such as tumoral invasion. Direct cortical stimulation (DCS) of language during awake surgery is aimed to test the function of cortical areas included in the surgical field. In this perspective, lack of speech arrest during stimulation of the left inferior frontal gyrus (IFG) may point to compensatory reorganization, while speech arrest may indicate disruption of the language network. We aimed to evaluate functional modifications of language in patients showing speech arrest or no speech arrest during DCS of the IFG, compared to healthy subjects, by employing graph theory on fMRI data



Methods

We reconstructed the functional language network from task-based fMRI of 20 patients with brain tumor and 10 healthy age/handedness matched controls.

The following inclusion criteria were applied: right-handed, left-side tumor invading the IFG, awake surgery with language DCS, no chemo/radiotherapy. At DCS, 10 patients presented speech arrest and 10 did not.

From the fMRI time signal of active clusters, we constructed the pairwise correlation and connectivity matrix by means of statistical inference techniques (LASSO). We run multiple centrality measures to characterize network differences: high degree, eigenvector centrality, closeness centrality, betweenness centrality, k-core, page rank, collective influence

Result

The common functional network of healthy subjects displayed a triangular structure, involving Broca's area (BA), supplementary motor area (SMA) and pre-motor area (pre-MA), with the highest score in centrality measures. Patients with speech preservation at DCS showed similar functional architecture to healthy controls. Moreover, in patients with no speech arrest, BA was integrated into a larger circuit together with other left and right sided cortical areas

Discussion & Conclusion

This study sheds light on the modifications of language network due to tumor-induced plasticity by correlation with intraoperative direct cortical stimulation. The conservation of a triangular-shaped core formed by BA, SMA and pre-MA correlates with absence of speech arrest at DSC. Furthermore, patients with preserved speech show increased connection sparsity: BA is a node of a wider and denser network in patients with putative reorganization

1-O14

INTEGRITY OF THE CORTICO-STRIATAL PATHWAY IN FABRY DISEASE INVESTIGATED VIA DIFFUSION MRI CONNECTOMETRY ANALYSIS

*C. Paoletta*¹, M. Battocchio², G. Pontillo¹, S. Schiavi², C. Russo¹, A. Pisani³, A. Daducci², S. Coccozza¹, A. Brunetti¹

¹ Department of Advanced Biomedical Sciences, University Federico II, Naples, ITALY, ² Department of Computer Science, University of Verona, Verona, ITALY, ³ Department of Public Health, Nephrology Unit, University Federico II, Naples, ITALY

Introduction

Recent evidences have suggested the possible presence of an involvement of the extrapyramidal system in Fabry Disease (FD), a rare X-linked lysosomal storage disorders long considered to be characterized by major cerebrovascular events only. Aim of this study was to investigate the microstructural integrity of the cortico-striatal connections in FD patients.

Methods

Forty-seven FD patients (M/F=19/28, mean age 42.3±13.1 years) and 49 healthy controls (HC) (M/F=21/28, mean age 42.3±16.3 years) were enrolled. All subjects underwent an MRI scan on a 3T machine, acquiring a Diffusion Tensor Images (DTI) sequence (voxel size 2.2×2.2×2.2mm³, 64 directions with b-value=1000s/mm² and nine b=0s/mm²). Fractional Anisotropy (FA), axial (AD), radial (RD) and mean diffusivity (MD) maps were computed for each subject using MRtrix. Anatomically-Constrained Tractography (ACT) with iFOD2 algorithm was performed to obtain 1 million streamlines. Connectomes were built using the

standard FreeSurfer Desikan-Killiany atlas and for each subject, DTI metrics and connectomes were combined to carry on diffusion MRI connectometry [10]. Finally, values corresponding to bundles connecting the precentral gyrus (PreCG) with the striatum were extracted.

Result

We found the presence of a microstructural involvement of cortico-striatal tracts in FD patients, predominantly affecting the left side. In particular, we found a significant reduction of mean FA values of the left cortico-striatal fibers (0.43±0.02 vs 0.41±0.02 for HC and FD, respectively, p=0.001), coupled to an increase in MD (0.67·10⁻³±0.02·10⁻³mm²/s vs 0.68·10⁻³±0.03·10⁻³mm²/s, p=0.001) and RD (0.50·10⁻³±0.02·10⁻³mm²/s vs 0.52·10⁻³±0.03·10⁻³mm²/s, p<0.001) values, while no differences emerged when AD maps were evaluated (1.00·10⁻³±0.03·10⁻³mm²/s vs 1.01·10⁻³±0.03·10⁻³mm²/s, p=0.11).

Discussion & Conclusion

We confirmed the presence of an alteration of the extrapyramidal system in FD patients, in line with the recent evidences suggesting the presence of brain changes as a possible reflection of the subtle motor symptoms present in this condition. In particular, our results show that along with functional changes, a microstructural damage of this pathway, predominantly affecting the left cortico-striatal connections, is present in FD patients.

1-O15

BRAIN CHANGES INDUCED BY ELECTROCONVULSIVE THERAPY

L. Oltedal^{1,6}, M. Argyelan², K.L. Narr³, C. Abbott⁴, H. Bartsch^{7,5}, U. Kessler¹, K.J. Oedegaard¹, A.M. Dale^{7,8}, F. GEMRIC⁹, O.T. Ousdal⁶

¹ Department of Clinical Medicine, University of Bergen, Bergen, NORWAY, ² Center for Psychiatric Neuroscience at the Feinstein Institute for Medical Research, New York, USA, ³ Departments of Neurology, Psychiatry, and Biobehavioral Sciences, University of California Los Angeles, Los Angeles, USA, ⁴ Department of Psychiatry, University of New Mexico School of Medicine, Albuquerque, New Mexico, USA, ⁵ Mohn Medical Imaging and Visualization Centre, Department of Radiology, Haukeland University Hospital, Bergen, NORWAY, ⁶ Department of Radiology, Haukeland University Hospital, Bergen, NORWAY, ⁷ Center for Multimodal Imaging and Genetics, University of California, San Diego, La Jolla, USA, ⁸ Department of Radiology, University of California, San Diego, La Jolla, USA, ⁹ The Global ECT-MRI Research Collaboration, Bergen, NORWAY

Introduction

Major depressive disorders (uni/bi-polar) are common and serious medical disorders that may lead to profound suffering for affected individuals and families. According to the World Health Organization (7. April 2017), more than 300 million people are living with depression worldwide, and the disorder is regarded as a primary cause of disability.

Electroconvulsive therapy (ECT) has remained the most effective acute treatment for otherwise treatment resistant major depressive episodes over the past 80 years. However, the mechanisms of action remain elusive. Patients receive ECT under general anesthesia 2-3 times per week for 2-4 weeks. Electric currents are delivered through scalp electrodes, intentionally triggering a brief seizure. While ECT is known to be associated with volumetric enlargements of cortico-limbic brain regions, the pattern of whole-brain structural alterations following ECT remains unresolved. Here, we examined the longitudinal effects of ECT on global and local variations in gray matter, white matter and ventricle volumes in major depression as well as predictors of ECT-related clinical response.

Methods

Longitudinal MRI and clinical data from the Global ECT-MRI Research Collaboration (GEMRIC) were used to investigate changes in white matter, gray matter and ventricle volumes before and after ECT in 328 patients experiencing a major depressive episode. In addition, 95 non-depressed control subjects were scanned twice. We performed a mega-analysis of single subject data from 14 independent GEMRIC sites.

Result

Volumetric increases occurred in 79 of 84 gray matter regions of interests. In total, the cortical volume increased by (mean \pm SD) 1.04 ± 1.03 % (Cohen's $d=1.01$, $p<0.001$) and the subcortical gray matter volume increased by 1.47 ± 1.05 % ($d=1.40$, $p<0.001$) in patients. The subcortical gray matter increase was negatively associated with total ventricle volume (Spearman's rank correlation $\rho=-0.44$, $p<0.001$), while total white matter volume remained unchanged ($d=-0.05$, $p=0.41$). The changes were modulated by number of ECTs and mode of electrode placements. However, the gray matter volumetric enlargements were not associated with clinical outcome.

Discussion & Conclusion

The findings suggest that ECT induces gray matter volumetric increases that are broadly distributed. However, gross volumetric increases of specific anatomically defined regions may not serve as feasible biomarkers of clinical response.

1-O16

ENDOGENOUS CHEMICAL EXCHANGE SATURATION TRANSFER (CEST) MR IMAGING FOR THE DIAGNOSIS AND THERAPY RESPONSE ASSESSMENT OF BRAIN TUMORS: A SYSTEMATIC REVIEW

S. Okuchi¹, A. Hammam¹, X. Golay¹, M. Kim¹, S. Thust¹

¹ University College London, Institute of Neurology, London, UNITED KINGDOM

Introduction

To generate a narrative synthesis of published data on the use of endogenous chemical exchange saturation transfer (CEST) MR imaging in brain tumors.

Methods

A systematic database search (PubMed, Ovid Embase, Cochrane Library) was used to collate eligible studies. Two researchers independently screened publications according to predefined exclusion and inclusion criteria. All included studies underwent a bias risk assessment using the Quality Assessment of Diagnostic Accuracy Studies (QUADAS-2) instrument, with each assessor independently evaluating concerns regarding applicability in 3 domains and bias risk in 4 domains. Disagreements were resolved in consensus with a third researcher.

Result

The electronic database search identified 430 studies, of which 36 studies (totaling 596 gliomas) fulfilled the inclusion criteria. The final selection of studies was categorized into 5 groups as follows: grading gliomas, 19 studies (areas under the curve (AUC) 0.500-1.000); predicting molecular subtypes of gliomas, 5 studies (AUC 0.610-0.920); distinction of different brain tumor types, 7 studies (AUC 0.707-0.905); therapy response assessment, 3 studies (AUC not given) and differentiating recurrence from treatment-related changes, 5 studies (AUC 0.880-0.980). A substantial bias risk was observed for several studies regarding the selection of patients (17/36), and concerning the conduct or interpretation of the index test (6/36). No relation was apparent between the severity of bias risk and the study results accuracy. The current published data predominantly consist of observational and comparative single center studies.

Discussion & Conclusion

CEST imaging potentially offers valuable, unique information in brain tumors to address typical clinical questions in neuro-oncology. Further research is required to assess its role in support of molecular genetic diagnosis and to investigate use in the post treatment phase.

1-O17

MRI ASSESSED RESPONSES IN TUMOR AND WHOLE BRAIN TO SRS ALONE OR COMBINED WITH IMMUNOTHERAPY IN PATIENTS WITH BRAIN METASTASES

L.B. Nilsen¹, E. Grøvig¹, I. Digernes¹, C. Saxhaug², A. Latysheva², O. Geier¹, T. Hellebust³, D. Sætre⁴, B. Breivik⁵, K. Jacobsen⁶, Å. Helland⁶, K. Emblem¹

¹ Oslo University Hospital (OUH) - Dept. of Diagnostic Physics, Oslo, NORWAY, ² OUH - Dept. of Radiology and Nuclear Medicine, Oslo, NORWAY, ³ OUH - Dept. of Medical Physics, Oslo, NORWAY, ⁴ Østfold Hospital Trust - Dept. of Radiology, Kalnes, NORWAY, ⁵ Hospital of Southern Norway - Dept. of Radiology, Kristiansand, NORWAY, ⁶ OUH - Dept. of Oncology, Oslo, NORWAY

Introduction

Pre-clinical studies suggest that combined use of stereotactic radiosurgery (SRS) and immunotherapy can provide a synergistic response, leading to improved local control and potential abscopal effects. The aim of this study was to compare MRI assessed responses in patients treated with

SRS alone to SRS combined with immunotherapy in tumor and normal brain of patients with brain metastases.

Methods

We analyzed 40 patients with brain metastases from NSCLC (N=26) or malignant melanoma (N=14), treated with SRS (15–27Gy). Six of the patients (5 mal.mel., 1 NSCLC) also received immunotherapy every third week (pembrolizumab (2mg/kg) and/or ipilimumab (3mg/kg)). MRIs were performed pre-SRS and then every third month for one year. Tumor and associated edema were delineated by experienced neuroradiologists. Cerebral blood volume from micro- and macro-vasculature, vessel calibers, and mean vessel density were obtained from spin- and gradient-echo DSC-MRI. All metrics were normalized to white-matter receiving <2Gy. Normal brain tissue was segmented from T1w-pre-contrast images (Matlab; SPM12). MRI responses were assessed in: Tumor, edema, and normal brain tissue receiving >1-2Gy, >2-10Gy, >10-15Gy, and >15Gy (peri-tumoral region) (Fig.1A).

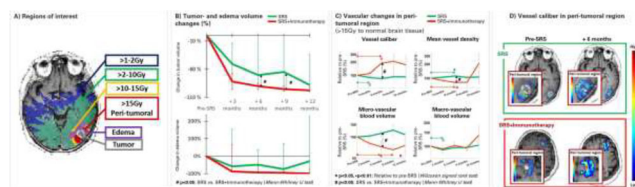


Fig. 1 Comparison of tumor and peri-tumoral MRI assessed responses in patients treated with SRS alone or SRS combined with immunotherapy. **A** ROIs responses were assessed in 4 regions of interests: normal brain receiving >1-2Gy, >2-10Gy, >10-15Gy, and >15Gy (defined peri-tumoral region), edema, and tumor. **B** Median reduction in tumor volume (top) and edema volume (bottom) with interquartile range. **C** Log transformed mean ± SEM of vascular metrics in the peri-tumoral region. Significant differences at 6 months post-SRS between the two treatment groups in vessel caliber (top right), mean vessel density (left right), and micro-vascular blood volume (bottom left). No difference in macro-vascular blood volume was observed (bottom right). The relative decrease in micro-vascular blood volume and vessel density, together with increase in vessel calibers in patients treated with additional immunotherapy, suggest that immunotherapy targets small and remains blood vessels in high dose regions. **D** Peri-tumoral vessel caliber pre- and 6 months post-SRS (superimposed T1w and contrast images) in a patient treated with SRS alone (red) and in a patient treated with combined SRS and immunotherapy (green)

Result

There was no difference in tumor- or edema volumes, pre- or post-SRS, between the two treatment groups. However, patients treated with additional immunotherapy showed greater tumor volume reduction than those treated with SRS alone at 6 months (90% vs. 70%, $p < 0.05$) and 9 months (95% vs. 65%, $p < 0.05$) post-SRS (Fig.1B). Pre-SRS, the vascular status in the whole brain was similar between the two treatment groups. Six months post-SRS, the vasculature of the peri-tumoral region was significantly different in patients treated with additional immunotherapy compared to SRS alone ($p < 0.05$) (Fig.1C-D): Increase (89%) vs. decrease (16%) in vessel caliber, decrease (19%) vs. increase (12%) in mean vessel density, and decrease (27%) vs. increase (12%) in micro-vascular blood volume. No differences were observed in tumor, edema or normal brain receiving <15Gy.

Discussion & Conclusion

Our preliminary results indicate that the addition of immunotherapy to SRS contributes to enhanced treatment response, including increased tumor volume reduction and micro-vascular changes in normal brain tissue receiving high SRS doses.

1-O18

CLINICAL MR IMAGING FOR WHO GRADE II/III GLIOMA MOLECULAR SUBTYPING: DIFFUSION, AGE AND MORPHOLOGY EVALUATION SYSTEM

J. Maynard¹, S. Okuchi¹, S. Wastling^{1,2}, O. Almosawi³, A. AL Busaidi², W. Mbatha², L. Mancini^{1,2}, S. Brandner⁴, Z. Jaunmuktane⁴, M. Koc², R. Jäger^{1,2,5}, S. Thust^{1,2,5}

¹ Neuroradiological Academic Unit, Department of Brain, Repair and Rehabilitation, UCL Institute of Neurology, London, UNITED KINGDOM, ² Lysholm Department of Neuroradiology, National Hospital for Neurology and Neurosurgery, London, UNITED KINGDOM, ³ Department of Statistics, UCL Great Ormond Street Institute of Child Health, London, UNITED KINGDOM, ⁴ Department of Neurodegenerative Disease, UCL Institute of Neurology and Division of Neuropathology, London, UNITED KINGDOM, ⁵ Imaging Department, University College London Foundation Hospital, London, UNITED KINGDOM

Introduction

Diffuse astrocytoma, isocitrate dehydrogenase wild-type (IDHwt) is a recently defined entity, which shares genetic features with primary glioblastoma (GBM). IDHwt gliomas progress rapidly, but are indistinguishable from lower grade IDH-mutant (IDHmut) astrocytomas and oligodendrogliomas with respect to proliferative indices and cell morphology. Early prediction of glioma IDH status has important clinical implications, but in practice this remains unsolved by standard MR imaging. We propose an algorithm for glioma molecular typing based on conventional MRI sequences and demographics alone.

Methods

Institutional review board approval was secured. 290 World Health Organization (WHO) grade II/III gliomas (80 IDHwt, 210 IDHmut), were subjected to apparent diffusion coefficient (ADC) region of interest measurements ($n=2900$) by three independent observers, blinded to tissue results. A visual assessment of glioma morphology was performed at a separate time point according to pre-specified morphological categories. Feature categories with good to excellent concordance ($\kappa > 0.6$) for three observers were tested in univariate analysis for IDH prediction. Predictive features ($p < 0.05$) were subsequently entered into a multivariate logistic regression model. The prediction system was then tested in an independent validation cohort.

Result

Amongst 4 ADC metrics; the best accuracy with good reproducibility (intraclass correlation coefficient (ICC) 0.85-0.92) was observed for the ratio of ADC in largest tumour cross-section: normal appearing white matter. The correlation between ADC values and IDH subtype was strong for non-Gadolinium enhancing and solidly enhancing tumours, but weak for rim enhancing tumours when measured in solid tumour components. A significant association was identified between age and IDH status ($p < 0.01$). Glioma location, enhancement characteristics, calcification and cyst formation were multivariate predictors ($p < 0.05$) of IDH subtype. Excellent accuracy was achieved using two slightly different prediction models incorporating diffusion, patient age, and morphology with 89% and 90.5% tumours correctly classed (AUC 0.93-0.96). The formula was subsequently applied to an unseen cohort ($n=49$) of WHO grade II/III

gliomas by a radiologist in training, achieving 84% accuracy for IDH typing.

Discussion & Conclusion

An evaluation system for IDH status prediction using a combination of ADC mean ratio measurements, age and reproducible tumour features may support clinical practice. Validation and model calibration in a multi-institutional setting will be considered.

1-O19

AGE- AND GENDER EFFECTS ON BRAINSTEM MR-PLANIMETRY

*S. Mangesius*¹, A. Hussl², C. Müller², F. Krismer², P. Mahlknecht², M. Schocke^{1,3}, E.R. Gizewski^{1,3}, W. Poewe^{2,3}, K. Seppi^{2,3}

¹ Department of Neuroradiology, Innsbruck Medical University, Innsbruck, AUSTRIA, ² Department of Neurology, Innsbruck Medical University, Innsbruck, AUSTRIA, ³ Neuroimaging Core Facility, Innsbruck Medical University, Innsbruck, AUSTRIA

Introduction

MR planimetry of brainstem structures can be helpful for the discrimination of parkinsonian syndromes. The aim of this study was to evaluate age- and gender effects on brainstem MR-planimetric measures.

Methods

MR-planimetric measures including brainstem diameters (midbrain, pons, middle and superior cerebellar peduncle) and areas (pontine and midbrain), the ratios derived from both midbrain-to-pons diameters and areas as well as the Magnetic Resonance Parkinson Index (MRPI) were assessed on 1.5 Tesla weighted MR images in a large cohort of 97 healthy controls (mean age 62.8 years; SD 10.9 years; female-to-male-ratio = 49:48). Planimetric measures were performed on an imaging database program (IMPAX EE). Gender- and age-related differences of all as well as of combined planimetric measurements were calculated using univariate and multivariate GLMs, and repeated for the population relevant for the differential diagnosis of parkinsonism, aged 50 to 80 years.

Result

Univariate and multivariate analyses showed significant effects of gender on both pontine measurements ($p < 0.05$ for all) with male subjects showing larger measurements, and significant effects of age on midbrain measurements ($p < 0.001$ for all) as well as on combined measurements and ratios derived from midbrain-to-pontine measurements ($p < 0.01$ for all). Intriguingly, there were neither gender nor age effects on combined measurements nor midbrain diameter in the population aged 50 to 80 years.

Discussion & Conclusion

Although age and gender might influence single brainstem MR-planimetric measures, our results indicate that there is no need for age- or gender-specific cut-offs for the age group relevant for the differential diagnosis of neurodegenerative parkinsonism.

1-O20

MRI-COMPATIBLE PNEUMATIC STIMULATOR FOR SENSORIMOTOR MAPPING IN PATIENTS WITH BRAIN TUMOURS

*V. Lolli*¹, A. Rovai², N. Trotta², S. Goldman², N. Sadeghi¹, F. Lefranc³, V. Jousmäki⁴, X. De Tiege²

¹ Department of Radiology, CUB Hôpital Erasme, Brussels, BELGIUM, ² Department of Nuclear Medicine, CUB Hôpital Erasme, Brussels, BELGIUM, ³ Department of Neurosurgery, Brussels, BELGIUM, ⁴ Department of Neuroscience and Biomedical Engineering, School of Science, Aalto University, Espoo, FINLAND

Introduction

This study aims at validating a magnetic resonance imaging (MRI)-compatible stimulator based on a pneumatic artificial muscle (PAM) eliciting computer-controlled timely and repetitive passive movements of fingers/toes for pre-operative functional MRI (fMRI) mapping of the primary sensorimotor (SM1) cortex in fourteen patients with brain tumours centered on or adjacent to the central sulcus. The robustness of the device to accurately map the SM1 cortex was previously validated in a series of fifteen healthy subjects.

Methods

Patients performed comparable active and passive PAM-induced flexion-extensions of the contralesional index finger while undergoing classical block-design fMRI alternating blocks of movement with rest periods. Conventional fMRI data analysis was performed in SPM12. The fMRI datasets of patients with right hemispheric lesions were flipped along the x-axis in order to obtain a cohort of patients with uniquely left-sided tumours.

Result

PAM-induced movements of the index finger resulted in a significant increase in blood-oxygen-level-dependent (BOLD) signal in the contralesional SM1 cortex in all patients ($p < 0.01$ Family Wise Error [FWE] corrected in 12/14 and < 0.001 uncorrected [unc.] in 2/14 subjects). Similar networks were recruited by active and passive index finger movements. At the group level, we observed no significant difference in mean contrast magnitude when comparing active with PAM-induced passive movement of the contralesional index finger and viceversa.

Discussion & Conclusion

Whereas PAM-based movement of the index finger produced weaker group-level increase in BOLD signal within the sensorimotor network than analogous active index finger movements in healthy subjects, the PAM-induced BOLD signal increase observed in brain tumour patients is comparable to that of active movement. The present results suggest that PAM-based motor fMRI is as reliable as active motor fMRI for pre-operative mapping of the SM1 cortex in brain tumour patients. The use of our PAM-based stimulator may therefore be preferred over active or passive experimenter-controlled fMRI in patients presenting with motor

deficits that could hinder their performance in executing the required motor task.

1-O21

MAGNETIC RESONANCE DIFFUSION-TENSOR IMAGING METRICS IN HIGH GRADE GLIOMAS: CORRELATION WITH IDH1 GENE STATUS IN WHO 2016 ERA

*R. Augelli*¹, A. Agnello¹, A. Bucci¹, N. Mandruzzato¹, G. Zoccatelli¹, A. Nicolato², G. Talenti¹, A. Gasparini¹, F.B. Pizzini¹, A. Beltramello³, G. Pinna², G.K. Ricciardi¹, E. Ciceri¹

¹ Neuroradiology Department, University Hospital of Verona, ITALY, ² Neurosurgery Department, University Hospital of Verona, ITALY, ³ Department of Radiology, IRCCS Sacro Cuore Don Calabria Hospital, NEGRAR (VR), ITALY

Introduction

To evaluate any possible correlation between the presence of Isocitrate DeHydrogenase 1 mutation (IDH1m) and specific DTI (Diffusion Tensor Imaging) metrics, such as Fractional Anisotropy (FA), Mean Diffusivity (MD), Radial Diffusivity (RD) and Axial Diffusivity (AD) in high grade cerebral lesions according with the recent WHO 2016 classification.

Methods

We retrospectively analyzed 47 patients who underwent an advanced-MR study with DTI followed by surgical intervention with a subsequent histological diagnosis of High-Grade Glioma (HGG) and immunohistochemical evaluation of IDH1 (Isocitrate DeHydrogenase) mutation status. For each DTI metrics we measured the ratio between tumor and normal tissue and we evaluated the correlation with IDH1 mutation.

Result

According to 2016 WHO classification, our series included grade III glioma in 18 patients (13 M; 5 F) and grade IV glioma in 29. IDH1 was mutated in 10 patients (IDHm group) and non-mutated in 37 patients (IDHwt group). We observed a positive correlation between IDH1 status and RD (P-value < 0.0001 for minRDratio and meanRDratio and < 0.0011 for maxRDratio. Cut-off of 3.151, 2.389 and 2.023, respectively; Area-Under-Curve (AUC) 0.895 for minRDratio, 0.878 for meanRDratio and 0.824 for maxRDratio) and between IDH1 status and MD (P-value 0.005 for minMDratio, 0.018 for meanMDratio and 0.089 for maxMDratio. Cut-off of 1.639, 1.641 and 1.49, respectively; AUC of 0.895 for minMDratio, 0.743 for meanMDratio and 0.678 for maxMDratio). No correlation was demonstrated between IDH1 status and FA and AD.

Discussion & Conclusion

Our results support the hypothesis that the number of residual axonal fibers, extracellular matrix composition and the presence of colliquative tissue, may together contribute to a global RD increase in HGG, with a relatively higher increase in IDH1m tumors. Our data are in favour of a multimodal advance evaluation of HGG. DTI metrics in our opinion help

to analyze IDH1 mutation status, in order to better characterize the lesions tailoring the treatment and the follow up in selected cases.

1-O22

PREDICTOR OF PROGNOSIS IN PATIENTS WITH NEWLY DIAGNOSED GLIOBLASTOMA USING PRE-TREATMENT INTRA- AND PERITUMORAL RESTRICTION SPECTRUM IMAGING

*A. Latysheva*¹, A. Server¹, O.M. Geier², T. Hope²

¹ Oslo University Hospital - Rikshospitalet - Department of radiology, Oslo, NORWAY, ² Oslo University Hospital - Rikshospitalet - Department of Diagnostic Physics, Oslo, NORWAY

Introduction

Apparent diffusion coefficient (ADC) previously demonstrated ability to improve detection of regions with high cellularity, but is also a prognostic marker in patients with glioblastoma. However, edema associated with intra- and peritumoral inflammation, infiltration and necrosis increases extracellular diffusion and affects ADC value in opposite way. We assessed the potential prognostic value of CI (cellularity index) derived from Restriction Spectrum Imaging (RSI), diffusion-weighted MRI technique with multi-b-value multi-diffusion time acquisitions, which have primary goal to maximize sensitivity to intraaxonal/intracellular restricted diffusion.

Methods

CI and ADC maps were analyzed for twelve patients with untreated glioblastoma, IDH-wildtype. The volume of interest (VOI) was obtained semi-automatically from the contrast-enhancing portion of tumor (VOI-CE) and from the peritumoral brain zone that extends 5 mm outside the enhancing tumor (VOI-PT) in all representative slides. Whole-tumor normalized histogram parameters were calculated for each VOI. The ability of CI and ADC to stratify progression-free survival (PFS) and overall survival (OS) were analyzed by Kaplan-Meier and Cox survival analysis adjusted for known survival predictors (MGMT methylation status, age, Karnofsky performance status and extent of surgical resection).

Result

Higher 95th percentiles CI both in VOI-CE and VOI-PT was associated with significantly longer PFS median (236 versus 171 days, HR=4.2, P=0.03, logrank test) and trended with longer overall survival (394 versus 236 days, HR=2.2, P=0.52, logrank test). Poorer OS was also associated with lower 5th percentiles ADC in VOI-PT (HR=3.2, P=0.02, logrank test).

Discussion & Conclusion

Pretreatment RSI may be used as a biomarker for stratification PFS and OS in patients with primary glioblastoma. The association between RSI metrics and clinical outcome requires further analysis in studies with larger samples.

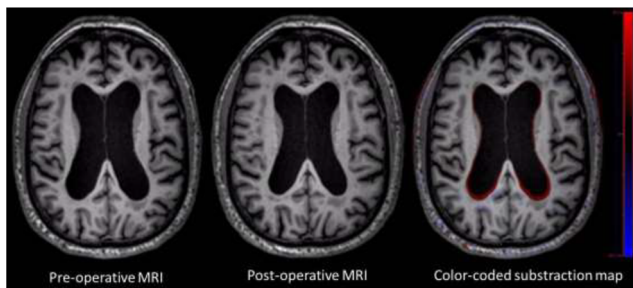
1-O23**ADDED VALUE OF AN AUTOMATIC REGISTRATION AND SUBTRACTION TOOL FOR MONITORING PATIENTS WITH NORMAL-PRESSURE HYDROCEPHALUS**

G. Kuchcinski¹, C. Jacquiez¹, R. Dagniaux¹, M. Baroncini², G. Ramette¹, J. Pruvo¹, X. Leclerc¹, J. Hodel³

¹ CHU Lille, Department of Neuroradiology, Lille, FRANCE, ² CHU Lille, Department of Neurosurgery, Lille, FRANCE, ³ CHU Mondor, Department of Neuroradiology, Créteil, FRANCE

Introduction

The aim of our study was to evaluate the added value of an automatic tool for the registration and subtraction of MRI images in the follow-up of patients with normal-pressure hydrocephalus treated with surgery

**Methods**

Forty-five patients with clinical and radiological criteria for normal-pressure hydrocephalus according to international guidelines, who underwent surgical treatment and 3T MRI follow-up, were prospectively included.

The ventricular size was compared on pre- and post-operative 3DT1 images by a senior and a junior neuroradiologist, independently and blinded from clinical data, according to a standard method (visual analysis, measurement of the callosal angle and Evans' index). The final interpretation was scored on a 5-point semi-quantitative scale ranging from -2 = significant decrease to +2 = significant increase. Confidence in the interpretation was self-assessed by a semi-quantitative scale ranging from 0 to 5.

After a month, the 3DT1 sequences were again compared, independently, using an automatic tool for image registration and subtraction.

The gold standard was the measure of the ventricular volume obtained by manual segmentation, conducted by third neuroradiologist.

Result

Compared to the standard method, the use of an automatic tool for 3D registration and subtraction significantly:

(a) improved the sensitivity of the interpretation for the junior: sensitivity = 29/33 = 80.6% [95% CI: 63.4 - 91.2] vs 20/33 = 55.6% [95% CI: 38.3 - 71.7] (p < 0.05) (no difference for the senior: 32/36 = 88.9% vs 30/36 = 83.3%)

(b) increased diagnostic confidence: junior = 4.7 vs 3.0 / senior 4.6 vs 3.2 (p < 0.001)

(c) improved the inter-observer agreement: weighted kappa = 0.613 [95% CI = 0.405 - 0.821] vs weighted kappa = 0.216 [95% CI = 0.014 - 0.418]

(d) reduced interpretation time: junior = 1.3 min vs 5.6 min / senior = 2.1 vs 4.4 min (p < 0.001)

Discussion & Conclusion

In the follow-up of patients with hydrocephalus, the use of an automatic tool for image registration and subtraction reduces the interpretation time while improving the diagnostic confidence, the inter-rater reproducibility and the sensitivity, especially for junior radiologists.

1-O24**TMS-EEG AND RESTING-STATE FMRI ACCURACY COMPARISON IN DIFFERENTIATION OF CHRONIC DISORDERS OF CONSCIOUSNESS**

D. Sinityn¹, E. Kremneva¹, L. Legostaeva¹, E. Yazeva¹, D. Sergeev¹, A. Poidasheva¹, A. Sergeeva¹, N. Suponeva¹, Y. Ryabinkina¹, M. Piradov¹

¹ Research center of neurology, Moscow, RUSSIA

Introduction

Diagnostic accuracy of different chronic disorders of consciousness (DOC) can be affected by the false negative errors in up to 40% cases. We aimed to investigate the accuracy of patient differentiation between VS (vegetative state) and MCS (minimally conscious state) based on TMS-EEG and resting-state fMRI data.

Methods

35 patients were enrolled into the study (21 VS, 14 MCS), all patients underwent 3 T resting-state fMRI and TMS-EEG. The analysis of functional connectivity according to TMS-EEG obtained the values of perturbation complexity index (PCI). For FMRI index of connectome intactness (ICI) was computed as the correlation coefficient of an individual connectivity vector and the mean vector of the reference group. A variant of the index (index of thresholded connectome intactness, ITCI) was evaluated by the same procedure after thresholding connectivity vectors at a given level. Hub disruption index (HDI) was calculated as index measuring the disruption of the nodal degrees in the connectom graph.

Result

PPCI index provides a more accurate VS and MCS group separation (area under the ROC curve: AUC = 0.86) than ITCI (AUC = 0.69) and HDI (AUC = 0.72) indices. Comparison of the results of clinical evaluation, as well as the data obtained by the TMS-EEG and rs-fMRI methods, showed that PCI index has a significant correlation with the average strength CRS-R scale (p = 0.0002). The correlation between ITCI and HDI indices with the CRS-R scale does not reach statistical significance (p = 0.08 and p = 0.06, respectively). The values of PCI index do not have a significant correlation with ITCI and HDI indices (p = 0.3 and p = 0.2, respectively).

At the same time, the indices based on rs-fMRI have a strong correlation between each other ($p < 0.0001$).

Discussion & Conclusion

TMS-EEG showed prevalence in DOC differentiation and higher correlation with clinical scale than resting-state FMRI. But FMRI makes it possible to visualize resting-state networks and their connections that are most severely disturbed in VS patients compared to MCS, which means, presumably, to maintain the process of consciousness. So both methods are feasible in consciousness and its disorders research.

Study was supported by RSCF grant 16-15-00274

1-O25

AMBULATORY BLOOD PRESSURE MONITORING AND DTI-BASED MICROSTRUCTURAL CHANGES IN PATIENTS WITH HYPERTENSION-RELATED CEREBRAL SMALL VESSEL DISEASE

*E. Kremneva*¹, L. Dobrynina¹, K. Shamtieva¹, M. Krotenkova¹, L. Kalashnikova¹

¹ Research center of neurology, Moscow, RUSSIA

Introduction

Application of modern antihypertensive drugs has improved the course of arterial hypertension (AH), but has not led to the expected decrease in cerebral small vessel disease (SVD) incidence and its complications. This fact encourages further investigation of hypertension-related mechanisms of brain damage. So we aimed to study the relation between daily profile of blood pressure and brain microstructure changes in patients with both SVD and AH.

Methods

The study included 64 patients (female – 38, mean age 59.4 ± 5.4 yo) with both SVD and AH. Ambulatory blood pressure monitoring (ABPM) and diffusion-tensor MRI (3 T, b-values 0, 1000 s/mm², 64 non-coplanar diffusion directions for each non-zero b-value (TE/TR 115/12600 ms; matrix 100 x 100, resolution 2 x 2 x 2 mm³) were obtained for all participants. The relation between studied parameters was estimated using the multivariate statistical analysis method - linear regression analysis.

Result

A statistically significant association was found between changes in daily profile of blood pressure according to ABPM data and microstructure abnormalities of the juxtacortical white matter hyperintensities (jWMH) of anterior frontal lobes, temporalparietal regions and left posterior cingulate cortex based on DTI data. An increase and variability of diastolic

blood pressure (DBP) were of primary importance in brain microstructural damage in mentioned areas leading to mean diffusivity and radial diffusivity increase.

Discussion & Conclusion

The revealed relation between microstructure abnormalities in jWMH and posterior cingulate cortex and an increase in DBP and its variability corresponds to the experimental data on the breakdown of the autoregulation reaction in cortex arteries and further descending vasogenic edema. It also indicates the significance of this mechanism in damage of white matter microstructure in patients with SVD. Predominant importance of both DBP increase and variability in brain microstructure damage suggests changes of cerebral blood flow autoregulation limits and related mechanisms of brain vessels and tissue damage. The study was supported by Russian Foundation for Basic Research grant 18-32-00852.

1-O26

AGREEMENT BETWEEN CT AND MRI IN PATIENTS WITH NORMAL PRESSURE HYDROCEPHALUS

*K. Kockum*¹, J. Virhammar², K. Riklund³, L. Söderström⁴, E. Larsson⁵, K. Laurell¹

¹ Umeå University, Dept. of Pharmacology and Clinical Neuroscience, Östersund, SWEDEN, ² Uppsala University Hospital, Dept. of Neuroscience, Neurology, Uppsala, SWEDEN, ³ Umeå University, Dept. of Radiation Sciences, Diagnostic Radiology, Umeå, SWEDEN, ⁴ Umeå university, Unit of Research, Education and Development, Östersund, SWEDEN, ⁵ Uppsala university, Dept. of Surgical Sciences, Radiology, Uppsala, SWEDEN

Introduction

Imaging is critical for diagnosing idiopathic normal pressure hydrocephalus. The aim of this study was to assess the agreement between CT and MRI for seven imaging features included in the iNPH Radscale, a radiological screening tool.

Methods

The study included 35 patients with idiopathic normal pressure hydrocephalus who were treated surgically from 2011 to 2015 at Uppsala University Hospital with preoperative CT and MRI performed with maximum three months between scans. Seven features were assessed: Evans' index, temporal horn size, callosal angle, periventricular white matter changes, narrow high convexity sulci, focally enlarged sulci, and enlarged Sylvian fissures. All scans were assessed by two radiologists who were blinded to each other's results and to clinical data.

Result

The agreement between CT and MRI was almost perfect for Evans' index, temporal horns, narrow sulci, and Sylvian fissures (kappa and intraclass correlation, 0.84–0.91, $P < .001$). There was substantial to almost perfect agreement for callosal angle and focally enlarged sulci. The concordance between modalities was fair for changes in periventricular white matter.

Discussion & Conclusion

CT and MRI are equally good for assessing radiological signs associated with idiopathic normal pressure hydrocephalus except for periventricular white matter changes, as MRI has superior soft tissue contrast. The wide availability, low cost, and acceptable reliability of brain CT makes it suitable as a first line investigation for detection of the disease.

1-O27

ASSESSING THE OPTIMAL FDG PET IMAGING TIME POINT IN GLIOBLASTOMA

M. Gule¹, M. Chen¹, S. Prabhu¹, J. Weinberg¹, O. Mawlawi¹, J. Johnson¹

¹ The University of Texas MD Anderson Cancer Center, Houston, USA

Introduction

Given the ongoing challenges faced with the non-invasive assessment of true progression of disease versus pseudoprogression (radiation necrosis/treatment changes) in glioblastoma, we sought to optimize our FDG PET imaging protocol. Prior research has suggested that conspicuity of high-grade gliomas with FDG PET is improved at delayed time points over the traditional approximately one-hour post-injection imaging time point.

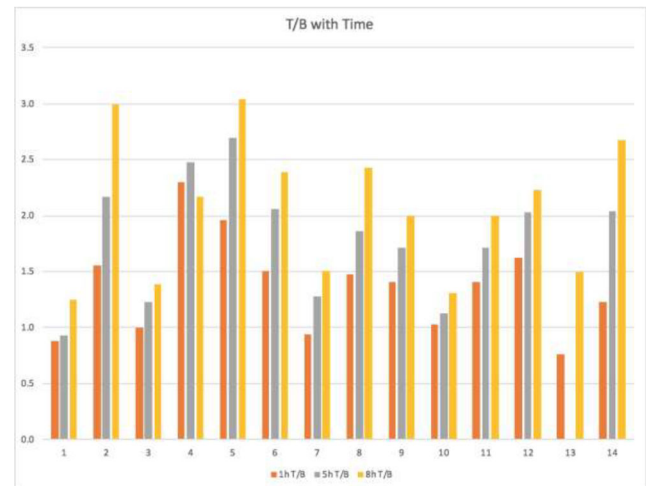
Methods

Seventeen untreated adult patients with suspected glioblastoma were imaged with FDG PET CT at 1, 5 and 8 hours post-FDG injection. All patients had surgery within three days of imaging. Maximum standard uptake values (SUV) were calculated for the central enhancing component of the suspected glioblastoma (lesion) and compared to normal appearing contralateral brain (background) at each time point.

Result

Thirteen patients (8 male) had pathology proven glioblastoma. The mean maximum SUV (Tmax) for the tumors at 1h, 5h, and 8h was 1.4 ± 0.4 , 1.8 ± 0.5 and 2.1 ± 0.6 , respectively. The Tmax for the lesions were statistically significantly increased for the 5h time point over the 1h time point ($p > 0.001$), the 8h time point over the 1h time point ($p = 0.026$) and the 8h time point over the

5h time point ($p = 0.036$). There were statistically significant increases in tumor to background (T/B) ratios also seen as 5h over 1h ($p > 0.001$), 8h over 1h ($p > 0.001$), and 8h over 5h ($p > 0.001$).



Discussion & Conclusion

Glioblastoma metabolism as measured by Tmax, as well as conspicuity as measured by L/B ratios, is significantly higher at 5h and 8h post-FDG injection over a 1h time point. This data suggests a delayed imaging time point may be superior in assessing post-treated glioblastoma for true progression over pseudoprogression. These results are promising, and further investigation is warranted.

1-O28

COMPARISON OF CNR OF ANTIDRIVE-3D-TSE BLACK-BLOOD IMAGING COMBINED WITH IMSDE TAKEN IN CLINICAL CASES IN OUR HOSPITAL

T. Hiraka¹, Y. Toyoguchi¹, Y. Sugai¹, Y. Konno¹, K. Kirii¹, F. Watarai¹, M. Kanoto¹

¹ Department of Radiology, Division of Diagnostic Radiology, Yamagata University Graduate School of Medical Science, Yamagata, JAPAN

Introduction

In our hospital, two types of iMSDE combining AntiDrive-3D-TSE black-blood imaging (iMSDE-AntiDRIVE-VISTA) were simultaneously taken to diagnose arterial wall disease in the posterior fossa: a Pd-type with an emphasis on the intravascular signal suppression effect and a T1-type used after angiography. The purpose of this study is to measure and compare the contrast-to-noise ratio (CNR) of the basilar artery wall of the two images taken at our hospital, and to confirm whether it is suitable for the diagnosis of artery wall disease.

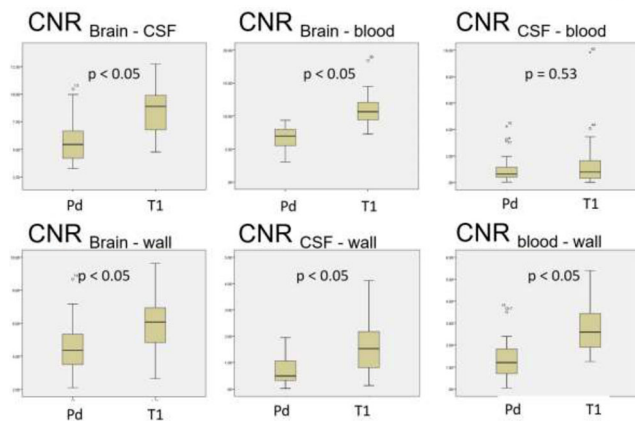
Methods

A total of 27 examinations (18 patients plus follow-ups) were performed between April and December 2017. All subjects had two types of iMSDE-AntiDRIVE-VISTA taken simultaneously. There were 12 males and 6 females, with a mean age of 64.7 (\pm 16.1) years. CNR was calculated from two types (measurement on Ax and Sag) of signal values and noise from the region of interest (ROI). CNR between brain parenchyma (brain), cerebrospinal fluid (CSF), vascular lumen (blood), and basilar arterial wall (wall) with Pd-type and T1-type were calculated, and statistical comparisons were made using the Mann-Whitney U test with SPSS ver. 22 for Windows.

Result

In measurements on Ax images, except for the CNR between CSF and the wall, the T1-type tended to have a significantly higher CNR, and in measurements on Sag images, except for the CNR between CSF and blood, the T1-type tended to have a significantly higher CNR. In all three CNRs associated with the wall, the T1-type also tended to have a significantly higher CNR.

Result : Pd vs T1 measurement on Sag



Discussion & Conclusion

Discussion

CNR associated with the basilar arterial wall was higher in the T1-type. It was believed that the signal value of the T1-type increased by AntiDrive and that the signal value of the Pd-type decreased because TR is as short as the proton density-weighted image, and that the standard deviation of the signal within the ROI was greater for the Pd-type because the noise of the Pd-type image quality is strong.

Conclusion

As a result of comparing the CNR of two types of iMSDE-AntiDrive-VISTA, the CNR of the arterial wall tended to be higher in the T1-type.

1-O29

CLINICAL USEFULNESS OF DEEP LEARNING BASED AUTOMATED DETECTION ALGORITHM IN THE INTRACRANIAL HEMORRHAGE

*M.H. Hahm*¹, H.J. Lee², J.K. Lim², H.S. Lee²

¹ Kyungpook National University Chilgok Hospital, Daegu, SOUTH KOREA, ² Kyungpook National University Hospital, Daegu

Introduction

There are various doctors in hospital who should order a brain computed tomography (CT) to rule out intracranial hemorrhages. The purpose of this study was to investigate the clinical usefulness of deep learning based automated detection algorithm in terms of physicians.

Methods

Between January 1, 2011, and December 31, 2017, a total of 5702 patients' brain CTs including 3055 cases with no intracranial hemorrhage and 2647 cases with intracranial hemorrhages, including traumatic and non-traumatic intracerebral hematoma, subarachnoid hemorrhage, intraventricular hematoma, epidural hematoma, and subdural hematoma, were used to develop the cascaded deep learning (CDL) automated detection algorithm.

A total of 38 physicians were recruited for test and categorized into 12 groups as follows: 4 interns, 4 internal medicine residents, 4 pediatrics residents, 4 emergency medicine junior residents, 4 emergency medicine senior residents, 4 neurosurgery junior residents, 4 neurosurgery senior residents, 2 radiology junior residents, 2 radiology senior residents, 2 emergency medicine specialists, 2 neurosurgery specialists, 2 neuroradiology specialists. These physicians were examined by test data set, and the diagnostic accuracy of hemorrhage and diagnostic time were evaluated in terms of physician alone and physician assisted by CDL.

Result

In terms of the binary classification, the performance of the CDL in test data set showed an AUC of 0.989. In terms of differential diagnosis among intracranial hemorrhages, the performance of the CDL in test data set revealed an AUC of 0.966. There were specific physician groups whose diagnostic accuracy were significantly improved by CDL, such as interns, internal medicine residents, pediatrics residents, and emergency junior residents ($p=0.029$). Additionally, emergency medicine senior residents and neurosurgery junior residents got help from CDL ($p=0.057$). However, the difference of diagnostic time between physician alone and physician assisted CDL revealed no statistical significance, and the mean value of diagnostic time in physician assisted by CDL showed higher than those in physician alone.

Discussion & Conclusion

Even though CDL may not reduce the diagnostic time unlike expectation, it is expected to play a role in improving the diagnostic accuracy in specific physicians groups.

1-O30

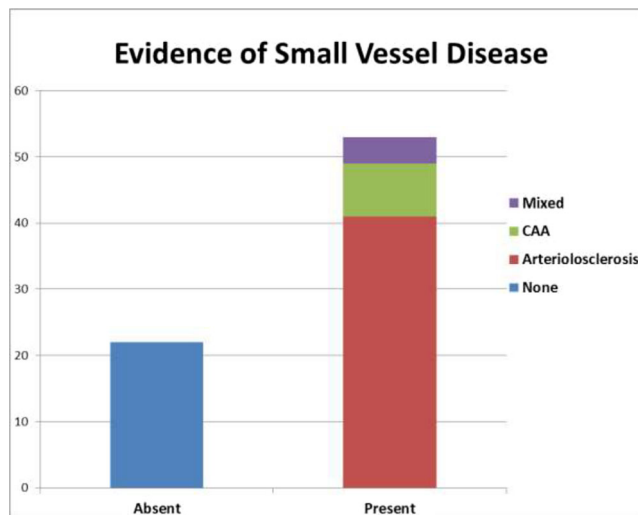
ACUTE SYMPTOMATIC LACUNAR ISCHEMIC STROKE AS FIRST PRESENTATION OF SMALL VESSEL DISEASE: HOW COMMON IS IT?

A. Guarnera¹, C. Barbato², L. Ulivi³, S. Browning⁴, D. Werring⁵, R. Simister⁴, R. Jager⁶

¹ Sant'Andrea Hospital, La Sapienza, Rome, ITALY, ² University of Florence, Florence, ITALY, ³ University of Pisa, Pisa, ITALY, ⁴ UCL Hospital, NHS Trust, London, UNITED KINGDOM, ⁵ NHNN, Queen Square, UCL, Institute of Neurology, London, UNITED KINGDOM, ⁶ NHNN, Queen Square, UCL, Institute of Neuroradiology, London, UNITED KINGDOM

Introduction

Acute symptomatic lacunar ischemic stroke (ASLIS) represents a common cause of stroke with a variable age of presentation. It may have several different underlying pathomechanisms which are incompletely understood. In this study, we investigated the prevalence of pre-existing small vessel disease burden in patients presenting with ASLIS using a number of small vessel disease (SVD) imaging markers. Specifically, we aimed to ascertain how frequently an ASLIS represents the initial radiological manifestation of SVD.



Methods

We retrospectively reviewed 546 consecutive patients, undergoing MRI for acute stroke between July 2018 and December 2018, and identified 75 subjects with a DWI+ ASLIS. We excluded patients with haemorrhagic strokes, large vessel disease and multi-territory infarcts suggestive of an embolic aetiology. MRIs were analysed for presence of the following imaging markers of cerebral SVD: white matter hyperintensities, lacunes, enlarged perivascular, cerebral microbleeds, and cortical superficial siderosis, using a number of established scoring systems. First, we divided the subjects of our cohort into those with and without clear evidence of concomitant SVD imaging markers. The former, we assigned to three categories of SVD: arteriolosclerosis; probable or possible cerebral amyloid angiopathy (CAA); and mixed disease.

Result

Of 75 subjects (46 males and 29 females, mean age: 70y±15.87), 22 (29%) did not have other imaging evidence of SVD. Of the 53 remaining cases, 41 (77%) had evidence of arteriolosclerosis, 8 (15%) of CAA and 4 (7.7%) of mixed disease. Subjects with no evidence of co-existing SVD markers were younger (mean age 58.5y±16.21 vs 72y±13.73)

Discussion & Conclusion

DWI+ ASLIS was the first imaging manifestation of SVD in about 30% of subjects. In the remaining 70% of cases, presence of SVD imaging markers suggested arteriolosclerosis as the predominant type of SVD, CAA being relatively rare. Patients with isolated perforating artery infarcts may well have a different pathophysiology (such as junctional atheroma) and risk of recurrence stroke than those where imaging markers indicate more widespread SVD. Our findings pave the way for future studies to address these issues.

1-O31

CLINICAL EVALUATION OF QUANTITATIVE REPORTS FOR MRI ASSESSMENT OF SUSPECTED MEDIAL TEMPORAL SCLEROSIS (MTS)

O. Goodkin¹, H. Pemberton^{1,2}, S. Vos^{1,3}, F. Prados^{1,4}, R. Das⁵, J. Moggridge^{2,6}, B. De Blasi⁷, P. Bartlett^{3,8}, E. Williams⁹, T. Campion⁶, L. Haider^{10,11}, K. Pearce⁶, N. Bargallo¹², E. Sanchez¹³, S. Bisdas^{2,6}, M. White¹⁴, S. Ourselin^{7,15}, G. Winston^{3,8,16}, J. Duncan^{3,8}, J. Thornton^{2,6}, M. Cardoso^{7,15}, T. Yousry^{2,6}, F. Barkhof^{1,2,6,13}

¹ Centre for Medical Image Computing (CMIC), Department of Medical Physics and Bioengineering, University College London, London, UNITED KINGDOM, ² Neuroradiological Academic Unit, UCL Queen Square Institute of Neurology, University College London, London, UNITED KINGDOM, ³ Epilepsy Society MRI Unit, Chalfont St Peter, UNITED KINGDOM, ⁴ Universitat Oberta de Catalunya, Barcelona, SPAIN, ⁵ Clinical, Educational and Health Psychology, University College London, London, UNITED KINGDOM, ⁶ Lysholm Department of Neuroradiology, National Hospital for Neurology and Neurosurgery, UCLH NHS Foundation Trust, London, UNITED KINGDOM, ⁷ Department of Medical Physics and Biomedical Engineering, University College London, London, UNITED KINGDOM, ⁸ Department of Clinical and Experimental Epilepsy, University College London, London, UNITED KINGDOM, ⁹ Wellcome Trust Centre for Neuroimaging, UCL Queen Square Institute of Neurology, University College London, London, UNITED KINGDOM, ¹⁰ Department of Biomedical Imaging and Image Guided Therapy, Medical University of Vienna, Vienna, AUSTRIA, ¹¹ Faculty of Brain Science, UCL Queen Square Institute of Neurology, University College London, London, UNITED KINGDOM, ¹² Radiology Department, Hospital Clinic de Barcelona and Magnetic Resonance Image Core Facility, IDIBAPS, Barcelona, SPAIN, ¹³ Radiology & Nuclear Medicine, VU University Medical Center, Amsterdam, THE NETHERLANDS, ¹⁴ Digital Services, University College London

Hospital, London, UNITED KINGDOM, ¹⁵ School of Biomedical Engineering and Imaging Sciences, Kings College London, London, UNITED KINGDOM, ¹⁶ Department of Medicine, Division of Neurology, Queens University, Ontario, CANADA

Introduction

MTS is a common cause of temporal lobe epilepsy. Current neuroradiological practice is largely subjective, but accurate assessment of key MTS imaging biomarkers – hippocampal volume loss and T2 signal change – could better inform treatment decisions. We tested whether reporting global and cross-sectional volumetric and qT2 measures, referencing normative data, improved diagnostic accuracy and confidence vs. visual assessment alone.

Methods

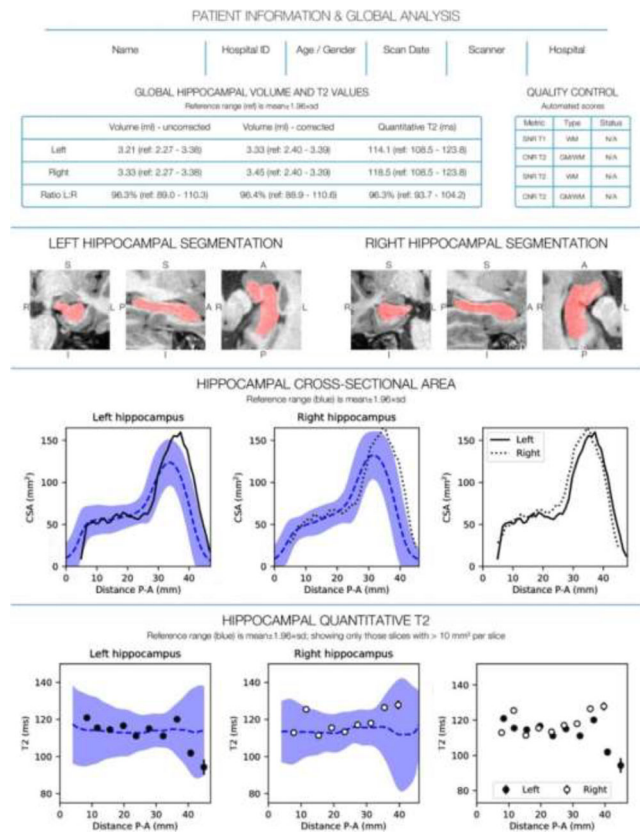
Quantitative reports of hippocampal qT2 and volume were generated for 43 cases (15 histologically-confirmed unilateral MTS, 5 with anterior pathology; 5 clinically-determined bilateral; 23 age-matched MR-negatives) with reference values from 115 controls. Raters with different radiological experience (3 each of neuroradiology consultants, registrars, and image analysts) assessed all cases with and without the report in random order, blinded to demographics except age and gender. Raters assigned cases normal/abnormal (‘correct assessment’), and, if abnormal, right, left or bilateral (‘correct detection’). Accuracy was calculated as (true positives + true negatives)/ total rated. Confidence for each decision was rated 1-5.

Result

Detection was initially high but showed trend-level improvement with the quantitative report from 87.5% to 92.5% (p=0.07, d=0.69). A large-magnitude improvement effect (84.5% to 93.8%) was seen in the image analyst group, although this did not reach significance (p=0.27, d=0.87). There was greater detection accuracy for anterior vs. all other unilateral cases (p= 0.07*) with the report and no difference without the report. For MTS cases, the report improved overall accuracy, largely due to improvements in detecting bilateral cases (p=0.028*). Confidence increased in the image analyst group when correctly identifying both normal (p<0.01*) and abnormal (p=0.025*) scans and at trend level for the other two groups. Agreement per rater with the correct diagnosis (Cohen’s kappa) increased from ‘fair’ to ‘excellent’ (0.74 – 0.87; p=0.063) with the report across all rater groups.

Discussion & Conclusion

MTS quantitative profiles could improve detection accuracy and diagnostic confidence. They may be of particular use in assessment of challenging anterior or bilateral cases. Although improvements were seen across rater experience levels, the largest were for less-experienced radiologists and image analysts. These findings have positive implications for patient care across clinical services and justify further validation with larger group sizes.



1-032

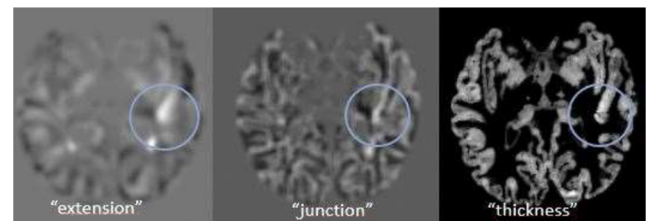
CONTRIBUTION OF MRI VOXEL-BASED MORPHOMETRY IN THE DIAGNOSIS OF FOCAL CORTICAL DYSPLASIAS

S. González-Ortiz¹, R. Medrano¹, R. Rocamora¹, G. Conesa¹, T. Mestre¹, J. Capellades¹

¹ Hospital del Mar, Barcelona, SPAIN

Introduction

Magnetic resonance imaging (MRI) is crucial in the diagnosis of pharmacoresistant epilepsy (PRE), since patients with lesions detected by MRI have a better prognosis after surgery. On the other hand, one of the most frequent etiologies in PRE, focal cortical dysplasia (FCD), can be difficult to identify in the MRI, with studies indicating that up to 50-80% of FCD escape visual diagnosis. In order to improve their detection, some voxel-based morphometry programs (VBM) have been developed. One of these is the MAP (Morphometric Analysis Program). Our objective is to evaluate the usefulness of this program in the diagnosis and management of patients with PRE.



Methods

We retrospectively review a group of 73 patients with focal PRE and a diagnosis of “non-lesional” MRI. All patients have a 3 Tesla MRI with Epilepsy protocol, which includes a T13D. This group of non-lesional MRI includes patients with a strictly normal MRI and those with some subtle finding or asymmetry that were not conclusive as a real lesion.

Each MRI is processed by MAP, obtaining 3 z-score maps called 'junction', 'extension' and 'thickness'. These maps are visually analyzed and guide a second look of the MRI. Then the patients are classified as: MAP+: one or more z-score maps are positive and a structural lesion is found in the MRI

MAP-: z-score maps are negative

MAP?: one or more z-score maps are positive but not structural lesion is found in the MRI

Result

In a preliminary analysis, more than 15% of patients are MAP+, around 70% are MAP-, and the rest of patients are MAP?.

Discussion & Conclusion

More than 15% of patients have changed from having a negative MRI to having a positive MRI, with a structural lesion detected after a focused evaluation of the images, guided by the z-score maps. These results have important repercussions in the clinical management and postoperative prognosis of patients with PRE.

1-O33

CERVICO-CRANIAL ARTERIAL DISSECTIONS -CLINICAL AND NEURORADIOLOGY CORRELATIONS

*B. Georgievski-Brkic*¹, T. Jaramaz-Ducic², M. Vukicevic², B. Vukomancic¹, V. Mileusnic², M. Savic², D. Kostic³, M. Lucic⁴

¹ Stroke hospital, Department of Radiology, Belgrade, SERBIA, ² Stroke hospital, Department of Neurology, Belgrade, SERBIA, ³ Military Medical Academy, Institute of Radiology, Belgrade, SERBIA, ⁴ Oncology Institute Sremska Kamenica, Department of Radiology, Novi Sad, SERBIA

Introduction

Cervico-cranial arterial dissection (CCAD) is a major cause of cerebral ischemia in young adults and can lead to various clinical symptoms, some of them are benign: headache, neck pain, Horner's syndrome but most patients have a stroke or transient ischemic attack (TIA).

Methods

We analyzed 214 CCAD in 188 patients diagnosed by MR imaging in Stroke Hospital in last ten years. 53 patients had 61 vertebro-basilar artery dissections (VBAD) and 135 patients had 153 carotid artery dissections (CAD). 6 different types of vessels pathologies were detected on MRI: intramural hematoma, “string” sign stenosis, tapering occlusion, pseudoaneurysms, intimal flap/ double lumen and “string and pearl” sign of stenosis. We compared the patients with CAD and VBAD.

Result

Patients with CAD were older ($X=45,1\pm 11,5$ versus $X=42,7\pm 12,7$, $p=0,463$) with more severe ischemic strokes (median National Institutes of Health Stroke Scale, $1,83\pm 2,6$ versus $7,04\pm 8,54$ $p<0,001$). Headache (64, 2% versus 42,2%; $p=0,008$) and neck pain (35,8% versus 17,8%; $p=0,007$) were more common in VBAD. TIA were more frequent in VBAD (33, 96% versus 20%, $p=0,007$). In patients with CAD there was significant correlation between cerebral ischemia and headache (68,4%, $r= 0,247$, $p=0,004$), amaurosis fugans (53,5%, $r= 0,236$, $p=0,006$) and Horner's syndrome (52,6%, $r= 0,277$, $p=0,001$). In VBAD intracranial arterial dissections (36,2% versus 11,1 %, $p<0,001$) and intimal flap/double lumen (41% versus 21,6%, $p=0,004$) were more common. In CAD, tapering occlusion pattern of dissection was more common presented with brain infarct than string sign stenosis (56,2% versus 34,4%, $p=0,001$) rather than VBAD (54,8% versus 42,9%, $p=0,222$). Intimal flap was more frequent presented with persistent neurological deficits (cerebral infarcts) rather than TIA (27,8% versus 20, 6%, $p=0,010$) in all patients with CCAD. Patients with VBAD had better favorable outcome after 3 months of ischemic stroke (modified Rankin score 0-2: 77,4% versus 54,8% , $p<0,001$). Recurrent brain infarcts were common in CAD (3 % versus 1,9% , $p=0,259$), but recurrent TIA-s were frequent in VBAD (5,7% versus 1,5%, $p=0,1$).

Discussion & Conclusion

VBAD and CAD have some different features in clinical and radiological presentations, outcome and rates of recurrent of ischemic event or TIA.

1-O34

COMPARISON OF ASL PERFUSION AND SPECT EXAMINATION IN LATERISATION OF SEIZURE FOCUS IN PATIENTS WITH INTRACTABLE TEMPORAL LOBE EPILEPSY

*A. Garg*¹, K. Bhullar², M. Tripathi³, S.P. Chandra⁴

¹ All India Institute of Medical Sciences, New Delhi, INDIA, ² All India Institute of Medical Sciences, New Delhi, INDIA, ³ All India Institute of Medical Sciences, New Delhi, INDIA, ⁴ All India Institute of Medical Sciences, New Delhi, INDIA, ⁵

Introduction

The aim of present study is to compare the diagnostic performance of ASL perfusion and SPECT examination in laterisation of seizure focus in patients with intractable temporal lobe epilepsy.

Methods

Forty-three patients with intractable temporal lobe epilepsy underwent conventional MR examination on 3T scanner and ASL perfusion on 1.5 T scanner using 3D pseudocontinuous ASL. Interictal and Ictal SPECT was done, dye was injected within 20 sec of seizure for ictal SPECT. Ictal SPECT was substrated from interictal SPECT and overload on MR scan (SISCOM).

The finding on conventional MR examination, ASL perfusion maps and SISCOM were noted to localise the seizure focus.

Result

Total 43 patients (M: 29, F-14; mean age 22.29 (range; 4-50 yrs)) were included. On conventional MR imaging, 4 patients had normal MRI, 10 had isolated medial temporal sclerosis (MTS) (L-5, R-2 and B/1-3), MTS with focal cortical dysplasia (FCD) (7), MTS with perinatal insult (5), neoplasms (4), isolated Type 1 FCD (4), type 2B FCD (4) and other lesions (5).

SPECT showed ipsilateral temporal lobe (22), contralateral temporal lobe (2), no localisation (11) and extra-temporal localisation (8 patients).

ASL perfusion was increased in 2 patients, decreased in 28 and normal in 13 patients. ASL perfusion maps showed ipsilateral temporal lobe (23), contralateral temporal lobe (1), no localisation (13) and extra-temporal localisation (6 patients).

Discussion & Conclusion

ASL perfusion maps are comparable of SPECT data in lateralising the seizure focus in patients with intractable temporal lobe epilepsy.

Reference

Stamoulis C, Verma N, Kaulas H, Halford JJ, Duffy FH, Pearl PL, Treves ST. The promise of subtraction ictal SPECT co-registered to MRI for improved seizure localization in pediatric epilepsies: Affecting factors and relationship to the surgical outcome. *Epilepsy Res* 2017, Jan;129:59-66.

Blauwblomme T, Boddaert N, Chemaly N, Chiron C, Pages M, Varlet P, et al. Arterial spin labeling MRI: A step forward in non-invasive delineation of focal cortical dysplasia in children. *Epilepsy Res* 2014, Dec;108(10):1932-9.

Cha YH, Jog MA, Kim YC, Chakrapani S, Kraman SM, Wang DJ. Regional correlation between resting state FDG PET and pcasl perfusion MRI. *J Cereb Blood Flow Metab* 2013, Dec;33(12):1909-14.

1-O35

VESSEL WALL ENHANCEMENT OF INTRACRANIAL ANEURYSMS ON HIGH RESOLUTION MRI: A RUPTURE SIGN? THE ICARUS STUDY

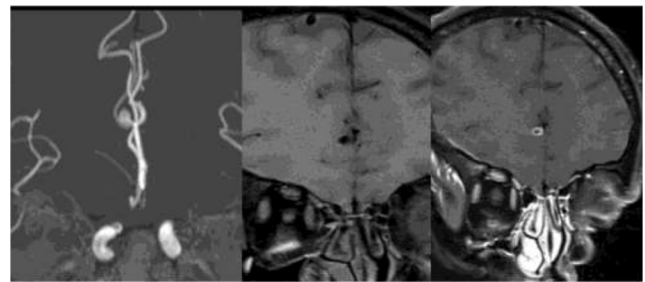
L. Dinia¹, L. Gramegna², C. Vert³, F. Arikan⁴, M. Luzi⁵, D. Hernandez⁶, P. Coscojuela⁷, E. Martinez⁸, A. Tomasello⁹, A. Rovira¹⁰

¹ Section of Diagnostic and Interventional Neuroradiology Department of Radiology Hospital Universitari Vall d Hebron, Barcelona, SPAIN, ² Section of Neuroradiology. IRCCS Istituto delle Scienze Neurologiche, Bologna, ITALY, ³ Section of Diagnostic and Interventional Neuroradiology Department of Radiology Hospital Universitari Vall d Hebron, Barcelona, SPAIN, ⁴ Department of Neurosurgery. Hospital Universitari Vall d Hebron., Barcelona, SPAIN, ⁵ Department of Neurosurgery. Universita Politecnica delle Marche, Ancona, ITALY, ⁶ Section of Diagnostic and Interventional Neuroradiology Department of Radiology Hospital Universitari Vall d Hebron, Barcelona, SPAIN, ⁷ Section of Diagnostic and Interventional Neuroradiology Department of

Radiology Hospital Universitari Vall d Hebron, Barcelona, SPAIN, ⁸ Department of Neuropathology. Hospital Universitari Vall d Hebron., Barcelona, SPAIN, ⁹ Section of Diagnostic and Interventional Neuroradiology Department of Radiology Hospital Universitari Vall d Hebron, Barcelona, SPAIN, ¹⁰ Section of Diagnostic and Interventional Neuroradiology Department of Radiology Hospital Universitari Vall d Hebron, Barcelona, SPAIN

Introduction

Saccular intracranial aneurysm (SIA) rupture has still devastating consequences. Instability state is still difficult to estimate. Inflammation plays a major role in aneurysm formation and rupture and literature suggests that aneurysm wall enhancement (WE) on magnetic resonance imaging (MRI) may be a surrogate of vessel wall inflammation. Main aim of the study is to assess the capability of WE to identify intracranial aneurysms in real danger for rupturing.



Methods

Cohort prospective observational study. Consecutive patients with ruptured and un-ruptured aneurysms underwent contrast 3T-MRI and histology to confirm wall inflammation. Statistical analysis was performed to investigate the association of WE with risk factors and histological markers of inflammation.

Result

A preliminary group of 50 patients was included. WE was present in 100% of ruptured, in 50% of unruptured symptomatic, and in 33% of asymptomatic aneurysms ($p=0.003$). Cut-offline of 4 in PHASES score was found, above which most of the aneurysms begin to enhance ($p<0.001$). Logistic regression analysis demonstrated as independent predictors of rupture: WE ($p=0.018$) and presence of multiple aneurysms ($p=0.016$). Independent predictors of wall enhancement were: size ($p=0.001$), presence of variables of circle of Willis ($p=0.005$) and irregular morphology ($p=0.016$). Analysis of WE as a predictor of rupture has shown ($p=0.002$): 100% sensitivity, 64% specificity, 28% VPP, 100% VPN. At a cut-off of 7, there is a direct correlation between the number of altered immunohistochemical inflammation markers and presence of WE ($p=0.043$). A score higher than 7 entails a 100% sensitivity, specificity, VPP and VPN in relation to presence of WE.

Discussion & Conclusion

Wall enhancement identifies instability-state in SIA and can be a new and powerful rupture sign that could be crucial in deciding whether and how

to treat SIA, even in small aneurysms. Final purpose is to offer a practice tool to personalize the therapeutic approach, distinguishing different aneurysm “activation” stages, in order to reduce intracranial bleeding and improving long-term outcome. Taking into account not only the dimensions and the morphology but, above all, the pathophysiology of the aneurysm itself, will allow tailoring therapeutic options. Further implication of the results will be the development of new personalized devices aiming at lowering the inflammation of the wall.

1-O36

PREDICTION OF LONG-TERM DISABILITY IN MULTIPLE SCLEROSIS: A ROLE FOR LINEAR MEASURES OF BRAIN ATROPHY?

*M. Di Stasi*¹, G. Pontillo¹, C. Russo¹, M.B. Cipullo¹, C. Paoletta¹, T. Petrillo¹, E.A. Vola¹, R. Lanzillo², A. Carotenuto², M. Masullo², A. Elefante¹, V. Brescia Morra², M. Quarantelli³, S. Cocozza¹, M. Petracca², A. Brunetti¹

¹ Department of Advanced Biomedical Sciences, University Federico II, Naples, ITALY, ² Department of Neurosciences and Reproductive and Odontostomatological Sciences, University Federico II, Naples, ITALY, ³ Institute of Biostructure and Bioimaging, National Research Council, Naples, ITALY

Introduction

Brain atrophy has been consistently identified as one of the strongest predictors of clinical disability in Multiple Sclerosis (MS). Aim of our study was to assess the validity of linear measures of ventricular enlargement as indicators of global brain atrophy and their possible role as surrogate markers of clinical disability.

Methods

In this longitudinal, retrospective study, 87 patients with Relapsing-Remitting MS, two MRI scans performed with a 2-year interval (2.02 ± 0.06 y) and a long-term clinical follow-up (9.76 ± 0.99 y) were selected. As a measure of clinical disability, the Expanded Disability Status Scale (EDSS) score was determined at each timepoint.

MRI images were visually assessed by 5 independent readers to determine the following linear measures of ventricular enlargement: Frontal Horn Width (FHW), Inter-Caudate Diameter (ICD), Third Ventricle Width (TVW) and Fourth Ventricle Width (4VW). Total Skull Diameter (TSD) was also determined to normalize for head size. Normalized Brain Volume (NBV) and percentage BV change (PBVC) were also calculated using SIENAX and SIENA, respectively. Intra-rater reliability for linear measures was tested on baseline scans via intra-class correlation coefficient (ICC). Correlation between linear and volumetric measures were assessed via Spearman correlation coefficient. The relationship between MRI metrics and disability was assessed via linear and binary logistic regression models for the prediction of baseline EDSS score and confirmed disability at 10-y FU, respectively, accounting for age, gender and DD.

Result

For linear measures, ICC ranged between 0.923 and 0.975. At baseline, normalized ICD and TVW showed a significant correlation with NBV ($\rho = -0.484, p < 0.001$ and $\rho = -0.440, p < 0.001$). Annual PBVC was significantly correlated with annual percentage change in FHW, ICD and TVW ($\rho = -0.299, p = 0.005$; $\rho = -0.338, p < 0.001$ and $\rho = -0.292, p = 0.006$). At baseline, EDSS score was significantly predicted by NBV ($R^2 = 0.243, p < 0.001$), normalized ICD ($R^2 = 0.203, p < 0.001$) and normalized TVW ($R^2 = 0.257, p < 0.001$). Confirmed disability at 10-years was significantly predicted only by annual PBVC (Nagelkerke $R^2 = 0.183, p = 0.01$).

Discussion & Conclusion

Linear measures of ventricular enlargement serve as rapid and reproducible indicators of brain atrophy at both cross-sectional and longitudinal analyses. Similarly to NBV, they correlate with EDSS score, while their change over time is not a valid surrogate of PBVC in predicting long-term disability progression in MS.

1-O37

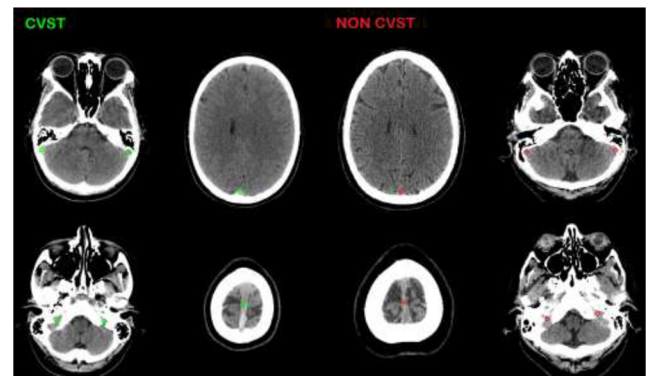
ASSESSMENT OF DURAL SINUS THROMBOSIS BY MEANS OF DENSITY VALUES: A TOOL FOR THE EMERGENCY RADIOLOGIST

*F. Dellepiane*¹, A. Romano¹, L. Pasquini¹, M. Rossi Espagnet¹, A. Napolitano², A. Bozzao¹

¹ La Sapienza University - Sant'Andrea Hospital, Rome, ITALY, ² Bambin Gesù Hospital, Rome, ITALY

Introduction

We wanted to define a quantitative, objective and easy-to acquire and interpreted parameter to be used in the evaluation and diagnosis of cerebral venous sinus thrombosis (CVST) on unenhanced CT images in both adult and pediatric population.



Methods

We retrospectively selected 30 adults and 30 pediatric patients with confirmed CVST diagnosis and two age-matched control groups (30 adults, 30 pediatric patients) and compared the densitometric values (HU)

measured in unenhanced TC, by positioning ROIs in six standardized key regions of the cerebral venous system: both sigmoid and transverse sinuses, confluence of sinuses and superior sagittal sinus. Three different radiologists repeated the measurements for every group and inter-observer reliability was assessed.

From every ROI, we obtained max and mean HU values and calculated the ratio “maximum HU value / (mean HU value) – (maximum HU value)” as parameter to discriminate patients with CVST. All the measurements in adult and pediatric population were compared with the respective control group through the Student t-test. Moreover, we obtained ROC curves to identify the best cut-off values for the significant parameters.

Result

He ratio max/mean-max was statistically significant in discriminating patients with CVST in both adult and pediatric population ($p < 0.05$). The cut off value of 1.2 showed a sensitivity and specificity of 91.7% in both groups. The maximum HU value was significantly higher in patients with CVST ($p < 0.05$), with the best cut-off value of 64.5 HU. We found an interclass correlation coefficient for HUMax and HUMax/ Mean-Max ratio respectively of 0.806 and 0.725 in the adult and 0.762 and 0.749 in the pediatric population; this means high concordance in the measurements made by the three observers, confirming a high reliability of the method.

Discussion & Conclusion

Misdiagnosis of CVST can deeply impact patient outcome. Currently, the diagnosis of CVST requires many diagnostic tests, with high inter-observer variability in interpretation. The standardized method that we propose may represent an objective, easy-to acquire diagnostic tool for the correct identification of patients with suspicion of CVST. The proposed method aims to provide the ER radiologist with a standardized and reliable diagnostic tool for an early diagnosis, with minimal inter-observer variability.

1-O38

MACHINE LEARNING APPROACH TO TEXTURE ANALYSIS PARAMETERS CAN PREDICT CLINICAL DISABILITY IN MULTIPLE SCLEROSIS PATIENTS

*S. Cocozza*¹, R. Cuocolo¹, G. Pontillo¹, L. Ugga¹, C. Russo¹, M. Petracca², R. Lanzillo², V. Brescia Morra², A. Elefante¹, A. Brunetti¹

¹ Univerity Federico II, Department of Advanced Biomedical Sciences, Naples, ITALY, ² Univerity Federico II, Department of Neurosciences, Reproductive Sciences and Odontostomatology, Naples, ITALY

Introduction

Multiple Sclerosis (MS) is a chronic inflammatory disease of the Central Nervous System, representing the first cause of neurological disability among young adults. Despite the use of advanced MRI techniques, imaging markers often fail to accurately predict the accumulation of physical disability in this condition. In an attempt to solve this clinico-radiological

paradox, aim of our study was to investigate the possible role of radiomics analyses for the prediction of physical disability in MS, by applying a machine learning approach to Texture Analysis (TA) parameters.

Methods

Seventy-nine patients with MS (according to 2010 McDonald criteria) were recruited. All patients underwent a neurological examination with the determination of the Expanded Disability Status Scale (EDSS) as an index of clinical disability, along with an MRI protocol on a 3T scanner including 3D-T1-weighted and 3D-FLAIR sequences.

On FLAIR images, hyperintense lesions were segmented using a semi-automated method (Jim 7), while T1 volumes were used to segment White Matter (WM) and both cortical and deep Gray Matter (GM). Then, FLAIR images were co-registered to the T1w volume in order to extract ROIs from both sequences.

For each ROI, 26818 features were extracted using an open source software (Pyradiomics v2.1.2). The resulting dataset was processed with a data mining software (Weka v3.8) and a regression Support Vector Machine was used for EDSS score prediction.

Model validation was performed with a train-test approach, with the test group constituted by 25% of the total population.

Result

MS patients (M/F=44/35; 41.5±11.0 years; 54 Relapsing Remitting MS, 25 Progressive MS) showed a median EDSS score of 3.5.

The subset evaluator produced a dataset containing 47 features (22 from T1w and 25 from FLAIR sequences, mainly derived from deep GM).

The Support Vector Machine allowed to obtain a correlation coefficient of 0.87, with a mean absolute error of 0.5 and a root mean square error of 0.7.

Discussion & Conclusion

Our results demonstrate that a machine learning-derived model including TA parameters mainly related to deep GM is able to predict physical disability in MS patients with great accuracy.

1-O39

AUTOMATED MRI HIPPOCAMPAL SUBFIELD MEASUREMENT IN MILD COGNITIVE IMPAIRMENT IN AN AMYLOID PROJECT

*O. Chawalparit*¹, C. Ngamsombat¹, K. Ningunha¹, W. Muangpaisan², T. Thientunyakit¹, P. Chamchaowanish¹, Y. Vichianin³

¹ Department of Radiology, Faculty of Medicine Siriraj Hospital, Mahidol University, Bangkok, THAILAND, ² Department of Preventive and Social Medicine, Faculty of Medicine Siriraj Hospital, Mahidol University, Bangkok, THAILAND, ³ Department of Radiological Technology, Faculty of Medical Technology, Mahidol University, Bangkok, THAILAND

Introduction

Studies of AD patients revealed brain volume loss which is also displayed in normal aging and mild cognitive impairment (MCI). More sensitive

diagnostic tool such as amyloid-PET study has been accepted for identifying early stage of the disease especially in MCI. However, more availability of MRI is still impressive for using as the screening tool for early AD detection.

This study aimed to identify regional brain atrophy by using automated MR-base volumetric measurement to differentiate MCI from normal elderly with the result of amyloid-PET study as the reference standard.

Methods

This study was a retrospective study from an amyloid project in dementia at our institute. Twenty-nine AD patients (mean 75.6 ±7.3 years), 11 MCI patients (mean 68.8±3.9 years) and 27 healthy control (HC) subjects (mean 69.3±4.7 years) were included in this study with analysis of neurological and neuropsychiatric test and underwent MRI (3-Tesla) with high-resolution 3D-T1W covering the whole brain. Quantitative volumetric analysis of brain including surface area, cortical gray matter volume, cortical thickness and hippocampal subfields was performed by using Freesurfer (v. 6.0).

Result

The diminishment of cortical gray matter volume and cortical thickness are involved in almost every brain regions with statistical significance in AD compared with MCI and HC. However, there was statistically significant different only of left granule cell layer and molecular layer of dentate gyrus (Lt.GC-ML-DG) ($p=0.02$) in amyloid PET positive MCI subjects compared to HC with the accuracy of 81.8%. Other hippocampal structures from subfield volume analysis including left whole hippocampus did not reach the statistical significance ($p=0.08$, accuracy of 87.9%) when compared between the two groups.

Discussion & Conclusion

Many of the studies of MRI in dementia to identify AD-converter MCI showed negative result. With the development of automated software for subfield hippocampal volume, e.g., FreeSurfer toolbox in this study, our study confirmed the improved sensitivity of MRI volumetric measurement with hippocampal subfield analysis to identify early stage of disease in MCI, at least compared with positive amyloid PET MCI. Study with higher number of subjects using this method to discriminate MCI and normal aging control would provide benefits as the screening tool in elderly population.

1-O40

A COMPARISON OF MICROSTRUCTURAL DIFFUSION MRI TECHNIQUES FOR THE IN-VIVO ASSESSMENT OF GLIOMA GRADING

*F. Carletti*¹, L. Mancini^{1,2}, S. Brandner³, L. Thorne⁴, A. Misericocchi^{4,5}, A. McEvoy^{4,5}, G. Samandouras⁴, S. Thust^{1,2}, J. Rees⁶, E. Sanverdi¹, S. Bisdas^{1,2}

¹ Lysholm Department of Neuroradiology, National Hospital for Neurology and Neurosurgery, UCLH NHS Foundation Trust, London,

UNITED KINGDOM, ² Neuroradiological Academic Unit, Department of Brain Repair and Rehabilitation, UCL Institute of Neurology, London, UNITED KINGDOM, ³ Department of Neurodegenerative Disease, UCL Institute of Neurology and Division of Neuropathology, London, UNITED KINGDOM, ⁴ Department of Neurosurgery, National Hospital for Neurology and Neurosurgery, UCLH NHS Foundation Trust, London, UNITED KINGDOM, ⁵ Department of Clinical and Experimental Epilepsy, UCL Queen Square Institute of Neurology, London, UNITED KINGDOM, ⁶ Department of Clinical Neurology, National Hospital for Neurology and Neurosurgery, London, UNITED KINGDOM

Introduction

The 2016 World Health Organization (WHO) classification of gliomas has introduced two critical molecular markers (IDH status and 1p19q co-deletion) adding higher prognostic value to the histopathologic findings. Diffusion MRI (dMRI) allows to probe the tumour microstructure and represents a candidate in-vivo technique for the prediction of these molecular markers. We aimed to assess the diagnostic performance of Diffusion Tensor Imaging (DTI), Diffusion Kurtosis Imaging (DKI) and neurite orientation dispersion and density imaging (NODDI) in glioma grading according to the latest integrated histomolecular WHO classification.

Methods

Forty-one patients with primary, treatment-naïve gliomas confirmed on histopathology (23 grade II and 18 grade III-IV tumours; 10 IDH wild-type, 17 IDH mutant 1p/19q retained and 14 IDH mutant 1p/19q codeleted; 33 non-oligodendroglial and 8 oligodendroglial tumours) were investigated using a multi-shell diffusion-weighted MRI protocol and morphological imaging. Tumours were segmented from morphological images. dMRI data were fitted at the voxel level using three different models (DTI, DKI, and NODDI). Multiple DTI, DKI and NODDI indices were extracted from the whole tumour segmentations and analysed by descriptive statistics and linear regression (Stata software).

Result

IDH wild-type (IDHwt) and mutant (IDHmut) gliomas showed different values of apparent diffusion coefficient (ADC) and average tumour mean kurtosis (MK) (p -value=0.02; Fig.1); IDHmut 1p/19q retained and IDHwt gliomas had different ADC values, average MK and intra-cellular volume fraction (ficvf) (p -value=0.004; Fig.2). The area under the receiver-operating characteristic curve showed a moderate (0.72-0.75) diagnostic ability of all DTI, DKI and NODDI metrics to distinguish patients with IDHmut from those with IDHwt gliomas. Finally, CSF volume fraction (fiso) and ficvf differed (p -value=0.002; Fig.2) between 1p/19q retained and codeleted gliomas, although the significance for differentiating IDHmut from IDHwt gliomas was weak (p -value=0.05-0.07; Fig.1).

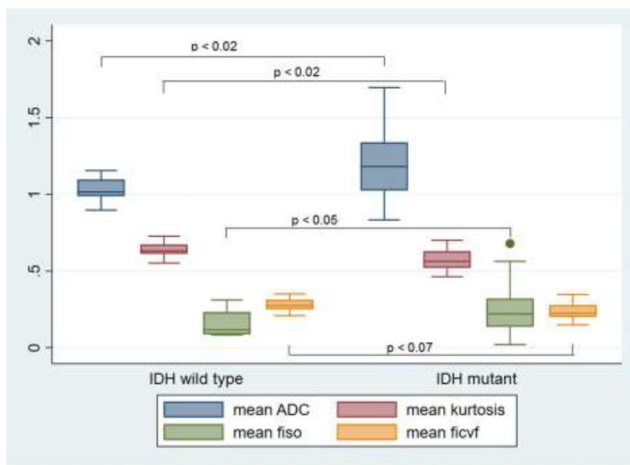


Fig. 1

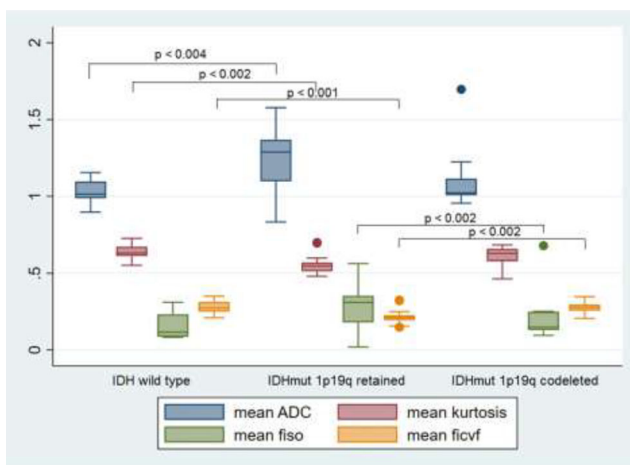


Fig. 2

Discussion & Conclusion

Microstructural dMRI techniques differentiated IDHwt from 1p/19q retained IDHmut gliomas, but only NODDI parameters could reliably probe the 1p/19q codeletion effect on the tumour microstructure in the IDHmut tumours.

1-O41

ASL-PERFUSION IN PREDICTING OF BRAIN GLIOMA MALIGNANCY AND IDH1 STATUS

A. Batalov¹, N. Zakharova¹, S. Goriaynov¹, E. Pogosbekian¹, A. Potapov¹, I. Pronin¹

¹ Federal State Autonomous Institution «N. N. Burdenko National Scientific and Practical Center for Neurosurgery» of the M, Moscow, RUSSIA

Introduction

Purpose: to assess correlation between the tumor blood flow (TBF) in the supratentorial brain gliomas on the base of ASL-perfusion with

histopathological markers of malignancy (WHO Grades, IDH-1 status, Ki-67 value).

Methods

The study group included 253 patients (135 female, 118 male, avg. age 45 ± 15 years) with primary supratentorial gliomas: 65 - low-grade (LGG) and 188 - high-grade (HGG (68-Gr.III, 120-Gr.IV)) status. Patients were examined on 3T MR-scanner. The pseudo-continuous ASL (pcASL) technique was used to determine TBF. TBF was normalized regarding to intact white matter (nTBF). In 72 of 120 patients with HGG immuno-histochemical assessment was conducted to determine the IDH-1 mutation (30-IDH1-mutant, 42-IDH1-wild-type). Ki-67 index was evaluated in 64 of 253 patients after tumor resection. All patients were divided into 2 groups: with a low proliferative activity of tumors (Ki-67 from 0 to 9%) and with a high level of cellular proliferation (Ki-67 more than 10%).

Result

TBF and nTBF in groups of LGG and HGG was significantly different ($p < 0.0001$). The sensitivity and the specificity of ASL in diagnosis of LGG and HGG were 85.1% and 96.9%, accordingly, AUC 0.954, cut-off-64 ml/100g/min. Maximum and normalized TBF in glioblastomas was significantly higher than in anaplastic astrocytomas. However, ASL showed low sensitivity and specificity in differential diagnosis within of high grade glioma's group. TBF and nTBF in IDH1-wild-type HGG was significantly higher than in IDH1-mutant HGG ($p < 0.001$). The sensitivity and the specificity of ASL in diagnosis of IDH1-wild-type and IDH1-mutant HGG were 64.3% and 84.1%, accordingly, AUC 0.750, cut-off - 84,2 ml/100g/min. We found the significant positive correlation between TBF and Ki-67 value ($r = 0.64$, $p < 0.001$). TBF and nTBF in groups of low- and high-Ki-67 values was significantly different. The sensitivity and the specificity of ASL in diagnosis of this two groups of gliomas were 82.6% and 85.4%, accordingly, AUC 0.837, cut-off - 66,7 ml/100g/min.

Discussion & Conclusion

pcASL is a reliable quantitative technique for the differential Ds between LGG and HGG, differentiation between IDH1-mutant and IDH1-wild-type of HGG, and between gliomas with low and high Ki-67 values as well.

The study was supported by RFBR N 18-29-01018.

1-O42

AN OBSERVATIONAL STUDY TO EVALUATE THE MANAGEMENT OF PATIENTS WITH CHRONIC HEADACHE WITH REFERRAL FROM PRIMARY CARE TO DIRECT ACCESS TO MAGNETIC RESONANCE IMAGING (MRI) COMPARED TO NEUROLOGY SERVICES

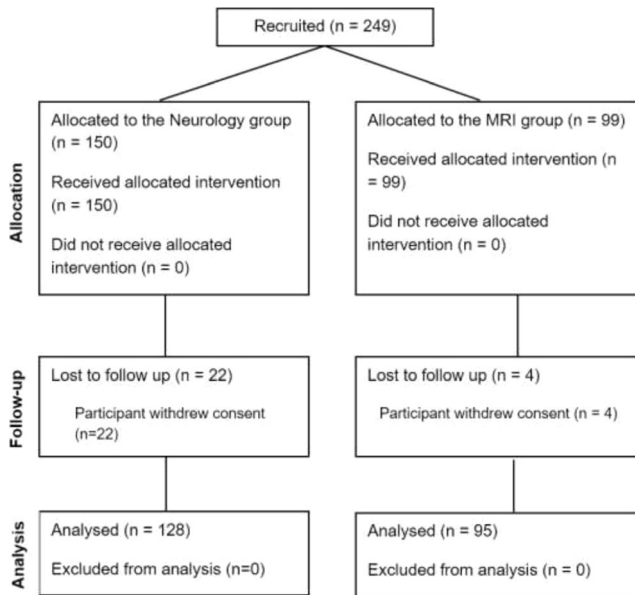
M. Asif¹, T. Rua^{1,2}, Y. Akande¹, C. Margariti³, J. Turville¹, R. Razavi^{1,3}, J. Peacock⁴, J. Shearer², V. Goh^{1,3}, P. McCrone², S. Afridi⁵

¹ Department of Clinical Imaging and Medical Physics, Guys and St Thomas NHS Foundation Trust, London, UNITED KINGDOM, ² Kings Health Economics, Kings College London, London, UNITED

KINGDOM,³ School of Biomedical Engineering and Imaging Sciences, Kings College London, London, UNITED KINGDOM,⁴ School of Population Health and Environmental Sciences, Kings College London, London, UNITED KINGDOM,⁵ Department of Neurology, Guys and St Thomas NHS Foundation Trust, London, UNITED KINGDOM

Introduction

To evaluate two existing clinical pathways used in the management of patients with chronic headache based on referral from General Practitioners (GPs) for a Neurologist appointment or direct access to Magnetic Resonance Imaging (MRI) brain scan.



Methods

A pragmatic, non-randomised, prospective single-center study compared the two clinical pathways used in the management of chronic headache following referral from GPs that differed in the first appointment, either a Neurology appointment or a MRI brain scan. Subsequent participants' use of health care services and costs were estimated using primary and secondary care databases and questionnaires at baseline, 6 and 12 months post-recruitment. Cost analyses at 6 and 12 months were compared using generalized linear models (GLM). Secondary outcomes assessed access to care, headache burden and self-perceived quality of life using headache-specific (MIDAS, HIT-6) and general questionnaires (EQ-5D-5L).

Result

The MRI group improved access to care (39.2 and 70.4 days from referral to MRI scan and report, respectively) compared to the Neurology group (110 days) ($p < 0.001$). The Neurology group was associated with a trend ($p > 0.05$) of better self-perceived quality of life using a generic questionnaire and an opposite trend from headache-specific questionnaires, exhibiting a trend ($p > 0.05$) of higher headache burden (HIT-6 score, MIDAS score and headache days). Mean (SD, n) cost up to 6 months post-recruitment per participant was £578 (£420, n=128) for the

Neurology group and £245 (£172, n=95) for the MRI group, leading to an estimated cost difference of £333 (95% CI £253 to £413, $p < 0.001$). The cost difference at 12 months increased to £518 (95% CI £401 to £637, $p < 0.001$). This cost difference derives from the lower utilization of participants in the MRI group of both GP visits (1.8 vs 1.2, $p = 0.006$) and hospital appointments (2.5 vs 0.3, $p < 0.001$) and despite the higher utilization of MRI scans (0.6 vs 1.1, $p < 0.001$).

Discussion & Conclusion

Direct referral to brain MRI from Primary Care led to cost-savings and quicker access to care compared to the management of chronic headache with referral to Neurology services. Direct referral to MRI should be incentivised for a subset of patient population more likely to be reassured by a negative brain scan.

1-O43

DOSE FINDING STUDY OF GADOPICLENOL, A NEW MACROCYCLIC GADOLINIUM-BASED CONTRAST AGENT (GBCA), IN MRI OF CENTRAL NERVOUS SYSTEM

*N. Anzalone*¹

¹ University Vita e Salute, Milan, ITALY

Introduction

The aim of this study was to determine a safe and effective dose of gadopixelenol, a new high relaxivity macrocyclic GBCA, based on the Contrast-to-Noise Ratio (CNR) and compared to gadobenate dimeglumine in patients with brain lesions.

Methods

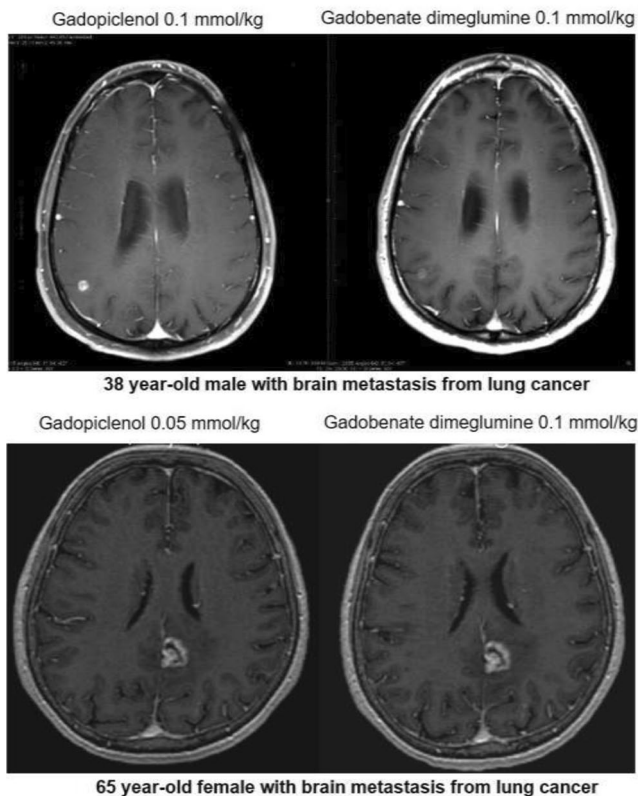
This double-blind, randomized, dose-parallel group and cross-over study included patients with known or highly suspected focal areas of disrupted blood brain barrier. Patients were randomized to one of four doses of gadopixelenol (0.025, 0.05, 0.1, 0.2 mmol/kg) and to one series of two MRIs: gadopixelenol and then gadobenate dimeglumine or vice versa, separated by a wash out period ranging from 2 to 14 days. Three independent off-site blinded readers performed the signal intensity measurements. Adverse events were collected up to one day post second MRI.

Result

The study population included 272 patients (58.5% females) with a mean \pm SD age of 53.8 ± 13.6 years. The superiority of gadopixelenol over gadobenate dimeglumine was statistically demonstrated at 0.2 and 0.1 mmol/kg for all readers with an increase in CNR $> 30\%$. At 0.05 mmol/kg, gadopixelenol showed a similar CNR as gadobenate dimeglumine at 0.1 mmol/kg (Figure 1). A linear relationship between CNR and dose of gadopixelenol was demonstrated for all readers. Similar results were observed for the other quantitative assessments (lesion to brain ratio and contrast enhancement percentage). When comparing paired images for diagnostic preference, at the same dose of 0.1 mmol/kg, the readers mostly prefer gadopixelenol (45.2% to 86.8% of cases) or express no preference (9.4% to 49.1%). With gadopixelenol at a dose of 0.05 mmol/kg, all

readers predominantly reported no preference between GBCAs (46.5% to 77.6%). Similar rates of adverse reactions were reported with gadopicolenol (11.7%) and gadobenate dimeglumine (12.1%).

Figure 1: Examples of MR images



Discussion & Conclusion

Gadopicolenol at 0.1 mmol/kg led to significant higher CNR, and at 0.05mmol/kg showed similar CNR magnitude as compared to gadobenate dimeglumine at the standard dose of 0.1 mmol/kg. A good safety profile was observed for both doses.

1-O44

SUPRA- AND INFRATENTORIAL ATROPHY FOLLOWING CLINICALLY ISOLATED SYNDROMES: A 30-YEAR FOLLOW-UP STUDY

*L. Haider*¹, K. Chung¹, G. Birch¹, A. Eshaghi^{1,3}, S. Mangesius⁴, F. Prados^{1,3,5}, D. Altmann^{1,6}, O. Ciccarelli^{1,7}, F. Barkhof^{1,3,7,8}, D. Chard^{1,7}

¹ NMR Research Unit, Queen Square Multiple Sclerosis Centre, University College London Institute of Neurology, UK, London, UNITED KINGDOM, ² Department of Biomedical Imaging and Image Guided Therapy, Medical University of Vienna, AUT, Vienna, AUSTRIA, ³ Centre for Medical Image Computing (CMIC), Department of Medical Physics and Biomedical Engineering, University College, London, UNITED KINGDOM, ⁴ Department of Radiology, Medical University Innsbruck, AUT, Innsbruck, AUSTRIA,

⁵ Universitat Oberta de Catalunya, Barcelona, Spain, Barcelona, SPAIN, ⁶ Medical Statistics Department, London School of Hygiene and Tropical Medicine, London, UK, London, UNITED KINGDOM, ⁷ National Institute for Health Research (NIHR) University College London Hospitals (UCLH) Biomedical Research Centre, UK, London, UNITED KINGDOM, ⁸ Department of Radiology and Nuclear Medicine, VU University Medical Centre, Amsterdam, NL, Amsterdam

Introduction

Objectives: Brain atrophy, and the neurodegeneration underlying it, starts early in multiple sclerosis (MS), however the long-term clinical relevance of early atrophy is not known. We aimed to assess brain atrophy rates following clinically isolated syndromes (CIS) suggestive of MS, and their relationship with long-term clinical outcomes.

Methods

Methods: 132 people presenting with a CIS were recruited between 1984–87 and followed up clinically and with magnetic resonance imaging (MRI) one, five, ten, 14, 20 and now 30 years later. Using the MRI scans, third ventricular width and medullary width were measured. Clinical outcomes (CIS, relapsing remitting (RR) and secondary progressive (SP) MS, and death due to MS) and expanded disability status scale (EDSS) scores were determined at 30 years.

Result

Results: Infratentorial atrophy, as measured by the change in medullary width (MEDW) 0-5 differed significantly between CIS vs. SPMS ($p=0.000$) and CIS vs. MSRSD ($p=0.005$). Supratentorial atrophy, measured by the change in third ventricular width (TVW) 0-10 did not differ over 0-5 years, but did over 0-10 years between CIS vs. SPMS ($p=0.048$) and CIS vs. MSRSD ($p=0.043$). The change in medullary width and white matter lesions from 0-5 years was associated with Expanded Disability Status Scale scores at 30 years, correcting for the total intracranial volume and gender giving an R^2 of 0.413, $p=0.000$.

Discussion & Conclusion

Conclusions: Medullary atrophy measurements within 5 years of a CIS, and third ventricular width within 10 years, are related to clinical outcomes over the next 20 to 25 years. This suggests that the processes underlying brain atrophy, and ultimately less favourable clinical outcomes, are already active at, or soon after, the clinical onset of MS.

1-O45

THE DIAGNOSTIC VALUE OF SUSCEPTIBILITY-WEIGHTED IMAGING IN MULTIPLE SCLEROSIS: THE CENTRAL VEIN SIGN AND IRON RINGS ARE SPECIFIC MARKERS OF MULTIPLE SCLEROSIS LESIONS

*M. Clarke*¹, L. Pessini Ferreira², D. Pareto², G. Arrambide⁴, M. Alberich¹, F. Crescenzo⁵, A. Garcia Vidal¹, M. Tintore⁴, C. Auger², N. Evangelou⁶, A. Rovira^{1,2,3}

¹ Vall d'Hebron Research Institute, Department of Radiology, Barcelona, SPAIN, ² Vall d'Hebron University Hospital, Department of Radiology, Barcelona, SPAIN, ³ Universitat Autònoma de Barcelona, Barcelona, SPAIN, ⁴ Vall d'Hebron University Hospital, Centre d'Esclerosi Múltiple de Catalunya (Cemcat), Barcelona, SPAIN, ⁵ University of Verona, Department of Neurosciences, Biomedicine and Movement Sciences, Verona, ITALY, ⁶ University of Nottingham, Division of Clinical Neuroscience, Nottingham, UNITED KINGDOM

Introduction

The 2017 McDonald diagnostic criteria for multiple sclerosis (MS) incorporate oligoclonal bands (OCB) testing as an alternative to dissemination in time (DIT). This has increased their sensitivity but decreased their specificity. New MS-specific biomarkers are needed to prevent misdiagnosis.

We aimed to assess the prevalence and diagnostic value of white matter lesions (WMLs) with central veins (CVs) and iron rings (IRs), detected on clinical 3T SWI, in patients with clinically isolated syndrome (CIS) and MS-mimicking disorders.

Methods

CIS patients were scanned within 5 months of the first attack and had 1–5 years follow-up. Each patient had a 2D/3D FLAIR, used to identify WMLs >3mm, and SWI, to identify CVs and IRs. The radiological diagnoses made using CVs and IRs were compared to the known clinical diagnoses. For CIS patients who did not fulfil DIS+DIT at baseline, the added value of CVs and IRs in combination with DIS was assessed and compared to DIS+OCB.

Result

112 CIS patients and 34 patients with MS-mimicking conditions were included. 94 CIS patients had clinically defined MS at follow-up. A total of 953 WMLs were analysed. CIS patients had a median of 2 WMLs with CVs (range 0–20) and 48% of them had at least 1 lesion with an IR (range 0–8). Non-MS patients had a median of 1 WML with CVs (range 0–6) and none had any WMLs with IRs. The sensitivity and specificity of using at least 2 WMLs with CVs (2 CVs) to classify patients as MS and non-MS were 71.3% and 69.2%. When at least 1 WML with an IR (1R) was used, the sensitivity and specificity were 57.5% and 100%.

57 CIS patients did not fulfil DIS+DIT at baseline and 49 of them had their OCB tested. DIS+OCB resulted in 31 extra diagnoses (sensitivity: 79.5%; specificity: 100%) compared to DIS+DIT alone. In comparison, DIS+2CVs resulted in 22 extra diagnoses (sensitivity: 53.9%; specificity: 94.4%) and DIS+1R resulted in 17 extra diagnoses (sensitivity: 43.6%; specificity: 100%).

Discussion & Conclusion

CVs and IRs, detected on clinical 3T SWI images, appear to be highly-specific markers of MS WMLs. Their role in MS diagnosis, when OCB testing is not possible, should be assessed in prospective, multi-centre studies.

2. INTERVENTIONAL

2-01

EMERGENCY EVERSION CAROTID ENDARTERIECTOMY IN THROMBECTOMY STROKE PATIENTS

*O. Nikoubashman*¹, R. Singh¹, J. Kalder², A. Riabikin¹, H. Ridwan¹, A.E. Othman³, A. Reich⁴, A. Mpotsaris¹, M. Wiesmann¹

¹ University Hospital RWTH Aachen, Department of Neuroradiology, Aachen, GERMANY, ² University Hospital RWTH Aachen, Department of Vascular Surgery, Aachen, GERMANY, ³ University Hospital Tübingen, Department of Tübingen, Tübingen, GERMANY, ⁴ University Hospital RWTH Aachen, Department of Neurology, Aachen, GERMANY

Introduction

Data in the literature suggest that thrombectomy with emergency carotid artery stenting (CAS) in acute stroke is associated with an increased hemorrhage rate. As we perform thrombectomy under general anesthesia, we avoid emergency CAS and perform emergency eversion carotid endarterectomy (eCEA) in the same anesthesia session in our angiography suite. We perform eCEA 1) before thrombectomy whenever necessary and 2) after thrombectomy whenever possible. In this analysis we focus on hemorrhage rates in patients who receive thrombectomy and emergency CAS vs. eCEA.

Methods

We retrospectively analyzed data from our prospectively maintained stroke registry and identified 31 thrombectomy patients who received emergency eCEA and 117 patients who received emergency CAS with GP2b/3a-inhibitors or dual antiplatelet therapy. One of the former was excluded from further analysis, because there was intracerebral hemorrhage prior to thrombectomy and one of the latter was excluded, because hemorrhage was due to vessel perforation during the intervention, which left 146 patients to be included in our study.

Result

Baseline characteristics (NIHSS, age, sex, rate of IV and IA thrombolysis, patients with unknown time window) were comparable ($p \geq .057$). Symptomatic hemorrhage rate was 0% (0/30) in the eCEA group and 3% (4/116) in the CAS group ($p = .358$). Parenchymal hemorrhage rate was 7% (2/30) in the eCEA group and 14% (16/116) in the CAS group ($p = .235$). Both parenchymal hemorrhages in the eCEA group occurred during the intervention and were diagnosed on immediate post-interventional imaging, whereas 5 parenchymal hemorrhages in the CAS group occurred during the intervention and the remaining 11 hemorrhages occurred within three days after the intervention ($p = .098$). There were no delayed hemorrhages in the eCEA group. Clinical outcome upon 90 days was comparable with 38% and 44% of patients achieving good clinical outcome (mRS 0–2) ($p = .545$).

Discussion & Conclusion

Parenchymal hemorrhage rate was half as high in the eCEA group, albeit this difference did not reach statistical significance. All hemorrhages in the eCEA group occurred during the intervention, implying that hemorrhage in this group was likely to be caused by reperfusion injury, whereas delayed hemorrhage is likely to be caused by dual antiplatelet therapy.

2-O2

HEMORRHAGE RATE AND ITS RISK FACTORS IN THROMBECTOMY PATIENTS RECEIVING EMERGENCY CAROTID ARTERY STENTING

*O. Nikoubashman*¹, R. Singh¹, A. Riabikin¹, H. Ridwan¹, A. Reich², A.E. Othman³, A. Mpotsaris¹, M. Wiesmann¹

¹ University Hospital RWTH Aachen, Departement of Neuroradiology, Aachen, GERMANY, ² University Hospital RWTH Aachen, Departement of Neurology, Aachen, GERMANY, ³ University Hospital Tübingen, Departement of Radiology, Tübingen, GERMANY

Introduction

Hemorrhage rates in the literature after thrombectomy with emergency carotid artery stenting (CAS) in acute stroke vary considerably, ranging from 0–22% for symptomatic hemorrhage and from 0–43% for parenchymal hemorrhage. Larger studies dealing with this issue consist of multicenter studies with heterogeneous patient cohorts and widely differing periprocedural management. This is why it was our aim to analyze parenchymal hemorrhage rates (ECASS PH2) in a homogeneous patient cohort of thrombectomy patients with additional CAS and to identify risk factors for hemorrhage, hypothesizing that intravenous thrombolysis and high blood pressure during the intervention are risk factors for hemorrhage.

Methods

We retrospectively analyzed data from our prospectively maintained stroke registry and identified 122 consecutive patients who received thrombectomy and emergency CAS. We focused our analysis on parenchymal hemorrhage rates in 117 patients, who received CAS with GP2b/3a-inhibitors or dual antiplatelet therapy, which is the standard in our institution. One patient was excluded from further analysis, because hemorrhage was due to vessel perforation during the intervention, which left 116 to be included.

Result

Symptomatic hemorrhage rate was 3% (4/116) and parenchymal hemorrhage rate was 14% (16/116). 5 (4%) of these parenchymal hemorrhages occurred during the intervention and were diagnosed on immediate postinterventional CT, whereas 8 hemorrhages occurred on the first day after intervention and the remaining 3

hemorrhages occurred on the second (n=1) and third (n=2) days. All hemorrhages occurred under either GP2b/3a-inhibitor or dual antiplatelet therapy. There was re-hemorrhage in 7 (44%) cases. All but one hemorrhage, which occurred two days after the intervention and was located atypically, were located within the infarcted area, with 13 of 16 (81%) hemorrhages being mainly located in the basal ganglia. Older age was a risk factor for hemorrhage (p=.03), whereas IV thrombolysis (p=.782), IA thrombolysis (p=.357), the occurrence of contrast extravasation (p=.759), unknown time window (p=.772), NIHSS (p=.090), initial infarction size (p=.926), and blood pressure (p>=.266) were not.

Discussion & Conclusion

There is an increased hemorrhage risk in thrombectomy patients who receive emergency stenting with dual antiplatelet therapy. IV thrombolysis and high blood pressure are no risk factors for hemorrhage, whereas older age is.

2-O3

STASIS INDEX FROM QUANTITATIVE HEMODYNAMIC ASSESSMENT AS A PREDICTOR OF BRAIN ARTERIOVENOUS MALFORMATION OBLITERATION AFTER GAMMA KNIFE SURGERY

*Y. Hu*¹, C. Lee², H. Wu¹, H. Yang², T. Lin¹, C. Luo¹, W. Guo¹, Y. Kao³, W. Chung², C. Lin¹

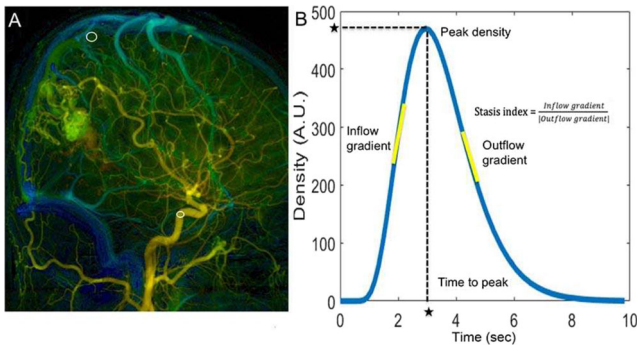
¹ Department of Radiology, Taipei Veterans General Hospital, Taipei, TAIWAN, ² Neurological Institute, Department of Neurosurgery, Taipei Veterans General Hospital, Taipei, TAIWAN, ³ Department of Biomedical Imaging and Radiological Science, National Yang-Ming University, Taipei, TAIWAN

Introduction

Gamma Knife surgery (GKS) obliterates 60%–80% of brain arteriovenous malformations (BAVMs). However, the hemodynamic effect on GKS outcomes is relatively unclear. We used quantitative digital subtraction angiography (QDSA) to explore this effect.

Methods

We retrospectively (2011–2017) included 98 patients with BAVM who received GKS alone. Two evaluators, blinded to the outcomes, analyzed the pre-GKS angiography and MR images to obtain the morphological characteristics and QDSA parameters. The time density curves of the arterial and venous regions of interest were used for hemodynamic analysis. The stasis index was defined as the inflow gradient divided by the absolute value of the outflow gradient. Patients' follow-up MR or DSA images were evaluated for the presence of complete obliteration (CO). Cox regression and Kaplan-Meier analyses were conducted to determine the correlations between the parameters and outcomes.



Result

Among the 98 patients, 63 (63.4%) achieved CO after GKS at a median latency period of 31 months. In the multivariate analyses with adjustment for age and sex, increased BAVM volume (HR 0.949, $p = 0.022$) was the independent demographic predictor, and venous stenosis (HR 2.595, $p = 0.009$), venous rerouting (HR 0.375, $p = 0.022$), and larger stasis index (HR 1.227, $p = 0.025$) were the independent angiographic predictors of CO. BAVMs with stasis index of >1.71 had a higher 36-month probability of CO than those with stasis index of <1.71 (61.1% vs 26.7%, $p = 0.045$).

Discussion & Conclusion

BAVMs with increased volume or venous rerouting were less likely to be obliterated. Venous stenosis and larger stasis index, indicating more stagnant venous outflow, may predict BAVM obliteration after GKS. QDSA analysis may help in predicting BAVM treatment outcomes and making therapeutic decisions.

2-O4

COMPLICATIONS IN POSTERIOR CIRCULATION MECHANICAL THROMBECTOMY. A RETROSPECTIVE REVIEW

*M.A. De Miquel*¹, L. Aja¹, S. Aixut¹, R. Barranco¹, O. Chirife¹, P. Cardona², H. Quesada², B. Lara², A. Paipa²

¹ Hospital Universitari de Bellvitge, Sección de Neuroradiología, L'Hospitalet de Llobregat, SPAIN, ² Hospital Universitari de Bellvitge, Servicio de Neurología, L'Hospitalet de Llobregat, SPAIN

Introduction

Vertebrobasilar stroke presents differences with carotid territory stroke. Diagnostic workout, imaging evaluation, time from symptoms onset and etiological frequency differ between supra and infratentorial regions. Mechanical thrombectomy is accepted as the best treatment in cases of ischemic stroke and adds some challenges in the posterior circulation. We present a review of our complications in terms of frequency, location and technique to help us in taking better treatment decisions.

Methods

This study is based in a retrospective review of our database. Since 2010 we have registered 629 cases of mechanical thrombectomy. Out of them,

60 (9.5%) cases corresponded to vertebrobasilar stroke and have been entered in this study.

Result

Out of 60 posterior circulation thrombectomies included in this review, no incidents have been recorded in 51 (85%) cases. The nine complicated cases corresponded to 5 (6.66%) dissections, 3 (5%) haemorrhages or contrast extravasation, and one (1.66%) case of puncture site hematoma. 17.5% of 23 treatments performed before 2015 achieved a mRS 0-3, while 48.4% of 31 thrombectomies done between 2015 and 2019 presented a good evolution.

Discussion & Conclusion

Dissection in atheromatous vertebral arteries resulted in bad prognosis in four out of five cases.

Mortality due to clinical worsening or directly attributed to the technique has been considered in 5 (6.66%) cases, most of them in keeping with dissection. Evolution of the material used for the treatment, mainly aspiration catheters, offer better guaranties to these patients.

2-O5

CUMULATIVE INCIDENCE OF RESTENOSIS IN THE ENDOVASCULAR TREATMENT OF EXTRA CRANIAL CAROTID ARTERY STENOSIS: META-ANALYSIS

*P. Clavel*¹, S. Hebert², C. Mounayer³, A. Rouchaud⁴, B. Marin⁵

¹ CHU Limoges, radiologie, Limoges, FRANCE, ² CHU Limoges, neurologie, Limoges, FRANCE, ³ CHU Limoges, radiologie, Limoges, FRANCE, ⁴ CHU Limoges, radiologie, Limoges, FRANCE, ⁵ CHU Limoges, radiologie, Limoges, FRANCE

Introduction

To assess the cumulative incidence of restenosis and stroke after stenting for cervical carotid artery stenosis, we performed a systematic review and meta-analysis.

Methods

We reviewed PubMed, Science direct and Scopus and included all studies reporting restenosis after stenting. Cumulative incidence of restenosis at 6 and 12 months were calculated. We also estimated the cumulative incidence of ipsilateral stroke within 30 days after stenting. Random effect meta-analysis and meta-regression were performed using relevant study level covariates. Sources of heterogeneity were investigated.

Result

Among 7 765 records, 40 studies were selected. 15 943 patients and 16 337 carotids were considered. The overall pooled cumulative incidence of restenosis $>50\%$ at 12 months was 5.7% (95%CI 3.8-8.6), $> 70\%$ at 12 months was 5.2% (3.3-8.2), $> 50\%$ at 6 months was 3.9% (2.2-6.8) and ipsilateral stroke within 30 days after stenting was 1.6% (1.0-2.5) without association with the use of an embolic protection device. We did not identify any relevant source of heterogeneity of the cumulative incidence

of restenosis >50% at 12 months. Mean age explained 80.9 % (R2=80.9%,p=0.01) of heterogeneities of restenosis >70% at 12 months. Presence of hostile neck explained 53.9%(R2 = 53.9%p=0.03) of heterogeneities of restenosis > 50% at 6 months.

Discussion & Conclusion

This meta-analysis showed a low cumulative rate of restenosis at 12 months and ipsilateral stroke within 30 days after stenting. Older age and hostile neck patients present a lower risk of in-stent restenosis. Embolic protection device was not associated with a lower risk of stroke.

2-O6

TREATMENT OF ESSENTIAL TREMOR (ET) AND PARKINSON DISEASE (PD) TREMOR WITH MRGFUS: PRELIMINARY LONG-TERM RESULTS AND EVALUATION OF IMAGING FINDINGS PREDICTIVE VALUE

*F. Bruno*¹, M.V.M. Micelli¹, L. Panebianco¹, S. Torlone¹, A. Corridore¹, M. Martino¹, A. Gagliardi¹, E. Tommasino¹, F. Arrigoni¹, A. Catalucci¹, M. Varrassi¹, A. Splendiani¹, C. Masciocchi¹

¹ University of L'Aquila, L'Aquila, ITALY

Introduction

To report our experience in the treatment of ET and PD tremor using MRgFUS thalamotomy and to evaluate the correlation between peri- and postprocedural imaging findings and treatment outcome

Methods

We evaluated 38 patients subjected to unilateral Vim ablation using MRgFUS In the period February 2018-March 2019 (18 ET, 20 PD tremor, mean duration of symptomatology 11.6 years). Pre and post-treatment evaluation included clinical evaluation using the Fahn-Tolosa-Marin scale (FTM) and the QUEST score. Sonication parameters and intraprocedural findings (accumulated thermal dose, ATD) were also recorded during all procedures. Instrumental MRI findings (lesion and edema size) were assessed after treatment.

Result

Treatment was effective (substantial and immediate reduction of tremor) in 36 out of 38 patients (93.3%). FTM scores decreased from mean values of 32.6 before treatment to 13.5 immediately after treatment. At 6 months, we found a minimal increase in mean FTM values due to the reappearance of tremor in 4 patients (p=0.132). In patients followed-up after 1 year, clinical evaluation showed a substantial stability of treatment effects. No major postoperative complications were recorded. We found a significant negative correlation between ATD size and FTM scores after the procedure, and a positive correlation between the presence of perilesional edema at 1 month with adverse clinical effects.

Discussion & Conclusion

MRgFUS thalamotomy is a safe and effective treatment option for tremor in patients with ET and PD. According to our preliminary results,

intraprocedural ATD and early postoperative MRI findings after the procedure may have a possible predictive value of treatment outcome after MRgFUS thalamotomy.

2-O7

6 TO 24 HOURS ENDOVASCULAR THROMBECTOMY FOR LARGE INTRACRANIAL VESSEL OCCLUSION WITHOUT PERFUSION CT PATIENT SELECTION: SINGLE CENTER EXPERIENCE

*A. Alexandre*¹, F. Giubbolini¹, I. Valente¹, E. Lozupone¹, F. D'Argento¹, C. Colosimo¹, A. Pedicelli¹

¹ Fondazione Policlinico Universitario A. Gemelli IRCCS, Roma, Italia. UOC Radiologia e Neuroradiologia., Roma, ITALY

Introduction

The effect of endovascular thrombectomy that is performed more than 6 hours after the onset of ischemic stroke has recently been shown by DAWN and DEFUSE-3 trial, and further validated by other studies. In these trials strict criteria were employed for patient selection, including perfusion CT.

We performed a retrospective single center evaluation of patient treated 6 to 24 hours after stroke onset without perfusion CT selection.

Methods

A retrospective single center evaluation of patient treated 6 to 24 hours after stroke onset in the period ranging from March 2016 to January 2019. On a total of 212 patients who received endovascular thrombectomy for a major intracranial vessel occlusion, we identified 55 patient who has been treated 6 to 24 hours after stroke onset. Patient has been selected on the basis of clinical and radiological criterias, including non contrast CT, multi-phase CT angiography.

Co-primary end points were the rate of functional independence (0, 1, or 2 on the mRS) at 90 days, and post-treatment symptomatic intracranial hemorrhage according to ECASS II criteria

Secondary end points were an early therapeutic response (defined as a decrease in the NIHSS score of > or = 10 from baseline or an NIHSS score of 0 or 1 on day 5, 6, or 7 of hospitalization or at discharge if it occurred before day 5), successful recanalization (which was defined as a grade of 2b or 3 on the mTICI scale on postprocedural conventional angiography)

Result

Out of 55 patient, 25 (45,4%) were functional independent at 90 days (mRS 0-2), of these 9 were mRS 0, 9 were mRS 1, and 7 were mRS 2; while the rate of symptomatic intracranial hemorrhage was 4 out 55 (7%), of which 1 was a parenchymal haematoma type 2, and 3 a parenchymal haematoma type 1.

Early therapeutic response was achieved in 22 patients out of 55 (40%) Successful recanalization (TICI score 2b or 3) was achieved in 44 patients out of 55 (80%).

Discussion & Conclusion

A larger population of patients can potentially benefit from endovascular thrombectomy, even without applying strict selection criterias, compared to DWAN and DEFUSE-3 trials.

2-O8

FEASIBILITY AND EFFICACY OF FLOW DIVERSION IN ANEURYSM MANAGEMENT OF SMALL CALIBER CEREBRAL ARTERIES: LONG TERM RESULTS OF A SINGLE CENTER EXPERIENCE WITH FRED JR

*N.D. Alberalar*¹, *D. Türeli*¹, *F. Baltacioglu*¹

¹ Marmara University School of Medicine - Department of Radiology, Istanbul, TURKEY

Introduction

Flow diversion is a valid option in endovascular treatment of challenging intracranial aneurysms. This study aims to evaluate feasibility and efficacy of Flow Re-Direction Endoluminal Device Jr (FRED Jr) designed for use in treatment of aneurysms of small caliber intracranial arteries.

Methods

Case files of 32 patients, and 37 aneurysms in total, treated with at least one FRED Jr. in a single tertiary referral center within a period of 42 months were retrospectively evaluated. Technical success, clinical outcomes, jailed and branch artery patencies and O'Kelly-Marotta (OKM) aneurysm occlusion grades were assessed based on immediate post-procedure controls along with 6th, 12th and 24th month follow-up digital subtraction angiography (DSA) images.

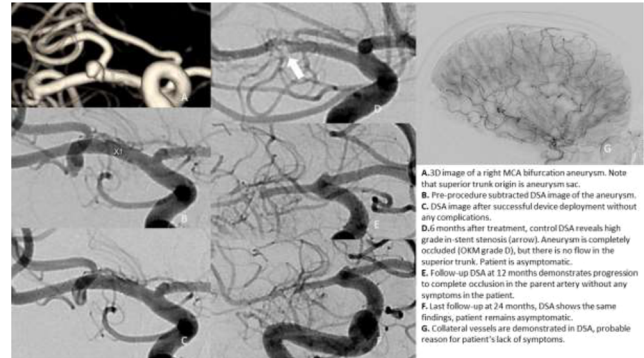
Result

FRED Jr. was deployed successfully, and without technical complications, in all cases. Immediate thromboembolic complications were observed in 4 patients (12.5%), all of which were discharged with unchanged modified Rankin scale scores. Compliance to follow-up at 6th, 12th and 24th months was 97.2% (n=36), 83.7% (n=31) and 29.7% (n=11), respectively. Complete to near-complete aneurysm occlusion was observed in 14 cases (38.8%) at 6 months; in 15 cases (48.4%) at 12 months; and in 7 cases (63.7%) at 24 months. Out of 24 aneurysms with branch arteries, 62.1% of all cases, branch artery occlusion was observed in 3 cases during follow-up; none was symptomatic. Complete occlusion of parent artery was observed in 1 patient during follow-up who remained asymptomatic. Patency of jailed arteries were preserved in all patients. None had permanent sequelae related to endovascular treatment.

Discussion & Conclusion

Lower occlusion rates, compared to other studies with flow-diverters in small vessels, are likely due to higher ratio of accompanying branch arteries; these are known for delaying thrombosis of aneurysm by ongoing blood supply demand to their corresponding territories. Occlusion of

parent and branch arteries were asymptomatic in all cases, implying formation of collateral vessels during gradual occlusion of aneurysms. Patency of jailed arteries underscores advantage of treatment with flow diversion in aneurysms of parent arteries with multiple branches. In conclusion, FRED Jr. is a feasible and safe treatment option for challenging aneurysms in small cerebral arteries.



3. HEAD & NECK

3-O1

COMPARISON BETWEEN CONTRAST-ENHANCED PROSET 3D-T1-TURBO FIELD ECHO(TFE) AND CONTRAST ENHANCED 3D- FLAIR VISTA FOR DIAGNOSING BELL'S PALSY

*J.H. Rhim*¹, *J. Kim*², *S. Park*¹

¹ SMG-SNU Boramae Medical Center, Seoul, SOUTH KOREA, ² Seoul National University Hospital, Seoul, SOUTH KOREA

Introduction

Principle of selective excitation (ProSet) is a type of fat suppression technique. The aim of this study was to investigate the usefulness of contrast-enhanced ProSet 3D-T1-TFE compared with contrast enhanced 3D-FLAIR VISTA for diagnosing Bell's palsy.

Methods

Total 92 facial nerves from 46 patients with unilateral Bell's palsy were analyzed in this study. Diagnosis of Bell's palsy was performed clinically and electrophysiologically. Two readers blinded to patients' information independently reviewed Proset 3D-T1-TFE and 3D-FLAIR VISTA images. Enhancement degree was visually assessed for each segment of facial nerves. Receiver operating characteristic (ROC) analysis was performed and sensitivity, specificity, accuracy, positive and negative predictive values were calculated. Signal intensities (SI) were measured in distal canalicular segment of facial nerves and brainstem in each sequence. SI ratio between the distal canalicular segment and brainstem in affected and unaffected facial nerves were compared. Interobserver agreements were also analyzed.

Result

The Area under the curve (AUC) of ProSet 3D-T1-TFE was greater than those of 3D-FLAIR VISTA for both readers (reader 1, 0.964 vs. 0.862; reader 2, 0.977 vs. 0.891). The sensitivities, specificities and accuracies were 96.7%, 91.3%, 94.2% for ProSet 3D-T1-TFE and 87.0%, 75.0%, 81.0% for 3D-FLAIR VISTA, respectively. The mean SI ratio between distal canalicular segment and brainstem was significantly higher in affected side than unaffected side in both sequences (0.56 vs. 1.28 on ProSet 3D-T1-TFE, $P < 0.001$; 0.70 vs. 1.09 on 3D-FLAIR VISTA, $P < 0.001$). The interobserver agreement for ProSet 3D-T1-TFE was higher than that of 3D-FLAIR VISTA (kappa -value, 0.847 vs. 0.493).

Discussion & Conclusion

ProSet 3D-T1-TFE is a very useful sequence for diagnosing Bell's palsy, with higher sensitivity, specificity, accuracy and interobserver agreement than 3D-FLAIR VISTA.

3-02

MICROSTRUCTURAL CHANGES IN CST ON CONTRALATERAL SIDES OF HIGH GRADE GLIOMAS

*E. Pogobekian*¹, A. Turkin¹, A. Baev¹, L. Fadeeva¹, I. Pronin¹

¹ FSBU N.N. Burdenko Neurosurgical Institute - department of Neuroimaging - Moscow - Russia, Moscow, RUSSIA

Introduction

High grade gliomas (HGG) usually expand by white matter [Kornienko V et al. Springer-Verlag 2009]. Thus infiltrative growth of lateral tumor to contralateral normal-appearing white matter (NAWM) is possible. Diffusion Kurtosis Imaging (DKI) [Jensen J et al. MRM 2005] and Spherical Mean Technique (SMT) [Kaden E et al. MRM 2016] are expansion of Diffusion Tensor Imaging approach, which can sense microstructural changes. Few researches demonstrated significant difference in NAWM between glioma patients and healthy controls [Horvath A et al., JMRI 2016; Turkin A et al., Medical Visualization 2017]. Estimation along tracts may be more sensitive to pathology [Reich DS, et al. AJNR 2008]. Aim of this work is to compare DKI and SMT metrics along corticospinal tract (CST) of normal appearing hemisphere in HGG patients with similar measurements in healthy volunteers.

Methods

In the study 13 HGG patients (6 men, 7 women, age from 29 to 65, average 50) and 13 healthy volunteers (8 men, 5 women; age from 21 to 55, average 34) were scanned on 3.0T MRI with following presets: voxel size 3x3x3 mm with interpolation to 1x1x1 mm, FOV 240 mm, b-values were 1000 and 2500 s/mm², 60 diffusion directions for each b-value. Fiber tracks were constructed by trained radiologist in TrackVis (www.trackvis.org). DKI and SMT values were measured in each voxel of CST. Voxels where mean kurtosis was greater than 3 or lower than 0 were excluded from statistical calculations. We processed voxelwise histogram analysis in order to get qualitative group comparison. For

quantitative comparison for each person we calculated averaged values in CST and compared groups using Mann-Whitney rank test.

Result

We didn't find significant difference between averaged CST values in groups ($p > 0.001$). But histograms showed noticeable deviation of medians for some DKI and SMT parameters (see image).

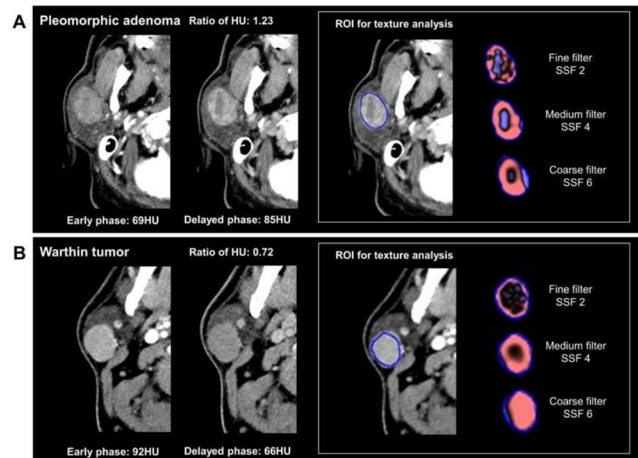
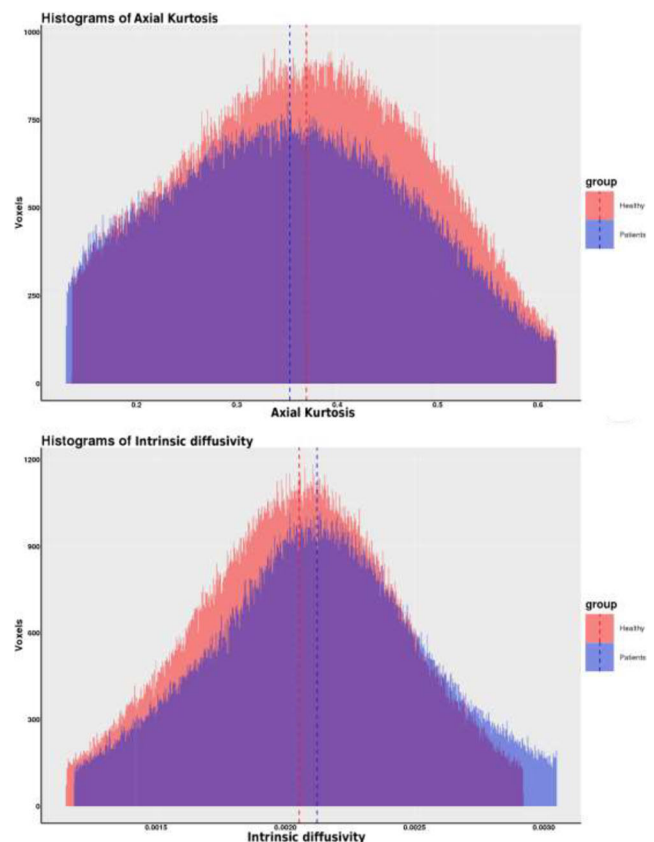


Figure. Enhancement pattern and texture analysis feature of pleomorphic adenoma (A) and Warthin tumor (B). Pleomorphic adenoma of the right parotid gland in a 57-year-old man shows gradual heterogenous enhancement. In contrast, Warthin tumor of right parotid gland in a 49-year-old man presents relatively homogenous enhancement and wash-out pattern. Corresponding representative texture images are shown with fine, medium, and coarse filters.



Discussion & Conclusion

Absence of changes in NAWM may be explained by small number of patients and healthy controls who participated in this study. Visible differences on some histograms led us suppose that DKI and SMT parameters may be helpful in future clinical diagnostics, but it must be proved on studies with larger groups.

3-O3

VISUALISATION OF THE INTRAPETROUS FACIAL NERVE CANAL ON BLACK BONE IMAGING AND A COMPARISON WITH PRE AND POST GADOLINIUM 3D SPACE SEQUENCES

*S. Kafiabadi*¹, S. Connor¹, B. Quirk¹

¹ King's College Hospital NHS Foundation Trust, London, UNITED KINGDOM

Introduction

Black bone MRI is a novel MRI sequence designed as an alternative to CT for osseous imaging. It employs a high-resolution volumetric sequence with a short TE and TR with a flip angle optimised to minimise soft tissue contrast, so enhancing bone-soft tissue boundaries. A series of papers have evaluated its potential contribution in the context of craniosynostosis, craniofacial disorders, 3D cephalometry and paediatric skull fractures. Whilst CT remains the imaging of choice to visualise the intrapetrous facial nerve canal in order to define the course of the facial nerve for petromastoid surgical approaches and involvement of the facial nerve by skull base pathology, it would be useful to explore the potential of black bone imaging to visualise the facial nerve canal and compare it with contemporary MRI sequences used for intrapetrous facial nerve imaging.

Methods

Black bone sequences (n=25) and pre and post gadolinium SPACE (Siemens -Sampling with perfection with application optimized contrasts using different flip angle evolution) sequences were reviewed by two independent neuroradiologists for the visibility of the intrapetrous facial nerve (labyrinthine, geniculate, tympanic, mastoid segments). Qualitative scoring of nerve visibility (on a 4 point Likert scale) and definition was assessed. Quantitative analysis of SNR and CNR was performed by placing regions of interest on the facial nerve. Results were compared with comparable literature values.

Result

Paired t tests were used to determine whether there was a statistical difference (p<0.05) between the sequences for the mean qualitative visibility and definition scores at each segment of the intrapetrous facial nerve canal. CNR was also compared between the sequences. Kappa tests was used to calculate qualitative scoring interobserver agreement. Black bone visibility scores compared favourably with the 3D SPACE sequence.

Discussion & Conclusion

Visibility of the intrapetrous segments of the petrous bone facial nerve on black bone imaging has been compared to more contemporary sequences.

The visibility and definition of the intrapetrous facial nerve canal on black bone imaging suggests a potential role in anatomical definition for surgical planning and in the context of skull base pathology.

3-O4

EXERCISE-INDUCED FLUCTUATION IN CEREBRAL BLOOD FLOW AMONG PATIENTS WITH MAIN ARTERIAL OCCLUSIONS IMPLIES A MECHANISM FOR CEREBRAL AUTOREGULATION: A PET STUDY

*M. Hiura*¹, T. Nariai², A. Muta², M. Sakata³, K. Wagatsuma³, T. Tago³, J. Toyohara³, K. Ishibashi³, K. Ishii³, Y. Katayama¹

¹ Aomori University - Center for Brain and Health Sciences, Aomori, JAPAN, ² Tokyo Medical and Dental University - Department of Neurosurgery, Tokyo, JAPAN, ³ Tokyo Metropolitan Institute of Gerontology - Research Team for Neuroimaging, Tokyo, JAPAN

Introduction

Cerebral autoregulation (CA) would be attributable to parenchymal arterioles and major cerebral arteries as well. To observe these two different roles for CA, changes in cerebral blood flow (CBF) were investigated while exercise caused increase and decrease in blood pressure (BP) among healthy volunteers and patients with major cerebral arterial occlusions.

Methods

Ten healthy male volunteers (HV) and five male patients with occlusive changes in the major arteries but were tolerable for regular exercise habit (IP) participated in this study. They performed 20 min cycling exercise and regional CBF (rCBF) were measured using oxygen-15-labeled water and PET at the baseline (Rest), onset (Ex1), continued phase (Ex2) and 10, 20 and 30 min after the cessation of exercise (Post 10, 20 and 30 min). Heart rate (HR) and mean blood pressure (MBP) were monitored. With the accumulated image and the measured arterial input function, rCBF was calculated using the autoradiographic method.

Result

These findings suggest that CA was identified at Ex2 in both HV and IP while CBF fluctuated at Ex1. Although BP increased greater in IP compared with HV, this fluctuation of CBF in IP was not larger than that in HV. By analysis with absolute values, global CBF (gCBF) increased by 10.5 % (P < 0.05) at Ex1 and tended to decrease at post 10 only in HV but not in IP. In both groups gCBF recovered to the level of Rest at Ex2. This changing pattern in CBF were similar when grey and white matters were analyzed separately. Brain areas where rCBF increased at Ex1 and decreased at post 10 were larger in HV compared with IP. For most of brain regions in the both groups, rCBF changed as the same manner in grey and white matters except for ischemic lesions in IP where rCBF did not changed during exercise.

Discussion & Conclusion

Differences in fluctuation of CBF elicited by exercise between IP and HV would be caused by structural alterations. Considering occlusive cerebral

arteries in IP, parenchymal arterioles, regulated by intrinsic factors which are associated with neuronal activation and astrocytic modulation, might have a role for the underlining mechanisms for changes in vascular resistance.

3-05

CT TEXTURE ANALYSIS FOR DIFFERENTIATION OF PLEOMORPHIC ADENOMA AND WARTHIN TUMOUR IN SALIVARY GLAND

M. Han¹, Y. Jung¹

¹ Department of Radiology, Ajou University Hospital, Suwon, SOUTH KOREA

Introduction

Pre-operative differentiation between pleomorphic adenoma and Warthin tumour is important, because the surgical strategies are different. This study aimed to evaluate diagnostic performance of CT texture analysis for differentiation of salivary gland tumours, pleomorphic adenomas and Warthin's tumours.

Methods

178 patients with pleomorphic adenomas and 84 patients with Warthin tumours who underwent two-phase CT were finally enrolled in this study. CT scans were obtained at early and delayed phases with scanning delays of 40 and 180 seconds. The CT texture analysis were performed on early and delayed phase scans separately, using TexRAD software that applies a filtration-histogram technique. The dynamic enhancement pattern of salivary gland tumours were also quantitatively evaluated with the Hounsfield units (HU). Differences between pleomorphic adenomas and Warthin tumour were analyzed using χ^2 test and independent t-test. ROC curve analysis was performed for discriminating tumours with texture parameters. Intraclass correlation coefficients (ICC) were estimated to assess intra- and inter-reader measurement reliability. Diagnostic performance of texture parameters were compared with conventional dynamic enhancement pattern using McNemar test.

Result

Warthin tumour showed cystic portion more frequently ($p<0.001$) and higher HU on pre-contrast ($p<0.001$) and early phase ($p<0.001$) enhanced images. Ratio of tumoral HU (HU on delayed phase/HU on early phase) was significantly different between two type of tumours ($p<0.001$). Standard deviation and entropy, texture parameters representing tumour heterogeneity, were significantly lower in Warthin tumours regardless of the type of filter used ($p<0.001$). Mean with coarse filter (AUC=0.944) and entropy with medium filter (AUC=0.901) were best discriminators between pleomorphic adenomas and Warthin tumours at early phase and delayed phase scans, respectively. Intra and inter-reader measurement reliability for mean and entropy are substantial to almost perfect (ICC, 0.65–0.99). Diagnostic accuracy of mean (90.5%) on early phase scan and entropy (84.7%) on delayed phase scan are not significantly different from the accuracy (89.3%) of conventional wash-out pattern for

distinguishing Warthin tumours from pleomorphic adenomas ($p=0.742$, $p=0.088$).

Discussion & Conclusion

Texture parameters from single phase CT scan is helpful for differentiating Warthin tumours from pleomorphic adenomas and the diagnostic performance is similar to two-phase enhancement pattern analysis.

4. PEDIATRICS

4-01

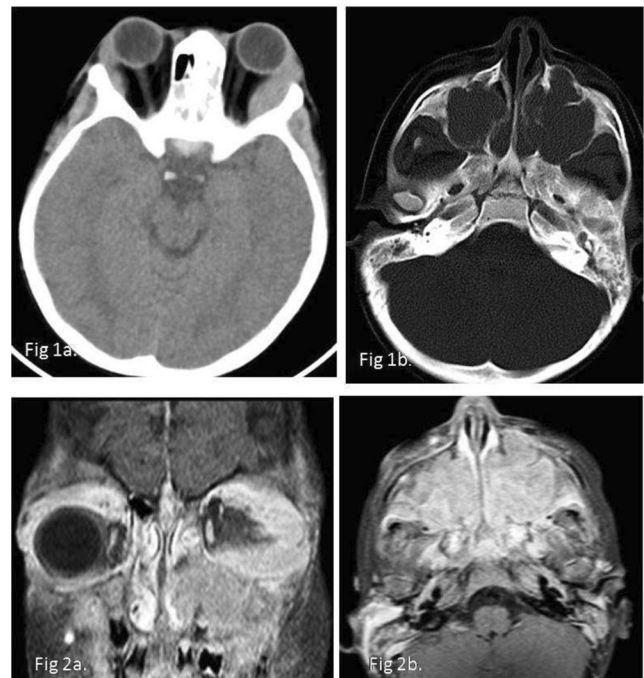
BILATERAL ORBITAL GRANULOCYTIC SARCOMA IN ACUTE MYELOID LEUKEMIA PRESENTING WITH PROPTOSIS

O. Yapici Ugurlar¹, H. Onder¹

¹ Okmeydani Research and Training Hospital, Istanbul, TURKEY

Introduction

Granulocytic sarcoma is a rare solid tumor derived from precursor cells of granulocytic series. Most commonly, these tumors happen in association with of acute myeloid leukemia (AML), but they may also occur with other myeloproliferative and myelodysplastic disorders. Almost any tissue can be affected, with skin and bone being the commonest. They have been reported in the skull, face, orbit, and paranasal sinuses. Here, we present radiological findings of a 6 years old girl with bilateral proptosis due to orbital granulocytic sarcoma.



Methods

A 6-years-old female patient, having the diagnosis of AML, referred to pediatric radiology department for evaluation of bilateral proptosis before her chemotherapy regimen has started. Cranial computerized tomography (CT) and magnetic resonance imaging (MRI) were performed respectively. According to the radiological work-up, the findings were consistent with GS. The patient started chemotherapy regimen. After five cycles of chemotherapy the periorbital swelling subsided. However the patient left the hospital without permission six days after the last chemotherapy and was lost to further follow-up.

Result

Non-contrast axial CT showed bilateral intraorbital solid tumors, prominent on the left side, homogenous slightly hyperdense with extension towards superior and lateral extra-conal fat planes and possibly touching the neighbouring extraocular musculature (Figure 1a). The paranasal sinuses, nasal cavity and nasopharynx were obliterated almost totally. Bilateral maxillary sinus walls were significantly thinned and partial erosion of the walls were noted due to infiltration (Figure 1b). MRI performed six days after CT, showed soft tissue mass in orbital region, paranasal sinuses, nasal cavity and nasopharynx, isointense in T2-weighted images, hypointense in T1-weighted images with homogenous enhancement after intravenous gadolinium administration (Figure 2a,b).

Discussion & Conclusion

GS is an unusual manifestation of AML, accounting for 3% of cases. The great majority occur in children before 15 years of age. It can also occur in association with other myeloproliferative or myelodysplastic disorders. The proptosis in GS is mainly due to leukemic infiltrates, retrobulbar hemorrhage, orbital muscle infiltration or venous blockage. Focal well-defined, homogeneous masses, may arise intraconally or extraconally, and invade orbital bones and contiguous structures. The primary differential diagnoses of an extraconal orbital mass in a child include rhabdomyosarcoma, metastatic neuroblastoma, Ewing's sarcoma, lymphoma, and idiopathic inflammatory pseudotumor. Chemotherapy is the main stay of treatment. The earlier detection of GS could better define prognosis.

4-O2

MAGNETIC RESONANCE IMAGING (MRI) PROTOCOL FOR CRANIOFACIAL PATHOLOGIES, REPLACING IONISING RADIATION-BASED COMPUTED TOMOGRAPHY

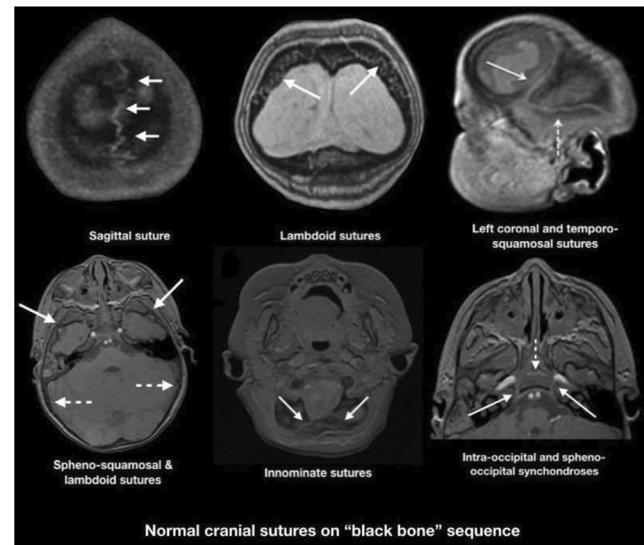
A.P. Tan¹

¹ National University Hospital, Singapore, SINGAPORE

Introduction

“Black bone sequence” has been used in our institution for a number of years, and is slowly finding its place in routine imaging of the craniofacial skeleton. We report our experience of utilising “black bone sequence” in children and young adults with craniofacial pathologies, ranging from craniosynostosis to traumatic injuries and craniofacial fibrous dysplasia. We will also present our MRI protocol for the imaging of

craniosynostosis, targeted at the demonstration of cranial vault anatomy as well as intracranial anomalies and potential complications associated with craniosynostosis.



Methods

Using the departmental database, patients who underwent “black bone” imaging in the preceding 3 years were identified and their imaging studies were retrieved. As this imaging sequence forms part of our routine clinical practice, ethical approval for this study was not required. All included imaging studies were reviewed by a paediatric neuroradiologist and comparison was made with computed tomography (CT) if available.

Result

We present 15 cases illustrating the reliability and potential benefits of our proposed MRI brain protocol which includes the “black bone sequence”, in the evaluation of craniofacial pathologies.

Discussion & Conclusion

Our proposed MRI brain protocol has the potential of replacing computed tomography (CT) as the modality of choice for the purpose of diagnosis and surveillance. Aside from the fact that MRI does not utilise harmful ionising radiation, it has excellent soft tissue resolution and hence is superior to CT in the detection of associated intracranial anomalies and potential complications (such as hydrocephalus and tonsillar herniation in the context of craniosynostosis).

4-O3

INVESTIGATING THE MYELINATION IN CHILDREN USING QUANTITATIVE T2 MAPPING

L. Porto¹, M. Bürger¹, U. Pilatus¹, A. Jurcoane¹, E. Elke Hattingen¹

¹ Neuroradiology, Frankfurt, GERMANY, ² Neuroradiology, Frankfurt, GERMANY, ³ Neuroradiology, Frankfurt, GERMANY, ⁴ Neuroradiology, Frankfurt, GERMANY, ⁵ Neuroradiology, Frankfurt, GERMANY

Introduction

This study investigates the age-related maturation of myelin in healthy children using quantitative T2 mapping. In conventional T2 weighted imaging, age-related changes are often only obvious until the age of two. The areas to myelinate last, the so-called terminal zones, were so far only described in conventional MRI. We chose these terminal zones to observe their myelination through quantitative T2 mapping.

Methods

We studied maps of T2 relaxation times, generated by a 1.5 tesla MRI of 13 subjects aged between 2 and 12 years. We measured T2 relaxation times in 8 different regions of interest (ROI) in the white matter of both hemispheres: frontal deep and subcortical, temporal deep and subcortical, parietal, occipital, corpus callosum and peritrigonal.

Result

In all ROIs except the corpus callosum, T2 relaxation times decreased continuously with increasing age (pearson correlation $r < -0,7$, $p < 0,05$). A mono-exponential function fitted the T2 decrease best. Absolute T2 values were highest in the subcortical frontal regions (max. 133ms). The negative slopes of the exponential function were steepest in the subcortical frontal regions followed by the subcortical temporal regions, indicating a more pronounced and persistent myelination in those regions. While high T2 relaxation times could be measured in the peritrigonal zones, the exponential curve did not show a steep decrease, which may indicate a slower myelination. The steepness of the T2 curve increased from the parietal, occipital and temporal up to the frontal lobes in this order. Afterwards subcortical regions myelinated, first temporal then frontal.

Discussion & Conclusion

The progression of changes related to myelination can be better defined after the 2nd year of life in the form of T2 relaxation time decrease correlated with increasing age. T2 mapping may provide a normal reference to pathologically altered development of myelination. The highest absolute T2 values and the steepest slope of the exponential function were located in the subcortical frontal region, indicating a faster and therefore not yet completed myelination.

4-04

GADOLINIUM RETENTION IN PEDIATRIC BRAIN: HYPERINTENSITY IN NUCLEUS DENTATUS AND GLOBUS PALLIDUS; WHEN IT APPEARS?

*R. Pitura*¹, G. Kruminā², D. Sosars³, I. Apine³

¹ Riga Stradins University - Faculty of Medicine, Riga, LATVIA, ² Riga Stradins University - Department of Radiology; Riga East University Hospital - Diagnostic Radiology Centre, Riga, LATVIA, ³ Children's Clinical University Hospital - Diagnostic Radiology Service, Riga, LATVIA

Introduction

Currently, there is no proof of clinical neuronal damage caused by Gadolinium deposits however the risk still persists, especially in

pediatrics due to longer life expectancy. By determining after how many contrast-MR examinations these deposits become obvious could point out the patients at highest risk and need for future observation.

Methods

Retrospective study performed at Children's Clinical University hospital included 37 pediatric patients (26 oncologic; 11 with other brain pathologies) with mean age 7.8 who received six or more post contrast head MRI with Gadodiamide. 193 subsequent pre-contrast MRI series were used for analysis. The regions of interest were pathology-free. The first examination was used as a reference. Other groups (Reference,1,2,3,4,5) were labeled based on serial number of contrast-MRI. Data were obtained from patient's medical records and radiological server. Signal intensity measurements were performed in axial pre-contrast T1wFFE images. Region of interest was 10mm² in four localizations: dentate nucleus (DN), globus pallidus (GP), pulvinar (TH) and pons (P), on the left side. Measurements were done by the same investigator repeatedly two times with 2-month interval. Mean DN:P and GP:TH ratios were calculated from both repetitions and compared with reference group using Wilcoxon signed rank test on SPSS 20.0.

Result

Statistically significant difference was found in both ratios (GP:TH; DN:P) between the reference and study group 4 ($p=0.037$; $p=0.016$) and study group 5 ($p>0.001$; $p=0.017$) with a confidence interval 95%.

Discussion & Conclusion

A significant change in GP: TH and DN:P ratios show that Gd deposits in globus pallidus and nucleus dentatus can be found in pediatric brain after the fourth Gd contrast MRI, suggesting that patients with at least 4 MRI with Gd are potentially in the risk of neuronal damage and development of neurological symptoms during their lives time until proven otherwise.

4-05

PRACTICAL CLINICAL USE OF MAGNETIC RESONANCE PERFUSION IMAGING FOR THE TREATMENT OF PEDIATRIC PATIENTS WITH MOYAMOYA DISEASE

*T. Nariai*¹, Y. Tanaka¹, S. Hara¹, Y. Ishii¹, T. Maehara¹

¹ Department of Neurosurgery, Tokyo Medical and Dental University, Tokyo, JAPAN

Introduction

We have been using various advanced magnetic resonance imaging (MRI) for the treatment and clinical research of pediatric patients with moyamoya disease. We report what type of new information has been obtained by them and how they improved the treatment of juvenile patients with moyamoya disease.

Methods

From 2001 to present, 205 juvenile patients (0-18 years old) were treated in our institute. All of them underwent at least one of perfusion MRI techniques, dynamic susceptibility contrast (DSC) MRI and/or arterial spin labeling (ASL) MRI.

Result

1) By setting threshold value for mean transit time (MTT) that is obtained by DSC-MRI, 85% of patients were selected for re-vascularized surgery using indirect bypass technique. MTT map was useful to decide the area of craniotomy. By this modification, good re-vascularization have been obtained without exception. 2) CBF map that is obtained with ASL-MRI was useful to evaluate the change (both amelioration by surgery and also worsening due to disease progress) of hemodynamic condition. Repeated measurement is available as the procedure is so non-invasive without any radiation exposure nor with use of contrast agent. 3) DSC- and ASL-MRI analysis revealed that hemodynamic condition start to ameliorate within two weeks after indirect bypass surgery.

Discussion & Conclusion

Because of its non-invasiveness, MRI must be the most suitable imaging modality for juvenile patients. Combined use of MR perfusion techniques for juvenile patients with moyamoya disease should be a key factor to perform a science-based treatment routinely and to broaden our knowledge on pathophysiology of this disease.

4-O6

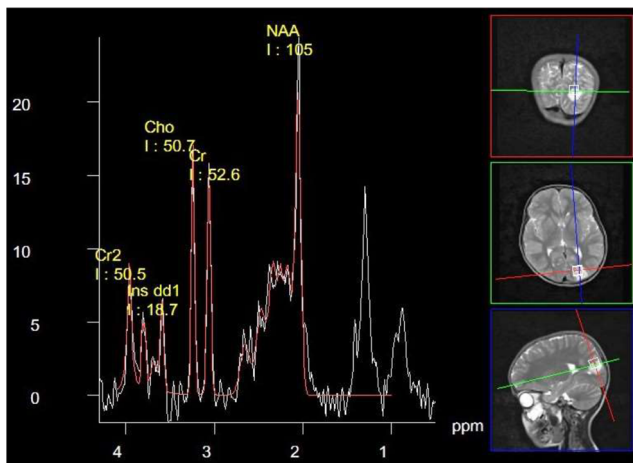
MAGNETIC RESONANCE SPECTROSCOPIC IMAGING IN NON-NEOPLASTIC PAEDIATRIC INTRACRANIAL LESIONS

*D.K. Narayana Vamyanmane*¹, S. Balakrishna¹, G. Sindu¹, L. Nidhi²

¹ Sri Siddhartha Medical College, Tumakuru, INDIA, ² The Aga Khan University Hospital, Nairobi, KENYA

Introduction

The intracranial non-neoplastic lesions, which may have similar imaging features with different pathological process, can be distinguished by in vivo magnetic resonance spectroscopic imaging (MRSI). Differentiating and categorizing non-neoplastic paediatric intracranial lesions with the help of metabolites in Magnetic Resonance Spectroscopic (MRS) Imaging using single voxel or multivoxel at spin echo 30ms and 135ms.



Methods

Paediatric patients with non-neoplastic intracranial lesions underwent magnetic resonance imaging and high-resolution proton MRS imaging before undergoing treatment. All intracranial non-neoplastic lesions studied, showed abnormal signal intensity on MR imaging compared with normal parenchyma. Proton MR spectroscopy was performed in single or multivoxel located within the lesion and perilesional areas. Proton MR spectroscopic images were acquired with spin-echo (SE) pulse sequences with parameters of 2000/135/128 (TR/TE/excitations) and 2000/30/128.

Result

The pattern of MRS metabolites consisted of abnormally increased or decreased metabolites. The intracranial non-neoplastic lesions showed metabolites consisted of Increased Choline, Inverted lactate or doublet peak, increased lipid, No reduction in N-acetyl aspartate (NAA) peak and decreased amino acids and creatinine (Cr). Phosphoserines and cyclopropane peaks are seen in tuberculoma. Diminished levels of NAA in early phase of ADEM and may persists in recovery phase. Lactate peak is increased and choline level maybe increased in acute phase or may be normal. In PVLM the concentrations of total N-acetyl aspartate and choline-containing compounds were reduced; and Myo-inositol concentrations were slightly increased. Elevated lactate helps in early detection of PVLM. The proton MR spectroscopy findings in toxic leukoencephalopathy revealed a decreased NAA peak & increase in Choline and lactate peak.

Discussion & Conclusion

In- vivo Magnetic Resonance Spectroscopic Imaging is non-invasive technique that gives relative concentrations of certain intracranial biochemical compounds. It provides biochemical information of the pathophysiological process of the tissue in question. Intracranial neoplastic and non-neoplastic lesions are characterized by using spectrum of different metabolites and its ratios – virtual biopsy.

4-O7

PREDICTION OF NEURODEVELOPMENTAL OUTCOME IN VERY PRETERM INFANTS WITH CEREBRAL MR SPECTROSCOPY AND DTI USING FEED-FORWARD NEURAL NETWORKS

*T. Janjic*¹, S. Pereverzyev Jr.¹, L. Lamplmayr¹, V. Wallner¹, R. Steiger¹, M. Zimmermann², M. Biermayr², V. Neubauer², U. Kiechl-Kohlendorfer², A.E. Grams¹, E.R. Gizewski¹

¹ Medical University of Innsbruck, Department of Neuroradiology, Innsbruck, AUSTRIA, ² Medical University of Innsbruck, Department of Paediatrics II, Neonatology, Innsbruck, AUSTRIA

Introduction

We aimed to evaluate if proton magnetic resonance spectroscopy (1H-MRS) and diffusion tensor images (DTI) performed in very preterm infants (VPIs) at term equivalent age (TEA) can predict their neurodevelopmental outcome (NDO) at the corrected age of

12 months using feed-forward neural-networks (fNNs).

Methods

From 346 VPIs born before 32 gestational weeks, 246 were excluded due to missing or poor-quality spectroscopy data and/or missing neurodevelopmental tests at 12 months corrected age. The data sets of 100 VPIs were considered for motoric and cognitive development, of whom 8 and 5, respectively were categorized as underdeveloped. We evaluated five potentially relevant metabolite ratios and two DTI characteristics, each in six different areas of the brain. We performed a feature selection algorithm for receiving a subset of those characteristics that we could assume as significant. To reduce bias by unbalanced classes, only VPIs that share approximate values of those characteristics with ones that had shown underdevelopment were considered for further calculations. On those smaller sets of VPIs, we finally constructed predictors using fNNs, which were able to predict underdevelopment in VPIs after considering the characteristics selected previously.

Result

The constructed predictors give a 100% accuracy in the case of the motoric underdevelopment. In the case of cognitive underdevelopment, we obtain a true positive rate of 100% and a positive predictive value of 83,3 %.

Discussion & Conclusion

1H-MRS and DTI obtained at TEA in VPIs allow prediction of their motoric and cognitive development at the corrected age of 12 months. The proposed approach using fNNs promises its use in clinical practice and could be useful for spotting those VPIs, who would mostly benefit from early intervention services.

4-08

ACCELERATED BRAIN AGING IN PREMATURE-BORN ADULTS

*D. Hedderich*¹, *M. Daamen*², *L. Scheef*², *H. Boecker*², *P. Bartmann*², *D. Wolke*³, *C. Zimmer*¹, *C. Sorg*¹, *C. Gaser*⁴

¹ Department of Diagnostic and Interventional Neuroradiology, Technical University of Munich, Munich, GERMANY, ² University of Bonn, Bonn, GERMANY, ³ University of Warwick, Coventry, UNITED KINGDOM, ⁴ University of Jena, Jena, GERMANY

Introduction

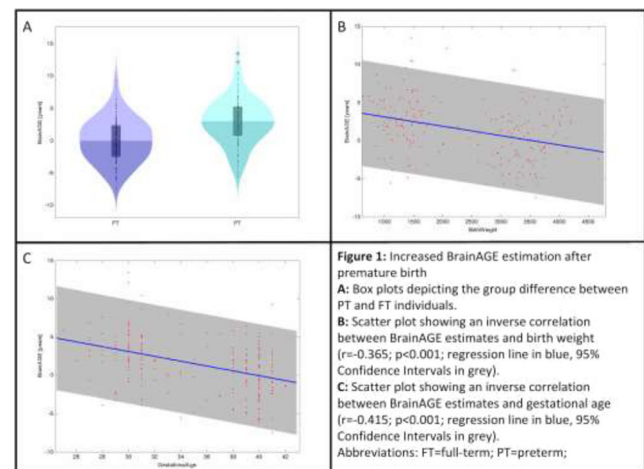
Premature birth is associated with disturbed brain development leading to structural brain alterations, which persist until adulthood, as well as with impaired cognitive and functional outcomes. Trajectories of brain development after premature birth are of particular interest but remain poorly studied. The present work aims at investigating estimations of biological brain age (i.e. “BrainAGE”) based on structural MRI in a large cohort of individuals born preterm (PT) and controls born at full term (FT).

Methods

T1-weighted structural MRI scans with an isotropic resolution of 1mm x 1mm x 1mm from 212 individuals (FT: 111; PT: 101; 124 male/88 female) were included. Participants were part of the Bavarian Longitudinal Study, followed from birth until adulthood and scanned approximately at the same age (mean age: 26.8±0.7 years). Individual offset of chronological brain age was estimated using the well-validated BrainAGE framework, which relies on complex multidimensional pattern analysis that aggregates the complex aging/developmental pattern across the whole brain to a single value. Estimated BrainAGE was compared between groups using two-sample t-tests and correlated with birth weight (BW) and gestational age (GA).

Result

BrainAGE estimations were increased for PT subjects by an overall mean of 2.9 years (see Fig. 1A). Increased BrainAGE showed inverse correlations with BW (-0.365; p<0.001; Fig 1B) and GA (-0.415; p<0.001; Fig 1C). We observed an emphasis of biological brain age increases for the right compared to the left hemisphere (3.2 vs. 2.3 years).



Discussion & Conclusion

We observed a considerable offset of biological brain age estimation towards older age in preterm-born adults based on structural MRI in a large cohort. This suggests accelerated brain aging in preterm-born adults and underscores evidence for lastingly shifted trajectories of brain development and aging processes. Our finding has implications for further investigations regarding the risk for age-related neurodegenerative disorders after preterm birth.

4-09

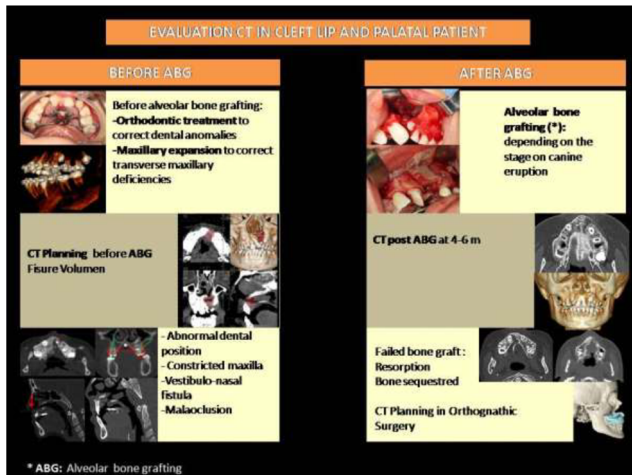
CT FINDINGS BEFORE AND AFTER SECONDARY BONE GRAFTING IN CLEFT LIP AND PALATE PATIENTS: OUR EXPERIENCE IN 120 PATIENTS

*M. Gómez-Chiari*¹, *E.J. Inarejos*², *J. Muchart*³, *M. Rebollo*⁴, *I. Barber De La Torre*⁵, *J. Munuera Del Cerro*⁶, *T. Maristany Daunert*⁷, *A. Rivera*⁸, *J. Rubio-Palau*⁹

¹ Hospital Sant Joan de Deu, Barcelona, SPAIN, ² Hospital Sant Joan de Deu, Barcelona, SPAIN, ³ Hospital Sant Joan de Deu, Barcelona, SPAIN, ⁴ Hospital Sant Joan de Deu, Barcelona, SPAIN, ⁵ Hospital Sant Joan de Deu, Barcelona, SPAIN, ⁶ Hospital Sant Joan de Deu, Barcelona, SPAIN, ⁷ Hospital Sant Joan de Deu, Barcelona, SPAIN, ⁸ Hospital Sant Joan de Deu, Barcelona, SPAIN, ⁹ Hospital Sant Joan de Deu, Barcelona, SPAIN

Introduction

Cleft lip and palate is the most frequent craniofacial anomaly. Treatment is complex and includes lip and palate repair (<1 y), bone graft before canine eruption and orthodontics. CT at diagnosis and follow-up is paramount for selecting the appropriate approach in each case.



Methods

We retrospectively reviewed the CT findings on patients with cleft lip and palate from January 2015 to April 2019 at a reference Pediatric Hospital. Images were evaluated on 3 planes with bone reconstruction algorithm and 3D post processed images.

Result

A total of 120 patients with this abnormality were included, 45 girls and 75 boys, aged from 6 to 22 years. There were 7 unilateral cleft lip and alveolar (UCLA), 80 unilateral cleft lip and palatal (UCLP) and 33 bilateral cleft lip and palate (BCLP). All patients underwent secondary bone grafting with particulate cancellous bone and marrow taken from the anterior iliac crest.

CT findings were classified according to:

- Dental anomalies (96% UCLP, 100% of BCLP and 70% en UCLA)
- Maxillary hypoplasia (93% UCLP, 100% of BCLP and 28% en UCLA)
- Malocclusion (70% UCLP, 96% of BCLP and 0% en UCLA)
- Naso-palatine fistula (7% UCLP, 24% of BCLP and 0% en UCLA)
- Velopharyngeal insufficiency (9% UCLP, 12% of BCLP)
- Temporalmandibular joint malformation in 2.5% UCLP
- Failed bone graft 6% in BCLP and 3.75% UCLP

Discussion & Conclusion

CT provides high anatomical resolution in the evaluation of patients with cleft palate abnormalities and other associated anomalies, and is useful for

treatment planning and follow-up. CT offers information about graft integration and quality of bone for future dental implant, dental eruption, occlusion and maxillary growth. These items should be assessed to plan a suitable orthodontic treatment with or without orthognathic or osteogenic distraction.

Treatment is important not only for aesthetic purposes but also for functional issues. It has a multidisciplinary and multistep approach from birth to adulthood. There are radiological key features that the radiologist should be aware in order to guide the surgeon and orthodontist to decide the best treatment option at different stages.

4-O10

HYPOTHALAMIC MALFORMATIONS IN PATIENTS WITH X-LINKED DEAFNESS AND INCOMPLETE PARTITION TYPE 3

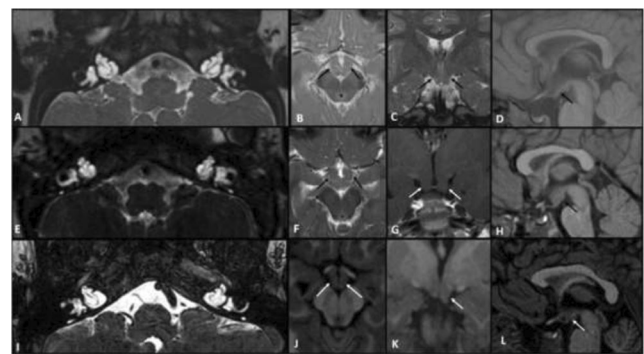
F. D'arco ¹, A. D'amico ², G.S. Colafati ³, D. Cicala ⁴, G. Talenti ⁵, K. Rajput ¹, L. Pinelli ⁶, A. Siddiqui ⁷

¹ Great Ormond Street Hospital, London, UNITED KINGDOM, ² University Hospital Federico II, Naples, ITALY, ³ Pediatric Hospital Bambino Gesù, Rome, ITALY, ⁴ Pediatric Hospital Santobono, Naples, ITALY, ⁵ Verona University Hospital, Verona, ITALY, ⁶ Spedali Civili Hospital, Brescia, ITALY, ⁷ King's College Hospital, London, UNITED KINGDOM

Introduction

X-linked deafness is a genetic disease characterised by mutation in POU3F4 gene.

Radiological diagnosis can be made on the basis of pathognomonic appearances of the cochlea (so called incomplete partition type 3) and large auditory canal. In this paper we describe a series of 15 patients from 6 institutions with this rare genetic anomaly in association with peculiar malformations in the hypothalamus.



Methods

Using EDM system and personal archives, a total of 17 patients with X-linked deafness, confirmed POU3F4 mutation and typical inner ear findings were found.

MRI of these 15 patients included high resolution T2 weighted images of the inner ears and standard sequences of the brain and were analysed in

consensus by the first and last authors for inner ears and other brain malformations.

Result

All of them had typical incomplete partition type 3 as described in literature (preserved interscalar septum and absent modiolus/lamina spiralis). 9/15 patients had mild but characteristic dysmorphism of the hypothalamus appearing thickened and irregular on axial, bulky on coronal and with a “bumpy” profile of the tuber cinereum on sagittal images. 3 patients demonstrated marked hamartoma-like enlargement of the hypothalamus. Only 3 patients had a normal looking hypothalamus.

Discussion & Conclusion

The existence of a syndrome characterised by mixed, bilateral, progressive sensorineural hearing loss in males with fixed stapes and high risk of stapes gusher was proposed for the first time in 1968. Subsequently several authors described a specific, symmetrical inner ear malformation in affected subjects (called IP3).

We describe for the first time a high prevalence of malformation of the hypothalamus in patients with POU3F4 mutation which are usually very subtle but may be also more pronounced.

Interestingly there is a possible role of this gene in the formation of the hypothalamic nuclei as well as regulation of the proglucagon promoter. This genetic link may explain coexistence of hypothalamic and inner ear malformations.

In conclusion, we report for the first time an association between incomplete partition type 3 and variable degree of hypothalamic malformations in patients with X-linked deafness and discuss genotype-phenotype correlation in patients with mutation of POU3F4 gene.

4-O11

MUSCLE- MRI PATTERN OF PROGRESSION IN SPINAL MUSCULAR ATROPHY PATIENTS

*L. Cristiano*¹, *T. Verdolotti*², *T. Tartaglione*¹, *C. Brogna*³, *A. Pichiechio*⁴, *C. Cinnante*⁵, *E.M. Mercuri*³

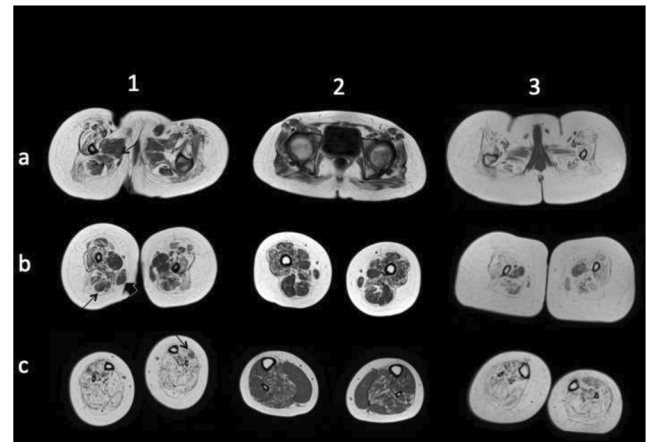
¹ Department of Radiology, Università Cattolica del Sacro Cuore- IDI IRCSS FLMM, ROME, ITALY, ² Department of Radiology, Università Cattolica del Sacro Cuore, Fondazione Policlinico Universitario A. Gemelli, Rome, ROME, ITALY, ³ Pediatric Neurology, Department, Università Cattolica del Sacro Cuore, Centro Clinico Nemo, ROME, ITALY, ⁴ Neuroradiology Department, IRCCS C. Mondino Foundation, Pavia, PAVIA, ITALY, ⁵ Neuroradiology Unit, Fondazione IRCCS Ca' Granda Ospedale Maggiore Policlinico, Milan, Italy, MILAN, ITALY

Introduction

Spinal muscular atrophy (SMA) is an autosomal recessive disorder characterized by degeneration of alpha motoneurons, clinically associated with muscle weakness, hypotonia and muscle atrophy. The weakness is predominant in the proximal muscles, with lower limbs often more involved than upper limbs with a typical

distribution that can also be observed on muscle Magnetic Resonance Imaging (MRI).

The aim of the present study was to perform lower limb muscle MRI in a large cohort of SMA II e III children and young adults, including both ambulant and non-ambulant patients, in order to define possible patterns of muscle involvement, assessing both muscle atrophy and fatty replacement.



Methods

The study is part of a larger multicentric study involving several Italian tertiary care centers for SMA in Rome and Milan. The study was approved by the Ethics committee of the different centers. We prospectively enrolled consecutive SMA patients attending their routine follow up appointments between March 2018 and January 2019.

Muscle MRI sequences were acquired on axial plane, using a flexible coil, covering the pelvis and the lower limbs. Each muscle was examined through its whole extension using the Mercuri classification, that allows a semi-quantitative evaluation of fatty infiltration.

Result

Fifty-four patients were included in the study; mean age 14.7 SD: ±10.3. Seventeen were type 2, 11 were type 3 non-ambulant patients, 21 SMA 3 ambulant.

None of the 54 patients had a completely normal MRI.

At pelvis level there was always involvement of the glutei, that was minimal in the very young children (age 2) and moderate or severe in the others.

At thigh level there was always involvement a predominant involvement of the anterior compartment compared to the posterior one. The more medial muscles, gracilis, sartorius and adductor longus were more often less involved. At leg level there was an overall more diffuse involvement. The soleus muscle was the most severely involved muscle.

Discussion & Conclusion

Our results suggest that, in addition to the well known patterns of involvement observed in SMA patients, a predominant involvement of the distal muscles can also be found, suggesting a possible larger variability than that reported so far.

4-O12**SURVEILLANCE IMAGING OF LOW-GRADE ASTROCYTOMAS IN CHILDREN: CAN WE REDUCE FOLLOW-UP AND THE USE OF CONTRAST AGENTS?***T. Campion*¹, B. Quirk¹, J. Cooper¹, K. Phipps¹, K. Mankad¹¹ Great Ormond Street Hospital, London, UNITED KINGDOM**Introduction**

The optimum strategy for the surveillance of low-grade gliomas in children has not been established, and there is increasing concern about the use of gadolinium-based contrast agents (GBCAs), particularly in children, due to their deposition in the brain. The number of surveillance scans and the use of GBCAs in surveillance of lower risk tumours should ideally be limited.

We aimed to investigate the consistency and utility of our surveillance imaging and also to determine to what extent the use of GBCAs contributed to decisions to escalate treatment in children with low grade gliomas.

Methods

This was a retrospective single centre study at a tertiary paediatric hospital. All children with a new diagnosis of a WHO grade 1 astrocytoma between 2007 and 2013 were included, with surveillance imaging up to December 2018 included in analysis. Patients without at least two years local follow-up available and those with tumour syndromes were excluded. The intervals of surveillance imaging were recorded, and the imaging and electronic health records, including multidisciplinary team meeting (MDT) notes were examined for decisions related to treatment escalation.

Result

88 patients were included. These included 20 optic pathway (OP) tumours, 42 cerebellar tumours and 26 supratentorial tumours in other locations.

64/88 had surgery as initial management, and 32 of these had a complete resection.

29/88 children had recurrence or progression of their tumours leading to a change in treatment, 28 of which were identified on surveillance imaging (12 in the OP group, 7 cerebellar and 11 other supratentorial). The mean time from first surveillance scan to recurrence/progression was 31 months (range 13-64 months).

4/32 patients had recurrence following complete resection, 16/32 patients had progression following incomplete resection.

On examination of the MDT notes, decisions to escalate treatment based on imaging were almost entirely founded on the T2 imaging characteristics rather than the post contrast appearances.

Discussion & Conclusion

Surveillance imaging studies could potentially be reduced in number, particularly in cerebellar tumours with complete resection. MDT decisions were rarely made on the basis of post-contrast imaging, and GBCA administration could be significantly

restricted in the setting of surveillance of low-grade gliomas in children.

5. SPINE**5-O1****ACQUIRED SPONDYLOLYSIS AND SPONDYLOLISTHESIS AFTER POST-DECOMPRESSION SURGERY OF LUMBAR SPINE WITHOUT FUSION***J.H. Yoo*¹¹ Mokdong Hospital, Seoul, SOUTH KOREA**Introduction**

The purpose of study is to describe acquired spondylolysis and spondylolisthesis after posterior decompression surgery of lumbar spine and to analysis of postoperative MDCT findings for assessing causative factors of postoperative spondylolysis.

Methods

Four patients with spondylolysis or spondylolisthesis after posterior decompression of lumbar spine without fusion were included in this study (mean age 44 years, range 29-51 years). All patients had preoperative spine MRI and postoperative spine MDCT. Before surgery, they showed neither spondylolysis nor spondylolisthesis in the segments operated on. We reviewed preoperative diagnosis, level and type of surgery from clinical data. Duration between surgery and postoperative images were calculated. We analyzed decompression size, location of spondylolysis or spondylolisthesis on MDCT images. The size of decompression was measured and expressed as percentage of width of laminectomy to total lamina length

Result

The diagnoses were disc protrusion in 4 patients. The levels of decompression were L3 in 2, and L4 in 2 patients. Two patients underwent bilateral partial laminectomy and two patients underwent right or left partial laminectomy. Mean follow-up duration was 25.5 months (6-66 months). Percentage of width of laminectomy was 70.2%, 68.2% in patients with bilateral laminectomy and 55.1%, 10.3% in patient with unilateral laminectomy. In patients with L3 laminectomy, spondylolysis of L3 and spondylolisthesis of L3-4 were developed. In patients with L4 laminectomy, spondylolysis of L4 and spondylolisthesis of L4-5 were developed. All postoperative spondylolysis were apart from pars interarticularis and extended to adjacent facet joint. Mean degree of spondylolisthesis were 17.8%.

Discussion & Conclusion

Large size of decompression was related with postoperative spondylolysis. All postoperative spondylolysis were developed at

laminectomy level with extension to adjacent facet joint. The patients treated with extensive laminectomy should be followed up carefully with spine radiograph and MDCT.

5-O2

GADOLINIUM-ENHANCED MAGNETIC RESONANCE IMAGING FINDINGS IN CERVICAL SPONDYLOTIC MYELOPATHY

*C. Auger*¹, L.M. Pessini Ferreira¹, F. Doniselli¹, E. Maciag¹, A. Rovira¹

¹ Hopsital Vall d'Hebron, Barcelona, SPAIN

Introduction

Cervical spondylotic myelopathy (CSM) consists of clinical myelopathy secondary to a spinal cord compression due to cervical spondylosis. Conventional magnetic resonance imaging (MRI) typically shows an intramedullary hyperintense signal on T2-weighted imaging (WI) and contrast enhancement on post-gadolinium T1-WI. We report a series of seven patients with CSM who had the typical MRI findings in CSM previously reported in the literature.

Methods

We retrospectively reviewed the medical records and gadolinium-enhanced MRI studies of seven patients who had been diagnosed with CSM, with the aim of characterizing the imaging findings and clinical presentation on T2-WI and post-gadolinium T1-WI MRI in both sagittal and axial planes.

Result

Our sample consisted of seven patients (42% females) with a mean age of 51 years at the moment of clinical onset. Six of them had experienced an insidious clinical onset of more than 8 weeks. Clinical manifestations included upper and/or lower limbs paresthesias and weakness and numbness, and otherwise unexplained gait impairment. All of them had a slow gradual progression of the symptoms. The MRI findings of our case series consisted of degenerative changes of the cervical spine, an intramedullary T2-signal hyperintensity, and an intramedullary enhancement on post-gadolinium T1-WI sequences. In this series we describe in detail the latter two, with no emphasis placed on degenerative changes.

Discussion & Conclusion

Our results support the statement that in patients with cervical spondylosis and clinical myelopathy, the presence on MRI of an intramedullary gadolinium-enhancement following a flat transverse pancake-like pattern (on sagittal images) and a circumferential pattern (on axial images), located within a T2-signal abnormality, is strongly indicative of spondylosis as the cause of the myelopathy.

5-O3

THE POTENTIAL ROLE OF INTERVERTEBRAL LUMBAR DISC FA (FRACTIONAL ANISOTROPY) MAP IN DIFFUSION TENSOR IMAGING (DTI) TO SELECT PATIENTS SUFFERING FROM LOW BACK PAIN AND WHO MAY BENEFIT FROM INTRADISCAL OXYGEN-OZONE INJECTION

*M. Perri*¹, F. Bruno¹, M. Varrassi¹, E. Tommasino¹, A. Di Sibio¹, G. Bianchi¹, A. Catalucci¹, A. Barile¹, C. Masciocchi¹, E. Di Cesare¹, Splendiani¹

¹ Dipartimento di Scienze Cliniche e Applicate e Biotecnologiche - Università degli Studi dell'Aquila, L'Aquila, ITALY

Introduction

To assess annular fibers anisotropy through the use of intervertebral disc FA map to select patients suffering from low back pain of lumbar disc origin and who may benefit from intradiscal oxygen-ozone injection.

Methods

A total of 75 patients suffering from back pain were selected for prospective non-randomized blinded trial approved by the Medical Ethical Committee of our Institution. Before treatment they underwent MRI 3 Tesla exams performed with conventional sequences (T2-FSE-WI, T2 fat-sat and T1 FSE-WI) and additional DTI sequence, respectively for assessing lumbar disc pathology according to the nomenclature and Fractional Anisotropy (FA) map of the involved intervertebral disc. Discography was obtained before treatments under CT guidance of the involved discs in order to confirm MRI reports. Patients were randomly assigned to two groups; control Group (20 men, 16 women; median age 45 years old) underwent intraforaminal injection of steroid and anesthetic. The remaining 39 patients (Study Group composed by 18 men, 21 women; median age 46 years old) underwent the same treatment with the addition of intradiscal oxygen-ozone (O2-O3) injection. Oswestry Low Back Pain Disability (ODI) Questionnaire was administered before treatment and at intervals, the last at 6-month follow-up. Results were compared with Chi2, t test and regression analysis.

Result

In cases of annular fissures without herniation or extrusion disc, O2-O3 intradiscal injection therapy was successful in 16 (41%) study group patients compared with 10 control group patients (27,5 %) (P < 0.01). ODI questionnaire showed significant improvement of symptoms in both Groups (P < 0.01). Similar results were observed in the remaining cases of both groups when the disc was involved with associated radicular pain (P < 0.01).

Discussion & Conclusion

An FA disc map congruous with a rupture of annular fibers could be considered as a predictive sign of response to oxygen-ozone lumbar intradiscal injection treatment so it could be added to the routine MR exam.

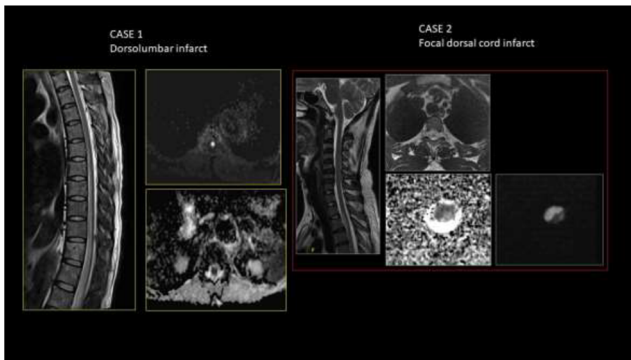
5-O4**SPINAL CORD INFARCTION, MANY MORE**

*H. Pendharkar*¹, N. Yadav¹, V. Murumkar¹, S. Biswas¹, S. Siddiqui¹, R. Chauhan¹, S. Jabeen¹

¹ Department of Neuro Imaging & Interventional Radiology, National Institute of Mental Health & Neuro Sciences, Bangalore, INDIA

Introduction

Spinal cord infarction is an uncommon disease varying in its clinical presentation. This study describes the clinical and radiological presentation of spinal cord infarcts in 20 consecutive patients.

**Methods**

Clinical and MR imaging data of 20 patients from Jan 2018 till April 2019 were reviewed. Inclusion criteria were acute or subacute presentation (peak within 72 hours) and MRI showing typical signal changes on T2WI compatible with spinal cord infarct. Exclusion criteria was signal change due to any other etiology.

Result

There were eight females & twelve males, age ranging from 13 yrs to 60 years, mean 35 years.

Clinical presentation included dissociative anesthesia, weakness of limbs, back or neck pain and autonomic symptoms with symptom onset to peak time ranging from few minutes to 48hrs in patients with Anterior spinal artery infarct (n=20). MRI findings in Anterior spinal artery infarcts included pencil like hyperintensities on T2 sagittal (n= 20, 100%) and “owl eye” appearance on T2 axial (n=6, 28%) images. Diffusion restriction was noted in all cases (n= 20, 100%).

The infarct was located in cervical region in 3, cervico dorsal in 3, upper dorsal in 5, mid dorsal to conus in 5, conus in 2 & was holocord - patchy in 2 patients.

Two patients had parainfectious infarcts with extensive arachnoiditis, two had iatrogenic infarcts , 1 atherosclerotic while while the etiology remained obscure in the remaining 15 patients. Follow up was available for 7 patients (period ranging from 3m-15d). Two patients had favorable outcome who could walk independently, two patients could walk with support, and three patients were wheelchair bound.

Discussion & Conclusion

Spinal cord infarction though a rare condition, needs a high index of suspicion. The signal changes are very typical; but its is important to include DWI in all these patients to identify the infarcts. It is an important cause of acute spinal syndrome. Typical distribution and appropriate imaging can help in timely diagnosis.

5-O5**EXTRAMEDULLARY SPINAL TUMORS: REPORT OF A SERIES CASES AND IMAGING FINDINGS WITH PATHOLOGIC CONFIRMATION**

*D. Maric*¹, S. Jelic², D. Mikic¹, B. Kecman¹

¹ University Clinical Centre of the Republic of Srpska, Department of Radiology, Banjaluka, BOSNIA AND HERZEGOVINA, ² Polyclinica Al-Tawil, Radiology Department, Sarajevo, BOSNIA AND HERZEGOVINA

Introduction

Tumors of the spine encompass a heterogeneous group of lesions that can be divided into three main subgroups: extradural, intradural extramedullary, and intradural intramedullary lesions.

Additionally, the cauda equina region is often considered separately as a number of lesions are particular to it. Defining the location of tumors and mass lesions of the spine in relation to the spinal cord and the dura is of the utmost importance as certain types of lesions tend to occur in certain locations.

Extradural tumors occur outside from dura. Primary extradural tumors of the spine comprise only a small percentage of all spinal tumors.

Intradural extramedullary neoplasms are located outside the spinal cord but within the dural sheath.

Methods

We present a pictorial review of the various extramedullary intradural and extradural lesions of the spine, as well as rare tumors such as isolated primary spinal epidural lymphoma (PSEL) and primary spinal extraskelatal Ewing's sarcoma.

The category of extramedullary intradural masses includes a variety of lesions from meningiomas and nerve sheath tumors (neurofibromas, schwannomas) to less common tumors (hemangiopericytoma), metastases, benign tumors (lipoma, dermoid, epidermoid), inflammatory disorders (arachnoid adhesions, sarcoidosis) vascular lesions (spinal-dural arteriovenous fistula), and cystic lesions (perineural or Tarlov cyst).

Result

Primary spinal extraskelatal Ewing's sarcoma are rare lesions appearing in the spinal extradural space. Isolated primary spinal epidural lymphoma (PSEL) is extremely rare, accounting for 0.9% of all extranodal NHL

Discussion & Conclusion

Magnetic resonance (MR) imaging plays a central role in the imaging of spinal tumors, allowing tumors to be classified as extradural, intradural-

extramedullary or intramedullary, which is very useful in tumor characterization. In the evaluation of lesions of the osseous spine both computed tomography (CT) and MR are important.

Although PSEL and primary spinal extraskelatal Ewing's sarcoma is a rare entity it should be considered in the differential diagnosis of the spinal epidural tumors.

5-O6

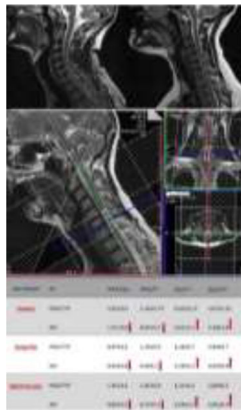
MAGNETIC RESONANCE SPECTROSCOPY: OPTIMIZATION AND CLINICAL APPLICATION OF CERVICAL CORD SINGLE VOXEL ACQUISITION AT 3 TESLA

M. Tuggia^{1,2}, M. Paccanaro¹, M. Mansour¹, V. Vitale¹, V. Pinna¹, G. Iannucci¹

¹ Neuroradiology Unit, San Bortolo Hospital, AULLS 8 Berica, Vicenza, ITALY, ² Istituto Poliambulatorio S. Gaetano, Thiene, Vicenza, ITALY

Introduction

INTRODUCTION: Magnetic Resonance Spectroscopy (MRS) is largely used in brain pathology; while there is poor literature of its use on spinal cord pathology, despite its value in differential diagnosis. One of the main limits of its application is of technical matter. Our study aimed to reduce technical difficulties and optimize MRS sequence, in order to standardize its application on cervical spinal cord pathology.



Methods

METHODS: 22 patients (7 males, 15 females) with multiple sclerosis (MS) and 5 healthy controls (2 males, 3 females), underwent MR 3Tesla scans between January and September (2016). A Head/Neck coil (64 channels) was used and MRI acquisition protocol for all patients consisted in sagittal plane turbo spin-echo (TSE) T1-Weighted (W), T2-W and short-TI Inversion Recovery (STIR), a TSE-T1w sequence after administration of gadolinium and a single voxel (SVS) non-isovoxel (7x7x35mm) Point-Resolved Spectroscopy (PRESS) sequence (prior its optimization on brain, consisting in reducing acquisition time, maintaining a good signal to noise ratio SNR, with a final result of a 6:48 minutes acquisition time vs 10-15min of the original sequence). In healthy patients the voxel was randomly positioned, whereas in MS

patients it was positioned on the demyelinating spinal cord lesion. All Patients were positioned in the coil so that cervical lordosis was straightened or at least reduced to its minimum; this technical strategy resulted in a greater amount of cord tissue included inside the voxel of MRS.

Post-processing spectroscopy data analysis was performed using three different softwares (Tarquin, Spectroscopy and SyngoVia), where lactate (Lac), N-acetylaspartate (NAA), creatine (Cr), choline (Cho), myoinositol (mIns) metabolites and their ratios were evaluated.

Result

RESULTS: All three post-processing techniques gave concordant results, where SM patients showed a reduction of NAA/Cho, NAA/Cr and mIns/Cr ratio, compared to healthy controls.

Discussion & Conclusion

DISCUSSION & CONCLUSIONS: MRs results in SM patients in our study were consistent with literature data. MRs can be a useful tool in the differential diagnosis of spinal cord lesions. Our study improves knowledge on this technique, underlining the importance of a stringent acquisition technique.

5-O7

STATISTICAL PARAMETRIC MAPPING OF REGIONAL BONE DENSITY AT THE THORACOLUMBAR SPINE FOR OPPORTUNISTIC OSTEOPOROSIS SCREENING

M. Löffler¹, A. Valentinitich¹, A. Jacob¹, B. Schmitz-Koep¹, T. Baum¹, C. Zimmer¹, Y. Ryang^{2, 3}, J. Kirschke¹

¹ Department of Neuroradiology, School of Medicine, Klinikum rechts der Isar, Technical University of Munich, Munich, GERMANY, ² Department of Neurosurgery, School of Medicine, Klinikum rechts der Isar, Technical University of Munich, Munich, GERMANY, ³ Department of Neurosurgery, Helios Klinikum Berlin-Buch, Berlin, GERMANY

Introduction

Osteoporosis is a major risk factor for procedure related complications in neurosurgical operations at the spine. With statistical parametric mapping (SPM) regional bone loss at the thoracolumbar spine can be analyzed using routine CT data. The aim of this study was to compare regional trabecular bone mineral density (BMD) between patients with normal, low, and osteoporotic bone mass as defined by dual energy X-ray absorptiometry (DXA).

Methods

In this retrospective study, 252 patients with lumbar DXA and a CT scan within 12 months were included. Clinical CT scans were performed for reasons other than densitometry on four different CT scanners each asynchronously calibrated to yield volumetric BMD. SPM of thoracolumbar vertebral bodies implied (1) individual registration of each vertebra to a standard spine template, (2) normalization of shape to match the template, and (3) calculation of voxel-wise statistics (gender-adjusted ANOVA and

t-test, $p = 0.05$ corrected for multiple testing). Patients with spinal metastasis and vertebrae with compression fractures or degenerative sclerosis were excluded from the analysis.

Result

According to DXA, 84 patients had osteoporosis, 91 had low bone mass, and 77 were healthy with normal bone mass. In healthy patients, mean BMD was lowest at L3 with $129.0 \pm 54.3 \text{ mg/cm}^3$ and highest at T1 with $208.7 \pm 54.8 \text{ mg/cm}^3$ (Table 1). Similar trends were observed for patients with osteoporosis and low bone mass. Compared to healthy patients, statistically significant decreases in BMD were observed in osteoporotic patients at all vertebral levels with an emphasis on the upper thoracic (minimum at T4 with T-score = -3.2 and 91% affected volume) and on the thoracolumbar junction/upper lumbar spine (minimum at L2 with T-score = -0.94 and 83% affected volume; Table 2, Figure 1). Similar tendencies were observed for patients with low bone mass (minima at T5 and T11).

Discussion & Conclusion

SPM can quantify and visualize regional bone loss at the spine for opportunistic osteoporosis screening and may impact neurosurgical planning. SPM revealed reduced trabecular BMD in osteoporotic patients pronounced at the upper thoracic spine and thoracolumbar junction. The mid-thoracic spine (T6–T10) with the least overall motion range due to ribcage stiffness seems to be less prone to osteoporosis-related deterioration of trabecular BMD.

Table 1: Characteristics of the reference group (normal bone mass: DXA T-score > -1) and comparison groups (low bone mass: $-2.5 < T \leq -1$ and osteoporosis: $T \leq -2.5$) stratified by vertebral level with the number of included vertebrae (n), BMD, volumetric bone mineral density, SD, standard deviation; DXA, dual energy X-ray absorptiometry.

Vertebral level	Normal (reference)		Low bone mass		Osteoporosis	
	n	BMD, mean \pm SD	n	BMD, mean \pm SD	n	BMD, mean \pm SD
T1	23	208.7 \pm 54.8	26	176.3 \pm 50.7	27	164.4 \pm 48.9
T2	27	192.4 \pm 42.4	31	154.8 \pm 33.7	26	139.1 \pm 34.8
T3	27	186.4 \pm 41.5	32	150.1 \pm 33.3	31	128.9 \pm 33.6
T4	28	175.3 \pm 40.3	34	143.5 \pm 31.0	30	116.7 \pm 29.4
T5	27	173.1 \pm 36.8	32	138.3 \pm 32.6	32	116.3 \pm 31.9
T6	31	163.4 \pm 37.6	31	136.0 \pm 33.7	29	124.3 \pm 40.2
T7	25	158.3 \pm 37.0	29	138.4 \pm 34.1	25	123.3 \pm 38.2
T8	34	154.6 \pm 41.8	36	128.0 \pm 33.4	31	142.0 \pm 53.3
T9	37	159.2 \pm 45.5	40	131.1 \pm 37.1	35	130.0 \pm 48.7
T10	40	159.7 \pm 44.8	48	129.9 \pm 37.4	42	114.8 \pm 42.7
T11	44	152.7 \pm 44.7	51	119.3 \pm 35.7	43	113.9 \pm 44.2
T12	42	141.6 \pm 39.5	56	112.7 \pm 32.0	44	99.6 \pm 41.9
L1	50	132.9 \pm 45.7	57	109.3 \pm 36.7	51	86.6 \pm 33.9
L2	53	135.1 \pm 52.6	57	106.8 \pm 44.0	57	87.3 \pm 40.1
L3	50	129.0 \pm 54.3	62	135.0 \pm 64.7	54	98.3 \pm 54.3
L4	54	135.6 \pm 61.3	58	149.5 \pm 73.3	48	92.7 \pm 45.5
L5	44	159.7 \pm 68.3	60	136.8 \pm 71.6	53	109.8 \pm 58.2

Table 2: Gender-adjusted T-score of patients with low bone mass and osteoporosis compared to the reference group and affected density regions (ADR), defined as proportion of significant voxels on P-maps with decreased bone mineral density.

Vertebral level	Low bone mass		Osteoporosis	
	T-score	ADR	T-score	ADR
T1	-2.3	0%	-3.1	21%
T2	-0.5	6%	-1.0	49%
T3	-2.3	11%	-3.2	80%
T4	-0.6	4%	-1.1	91%
T5	-2.1	29%	-3.0	85%
T6	-0.5	1%	-0.7	36%
T7	-0.7	0%	-1.1	11%
T8	-0.5	2%	-0.1	7%
T9	-0.5	5%	-0.4	13%
T10	-0.5	6%	-0.8	43%
T11	-0.6	30%	-0.7	38%
T12	-0.5	19%	-0.9	58%
L1	-0.4	3%	-0.9	82%
L2	-0.5	16%	-0.9	83%
L3	0.2	0%	-0.6	21%
L4	0.3	0%	-0.8	50%
L5	-0.2	5%	-0.8	52%

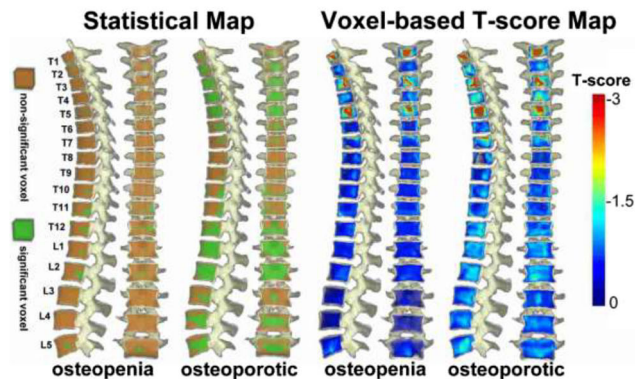


Figure 1: Statistical parametric maps of volumetric trabecular BMD at the thoracolumbar spine calculated between patients with normal bone mass (reference group, not shown) and low bone mass (osteopenia) or osteoporosis. Diagnostic categories of osteoporosis ($T \leq -2.5$) and low bone mass ($-2.5 < T \leq -1$) are defined by DXA reference standard. Gender-adjusted ANCOVA yielded P-maps illustrating in green color regions of statistically significant differences in BMD between the reference group and patients with low bone mass or osteoporosis ($p = 0.05$ corr.). Corresponding T-maps visualize the magnitude of regional BMD loss between the reference group and patients with low bone mass or osteoporosis ($p = 0.05$ corr.). BMD, bone mineral density; ANCOVA, analysis of variance; DXA, dual energy X-ray absorptiometry; corr., corrected for multiple comparisons per vertebra.

5-08

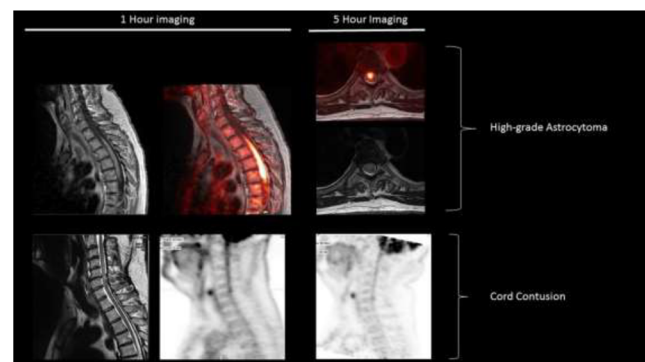
MULTI-TIME POINT FDG-18 PET/MR IMAGING OF SPINAL CORD LESIONS OF UNKNOWN ETIOLOGY

M. Gule-Monroe¹, C. Tatsui², J. Weinberg², M. Chen¹, O. Mawlawi³, D. Schomer¹, J. Johnson¹

¹ MD Anderson Cancer Center, Department of Diagnostic Imaging, Houston, USA, ² MD Anderson Cancer Center, Department of Neurosurgery, Houston, USA, ³ MD Anderson Cancer Center, Department of Imaging Physics, Houston, USA

Introduction

The purpose of this study was to evaluate the use of multi-time point F-18 FDG PET/MR imaging of spinal cord lesions of unknown etiology.



Methods

Prospective, single institution study of 7 adult patients. Imaging encompassed whole-body and spine FDG-18 PET/MR with imaging acquisition at standard of care 1 hour in addition to 5 and 8 hours after PET tracer administration. Lesion to Background (L/B) ratio was calculated by drawing a region of interest over the lesion and over background, normal cord and recording the Maximum Standard Uptake Values.

Result

In 1 patient, pathologically confirmed as high-grade astrocytoma, the L/B at 1 hour was high (4.6) and increased by 26% at 5 hours. 1 patient, pathologically confirmed as grade II ependymoma, demonstrated high L/B of 6.1 at 1 hour with L/B decrease of 24% and 44% at 5 and 8 hours. 1 patient with indeterminate imaging for neoplasm vs. benign process had L/B ratio of 2.5 at 1 hour, increasing 40% at 5 hours. The remaining 4/7 patients had imaging findings consistent with benign, nonspecific inflammatory process (3) or cord contusion (1). The L/B ratio in patients with a clear benign etiology ranged from 1-1.7 with no significant increase in L/B ratio at 5 and 8 hour imaging.

Discussion & Conclusion

Increasing L/B ratio has been reported as more accurate in predicting high-grade malignancy than absolute uptake values in brain gliomas. This was replicated in our study with increasing L/B ratio at 5 hours in a patient with high-grade astrocytoma. Conversely decreasing L/B ratio

on delayed time-point imaging was demonstrated in a patient with low-grade ependymoma. Furthermore lesions with benign etiology had clearly lower L/B and did not demonstrate significant increase in the L/B ratio on multi-time point imaging.

Our preliminary data supports the use of multi-time point F-18 FDG PET/MR for the evaluation of spinal cord lesions of unknown etiology, allowing for accurate separation of benign vs. high grade vs. low grade neoplasm. This is an ongoing trial and more data is needed to support these preliminary observations.

5-O9

ASSESSING SYMPTOM RELIEF FOLLOWING VERTEBROPLASTY IN MULTIPLE MYELOMA

*D. Connolly*¹, A. Martin¹, R. Batty¹, G. Tse¹

¹ Royal Hallamshire Hospital, Sheffield, UNITED KINGDOM

Introduction

Multiple myeloma is the second most common haematological malignancy characterised by uncontrolled proliferation of monoclonal plasma cells in bone marrow and blood leading to organ damage and osteolysis. Sixty to eighty percent of patients have spinal involvement at the time of diagnosis which can lead to severe pain and vertebral body fracture.

Vertebroplasty is a minimally invasive percutaneous procedure by which cement is injected into the vertebral body. Previous studies have shown this can improve pain as rated by a Visual Assessment Score (VAS).

The aim of this paper is to add to the current literature by assessing the response to treatment on more global aspects of quality of life using the Oswestry Disability Index (ODI).

Methods

An ongoing prospective study assessing patient's response to vertebroplasty using VAS, ODI and changes in analgesia using the WHO "analgesic ladder" as a system to score analgesia use.

Result

17 patients and 60 levels were treated between November 2017 and April 2018. The mean reduction in VAS was 3.2 points. The mean reduction in ODI was 40% from the patients original score with a range of between 12 and 100% improvement compared to their original score. Twelve patients reduced their analgesic requirement by at least 1 level on the WHO "analgesic ladder" and 5 remained on the same analgesia.

Discussion & Conclusion

Vertebroplasty provides excellent pain relief and improvement in quality of life in patients with multiple myeloma

5-O10

CERVICAL SPINE FRACTURE PATTERNS PREDICT DISSECTION OF VERTEBRAL ARTERY AFTER BLUNT INJURY

*J. Kostic*¹, I. Kostic², K. Davidovic¹, A. Stankovic¹, D. Masulovic²
¹ Center for radiology and MRI, Clinical Center of Serbia, Belgrade, SERBIA, ² Clinical Center of Serbia, Belgrade, SERBIA, ³ Center for radiology and MRI, Clinical Center of Serbia, Belgrade, SERBIA, ⁴ Center for radiology and MRI, Clinical Center of Serbia, Belgrade, SERBIA, ⁵ Center for radiology and MRI, Clinical Center of Serbia, Belgrade, SERBIA

Introduction

Cranio-cervical artery dissection is a potentially disabling yet probably underrecognized condition that often occurs in young and middle-aged adults. Because of the proximity of the cervical spine and vertebral arteries, the aim was to determine incidence of cervical artery dissections (CeADs), the value of various factors in predicting the existence of a vertebral artery injury (VAI) and to query whether all patients with cervical spine fractures required arteriography to rule out VAI.

Methods

A total of 230 consecutive trauma patients with an Injury Severity Score (ISS) of 16 and more admitted to our Level I trauma center during a 24-month period were prospectively included. Standardized whole-body CT in a 128-detector row scanner included a head-and-neck CT angiography and magnetic resonance angiography of their cervical spine. Incidence, mortality, patient and trauma characteristics, and concomitant injuries were recorded and analyzed retrospectively in patients with carotid artery dissection (CAD) and vertebral artery dissection (VAD). All magnetic resonance angiographies were examined for vertebral artery injury.

Result

Ninety-two patients with vertebral artery injuries were identified, two patients with vertebral injuries had minor cervical fractures, a C6 body fracture and a C7 spinous process/laminar fracture; both underwent diagnostic angiography for injury mechanism. Of the 21 patients without cervical spine fracture, angiographic screening for BCVI was performed for neurologic symptoms (11 patients), basilar skull fracture (6 patients), or severe facial fractures (4 patients). Cervical spine fracture was the sole indication for VAI in 69 patients. Age, sex, mechanism of injury, neurologic impairment, and associated injuries were not statistically significant in predicting the presence of a vertebral vessel occlusion. Of the 230 patients included, 6.2% had a CAD, and 2.7% had a VAD. One patient had both CAD and VAD. A total of 41.6% of the patients with traumatic CAD and 25% of the patients with VAD had neurological sequelae.

Discussion & Conclusion

Blunt vertebral artery injury is associated with complex cervical spine fractures involving subluxation, extension into the foramen transversarium, or upper C1 to C3 fractures. Routine screening should incorporate these findings to maximize yield while limiting the use of invasive procedures.

5-O11**INTRA-OSSEOUS BASIVERTEBRAL NERVE RADIOFREQUENCY ABLATION (BNRA) FOR THE TREATMENT OF CHRONIC VERTEBROGENIC LOW BACK PAIN**A.E. *De Vivo*¹, L. Manfre¹, H. AL Qatami²¹ Istituto Oncologico del Mediterraneo IOM, catania, ITALY, ² Hamad Medical Corporation, Doha, QATAR**Introduction**

The aim of our study is to evaluate new Basivertebral Nerve Radiofrequency ablation (BNRA) in treating patients affected by chronic vertebrogenic low back pain.

Methods

From January 2018 patients presenting with low back pain were evaluated at our institute.

A total of 28 patients were eligible for percutaneous CT-guided BNRA. 4/28 patients had 1 segment affected, 24/28 patients had 2 segments affected.

Inclusion criteria were:

Chronic LBP (>6 months), evidence at CT/MRI Imaging of disc degeneration and Modic 1 changes, evidence of vertebral body uptake on SPECT/TC imaging, failure of conventional therapies.

Pain intensity was rated by the VAS and ODI score.

BNRA was performed in a fully percutaneous procedure (STAR®). An 8G Jamshidi needle is introduced by unilateral trans-pedicular approach inside the vertebral body with the central part of the electrode located in the center of the vertebral body, where the majority of vertebral body nerves cluster.

After placing the electrode to the targeted location thermal ablation is delivered for 10 minutes at 85°C to create an approximately 1,5 cm spherical lesion; Conventional MRI performed 1 month after the procedure shows the size of the ablation area.

Result: The CT-guided procedure was well tolerated by all patients in simple local anesthesia, and mean operative time was approximately 45 minutes. No major or minor complications were detected at immediate post-operative CT control scan.

All 28 patients underwent 3 and 6 months clinical follow-up:

3 months follow-up VAS scores decreased significantly compared to baseline: mean change in VAS from baseline was -4.1 mm therefore showing a marked improvement in 28/28 of 28 enrolled patients, (VAS decreased more than 3.0 mm).

Post ablation ODI score showed marked improvement: At 3-months, the mean change in ODI from baseline was -26.2 points. Using a 10-point improvement threshold for success, 100% of patients reached clinical success.

Discussion & Conclusion

BNRA ablation seems to be a powerful technique for pain relief in patients with chronic vertebrogenic LBP. Therefore the CT-

guided procedure is fast and safe and can be performed in simple local anesthesia. Moreover SPECT/TC seems to be a reliable diagnostic tool to select patients that should undergo BNRA procedure.

5-O12**CT-GUIDED TRANSFACET PEDICLE SCREW FIXATION IN LUMBAR MICROINSTABILITY SYNDROME: A NOVEL APPROACH**A.E. *De Vivo*¹, L. Manfre¹, H. AL Qatami², I. Gil³¹ Istituto Oncologico del Mediterraneo IOM, CATANIA, ITALY, ² Hamad Medical Corporation, DOHA, QATAR, ³ Centro Hospitalar Lisboa Ocidental CHLO, LISBON, PORTUGAL**Introduction**

Lumbar instability is one of the most common cause for chronic low back pain (LBP).

The concept of vertebral instability has evolved in the last years, and the new concept of “micro-instability” was recently introduced, despite it's not yet unanimously recognized by the scientific community, to differentiate a specific syndrome.

Microinstability can be defined as a pure motion/bio-mechanical dysfunctional syndrome with no or minimal anatomical changes, in absence of spondylolisthesis. The aim of our study is to evaluate new percutaneous trans-facets fixation (TFF) in treating patients affected by chronic mechanical low back pain, due to single level microinstability.

Methods

From January 2014 patients presenting with low back pain and suspected microinstability syndrome were evaluated at our institute.

All the patients underwent conventional lumbar CT and MRI study. Additionally, a CT-guided Medial Branch Block (MBB), with injection of 1cc of Lidocaine at the level of the zygapophyseal nerve of the presumed facets responsible for LBP was performed.

A total of 84 patients (43 M; 41 F; median age 45 years old, age range 25-32) were eligible for percutaneous CT-guided trans-facet fusion.

All the patients presented disc degeneration classified according to Pfirrmann grading of lumbar disc degeneration (3 Grade I; 18 Grade II; 31 Grade III; 24 Grade IV; 8 Grade V).

Pain intensity was rated by the VAS and ODI score.

Result

Post-treatment VAS scores decreased significantly compared to baseline: mean 20.7 ± 8 (P < .001) VS 70 ± 5,4 (Fig), therefore showing a marked improvement in 81 of 84 enrolled patients (VAS decreased more than 30 mm)

Post fusion ODI score showed marked improvement; mean score: $2 \pm 3,4$ ($P < .001$) compared to the pre-operative score (15 ± 2).

Discussion & Conclusion

Transfacet pedicle screw fixation (TFF) seems to be a powerful technique for lumbar spine stabilization in patients with chronic mechanical LBP related to lumbar microinstability, and no side-effects or complications were observed. Mean working time was significantly reduced using a fully CT-guided technique in simple analgo sedation. In conclusion, CT-guided TFF is a fast and safe technique when facet posterior fixation is needed.

E-POSTERS (original and unedited texts as received by the authors)

1. DIAGNOSTIC

1-P1

ASSESSMENT OF 3D T2-WEIGHTED HIGH-SAMPLING-EFFICIENCY (SPACE) SEQUENCE FOR EVALUATION OF CHIARI I MALFORMATION

*S. Örs Kukurcan*¹, E. Inci¹, A. Kukurcan², G. Güclü³, M. Cirak³

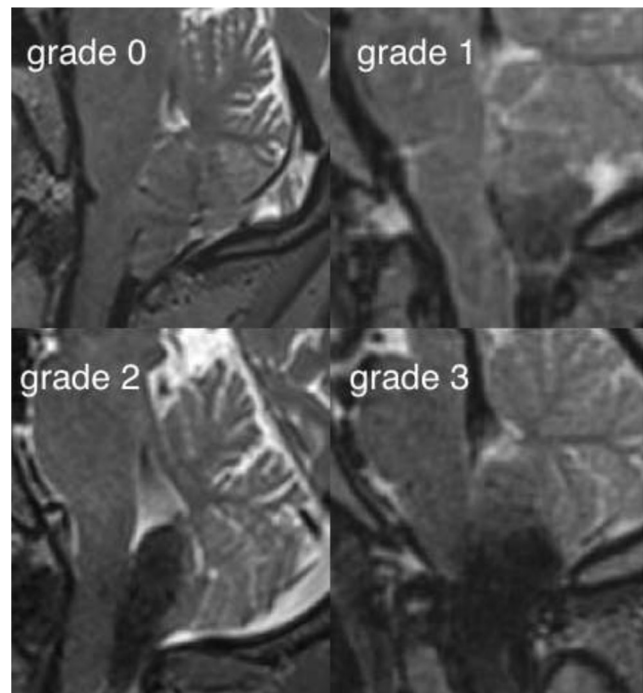
¹ Bakirkoy Dr Sadi Konuk Training and Research Hospital, Radiology Department, Istanbul, TURKEY, ² Van Training and Research Hospital, Van, TURKEY, ³ Bakirkoy Dr Sadi Konuk Training and Research Hospital, Neurosurgery Department, Istanbul, TURKEY

Introduction

3D-SPACE has become an essential component of routine CSF flow imaging protocol which has high sensitivity to motion where the detection signal becomes low in the moving regions. 3D-SPACE method provides a direct way to image the tonsillar motion which cannot easily be done using other motion-sensitive sequences. Tonsillar blackout sign (TBS) have identified a highly reliable imaging sign to diagnose CM1 by using 3D-SPACE sequence. In this study, we evaluate efficacy of TBS in identifying Chiari malformation (CM1) as diagnostic marker, correlation with degree of symptoms, investigate its role in follow-up of symptomatic CM1 patients.

Methods

112 patients who were diagnosed CM1 according to clinical and radiological findings were included in this study. All patients were divided into two groups: symptomatic CM1 (Group I) and asymptomatic-CM1 (Group II) by a neurosurgeon. Groups also subdivided into two: operated or non-operated CM1. All patients in operated groups were followed by two years. Two radiologists evaluated SPACE sequence and presence and grading of TBS to define cerebrospinal fluid flow abnormality in all groups (image 1).



Result

Presence and grading of TBS in symptomatic patients was significantly higher than that in asymptomatic patients ($P < .001$). In operated group, degree of TBS sign decreased after the surgery with the correlation of symptoms ($p < .001$). In grading of TBS on 3D-SPACE, the level of agreement between two readers was excellent. TBS had mostly disappeared in operated groups that who had benefit from surgery in third-sixth months and first year controls.

Discussion & Conclusion

TBS is highly suggestive, useful for diagnosis CM1 patients. TBS sign is particularly useful in the distinction of the symptomatic and the asymptomatic CM1 patients and helpful to decide which patients are likely to get benefit from the decompressive surgery. TBS is useful for follow up in symptomatic CM1 patients.

1-P2

A CASE OF ANTI-GLIAL FIBRILLARY ACIDIC PROTEIN (GFAP) ANTIBODY ASSOCIATED MENINGOENCEPHALOMYELITIS

*H. Zhang*¹, S. Kumar¹, T. Umaphathi¹

¹ Neuroradiology, National Neuroscience Institute, Singapore, SINGAPORE

Introduction

A distinctive, corticosteroid-responsive autoimmune meningoencephalomyelitis is recently characterized with anti-glial fibrillary acidic protein (anti-GFAP) antibody as the biomarker and shows a striking radiological appearance.

Methods

We report the MRI findings of a case of anti-GFAP antibody associated autoimmune meningoencephalomyelitis.

Result

A 68 year old lady presented with fever, headache, vomiting, visual hallucination and altered mental status. Clinical examination was consistent with acute meningoencephalomyelitis. Spinal fluid revealed lymphocytic pleocytosis, raised protein and low glucose. Standard bacteriological and virologic evaluation was unyielding.

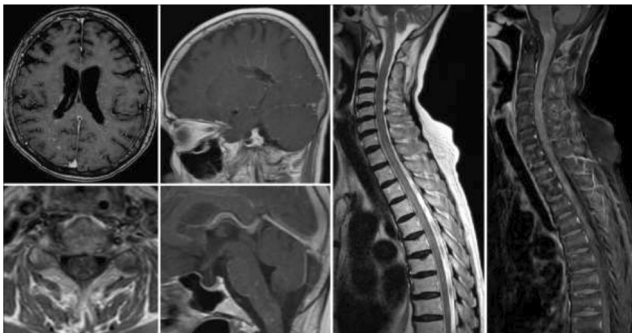
Meningitic antibiotics were started, but the patient continued to deteriorate neurologically. Anti-tuberculous (TB) treatment was then tried, with high dose corticosteroids. The patient started to improve. However, within two weeks of weaning-off corticosteroids she became confused again, with prominent upper limb and head tremor, and bilateral dysmetria. Blood and spinal fluid TB cultures all returned negative.

MR brain showed leptomeningeal enhancement and a striking radial pattern of perivascular enhancement oriented perpendicular to the ventricles in the deep and periventricular white matter. Linear and punctate enhancement was seen in the pons, medulla and cervicomedullary junction. MR spine showed multiple short segmental, intramedullary, T2 hyperintense, enhancing lesions along the entire length of spinal cord.

CSF sample was sent to MAYO clinic for analysis. Anti-GFAP antibody was detected at high titres. TB treatment was stopped and high dose corticosteroids therapy was started. The patient recovered gradually.

Discussion & Conclusion

Anti-GFAP antibody associated autoimmune encephalitis can present with a diverse clinical syndromes of encephalitis, meningoencephalitis, myelitis, encephalomyelitis, meningitis, neuropathy and ataxia. Typical MR findings include radial pattern of perivascular enhancement perpendicular to the ventricles, leptomeningeal enhancement and segmental T2 hyperintense and enhancing intramedullary lesions in the spinal cord. Therefore, it can mimic sarcoidosis, infective encephalitis, vasculitis, sarcoid, intravascular lymphoma and CLIPPERS syndrome. Anti-GFAP antibody is the key point for diagnosis, which can be found in serum or spinal fluid. The disease may be paraneoplastic, sometimes associated with an occult malignancy. PET/CT scan was performed for our patient and turned out to be negative. Corticosteroids are the treatment of choice, and our patient responded well.



1-P3

BASELINE INCREASED ADC VALUE WITHIN NORMAL APPEARING WHITE MATTER AS PREDICTOR OF NUMBER OF RELAPSES IN MULTIPLE SCLEROSIS PATIENTS TREATED WITH INTERFERON-BETA IN THE 4-YEAR FOLLOW-UP

A. Zacharzewska-Gondek¹, A. Pokryszko-Dragan², M. Sasiadek¹, J. Bladowska¹

¹ Wroclaw Medical University - Department of General and Interventional Radiology and Neuroradiology, Wroclaw, POLAND, ² Wroclaw Medical University - Department and Clinic of Neurology, Wroclaw, POLAND

Introduction

Diffusion-weighted imaging (DWI) is a sensitive technique in detection of subtle changes of tissue integrity in the normal appearing white and grey matter (NAWM, NAGM) that seem to be not affected in conventional MRI of MS patients. Several predictors of non-response to interferon-beta (IFN-beta) treatment have been proposed; however, the role of DWI has not been well investigated. The aim of the study was to assess the usefulness of apparent diffusion coefficient (ADC) measurements in the selected regions of NAWM and NAGM in MS patients at baseline MRI as potential predictors of poor response to interferon-Beta (IFN-B) treatment, defined as at least 1 relapse in the 4 year follow-up period.

Methods

Sixty-five MS patients underwent baseline MRI with DWI on a 1.5T MR unit at the beginning or after one year of treatment. Thirty-one sex- and age-matched control subjects (CG) were also included in the study. ADC values were measured in 13 regions of interest (ROIs). Twenty-nine patients (MS1 group) experienced at least one relapse. Thirty-six patients (MS0 group) remained free of relapses for more than 4 years. Associations between baseline ADC values, demographic, clinical, other radiological features and number of future relapses were studied by Poisson regression analysis. The statistical outcomes were expressed by a relative risk (RR) together with a confidence 95% intervals and a p-values.

Result

MS1 patients showed significantly higher ADC values in frontal and frontoparietal NAWM compared to MS0 and CG. ADC values in these regions (RR=1.01), baseline EDSS (expanded disability status scale) (RR=1.28) and baseline lesion load (RR=1.08) predicted number of relapses separately (p=0.026-0.000), prediction was further strengthened by presence of Gd-enhancing lesions at baseline.

Discussion & Conclusion

The prompt identification of MS patients with a poor response to the first-line therapy is pivotal to select potential candidates to receive alternative therapy earlier. We found that apart from commonly investigated potential predictors, higher ADC values in frontal and frontoparietal NAWM are also significant factors in predicting of poor response to IFN-Beta treatment.

1-P4
DIFFUSION TENSOR TRACTOGRAPHY OF NIGROSTRIATAL PATHWAY ON EARLY PARKINSON'S DISEASE: A LONGITUDINAL CASE-CONTROL STUDY

A. Yong¹, S. Hartono¹, L. Ooi¹, S. Ng², N. Chia², D. Heng¹, X. Choi¹, E.K. Tan^{1,2}, L. Tan², L.L. Chan¹

¹ Singapore General Hospital, Singapore, SINGAPORE, ² National Neuroscience Institute, Singapore, SINGAPORE

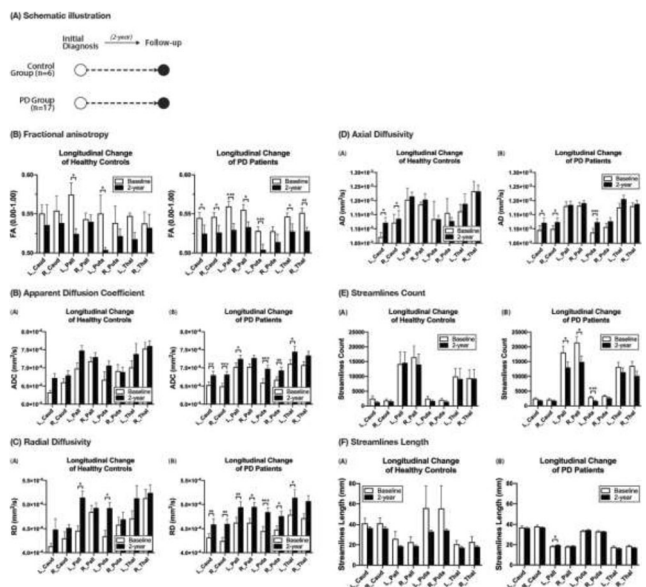
Introduction

Parkinson disease (PD) is associated with neuropathological degeneration in the substantia nigra (SN), with known neuronal loss in the nigrostriatal pathway (NSPs). However, the development of PD therapeutics is restricted by objective methods to demonstrate slowing or reversal of PD. To date, diffusion tensor tractography (DTT) has shown to objectively identify signs of NSPs degeneration in cross-sectional studies. However, the lack of DTT data documenting progressive NSPs changes creates a gap in assessing its feasibility in tracking PD progression.

Methods

Here, we present our longitudinal study on DTT changes of NSPs. We evaluated the NSPs of 17 PD patients (11 males, mean-age 61.2) at their initial diagnosis and at two-year follow-up, with six healthy controls (four males, mean-age 62.2). We isolated the NSPs with our proprietary pipeline developed with MRTrix. The pathways are connected between a striatal-nucleus and its ipsilateral-SN. The striatal-nuclei were segmented automatically, while ROIs encompassing SNs were hand-drawn. Fractional anisotropy (FA), apparent diffusion coefficient (ADC), radial diffusivity (RD), axial diffusivity (AD), streamline counts and streamline length of the NSPs were evaluated.

Result



FA of NSPs connecting all striatal-nuclei, except right-putamen, was decreased in PD after two-year. Meanwhile, only FA of NSPs connecting left-globus-pallidus and left-putamen was decreased in control. Likewise, ADC of NSPs connecting all striatal-nuclei, except right-globus-pallidus and right-thalamus, was increased in PD after two-year. RD of NSPs connecting all striatal-nuclei, except right-thalamus, was also increased in PD after two-year. Only RD of NSPs connecting left-globus-pallidus and left-putamen was increased in control. AD of NSPs connecting left-caudate, right-caudate, and left-putamen was increased in PD, while AD of NSPs connecting left-caudate and right-caudate was increased in control. Furthermore, there were lower streamline counts for NSPs connecting left-globus-pallidus, right-globus-pallidus, and left-putamen in PD after two-year. Finally, both groups have minimal change in streamline lengths after two-year.

Discussion & Conclusion

This is, to our knowledge, the first study on longitudinal DTT changes in PD. Our data suggests DTT can be a sensitive and robust method in tracking PD progression. We believe this study will create a novel option in tracking PD progression and assist the development of PD therapeutics.

1-P5

THE EFFECT OF CONTEXTUAL REPORTING IN THE WORK-UP OF SUBJECTIVE COGNITIVE DECLINE

C. Håkansson¹, G. Torisson², E. Londos², O. Hansson², I. Björkman-Burtscher¹, D. van Westen¹

¹ Diagnostic Radiology, Lund University, Lund, SWEDEN, ² Memory Research facility, Lund University, Malmö, SWEDEN

Introduction

Relevant imaging findings in the work up of cognitive decline are underreported. Here we determine the impact of contextual reporting on sensitivity, specificity and accuracy of clinical radiology reports for relevant findings in the diagnostic work up of subjective cognitive decline (SCD). Contextual reporting is an intermediate between structural reporting and free narrative reporting and resembles a checklist-inspired report adapted to a specific clinical question or disease with free text narratives allowed.

Table. Reported findings and compliance; all (N=236)

Pathology	Radiology reports		g-value
	Before (n=111)	After (n=125)	
	%	%	
Contextual compliance			
All pathologies reported	6	30	<.001
"Impression" in report	12	24	.015
Full compliance ^b	2	8	.031

Note: Pearson Chi-Square, *p* < .05 represents a significant difference.

^a Total of reported normal and abnormal findings.

^b I.e. reports where all pathologies were reported and report ended with an "Impression".

Methods

In our department templates are available that are based on a free text narrative, however medial temporal lobe atrophy (MTA), width of lateral ventricle (WLTV), white matter changes (WMC), global cortical atrophy (GCA) and a final “Impression” should always be assessed and reported regardless if findings are considered abnormal or not. For full compliance the report must include all pathologies and end with an “Impression”. We assessed reporting frequencies, correct classification, and compliance with contextual templates for MTA, WLTV, WMC, and GCA in two aged matched patient groups examined before (n=111) and after (n=125) the introduction of contextual reporting at our department. Sensitivity, specificity and accuracy of the radiology reports before and after were calculated using an online statistics calculator and exact Clopper-Pearson 95% confidence intervals (95%CI) were determined. Significance was assessed by visual comparisons of CI:s.

Result

Reporting frequencies and correct classification increased significantly for MTA (p<.001), WMC (p<.001), and GCA (p=.01) after the introduction of contextual reporting, but not for WLTV. There was also an increase in contextual compliance (see Table). Sensitivity, specificity and accuracy increased for MTA, WML and GCA with only the increase in sensitivity for GCA reaching significance.

Discussion & Conclusion

Our results suggest that the introduction of contextual reporting using visual rating scales may increase sensitivity, specificity and accuracy of the radiology reports in the diagnostic work up of SCD.

1-P6

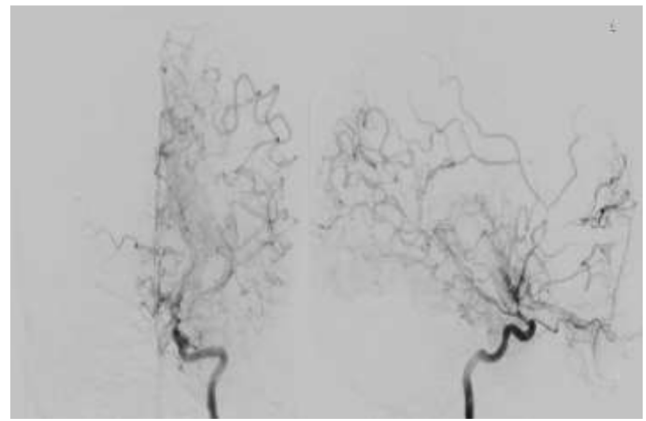
A RARE CASE OF POSTINFECTIOUS MOYAMOYA SYNDROME: CASE REPORT AND REVIEW OF THE LITERATURE

*P. Trombatore*¹, E. Lozupone¹, S. Gaudino¹, L. Milonia¹, A. Alexandre¹, I. Valente¹, F. D'argento¹, C. Colosimo¹, A. Pedicelli¹

¹ Fondazione Policlinico Universitario A.Gemelli IRCCS, Rome, ITALY

Introduction

Postinfectious Moyamoya syndrome (MMS) is a rare vasculopathy that can follow a bacterial meningitis. Few cases have been described in the literature related to different microorganisms such as M. Tuberculosis, S. Pneumoniae, H. Influence and T. Pallidum. We present a unique case of MMS following a bacterial meningitis caused by A. Fumigatus and E. Coli and we reviewed all cases of MMS post-meningitis in the literature.



Methods

A 41years-old man developed meningitis due to A. Fumigatus and E. Coli infection 4 days after neurosurgery for subependymoma of the fourth ventricle.

Two years later, the patient presented with mild left hemiparesis. The MRI revealed two acute ischemic lesions in the right centrum semiovale associated to bilateral chronic watershed cerebral ischemic lesions. Bilateral severe stenosis of distal ICA and the M1 segments of MCA were disclosed at the MR-angiography.

The cerebral DSA showed a typical Moyamoya pattern with occlusion of both the distal ICA, the M1 segments, the A1 segments and the presence of tangle of tiny vessels (“puff of smoke”) along the course of lenticulostriatal arteries; leptomeningeal and trans-dural collateral circulation was also detected. Posterior circulation was spared from the disease.

The cases of the review were identified through research on PUBMED and additional articles were considered basing on their references.

Result

9 cases of MMS following a bacterial meningitis were found after reviewing the literature. The Mycobacterium tuberculosis was isolated in 4 patients, the Streptococcus pneumoniae in 3 patients, the Treponema pallidum and the Haemophilus influenzae type C in one case each. Time between meningitis and onset of Moyamoya pattern was extremely variable. In 1 patient Moyamoya pattern developed after 30 days, in 5 patients between 6-12 months, and in 4 patients after one year; in the latter group, the infectious agent involved was the Mycobacterium tuberculosis. Involvement of posterior circulation was present in 7 cases, 3 of which were consequent to Streptococcus pneumoniae meningitis. All patients were medically treated.

Discussion & Conclusion

Clinicians should be aware of vascular complications such as MMS which can follow bacterial meningitis. Imaging is essential for diagnosis and to exclude other causes of late neurological symptoms in these patients.

1-P7

MAY AN AUTOMATIC FRAMEWORK BASED ON MR IMAGES REDUCE THE USE OF CONTRAST AGENTS IN MULTIPLE SCLEROSIS? PRELIMINARY RESULTS

*E. Tommasino*¹, G. Placidi², M. Polsinelli², C. Masciocchi¹, A. Splendiani¹

¹ Department of Life, Health and Environmental Sciences, University of L'Aquila, Coppito 2 AQ, 67100, Italy, L'AQUILA, ITALY, ² Department of Biotechnological and Applied Clinical Science, University of L'Aquila AQ, Via Vetoio 1 AQ, 67100, Italy, L'AQUILA, ITALY

Introduction

Multiple sclerosis is one among the chronic neurological conditions, in which MRI has been established as the most reliable exam in monitoring the evolution of the inflammatory plaques and the course of the disease. Gadolinium-enhanced T1-weighted MR images allow the identification of active lesions, since enhancement appears in the areas of increased permeability and ongoing inflammation. Nevertheless, the continuous use of gadolinium-based contrast agents (GBCAs) is not without risk. Firstly, the slow renal excretion of GBCAs is limited in patients with chronic renal failure. Secondly, evidences suggest the deposition of GBCAs in the brain, particularly in the dentate nucleus and the globus pallidus. Therefore, we propose a new automatic segmentation technique based on MR images, to rapidly identify new lesions.

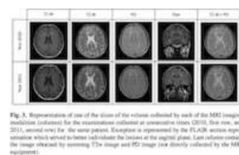


Fig. 3. Representation of one of the slices of the volume collected by each of the MRI imaging modalities (T1w, T2w, PDw and FLAIR) for the reconstruction of the volume (2010, 2011, 2017 and 2018), second row for the same patient. Examples are represented by the FLAIR images representing the image obtained by summing T1w image and PD image (see directly collected by the MRI equipment).

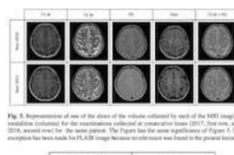


Fig. 5. Representation of one of the slices of the volume collected by each of the MRI imaging modalities (T1w, T2w, PDw and FLAIR) for the reconstruction of the volume (2010, 2011, 2017 and 2018), second row for the same patient. The figure has the same significance of Figure 3. The exception has been made for FLAIR image because in this case the image has been obtained by summing T1w image and PD image (see directly collected by the MRI equipment).

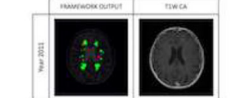


Fig. 4. The slice corresponding to Figure 3 after the combination with the proposed framework. The red color indicates the presence of new lesions (new) and the blue color indicates the presence of chronic lesions. Green is used for chronic lesions, and for new lesions red color is used. The image obtained by the proposed framework is shown in the right side of the image. The image obtained by the proposed framework is shown in the left side of the image. The image obtained by the proposed framework is shown in the right side of the image. The image obtained by the proposed framework is shown in the left side of the image.

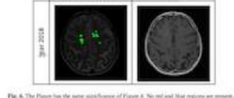


Fig. 6. The figure has the same significance of Figure 4. The red and blue regions are present to indicate the absence of new lesions (new) and of old lesions (old) respectively in the red and blue color in the image. The image obtained by the proposed framework is shown in the right side of the image. The image obtained by the proposed framework is shown in the left side of the image.

Methods

Based on T1-w, T2-w, PD-w and FLAIR images, we present an automated framework for the identification and segmentation of lesions by using convolutional neural network (CNN) architecture applied to the volumes collected by these different imaging modalities. The proposed framework has been tested on data collected at 4 different times (4 consecutive examinations: 2010, 2011, 2017 and 2018, compared in couples: 2010- 2011 and 2017-2018) collected from a 55 years old male with RR-MS with a 1.5 T MRI.

Result

The resulting binary masks obtained from the identification/segmentation strategy gave on each examination the possibility to calculate the volume of each lesions, their status (chronic or active) and, hence, to estimate the progression of the disease. The framework output (in each imaging modality), gave with the RED color information about new lesions, the GREEN color information about chronic lesions and the BLUE color information about

lesions segmented in the previous examination but absent in the following (outliers or reabsorbed edema).

Discussion & Conclusion

Preliminary results are reported demonstrating that the calculations performed by the proposed framework are capable, when the disease is stable, to gather the same information obtainable when the contrast agent (GBCAs) is administered to the patient. Being an automated method, it may give information about the plaque status in real time and thus, prevent the use of GBCAs in that situations, where any new plaque is detected.

1-P8

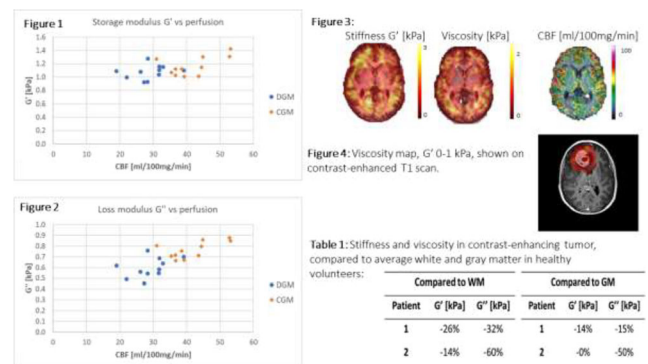
IN VIVO ASSESSMENT OF STIFFNESS, VISCOSITY AND PERFUSION – IN HEALTHY SUBJECTS AND BRAIN CANCER PATIENTS

*S.F. Svensson*¹, W. Nordhøy¹, G. Løvland², R. Sinkus^{3,4}, J.R. de Arcos³, O. Darwish³, S. Holm⁵, E. Vik-Mo⁶, K.E. Emblem¹

¹ Department for Diagnostic Physics, Oslo University Hospital, Oslo, NORWAY, ² The Intervention Center, Oslo University Hospital, Oslo, NORWAY, ³ Division of Imaging Sciences and Biomedical Engineering, Kings College, London, UNITED KINGDOM, ⁴ INSERM U1148, LVTS, University Paris Diderot, Paris, FRANCE, ⁵ Department of Informatics, University of Oslo, Oslo, NORWAY, ⁶ Department of Neurosurgery, Oslo University Hospital, Oslo, NORWAY

Introduction

MR Elastography¹ (MRE) can be used to noninvasively quantify the mechanical properties of tissue: shear stiffness (G') and shear viscosity (G''). The purpose of our study was to assess tissue stiffness and perfusion in the human brain, for both healthy subjects and brain cancer patients.



Methods

This preliminary study was performed in 11 healthy volunteers, and two patients diagnosed with glioblastoma. The exams were performed on a 3T MRI scanner, and the MR Elastography was performed using the Gravitational Transducer², which induced shear waves of 50 Hz into the head. To estimate brain perfusion in the healthy volunteers, we performed an Arterial Spin Labelling (ASL), according to the ASL White

Paper³. For patients, gradient-echo, spin-echo dynamic susceptibility contrast imaging was acquired.

Result

The cerebral blood flow (CBF) is 43 % higher in the cortical gray matter than in deep gray matter ($p=0.001$). The tissue viscosity G'' is 28% higher in cortical gray matter than in deep gray matter ($p=0.0002$). The shear stiffness G' shows a tendency towards higher values in cortical gray matter ($p=0.21$). Figure 1(2) show the relationship between stiffness (viscosity) and CBF in deep and cortical gray matter, Figure 3 shows example images of G' , G'' and CBF for a volunteer.

Two patients have been included so far; viscosity map shown in figure 4. The stiffness and viscosity differ from the values measured in both gray and white matter in the healthy volunteers, as shown in table 1.

Discussion & Conclusion

Results recently published(4) on ASL and MRE in sub-regions of deep gray matter, suggested a high sensitivity of MRE in deep gray matter to perfusion pressure. In this preliminary work, we show that both the perfusion and viscosity were higher in the cortical gray matter than in the deep gray matter in healthy volunteers. In patients, stiffness and viscosity differ from the values observed in healthy volunteers.

1-P9

THE PREDICTIVE VALUE OF ADVANCED TECHNIQUES OF BRAIN MRI IN PATIENTS WITH CLINICALLY ISOLATED SYNDROME

*J. Stulik*¹, M. Kerkovsky¹, M. Dostal^{1,2}, M. Kuhn^{3,4}, J. Losak³, P. Praksova⁵, M. Hulova⁵, Y. Benesova⁵, J. Bednarik⁵, A. Sprlakova-Pukova⁵, M. Mechl⁵

¹ Department of Radiology and Nuclear medicine, University Hospital Brno and Masaryk University, Brno, CZECH REPUBLIC, ² Department of Biophysics, Masaryk University, Brno, CZECH REPUBLIC, ³ Department of Psychiatry, The University Hospital Brno and Masaryk University, Brno, CZECH REPUBLIC, ⁴ Behavioural and Social Neuroscience, CEITEC MU, Brno, CZECH REPUBLIC, ⁵ Department of Neurology, University Hospital Brno and Masaryk University, Brno, CZECH REPUBLIC

Introduction

Several studies have demonstrated the diagnostic potential of advanced MRI techniques like diffusion tensor imaging (DTI) or functional MRI in patients with multiple sclerosis or clinically isolated syndrome (CIS). In this study we attempt to investigate the predictive power of these techniques together with volumetry to predict the clinical conversion in patients with CIS to clinically definite multiple sclerosis (CDMS).

Methods

The study group included 50 patients with CIS, who were followed for two years;. 15 patients have progressed to CDMS within this period, 35 patients remained clinically stable. All patients underwent multimodal

MRI. The evaluated parameters comprised brain volume, resting-state functional MRI (rsfMRI) data and DTI scalar parameters of the white matter (WM). rsfMRI data was analysed by supervised machine learning algorithm, DTI data was analysed by tract-based spatial statistics (TBSS) and SienaX was used for evaluation of the brain volumes. All parameters were compared mutually between the two above-mentioned subgroups.

Result

We found significant differences in brain connectivity of several brain regions between the patients with and without progression to CDMS revealing sensitivity and specificity of 0.87 and 0.60 respectively. Moreover, significant differences between the subgroups were found in fractional anisotropy by TBSS analysis within extensive areas of WM, also the volume of WM was significantly lower in patients with progression compared to the progression-free group.

Discussion & Conclusion

Our results suggest that the groups of patients with CIS differing by the presence or absence of the clinical progression to CDMS within two years of observation are rather different entities also from the perspective of functional connectivity, diffusivity and volumetry. Thus, these modalities appear as a promising diagnostic tool, which may complement the conventional MRI techniques to better identify the patients at risk of clinical progression of the demyelinating disease.

1-P10

PSYCHOPHYSIOLOGICAL OUTCOMES OF AGE-RELATED BRAIN ATROPHY

*Y. Statsenko*¹, K. N. Gorkom¹, M. Ljubisabljevic¹, M. Szolics¹, G.C. Baylis¹, T. al Mansoori¹, K. M. Das¹, E. Soteriades¹, I.A. Charykova², T. Dotsenko³, L.V. Kutniakhova³, M.E. Biandzetskaya⁴, I.V. Glebova⁵, A.S. Kulagin⁵

¹ UAEU, College of Medicine and Health Sciences, Al Ain, UNITED ARAB EMIRATES, ² Republican Scientific and Practical Centre for Sports, Minsk, BELARUS, ³ Byelorussian State Economical University, Minsk, BELARUS, ⁴ Minsk State Linguistic University, Minsk, BELARUS, ⁵ JSC Tensor, Dubna, RUSSIA

Introduction

Recent neuroimaging studies provided inconsistent results regarding the role of brain atrophy and impaired psychophysiological function. The early cognitive dysfunction in case of the age-related brain atrophy is of primary interest. Neurologists and radiologists commonly deal with age-related cognitive dysfunction.

Methods

Participants – $n=232$; 8-90-year-old, both gender. MRI-brain was performed with 1.5T Siemens equipment; a sagittal 3D-T1w image-set covering the entire brain and skull was used for the voxel-based morphometry (Computational Anatomy Toolbox CAT12). The total intracranial volume (TIV), the absolute and the relative values of gray matter (GM)

and white matter volume (WM) and cerebra-spinal fluid (CSF) were calculated. Psychophysiological testing included simple (pushing a button when a light indicator flashes) and complex visual-motor reaction (reacting in different ways according to the color of the presented signal), using the technique 'Reaction to a moving object' (the time preciseness of acting on an expected event), arm dynamometry with calculation of the Asymmetry Coefficient (AC). The Decision Making Time (DMT) was calculated as the difference between the mean time for complex and simple reactions. The correlation coefficients were calculated for each set of paired data of volumetric brain sizes and psychophysiological tests.

Result

Significant ($p < 0.05$) negative correlations were observed between the time for simple and complex visual-motor reaction and the volumes of GM and WM. Reasonably, significant positive correlations were found between these physiological indexes and the amount of CSF. No significant correlation between DMT and brain volumetric data was found. The correlation coefficients between volumetric brain data and each of the psycho-physiological indexes were almost similar both for WM and GM, with an exception for AC. Opposite changes are observed for the AC when WM compared GM.

Discussion & Conclusion

Unexpectedly brain aging doesn't slow the process of making a decision; the cognitive function does not significantly decline. However, the time for a simple motoric reaction increases, consequently the overall reaction time increases in the elderly cohort.

1-P11

TUBE CURRENT REDUCTION IN COMPUTED TOMOGRAPHY ANGIOGRAPHY – HOW LOW CAN WE GO IN PATIENTS WITH SUSPECTED ACUTE STROKE?

*N. Sollmann*¹, K. Mei², I. Riederer¹, S. Schön¹, F.K. Kopp², M.T. Löffler¹, J.S. Kirschke¹, E.J. Rummeny², C. Zimmer¹, P.B. Noel³, T. Baum¹

¹ Department of Diagnostic and Interventional Neuroradiology, Klinikum rechts der Isar, Technical University Munich, Munich, GERMANY, ² Department of Diagnostic and Interventional Radiology, Klinikum rechts der Isar, Technical University Munich, Munich, GERMANY, ³ Department of Radiology, Perelman School of Medicine, University of Pennsylvania, Philadelphia, USA

Introduction

Computed tomography angiography (CTA) as part of first-line stroke imaging protocols entails considerable radiation exposure for the patient. However, research on dose reductions for head and neck CTA is scarce. The aim of this study is to systematically evaluate image quality, detectability of large vessel occlusion (LVO) or dissection, and diagnostic confidence in CTA with virtually lowered tube current and iterative reconstruction (IR) in patients with suspected acute stroke.

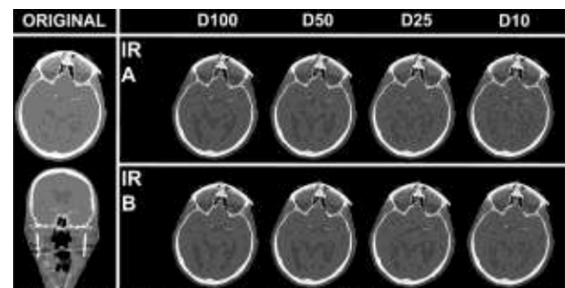


Fig. 1 79-year-old patient with a right-sided ischemic stroke of the middle cerebral artery (MCA, M1 segment). The figure illustrates axial (top) and coronal (bottom) computed tomography angiography (CTA) in two rows (A: similar regularization to clinical reconstructions, B: two times stronger regularization). Furthermore, axial slices of CTA scans reconstructed with 100%, 50%, 25%, and 10% (D10) of the original tube-current are shown, using two levels of iterative reconstruction (IR) algorithms (A, B)

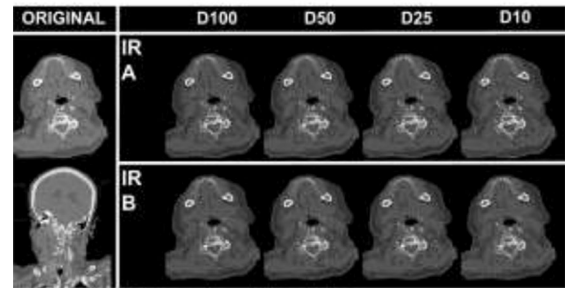


Fig. 2 81-year-old patient with a left-sided dissection of the extracranial internal carotid artery (ICA). The figure illustrates axial (top) and coronal (bottom) computed tomography angiography (CTA) in two rows (A: similar regularization to clinical reconstructions, B: two times stronger regularization). Furthermore, axial slices of CTA scans reconstructed with 100%, 50%, 25%, and 10% (D10) of the original tube-current are shown, using two levels of iterative reconstruction (IR) algorithms (A, B)

Methods

Thirty patients (age: 79.0 ± 10.4 years, 50% with LVO or dissection, affection of the middle cerebral artery in 53.3%) underwent CTA of the supraaortic up to the intracranial arterial vessels. CTA scans were simulated as if they were made at 50% (D50), 25% (D25), and 10% (D10) of the original tube current. Image reconstruction was achieved with two levels of IR (A: similar to clinical reconstructions, B: two times stronger regularization). Two readers (R1 and R2) performed qualitative image evaluation considering overall image quality and artifacts, vessel contrast, detection of vessel pathology, and diagnostic confidence (scoring: 1 – low, 2 – medium, and 3 – high confidence).

Result

Level B of IR was favorable regarding overall image quality and artifacts for D10, while level A was favorable for D100 and D50. CTA scans with D25 and both levels of IR still showed good vessel contrast, with even peripheral arterial branches of the anterior, middle, and posterior cerebral artery being clearly detectable. Further, CTA scans with D25 using level A of IR showed an adequate level of diagnostic confidence without any missed LVO or dissection according to evaluations of both readers (D25 A: R1: 2.5 ± 0.6 vs. R2: 2.6 ± 0.6 , $p > 0.05$). Inter-reader agreement was high for all items of evaluations, particularly when level A of IR was applied.

Discussion & Conclusion

CTA using IR and tube currents lowered down to 25% of original imaging is feasible without drawbacks regarding vessel contrast or detection of vessel pathology in patients with suspected acute stroke. Thus, our approach enables significant reductions in radiation exposure for head and neck CTA, with an average decrease from 8.5 ± 1.5 mGy to 2.1 mGy in our patients.

1-P12**EFFECT OF REPETITIVE TRANSCRANIAL MAGNETIC STIMULATION ON RESTING-STATE FUNCTIONAL CONNECTIVITY IN PATIENTS WITH CHRONIC DISORDERS OF CONSCIOUSNESS**

A. Sergeeva¹, E. Kremneva¹, S. Morozova¹, D. Sinitsyn², L. Legostaeva², A. Poydasheva², E. Iazeva³, D. Sergeev³, I. Bakulin², Y. Ryabinkina³, N. Suponeva², M. Piradov³

¹ Department of Neuroradiology, Research Center of Neurology, Moscow, RUSSIA, ² Department of Neurorehabilitation, Research Center of Neurology, Moscow, RUSSIA, ³ Department of Neurocritical Care, Research Center of Neurology, Moscow, RUSSIA

Introduction

Repetitive transcranial magnetic stimulation (rTMS) is a potentially effective approach to the recovery of chronic disorders of consciousness (DOC), i.e., vegetative state (VS) and minimally consciousness state (MCS), that may be explained by reorganization of large-scale cortical networks. We aimed to investigate the changes of resting-state functional connectivity (FC) patterns in DOC patients after rTMS.

Methods

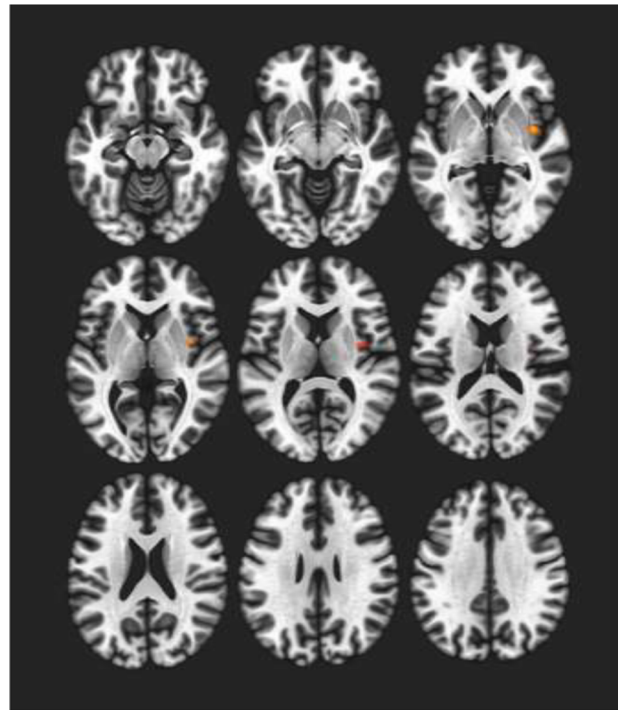
Twenty traumatic and non-traumatic DOC patients (10 VS and 10 MCS, 3 to 73 months post-injury) underwent 10 sessions of 20 Hz rTMS of the left angular gyrus. Resting-state FC was assessed before and after rTMS course. MRI data was analyzed using CONN toolbox ROI-to-ROI (with $p < 0.05$ corrected at the seed level) and Seed-to-Voxel (with cluster level of $p < 0.05$ corrected for FDR) approaches.

Result

Mild behavioral improvement (mean of 1.3 point, as assessed by Coma Recovery Scale-Revised) was seen in MCS patients (9 of 10 improved; $p = 0.006$). Among VS patients only 1 of 10 improved by 2 points ($p = 0.317$).

Effect of stimulation for the combined VS and MCS group was seen as increased FC between left lateral parietal cortex (within default mode network [DMN]) and the cluster of voxels within right insular cortex (Fig.). ROI-to-ROI analysis demonstrated decrease of connectivity between right anterior cingulate cortex (salience network) and right lateral prefrontal cortex, and between right lateral parietal cortex and right frontal eye fields (dorsal attention network). In MCS patients no changes were seen, while in VS patients FC between occipital visual network and sensorimotor superior network decreased. In a subset of anoxic MCS patients ($n = 4$) we observed increased connectivity between medial prefrontal cortex (MPFC) and right parietal cortex (components of DMN), and decreased connectivity between right intraparietal sulcus (dorsal attention network) and left posterior superior temporal gyrus (language network). Connections between MPFC and voxels

within right lateral occipital cortex, right angular gyrus and right middle temporal gyrus in this subgroup were also enhanced following non-invasive stimulation.

**Discussion & Conclusion**

Our non-randomized study demonstrated on a small sample of chronic DOC patients that rTMS may induce mild beneficial clinical effect in MCS patients, along with changes of FC of DMN regions.

Funding: the study is supported by RSF grant 16-15-00274

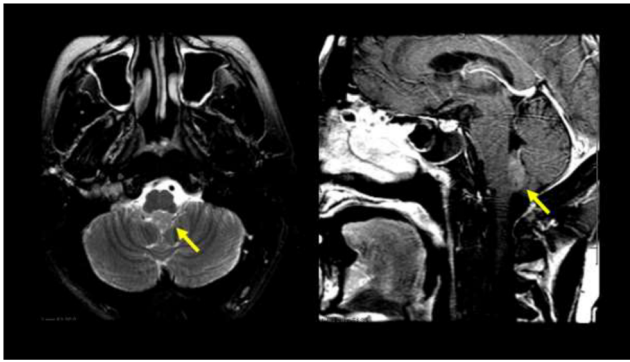
1-P13**IMAGING CHARACTERISTICS OF 4TH VENTRICLE SUBEPENDYMOMA**

A. Haider¹, R. Sawaya¹, G.N. Fuller², D.F. Schomer³, M. Gule-Monroe³

¹ MD Anderson Cancer Center, Department of Neurosurgery, Houston, USA, ² MD Anderson Cancer Center, Department of Pathology, Houston, USA, ³ MD Anderson Cancer Center, Department of Diagnostic Imaging, Houston, USA

Introduction

Subependymomas are rare, WHO Grade I central nervous system neoplasms of ependymal origin that represent approximately 0.2-0.7% of all intracranial tumors. Very little literature exists about the imaging characteristics of these tumors due to their scarcity. Here, we describe the clinical and radiological characteristics of 20 patients with 4th ventricle subependymoma.



Methods

This is a retrospective single-institution study performed after Institutional Review Board approval. Patients diagnosed with 4th ventricle subependymoma were identified via a search of the M.D. Anderson Cancer Center Brain and Spine Registry. A review of clinical, radiology and pathology reports and MRI images was performed.

Result

20 patients (14 male, 6 female) were identified. Nine patients underwent surgery, with histopathological confirmation of subependymoma. The median age at diagnosis was 53.7 years. Median tumor volume for the operative cohort was 4.32cm³, while for the non-operative cohort it was 0.48cm³. Eight patients in the operative group exhibited symptoms at diagnosis related to the 4th ventricular mass. For the total cohort, the majority of subependymomas (n=13) were isointense on T1, hyperintense (n=14) on T2, and enhanced (n=17). All tumors were located just below the body of the 4th ventricle, terminating at the level of the obex. The majority of operative cases (n=7) demonstrated extension of tumor into foramen of Magendie or Luschka, while only 1 case did so in the non-operative cohort.

Discussion & Conclusion

Our study is the first to identify a propensity for 4th ventricular subependymomas to be located below the body of the 4th ventricle. This novel finding may suggest that the subependymal glial cells that give rise to these lesions are the same cells that support the area postrema. Furthermore, the presence of tumor at the foramen of Luschka or Magendie was strongly linked to clinical symptoms requiring surgical resection. This is in contrast to the patients that were placed on imaging surveillance, where only one patient had minimal tumor at the foramen of Luschka.

This study is to the best of our knowledge the largest collection of 4th ventricular subependymomas with imaging findings published to date.

1-P14

THE INCIDENCE OF OCCULT BONE DEFECTS AT THE TEMPORAL BASE ON MRI

*S.E. Sanverdi*¹, M. A. Gurses¹, M.T. Kitapci¹

¹ Integra Imaging Center, Ankara, TURKEY

Introduction

Occult bony defects seen within the temporal base are relatively rare in comparison to the frontal and occipital regions. Although they are mostly congenital and asymptomatic, they have a potential risk for focal brain entrapments by increasing in size as a consequence of some certain situations such as over-sneezing, increased intracranial pressure, etc.

We herein aimed to investigate the incidence of those closure defects which are most likely to have ignored throughout a large number of series.

Methods

Patients: Magnetic resonance imaging of head, skull base, temporal bone and orbit of 1846 patients in total (F/M: 58/42%, median age: 47±6.3 year) who have been referred to our institution with various clinical indications have retro- and prospectively been evaluated within a period of 3 years between January, 2016 - January, 2019.

Image analysis: Axial and coronal SpinEcho T2-weighted images were evaluated by two radiologists in consensus to define the presence, the side and the size of the gap, and also to assess the meningo-/ encephaloceles and parenchymal changes in relevant cases. Heavy T2-weighted series and Computed Tomography images were applied where necessary and available.

Statistical analysis: Descriptives, Chi- Square and ANOVA tests were used in statistical analyses by accepting threshold of $p < 0.005$.

Result

An overall incidence of temporal base occult bony defect was found to be 4% with a slight male predominance (58%).

45 out of 74 in total were seen on the left.

18 of those patients revealed neural and/ or dural components trapped within the bony gap while only 9 of those showed cortical dysplasia.

The median width of the closure defect on either axial or coronal plane was measured 12±3.3 mm.

No side, age or gender predilection was obtained.

Discussion & Conclusion

Our results are in parallel to the literature which have been stated between 2-5% before, and with a regard to this consistency we do suggest that this entity should not be underestimated in daily imaging evaluations as bony gap may show changes in size by the time and new onset clinical manifestations may appear in some cases who were even asymptomatic in the past or with unexplained aetiology.

1-P15

RADIOLOGICAL FEATURES OF AUTOIMMUNE NEUROLOGICAL DISORDERS

*S. Ebden*¹, L. Guthrie¹, H. Jaber¹, M. Edwards², G. Ingram², O. Pearson², S. Sadiq¹

¹ Swansea Bay University Health Board, Department of Radiology, Swansea, UNITED KINGDOM, ² Swansea Bay University Health Board, Department of Neurology, Swansea, UNITED KINGDOM

Introduction

Antibody-mediated autoimmune neurological disorders are a group of rare but well described conditions that are rapidly expanding. Pathological autoimmune disease occurs due to a specific adaptive autoimmune response that targets an antigen occurring within the body. The antibodies involved can be classified by their target on either the cell surface, such as the NMDA-receptor or voltage-gated potassium channel, or aimed at intra-cellular components including anti-Hu, anti-Ri and anti-Yo syndromes.

Patients can present with a variety of disorders including limbic encephalitis, transverse myelitis and cerebellar dysfunction. Many of these disorders are paraneoplastic associated with underlying malignancy.

This review explores a series of antibody-mediated autoimmune neurological disorders describing the clinical and radiological features and commonly associated malignancies.

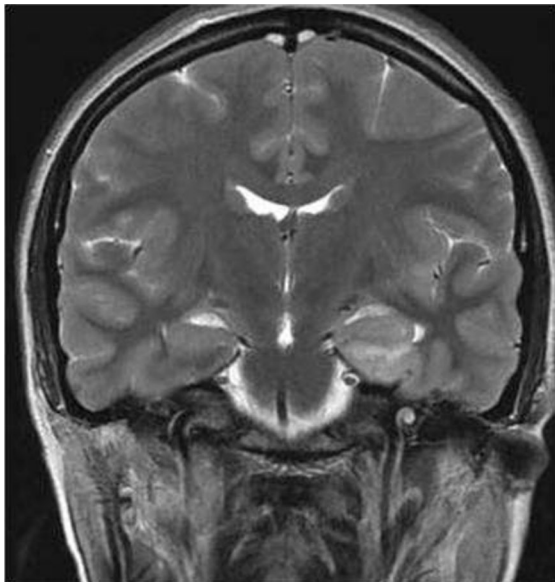
Methods

A group of patients have recently presented to our tertiary neurosciences department with subacute neurological deterioration and subsequently found to have positive serology for one of these recognised antibody-mediated autoimmune neurological disorders.

A retrospective analysis of the case notes and radiology was performed, together with the radiological differential diagnosis that was provided prior to the availability of the serology results. If appropriate, any subsequent investigations for malignancy were also reviewed.

Result

We describe a case series of different autoimmune neurological disorders including cases of anti-VGKC, anti-NMDA, anti-GFAP and anti-CRMP5 encephalitis; anti-Ri cerebellar disease and aquaporin -4 and anti-MOG neuromyelitis spectrum disorder. We compare the imaging features of these cases to other important radiological differentials including infection, inflammation and malignancy which would require other forms of treatment.



Discussion & Conclusion

We highlight the importance of considering autoimmune pathology in patients with subacute neurological disorders, some of whom are young adults. Many of these disorders have radiological findings which are similar to other pathologies making the initial diagnosis challenging and others have a strong clinical association with specific malignancies which maybe undiagnosed prompting onward urgent investigation and follow-up surveillance imaging.

Radiological recognition of this group of relatively new neuroradiological disorders, together with knowledge of the radiological differential diagnoses, is an integral part of the patient's care requiring close clinico-radiological correlation and discussion.

1-P16

SUSCEPTIBILITY-WEIGHTED IMAGING AS AN ALTERNATIVE TO CONTRAST-ENHANCED T1W IMAGES FOR DETECTING ACUTE MULTIPLE SCLEROSIS LESIONS

A. Rovira¹, L.M. Pessini Ferreira¹, A. Barros¹, A. Salerno¹, C. Auger¹

¹ Neuroradiology Section, Radiology Department, Vall d'Hebron Research Institute, Barcelona, SPAIN

Introduction

Multiple sclerosis (MS) is a chronic neuroinflammatory disease with spatiotemporal dissemination of lesions within the central nervous system. Gadolinium-enhancement of focal lesions on MRI indicates active inflammation, and represents a marker of disease activity. Susceptibility-weighted imaging (SWI) is an MRI technique that allows in vivo detection of iron content in tissues. We hypothesize that in gadolinium-enhancing lesions, no iron is present within the lesion, while on non-enhancing new T2 lesions iron deposition could be identified. Therefore, the absence of susceptibility effect on SWI would indicate active inflammation on new MS lesions. The aim of this study is to determine the utility of SWI for predicting gadolinium enhancement in a sample of new T2 MS lesions.

Methods

We retrospectively reviewed a set of 60 multiple sclerosis patients, who had undergone a baseline and a follow-up (maximum of 18 months) 3T MRI, in whom new T2 lesions were identified. Each new T2 lesion was evaluated in a blinded fashion: SWI were evaluated in a first reading session, and gadolinium-enhanced images in another session carried out three weeks later. Statistical analysis was based on 2 x 2 contingency tables using SPSS statistical software.

Result

We evaluated a total sample of 192 new T2 lesions. Based on the absence of signs indicating iron deposition (hypointense rim or dot not attributable

to a central vein), the sensitivity, specificity, positive predictive value, negative predictive value and accuracy of SW images for predicting gadolinium enhancement were 83.7%, 92.9%, 78.2%, 94.9% and 90.8%, respectively.

Discussion & Conclusion

The absence of iron deposition on SWI seems to be a useful marker of active inflammation in new MS brain lesions. SWI could be considered as an alternative to gadolinium-enhanced MRI for assessing disease activity in the monitoring process of MS patients.

1-P17

THE IMPORTANCE OF MRI PULSE SEQUENCE SELECTION IN DETECTING BRAIN HYPINTENSE LESIONS IN MULTIPLE SCLEROSIS. RELEVANCE FOR THE DEFINITION OF “BLACK HOLES”

*N. Romano*¹, *C. Lapucci*², *S. Schiavi*^{2,3}, *L. Saitta*⁴, *A. Signori*¹, *M.P. Sormani*¹, *G. Boffa*^{2,5}, *M. Pardini*^{2,5}, *A. Uccelli*^{2,5}, *M. Inglese*^{2,5}, *L. Roccatagliata*^{1,4}

¹ Department of Health Sciences (DISSAL), University of Genoa, Genoa, ITALY, ² Department of Neuroscience, Rehabilitation, Ophthalmology, Genetic, Maternal and Child Health, University of Genoa, Genoa, ITALY, ³ Department of Computer Science, University of Verona, Verona, ITALY, ⁴ Department of Neuroradiology, Ospedale Policlinico San Martino, Genoa, ITALY, ⁵ Department of Neurology, Ospedale Policlinico San Martino, Genoa, ITALY

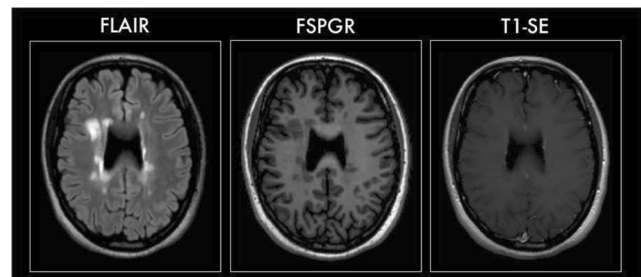
Introduction

In Multiple sclerosis (MS), T1-weighted spin echo (T1SE) sequences are used to detect chronic hypointense lesions. 3D-T1-weighted gradient-echo (3D-T1GE) are able to detect a greater number and volume of hypointense lesions with respect to T1SE images, but microstructural correlates of these different types of hypointensities has not been investigated.

The aims of our work are to evaluate lesions detectability on 2D-T1SE and 3D-FSPGR sequences, to quantify the degree of microstructural changes within lesions and to correlate them with patients' clinical status.

Methods

60 patients underwent brain MRI on 1.5T and 3T scanners. We identified T2-FLAIR hyperintense lesions with no hypointense signal on T1SE/3D-FSPGR (a), hypointense lesions only on 3D-FSPGR (b) and hypointense lesions on both T1SE and 3D-FSPGR sequences (c). We compared mean lesion number (LN) and volume (LV) identified on T1SE and 3D-FSPGR sequences. We correlated T1SE and 3D-FSPGR LN and LV with EDSS. Friedman test was performed to compare FA and MD inside each lesions type.



Result

35 patients were female. Mean age was 39.1 (± 7.8); mean EDSS was 3 (± 2). FSPGR and T1SE LN and LV were significantly different ($p < 0.001$) and both correlated with EDSS (for FSPGR: $r = 0.55$ and $r = 0.53$, $p < 0.001$; for T1SE: $r = 0.56$ and $r = 0.59$, $p < 0.001$). Mean FA and MD values inside lesions were 0.33 (± 0.06) and 0.9 (± 0.1) 10^3 mm²/sec (a), 0.31 (± 0.04) and 0.9 (± 0.1) 10^3 mm²/sec (b), 0.26 (± 0.05) and 1.1 (± 0.1) 10^3 mm²/sec (c). FA and MD inside (a), (b), and (c) were significantly different ($p = 0.008$, $p = 0.0003$).

Discussion & Conclusion

3D-FSPGR demonstrated a better sensitivity in detecting chronic hypointense lesions with respect to T1SE. MRI microstructural parameters revealed different degrees of tissue damage on different pulse sequences, suggesting a histopathological continuum with more severe damage in lesions detected on T1SE. These results have important implications on the definition of “black holes” particularly in the setting of MS monitoring in adult patients and on the role of T1 hypointense lesions in paediatric patients at the first episode.

MRI sequences standardization represents an issue for future investigations on clinical criteria for MS diagnosis and follow-up.

1-P18

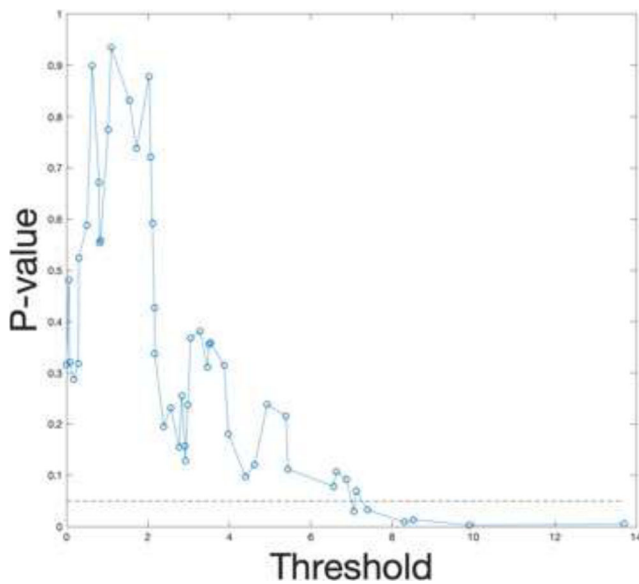
PROGNOSTIC FACTORS IN GBM: POST-OPERATIVE TUMOR VOLUME

*M. Fernandez-Taranilla*¹, *A. Hilario*¹, *E. Salvador*¹, *P. Martin-Medina*¹, *L. Koren*¹, *J. Sepulveda*¹, *A. Lain-Hernandez*¹, *A. Perez-Nuñez*¹, *V. Perez-Garcia*², *J. Perez-Beteta*², *D. Molina-Garcia*², *A. Ramos*¹

¹ Hospital Universitario 12 de Octubre, Madrid, SPAIN, ² University MOLAB, Ciudad Real, SPAIN

Introduction

Glioblastoma (GBM) is the most aggressive primary malignant brain tumor with poor survival outcomes. Surgical resection have shown impact on survival but complete resection is difficult to achieve due to the risk of neurologic function deficits. The aim of this study was to identify the relationship between the contrast enhancing (CE) tumor volume after surgery and overall survival, taking into account the location of the tumor.



Methods

Retrospective analysis and semi-automatic segmentation of pre and post-operative volumetric MRI (1.5T) of adults patients with unifocal gliomas. GBM grade IV WHO, demonstrated on biopsy/resection at a tertiary care institution between 2012 to 2018. We excluded secondary and recurrent GBM and IDH1- positive mutation patients due to different survival rates. Overall(OS) survival was defined as the interval from the date of post-operative MRI to the date of death. Tumor was classified on frontal,temporal,parietal, occipital,basal ganglia and corpus callosum locations depending on where the majority of the tumor was centered.

Result

We reviewed 395 gliomas, 246 were excluded because histology was not pure GBM grade IV WHO, 18 for lacking volumetric images, 21 with multicentered disease, 3 due to severe artifacts on images available and 11 with IDH-1positive mutation. Clinical, operative and hospital records of the remaining 96 patients were retrospectively reviewed: 55males and 41 women with a mean ages of 60years old. 45 patients with total resection,38 as subtotal and 13 with biopsy. Kaplan-Meier univariate analysis was performed on pre and post-operative volume, surgery/biopsy and location and multivariate analysis with Spearman correlation. Total/subtotal resection had higher survival rates than biopsy (p-value= 0-006). Patients with post-surgery volumes <10cm³ survived 7,79 months more that the group with higher residual volumes (p-value=0.003).

Discussion & Conclusion

Post-operative CE tumor volume, seems to be an independent prognostic factor on OS and residual CE volumes <10cm³ could increase survival rates in GBM patients.

1-P19

ASSESSING TREATMENT RESPONSE IN DIFFUSE GLIOMAS: KEYS TO DIFFERENTIATE TRUE PROGRESSION FROM PSEUDOPROGRESSION

A. Hilario ¹, E. Salvador ¹, P. Martin-Medina ¹, L. Koren ¹, J. Sepulveda ¹, A. Hernandez-Lain ¹, A. Perez-Nuñez ¹, A. Lagares ¹, A. Ramos ¹

¹ Hospital 12 de Octubre, Madrid, SPAIN

Introduction

The purpose of this study is to describe tips and tricks at MRI that helps us differentiate true progression (TP) from pseudoprogression (PsP) in the follow-up of treated gliomas.

Methods

This work has been carried out in a reference center in neuro-oncology. We review DWI, DCE and DSC perfusion MRI, as well as patterns of contrast enhancement in a group of glioblastomas treated surgically and with chemoradiotherapy according to STUPP scheme.

Result

PsP occurs in 20-30% of all patients treated for malignant glioma, and the risk is increased in patients with MGMT promoter methylation. PsP usually appears on MRI within the first 3 months of completing radiotherapy, but can occur 6 months after treatment or longer. Confirmation of PsP requires either stability or improvement of enhancement or histological diagnosis.

Conventional MRI signs have limited utility, but new enhancement outside the margins of irradiation or subependymal spread are useful MRI markers in identifying TP.

Analyzing DSC, longitudinal trends in rCBV may be more useful than absolute rCBV in distinguishing PsP from TP. Although one would expect lower rCBV less than 1.75 values in PsP, overlapping rCBV for PsP and TP at initial progressive enhancement has been demonstrated.

At DCE, patients with PsP have lower measures of V_p, V_e and K_{trans} than patients with TP. Due to the slow and progressive enhancement of post-treatment changes, pseudoprogression shows a smaller initial (iAUC) and higher final (fAUC) area under the time signal-intensity curve at the semiquantitative analysis.

On the basis of DWI, the mean ADC has a limited role, but the lower end values (5th percentile point) of the cumulative ADC histograms could help differentiating TP from PsP.

Discussion & Conclusion

Accurate differentiation between PsP and TP remains challenging for optimal treatment. Diffusion and perfusion imaging parameters may demonstrate different diagnostic values for predicting PsP in treated gliomas.

1-P20

CONTRAST ENHANCEMENT PATTERN IS PREDICTIVE OF SURVIVAL IN PEDIATRIC GLIOBLASTOMAS

H. Pokhylevych ¹, M. Gule-Monroe ¹, M. Chen ¹, G. Fuller ¹, S. Gruschkus ¹, J. Johnson ¹

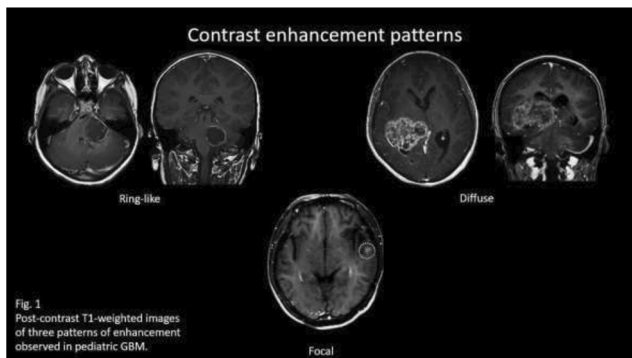
¹ The University of Texas MD Anderson Cancer Center, Houston, USA

Introduction

Pediatric glioblastomas have a dreadful prognosis, and are rare, comprising 2.9% of all central nervous system tumors in children. They have therefore received little attention in the literature. Available studies indicate that pediatric glioblastomas behave differently compared to adult glioblastomas. These tumors are also genetically distinct from adult glioblastomas. Contrast enhancement of gliomas on magnetic resonance (MR) images corresponds to break down of the blood-brain barrier related to vascular proliferation in malignant gliomas. The purpose of this study was to determine whether tumor enhancement is a prognostic factor that can be used to predict survival.

Methods

After obtaining IRB approval, imaging studies and clinical data from sixty-four pediatric patients with pathology-proven GBMs treated at our institution between May 2004 and December 2018 were evaluated. Imaging characteristics and treatment were analyzed. Contrast enhancement patterns were classified into three types: focal, ring-like and diffuse, based on preoperative post-contrast T1-weighted MR images (See Figure 1).



Statistical analysis was performed to evaluate the prognostic value of MR enhancement.

Result

Patients with focal-enhanced GBMs had a significantly longer progression free survival ($p = 0.0308$) comparing to other enhancing glioblastomas (diffuse and ring-like). Our data also confirmed that extent of resection remains the most important prognostic factor. Patients with GTR had a significantly longer overall survival and progression free survival ($p=0.0493$ and $p=0.0244$ respectively).

Discussion & Conclusion

Our findings show a strong relationship between the preoperative contrast enhancement pattern and survival in pediatric GBM. This finding can be useful to radiologists, clinical oncologists, and neurosurgeons for predicting outcomes as well as treatment planning. Based on prior publications predominantly on adult gliomas, the enhancement pattern may have a genetic basis and further research on this association is underway.

1-P21

THE USEFULNESS OF THREE-COMPARTMENT MODEL ANALYSIS DCE MRP IN THE EVALUATION OF POST-TREATMENT HIGH GRADE GLIOMA: EXPERIENCE AT SIRIRAJ HOSPITAL

*S. Piyapittayanan*¹, T. Sawangthap¹, O. Chawalparit¹, R.K. Gupta², C. Ngamsombat¹, S. Sathornsumtee³, J. Petsuksiri¹

¹ Siriraj Hospital - Department of Radiology, Bangkok, THAILAND, ² Fortis Memorial Research Institute - Department of Radiology, Haryana, INDIA, ³ Siriraj Hospital - Department of Medicine, Bangkok, THAILAND

Introduction

The differentiation between tumor recurrence and post-treatment related change in high grade glioma (HGG) is problematic and challenging. Dynamic contrast-enhanced (DCE) MRI provides the information of multiple pharmacokinetic parameters that could characterize the vascularity of a suspicious brain lesion and helps to differentiate the lesion's nature. Our purpose was to evaluate the usefulness and diagnostic accuracy in discriminating tumor recurrence from post-treatment change of HGG by using the three-compartment model analysis of DCE MRP.

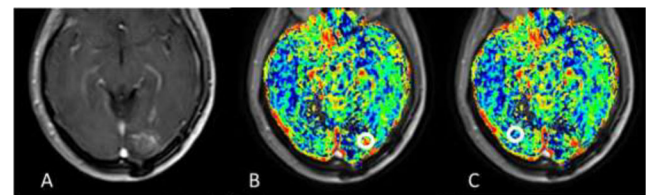


Fig.1 There was newly developed enhancement at the tumor bed area on contrast enhanced T1wi at left occipital region (picture A). On the CBV map, ROIs were drawn in the tumor bed area that showed highest perfusion (white circle in picture B) and the contralateral normal appearing white matter (white circle in picture C).

Methods

Twenty patients with HGG underwent cMRI and DCE MRP after standard treatment and were classified into two groups; tumor recurrence ($n=11$) and post-treatment related change ($n=9$). The DCE MRI derived parameters were obtained by using three-compartment pharmacokinetic model analysis and measured values in region of interest (ROI) at the lesion which showed highest perfusion in colored CBV map. Then, another same sized ROI was drawn at the contralateral normal appearing white matter and calculated parameter ratios.

Result

The ICC of all parameters are fair to excellent (0.303-0.969). The CBV, CBV corrected V_e , CBV corrected leakage, and CBF ratio from the recurrent lesions were significantly higher than those with post-treatment related change ($p = 0.02, 0.02, 0.02,$ and $0.38,$ respectively). The cutoff value of 1.72 for CBF ratio and the cutoff value of 2.069 for CBV, CBV corrected V_e , and CBV corrected leakage, would give accuracy of 75% with 72.7%

sensitivity, 80% and 77.8% specificity. The inter-observer reliability was accessed by intraclass correlation coefficient (ICC). Pairwise comparisons were performed by using the Mann-Whitney U test. The ROC curves of significant parameters were used to establish the cutoff value for differentiating the two entities.

Discussion & Conclusion

We found that the quantitative values of CBV, CBV corrected Ve, and CBV corrected leakage at the recurrent lesions were significantly higher than the lesions in those with post-treatment related change which concordant with prior studies. Because elevated CBV and Ve values in HGG are resulted from tumor angiogenesis, and subsequently increased microvascular density and altered capillary permeability. The three-compartment model derived DCE-MRI parameter is useful for discriminating between tumor recurrence and post-treatment related change in patient with high grade glioma.

1-P22

MRI ANATOMICAL VARIANTS OF THE HEAD OF THE HIPPOCAMPUS

*E. Piccirilli*¹, L. Gentile¹, V. Panara¹, P.A. Mattei¹, M. Caulo¹

¹ ITAB Institute for Advanced Biomedical Technologies Department of Neuroscience and Imaging, Chieti, ITALY

Introduction

The head of the hippocampus (H) is classically described as having 2 to 4 digitations both in ex-vivo specimens and in-vivo, on MRI coronal images. The systematic observation of brain MR of healthy subjects enrolled in research protocols reveals however a greater variability. Our aims were to use MRI in a large sample population of healthy subjects to define the spectrum of such variability and to provide a new, possibly extensive, classification of the different anatomical variants of the H in the coronal plane

	0A	0B	1A	1B	1C	1D	2A	Total
	No. (%)	No. (%)	No. (%)	No. (%)	No. (%)	No. (%)	No. (%)	No. (%)
OVERALL								
Right hemisphere	20 (8.4)	2 (0.8)	19 (8.0)	29 (12.2)	4 (1.7)	7 (2.9)	157 (66.0)	238
Left hemisphere	28 (11.8)	4 (1.7)	23 (9.7)	32 (13.4)	2 (0.8)	6 (2.5)	143 (60.1)	238
Total	48 (10.1)	6 (1.3)	42 (8.8)	61 (12.8)	6 (1.3)	13 (2.7)	300 (63.0)	476
MEN								
Right hemisphere	14 (10.1)	1 (0.7)	9 (6.6)	17 (12.3)	1 (0.7)	6 (4.4)	90 (65.2)	138
Left hemisphere	12 (8.7)	1 (0.7)	15 (10.9)	22 (15.9)	1 (0.7)	2 (1.4)	85 (61.7)	138
Total	26 (9.4)	2 (0.7)	24 (8.7)	39 (14.1)	2 (0.7)	8 (2.9)	175 (63.5)	276
WOMEN								
Right hemisphere	6 (6.0)	1 (1.0)	10 (10.0)	12 (12.0)	3 (3.0)	1 (1.0)	67 (67.0)	100
Left hemisphere	16 (16.0)	3 (3.0)	8 (8.0)	10 (10.0)	1 (1.0)	4 (4.0)	58 (58.0)	100
Total	22 (11.0)	4 (2.0)	18 (9.0)	22 (11.0)	4 (2.0)	5 (2.5)	125 (62.5)	200

Table 1 Overall frequencies and percentages of the morphological variants of H

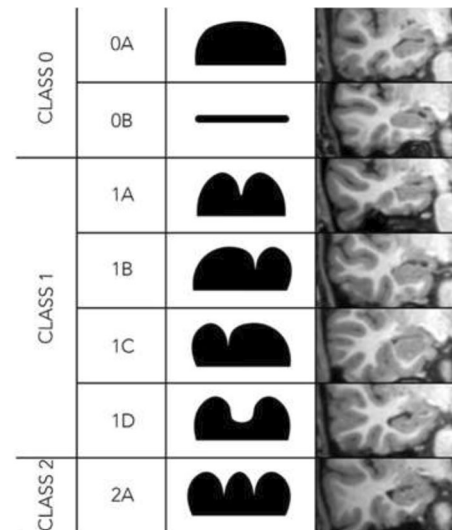


Fig 1. Schematic representation of the criteria used for morphological classification of the H

Methods

Brain MRI were obtained from 238 young healthy subjects (138 M; age 18-39). The H were identified on high resolution T1W 3D MRI images (1 mm thick), coronal reformatted according to a plane parallel to the fourth ventricle at the level of mammillary bodies. First, the H of a subset of 100 healthy subjects were analyzed and classified according to morphological criteria (the number of sulci and the number and size of the digitations) to identify the anatomical variants; then this classification was used to estimate the frequencies of the anatomical variants in a larger subset of 238 healthy subjects (a total of 476 H reviewed). The frequencies of the different anatomical variants of the H were reported for hemisphere and sex

Result

Class 0 variant (total absence of sulci, 11.3%) is subdivided in 0A (one digitation, 10.1%) and 0B (no digitations or “null variant”, 1.1%). Class 1 variant (25.6%, one single sulcus) is further subdivided into four types according to the location and the width of the sulcus [1A (8.8%), 1B (12.8%), 1C (1.3%) and 1D (2.7%)]. Class 2 variant (“classical variant”, two symmetrical sulci and three digitations, equal in size) is the most frequent overall (63%). A statistically significant difference between the hippocampal head classification of the two hemispheres was observed only in women (p=.035, Marginal Homogeneity Test) and overall (p=.047, Marginal Homogeneity Test). The prevalence of the anatomical variants did not differ between genders

Discussion & Conclusion

The large study population allowed the description of a new morphologic classification of the H which should allow to minimize the risk of misinterpreting anatomical variants as pathological conditions

1-P23

TUMEFACTIVE INFLAMMATORY LEUKOENCEPHALOPATHY IN COCAINE USERS: REPORT OF THREE CASES

*L.M. Pessini Ferreira*¹, S. Kremer², C. Auger¹, J. Castillo¹, J. Pottecher², J. de Sèze², B. Lhermitte², E. Maciag¹, A. Rovira¹

¹ Hopsital Vall d'Hebron, Barcelona, SPAIN, ² CHU de Strasbourg, Université de Strasbourg, Strasbourg, FRANCE

Introduction

Cocaine is the most common illicit stimulant drug used in Europe, and it can potentially affect the central nervous system due to a direct effect, or by means of additive drugs. Levamisole has been increasingly used as an additive drug since it extends the stimulating effects of cocaine. This has led to an increase in the detection of levamisole adverse reactions, including levamisole-induced multifocal inflammatory leukoencephalopathy (MIL), a potentially lethal monophasic cerebral demyelinating disease.

Methods

We present three clinico-radiological cases of tumefactive MIL. All of these patients had a history of cocaine abuse (chronic in the first two cases, and acute in the third one) but none had previously developed neurological symptoms. Our cases were retrospectively evaluated, accessing clinical data from medical records, as well as laboratory tests and MRI studies. Imaging findings revealed the presence of tumefactive MIL in all these cases. The first two patients had lesions following a Balo's Concentric Sclerosis (BCS) pattern.

Result

Levamisole-induced MIL may lead to the development of multiple demyelinating lesions affecting the subcortical and periventricular white matter, basal ganglia and/or brainstem. Tumefactive demyelinating lesions are an unusual finding in levamisole-induced MIL. Specifically, the BCS pattern is a rare finding in these patients: to our knowledge, only two more cases mimicking BCS have been reported in the literature, which have also occurred in chronic cocaine users.

Discussion & Conclusion

Based on the history and images of our patients and other two similar case reports, we suggest a probable pathophysiological relationship between levamisole-adulterated cocaine use and the occurrence of tumefactive MIL with atypical demyelinating lesions, even when they present following a BCS imaging pattern.

1-P24

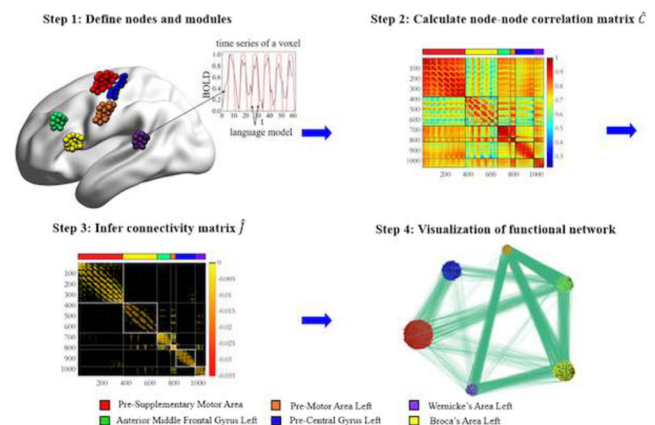
GRAPH THEORETICAL ANALYSIS OF TASK-BASED FUNCTIONAL MAGNETIC RESONANCE IMAGING OF HUMAN LANGUAGE: THE TRIANGLE OF SPEECH

*L. Pasquini*¹, Q. Li², G. Del Ferraro², F. Dellepiane¹, K. Peck³, M. Jenaby³, H. Makse², A. Holodny³

¹ Sant'Andrea Hospital, La Sapienza University, rome, ITALY, ² City college of New York, New York, USA, ³ Memorial Sloan Kettering Cancer Center, New York, USA

Introduction

The human language network has been investigated using different approaches, with variable results. Task-based functional MRI (tb-fMRI) is a powerful method to identify brain areas involved in cognitive performances, such as language production. Pre-surgical planning of brain tumors is routinely accompanied by fMRI to guide the neurosurgeon's understanding of the eloquent brain areas. Although tb-fMRI sheds light on areas involved in cognitive processes, it does not elucidate how they functionally interact with each other and integrate to form a comprehensive network. Our main objective was to investigate the language network of healthy subjects from tb-fMRI data by ad hoc implementation of statistical inference techniques (LASSO) based on graph theory. We further investigated the role of sub-divisions of Broca's Area in the network



Methods

We recruited 20 healthy right-handed subjects who performed a language production task. The active voxels were grouped into clusters according to their anatomical location on fMRI. Starting from the active clusters, we constructed the pairwise correlation matrix and inferred the connectivity matrix of the functional network using a penalization parameter. We set the penalization parameter to threshold the matrix based on brain integration (all the clusters are connected) and sparsity (minimal wiring)

Result

Our results show a triangular-shaped common functional language network across 20/20 subjects, which entangles Broca's area, supplementary motor area, and pre-motor cortex in the left hemisphere. The common network across 18/20 subjects also included left Wernicke's area. The pars opercularis resulted by far more connected with the other nodes of the network than Broca's pars triangularis.

Discussion & Conclusion

This new approach allows to gather valuable information about brain connectivity from the tb-fMRI examination routinely performed in clinical practice. This post-processing technique is general and not limited to language tasks, in addition to healthy controls it can be applied to patients and help understanding critical clinical questions, such as brain functional connectivity for pre-surgical planning.

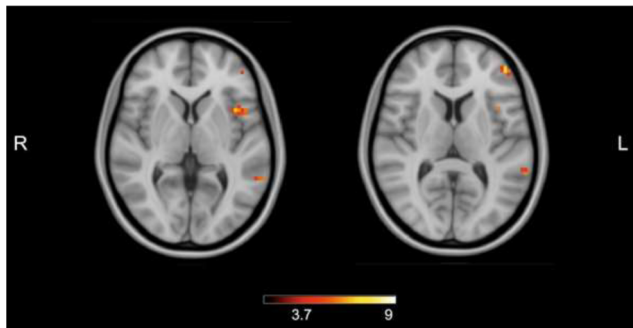
1-P25**REORGANIZATION OF BRAIN NETWORKS FOLLOWING CAROTID ENDARTERECTOMY: FUNCTIONAL CONNECTIVITY CHANGES AND COGNITIVE EVALUATION**

*L. Pasquini*¹, A. Romano¹, M. Rossi Espagnet^{1, 2}, M. Moraschi¹, F. Giove¹, D. Mascali¹, A. Di Vita¹, S. Lisi¹, R. Margiotta¹, T. Dezi¹, F. Dellepiane¹, M. Taurino¹, A. Bozzao¹

¹ Sant'Andrea Hospital, La Sapienza University, Rome, ITALY, ² Bambino Gesù Children's Hospital, Rome, ITALY

Introduction

To assess whether there is reorganization in brain networks after Carotid Endarterectomy (CEA) using resting state Magnetic Resonance, with a special focus in the Default Mode Network (DMN).

**Methods**

10 subjects with unilateral ICA stenosis and surgical indication for CEA according to the guidelines of the European Society for Vascular Surgery were recruited. Subjects were scanned in two conditions: few days before surgical operation (PRE-sur) and after six months from the intervention (POST-sur). Data were collected on a 1.5T MRI scanner equipped with a standard birdcage coil. FC maps of the DMN were produced using a Seed-to-Voxel approach. Patients underwent extensive neuropsychological testing before and after surgery, including the assessment of: general cognitive functioning by means of the Mini Mental State Examination; executive, attention, memory, language and visuo-spatial functions.

Result

In PRE-sur group, our results showed that FC of the injured hemisphere was decreased with respect to FC of the not-injured hemisphere in areas of the amygdala and frontal pole, while it was increased in areas of the occipital fusiform gyrus, temporal pole and anterior division of middle temporal gyrus. In POST-sur condition, our result showed that FC of the injured hemisphere was increased with respect to the not-injured hemisphere in areas of the temporal-occipital part of the middle temporal gyrus, frontal opercular cortex and frontal pole (figure). No significant decrease of FC between the injured and not-injured hemisphere was found. A Wilcoxon signed-rank test was used to assess any differences between the evaluations in any test. A qualitative analysis highlighted an improvement in 6/10

patients in the following cognitive domain: general cognitive functioning, verbal memory and executive function.

Discussion & Conclusion

CEA procedure is associated with improvement of neurocognitive performance and reorganization of functional connectivity, including the DMN. With further development, this analysis could provide significant parameters to predict clinical outcome of patients undergoing CEA

1-P26**CORTICAL THICKNESS AND GYRIFICATION INDEX IN PSYCHOTIC DISORDERS: FROM FIRST EPISODE PSYCHOSIS TO CHRONIC DISEASE**

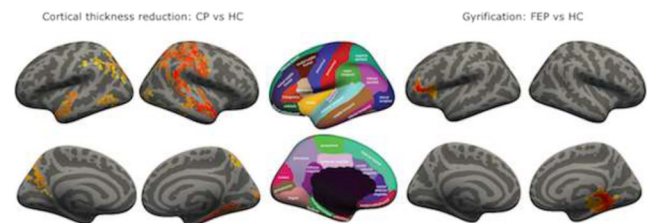
*L. Pasquini*¹, M.C. Rossi Espagnet^{1, 2}, A. Romano¹, M. Lucignani², A. Del Casale¹, F. Delle Piane¹, A. Napolitano², A. Bozzao¹

¹ Sant'Andrea Hospital, La Sapienza University, Rome, ITALY, ² Bambino Gesù Children's Hospital, Rome, ITALY

Introduction

Psychotic disorders are a disabling condition leading to severe functional impairment and increased mortality. Therefore identification of biomarkers is of great importance as it may provide a better understanding of the disease pathophysiology and a tool for diagnosis, especially in the early phase of the disorder.

The purpose of this study was to explore cortical morphometric parameters such as cortical thickness (CT) and Local Gyrification Index (LGI) in patients affected by chronic psychosis (CP) and first episode psychosis (FEP) and to evaluate differences between the two groups and with healthy controls (HC).

**Methods**

18 patients with a clinical diagnosis of FEP and 21 patients with a diagnosis of CP were enrolled. A group of age-matched 16 HC was included for comparison. All subjects underwent a brain MRI (1.5 T scanner, Siemens Sonata, Erlangen Germany) including a non-contrast 3D-T1 sequence.

FreeSurfer recon-all pipeline was used for image preprocessing, CT and LGI estimation. Cortical parameter differences among groups were assessed using permutation tests (Permutation Analysis of Linear Models FSL package with 1000 permutations). We produced Threshold-Free Cluster Enhancement (TFCE) statistical maps using group age as covariate and detected significantly altered cortical regions by thresholding at family-wise error

corrected $p < 0.05$. Results were displayed on a common inflated surface template.

Result

Statistically significant CT reduction was found in bilateral temporal and parietal lobes of CP when compared to HC, while no significant thickness differences resulted between FEP and HC. Comparing FEP and CP, we observed a CT thinning trend as disease progress from the onset to its chronic phase. Compared to HC, FEP LGI resulted significantly increased, especially in the left frontal and right temporal lobes. No significant LGI differences were found between CP and HC.

Discussion & Conclusion

This study provides possible markers for psychotic disorders as a tool for diagnosis, especially in the early phase of the disorder. Hypergyrification in FEP and reduction of CT in CP may represent markers of disease severity possibly reflecting the result of multiple processes including early alteration of neural development and delayed effects on neural connections.

1-P27

IMAGING OF GLOBE AND VISUAL PATHWAY: ANATOMY WITH RELATED COMMON PATHOLOGIES

*B. Nanda*¹, *K. Yeong*¹, *K. Lin*¹

¹ NG TENG FONG GENERAL HOSPITAL, SINGAPORE, SINGAPORE

Introduction

Disease processes affecting vision may be primarily related to the globe or visual pathway, or can be secondary to infiltration or mass effect from pathologies arising from adjacent structures. The visual pathway is divided into anterior and posterior pathways. The anterior pathway comprises of retina, optic nerve, optic chiasma, optic tract and lateral geniculate bodies. Whereas structures beyond it i.e. optic radiations and primary visual cortex are included in the posterior pathway.

Involvement of the globe and visual pathway produces characteristic clinical and radiological manifestations. Accurate knowledge of anatomy along with history and clinical examination is important to pin point site of disease process. Cross sectional imaging i.e. Computed tomography (CT) and Magnetic resonance imaging (MRI), is an important tool not only in disease localisation, characterisation and providing differential diagnosis but also helps to timely identify severe complications that may lead to devastating consequences such as vision loss.



Methods

1. Review imaging anatomy of the globe and anterior visual pathway.
2. Review differential diagnoses and imaging pearls of pathologies with pictorial illustrations.

Result

Various disease processes involve the globe and visual pathway, including traumatic pathologies, infection and inflammatory diseases, demyelination, optic neuropathies with multiple aetiologies (including the compressive neuropathies caused by orbital & supra-sellar masses or thyroid orbitopathy) and less common lesions like tumours and idiopathic intracranial hypertension.

CT scan is useful in identifying calcification, haemorrhage and provides excellent bony details. MRI on the hand allows better delineation of the anatomy of entire visual pathway due to its excellent soft tissue resolution without exposure to ionising radiation.

Discussion & Conclusion

This educational exhibit aims to identify and provide a broad overview of the anatomy and CT/MR imaging appearances of the various pathologies affecting the globe and visual pathway.

1-P28

EARLY OUTCOMES OF BRAIN ARTERIOVENOUS MALFORMATIONS TREATED WITH DIFFERENT THERAPEUTIC STRATEGIES: ONE HOSPITAL-BASED COHORT STUDY

*B. Milatovic*¹, *S. Milosevic*², *N. Vojvodic*², *I. Nikolic*²

¹ Clinical Center of Serbia, Belgrade, SERBIA, ² Clinical Center of Serbia, Belgrade, ³ Clinical Center of Serbia, Belgrade, ⁴ Clinical Center of Serbia, Belgrade

Introduction

Objective: Brain arteriovenous malformations (AVMs) are the leading cause of intracranial hemorrhage in young patients. Our aim was to estimate the early outcomes in patients with AVMs treated with different strategies and to investigate the possible factors that might be reliable predictors of those outcomes.

Methods

We performed a retrospective hospital-based cohort study, using data from 58 patients with clinically manifested intracranial AVMs. All of the patients were hospitalized and treated in oneneurosurgery center between 2010 and 2016. All relevant demographic, clinical, and neuroradiological data were analysed in terms of two possible outcomes: i) excellent outcome (patients without any symptoms or deficits) and ii) all other patients

Result

Our analysis showed that 39 treated patients (67.2%) with AVMs had excellent early outcomes. We found that Spetzler-Martin grades were

significantly lower in the group of patients with excellent outcomes ($p=0.021$). Among the patients with excellent outcomes, there was also a statistically higher proportion of AVMs with a shorter feeding artery ($p=0.012$). The absence of venous dilatation approached statistical significance ($p=0.052$)

Discussion & Conclusion

The majority of our patients treated due to AVMs had no symptoms or functional deficits at the time of hospital discharge. Our study showed that Spetzler-Martin grades and feeding artery length were the most reliable predictors of AVM early outcome.

1-P29

MEASUREMENT OF ACUTE CEREBRAL INFARCTION VOLUME: COMPARING ADC-BASED METHOD WITH DWI-BASED METHOD

E.J. Lee¹, M.S. Chung¹, J.S. Byun¹

¹ Chung-Ang University Hospital, Seoul, SOUTH KOREA

Introduction

In patients with acute ischemic stroke, patient selection for endovascular thrombectomy requires correct and fast estimation of infarct core on MRI. Recently, an automated software using Apparent Diffusion Coefficient (ADC) criteria is introduced for segmentation of infarct core. To compare with diffusion-weighted imaging (DWI)-based manual outlining of infarct core, we validate ADC-based autosegmentation in patients with acute cerebral infarction.

Methods

249 patients, undergone brain DWI MR between January 2017 and December 2018, were included. Patients with acute ischemic stroke due to intracranial large artery occlusion in anterior or posterior circulation were included. Exclusion criteria were as follows: 1) embolic infarction, 2) severe artifact, 3) multiple staged infarction, 4), acute infarction F/U, 5) hemorrhagic transformation, 6) DWI hyperintensity with other pathology (such as metabolic encephalopathy), 7) SAH complicating infarction, 8) mechanical error and 9) venous infarction.

On DWI, infarct core volume was quantitatively measured as total hyperintense area in single slices multiplied by slice thickness, using software (NordicICE, NordicNeuroLab, Bergen, Norway). ADC-based autosegmentation were fulfilled with commercial software (RAPID, iSchemaView Inc, Menlo Park, CA) and implemented threshold of $0.000620 \text{ mm}^2/\text{s}$ for infarct core. For comparison of DWI- and ADC-based infarct core volumes, Pearson correlation coefficients were estimated.

Result

Of 249 patients, mean age was 69.2 ± 13.2 years (31-101 years:male: female = 146:103). The mean infarct core volumes were 12.96 ml (0.03-232.4 ml) on DWI-based method and 13.90 ml (0-289 ml) on ADC-based method. In total patient group ($n=249$), two infarct core volumes revealed excellent correlation with R^2 of 0.924 ($p<0.0001$). In patients with anterior

territorial infarction ($n=155$), two infarct core volumes also depicted excellent correlation with R^2 of 0.973 ($p<0.0001$). But, in anterior territorial infarction patient with infarct volume of $< 51 \text{ ml}$ ($n=135$), two infarct volumes showed relatively lower correlation with R^2 of 0.794 ($p<0.0001$).

Discussion & Conclusion

ADC-based segmentation of infarct core was rapid. But it detected scattered noise voxels resulting unexpected segmentation, particularly in high cortical gray matter and small infarct volume. On the other hand, DWI-based method produced less noisy segmentation within acceptable outlining time. Therefore, applying DWI-based method complementarily to ADC-based method could help patient selection for endovascular thrombectomy.

1-P30

THE PEARLS AND PITFALLS OF ARTERIAL SPIN-LABELING(ASL)-MRI FOR VARIOUS INTRACRANIAL PATHOLOGIES IN DAILY PRACTICE

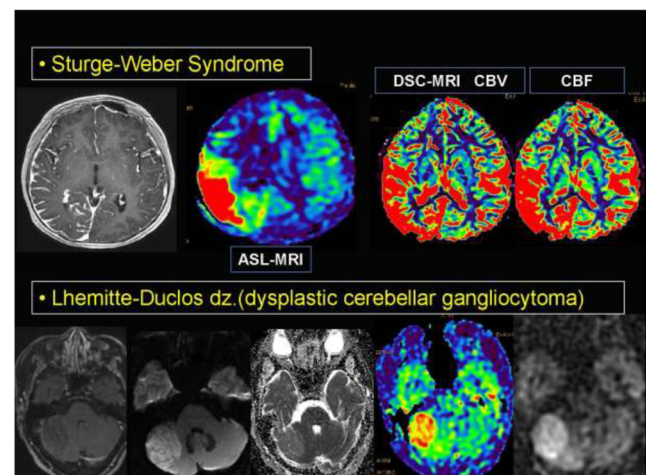
A. Lee¹

¹ Soonchunhyang University Bucheon Hospital, Bucheon, SOUTH KOREA

Introduction

TEACHING POINTS

1. To introduce the concept of Arterial Spin-Labeling Magnetic Resonance Imaging (ASL-MRI).
2. To present the category-based findings (CBF) of ASL-MRI for various conditions of the central nervous system (CNS)
3. To compare the findings of ASL-MRI with those of Dynamic Susceptibility Contrast Magnetic Resonance Imaging (DSC-MRI)
4. To summarize the ASL-MRI appearances based on relative CBF values and analyze the reason for the discrepancy between ASL-MRI and DSC-MRI.



Methods

TABLE OF CONTENTS/OUTLINE

1. Explanation of the scheme of the perfusion imaging acquisition by ASL-MRI.
2. Presentation of the CBF of ASL-MRI in various conditions of the CNS: (1) stroke, (2) tumor, (3) infection, (4) seizure, (5) congenital disorder (Sturge–Weber Syndrome, Neurofibromatosis), and (5) other miscellaneous conditions (brain death, diffuse hypoxic injury, etc.)
3. Summation of the ASL-MRI appearances based on relative CBF values.
4. Explanation of partial discrepancy in findings of ASL-MRI and DSC-MRI.

Result

Discussion & Conclusion: Merits and limitations of different methods for perfusion MRI

- Concordant vs. discordant finding between ASL-MRI and DSC-/DCE-MRI

Future directions and summary

1-P31

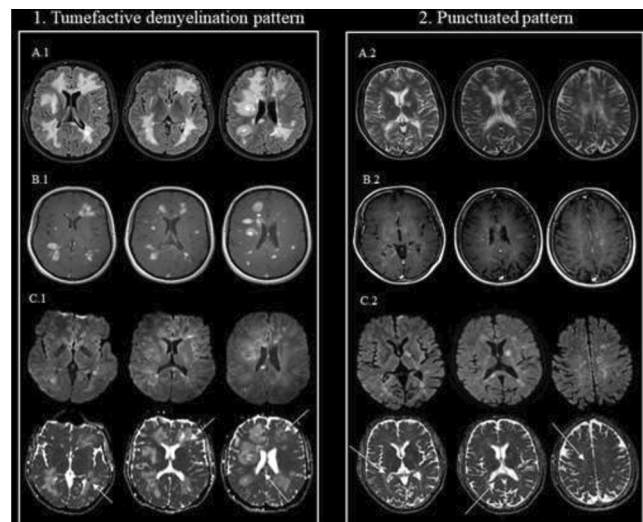
DIFFERENT MRI PATTERNS IN MULTIPLE SCLEROSIS WORSENING AFTER STOPPING FINGOLIMOD

C. Lapucci¹, D. Baroncini², M. Cellerino^{1,3}, G. Boffa^{1,3}, I. Callegari⁴, M. Pardini^{1,3}, G. Novi¹, M. Sormani⁵, G. Mancardi^{1,3}, A. Ghezzi², M. Zaffaroni², A. Uccelli^{1,3}, M. Inglese^{1,3}, L. Roccatagliata^{5,6}

¹ Department of Neuroscience, Rehabilitation, Ophthalmology, Genetics, Maternal and Child Health (DiNOGMI), University of Genoa, ITALY, ² Multiple Sclerosis Centre, Gallarate Hospital, ASST of Valle Olona, Gallarate, ITALY, ³ Department of Neurology, Ospedale Policlinico San Martino - Sistema Sanitario Regione, Genoa, ITALY, ⁴ IRCCS Foundation C. Mondino National Neurological Institute, Pavia, ITALY, ⁵ Department of Health Sciences (DISSAL), Ospedale Policlinico San Martino IRCCS, Genoa, ITALY, ⁶ Department of Neuroradiology, Ospedale Policlinico San Martino IRCCS, Genoa, ITALY

Introduction

The worsening of neurological status (WNS) after Fingolimod (FTY) discontinuation is a controversial phenomenon regarded as Multiple Sclerosis (MS) “reactivation” or considered a distinct “rebound” phenomenon. The aim of the study is to analyze MRI features of MS patients who experienced WNS after stopping FTY.



Methods

In this retrospective study, demographic, clinic-radiological data of MS patients who experienced WNS after stopping FTY were collected. A “ δ EDSS-ratio” was introduced to identify patients that showed an inflammatory flare-up exceeding the highest lifetime disease activity level. Patients with δ EDSS-ratio more than 1 were enrolled.

Result

Eight patients were identified. The mean (SD) age was 35.3 (4.9) years. The mean FTY treatment duration was 3.1 (0.8) years. The mean FTY discontinuation-WNS interval was 4 (0.9) months. The four patients with δ EDSS-ratio more than or equal 2 developed severe monophasic WNS, characterized by clinical features and MRI findings not typical of MS, classified “Tumefactive Demyelination” (TDL) and “Punctuated” (PL) pattern. Conversely, patients with more than 1 δ EDSS-ratio but less than 2 had clinical features and brain MRI compatible with a typical, aggressive, MS relapse. In patients with TDL and PL, the flare-up of inflammatory activity led to severe tissue damage resulting in T2 and also T1 lesion volume increase at 6-months follow-up.

Discussion & Conclusion

The small size of our cohort represents a limitation thus considering the δ EDSS-ratio as a parameter able to predict clinical and radiological worsening after FTY withdrawal could be speculative. Nevertheless, it has been a simple method to retrospectively identify and, particularly, stratify the patients who worsened after FTY suspension. Interestingly, patients with worse clinical course and outcome were those who showed peculiar MRI features that we defined TDL and PL, different from a typical MS flare-up. Further studies are necessary to investigate whether specific cellular subsets might play a role in patients who develop a particularly severe WNS after FTY cessation.

1-P32**5-YEAR FOLLOW-UP STUDY IN MULTIPLE SCLEROSIS: ATROPHY AND OTHER MRI-PARAMETERS AS PREDICTORS OF NEUROLOGICAL DEFICIT IN RELAPSING REMITTING MULTIPLE SCLEROSIS**I. Krotenkova¹, V. Bryukhov², M. Zakharova³, M. Krotenkova⁴¹ Research center of Neurology, Moscow, RUSSIA, ² Research center of Neurology, Moscow, RUSSIA, ³ Research center of Neurology, Moscow, RUSSIA, ⁴ Research center of Neurology, Moscow, RUSSIA**Introduction**

Multiple sclerosis (MS) is widely known to be not only a chronic inflammatory disease, but also a degenerative process, but the sequence of involvement of different regions and correlation with disability is still unclear. It has become increasingly clear that MRI techniques are needed to measure aspects of pathologic changes in MS.

The aim of this study was to determine atrophy rates in RRMS patients over the course of 5 years, using voxel-based morphometry (VBM), to access T2-lesion burden (T2LV) and to investigate the relationship between these measures and neurological disability.

Methods

25 RRMS patients (age 34.5±15.5years) underwent MRI and neurological examination in follow-up: first one – during relapse and then in 12 months after it. And 20 patients (among them) - in 60 months. Neurological deficit was measured with Expanded Disability Status score (EDSS): 4.5±2 at submission. VBM was performed to assess GM and WM volume changes in MS patients and T2LV was accessed 4 times in follow-up. Group comparisons were tested with family-wise error correction for multiple comparisons ($p < 0.05$). IBM SPSS Statistics 20 was also used for getting numerical data and evaluate statistically significant associations between MRI and clinical parameters.

Result

Over a period of 12 months patients experienced a decrease in the whole brain volume, total GM and WM volume (especially, corpus callosum), in right precentral and postcentral guri and in spine volume ($p < 0.05$). And in 60 months beside these changes MS patients showed pronounced atrophy of parahippocampal guri, left caudate, thalamus and anterior lobes of cerebellum.

A strong correlation between brain and spine atrophy rates was revealed. Subcortical GM volume changes were associated with EDSS score, disease duration and correlated with neurological deficit progression, but showed no association with T2LV.

Discussion & Conclusion

RRMS patients show rapid brain and spine volume loss and atrophy has distinct patterns of regional distribution. Deep GM volume is associated with disease duration and can predict neurological deterioration.

1-P33**LANGUAGE LATERALIZATION MAY BE DEPENDENT ON THE TEMPORO-PARIETAL HUBS OF THE STRUCTURAL CONNECTOME - A DTI-FMRI CORRELATION STUDY**L.R. Kozák¹, G. Gyebnár¹¹ MR Research Center, Semmelweis University, Budapest, HUNGARY**Introduction**

Language lateralization is usually considered in a generalized fashion, i.e. 95% of right handers and 75% of left handers have left lateralized language processing. Nevertheless, the issue of lateralization is more complex as different aspects of language processing are subserved by the balanced activations of overlapping brain networks [1]. Here we aimed to investigate if network analytics may be suitable for the discussion of lateralization with special respect to pre-surgical evaluation.

Methods

We retrospectively evaluated 39 consecutive patients from our clinical database who all underwent routine pre-surgical workup including BOLD fMRI with picture naming, synonym matching, speech comprehension and auditory decision tasks at 3mm isotropic spatial and 3s temporal resolution; and diffusion weighted imaging with 32 encoding directions, $b = 800$ s/mm², and 2mm isotropic resolution.

fMRI analysis was performed in SPM12 [2] with standard parameters, then the individual unthresholded activation maps were further analyzed using ICN_Atlas [3] with ROIs defined by the AAL atlas [4].

DWI data was processed and analyzed with ExploreDTI [5] including whole brain DTI tractography and calculating connectivity matrices using the same ROIs. Network characteristics of the whole DTI-based structural connectome were calculated with the Brain Connectivity Toolbox [6] and were compared to fMRI-based speech lateralization using conventional parametric statistics in Matlab, focusing on the bilateral AAL labels corresponding to Broca's and Wernicke's areas.

Result

Lateralization assessed with fMRI correlated significantly with structural network parameters in task dependent manner: temporal lateralization patterns of the speech comprehension and auditory decision tasks, and frontal lateralization patterns of the picture naming and synonym tasks showed significant positive correlations with the network metrics-based lateralization parameters of the temporo-parietal areas. The lateralization of frontal functional language areas was reflected in the lateralization of arcuate fasciculus.

Discussion & Conclusion

The importance of the temporo-parietal network hubs over different language tasks is emphasized by the observed functional-structural correlations. Our findings are in line with previous literature [7,8], suggesting that multi-modal network analysis may open new avenues in the pre-surgical evaluation of language processing.

References

- [1]Friederici, *PhysiolRev*, 91:1357–1392,2011
 [2]<https://www.fil.ion.ucl.ac.uk/spm>
 [3]Kozák, *NeuroImage*, 163:319-341
 [4]Tzourio-Mazoyer, *Neuroimage* 15(1):273-89.
 [5]Leemans, *ISMRM-2009* p3537
 [6]Rubinov&Sporns, *NeuroImage* 52:1059-69.
 [7]Wylie&Regner, *JNeurosci* 34(47):15505-15507
 [8]Propper, *BrainCogn* 73:85–92

1-P34

BILATERAL THALAMIC LESIONS: RADIOLOGICAL APPROACH TO DIAGNOSIS WITH A PICTORIAL REVIEW

*I. Khan*¹, C. Soke Miang¹

¹ National Neuroscience Institute, Singapore, SINGAPORE

Introduction

The thalami are paired ovoid masses of grey matter situated on each side of the third ventricle. They are a major sensory and motor relay station for the cerebral cortex, brain stem, hypothalamus and basal ganglia, involved in the regulation of sleep, consciousness and alertness.

Bilateral thalamic lesions are uncommon. They may be seen in different acute and chronic clinical situations. Early diagnosis facilitates prompt treatment, which is essential to avoid poor clinical outcome in certain acute pathologies.

Methods

1. Review differential diagnoses and pathologies involving bilateral thalami. These include arterial and venous ischaemia, neoplastic, infectious and demyelinating diseases, as well as metabolic-toxic aetiologies.
2. We propose an algorithm in the approach to imaging that may aid diagnosis, with clinical examples to illustrate.

Result

Proposed algorithm

1. Location of the lesion within the thalamus.

Different disease processes may have preferential involvement of different parts of the thalamus.

Conversely, involvement of the entire thalamus may be seen in tumour, certain infections, venous ischaemia and hypotensive or hypertensive brain injury.

2. Presence of thalamic expansion.

Tumour and venous ischaemia are often associated with significant oedema which results in swelling of the thalami.

3. Presence of extra-thalamic lesions in the brain.

The presence of other similar lesions in the brain may help narrow the differential diagnosis.

4. Awareness of salient imaging features.

The signal characteristics of the lesions on different MRI sequences, density on CT and presence of calcifications may help point towards certain pathologies. In addition, the judicious use of MR angiography,

MR venography or MR spectroscopy may provide more information to arrive at a diagnosis.

5. The evolution of the imaging findings over time.
6. Last but not least, the clinical presentation of the patient, other clinical tests and laboratory findings are essential for a complete evaluation.

Discussion & Conclusion

Bilateral thalamic lesions may be the result of both local or systemic disorders as well as acute and chronic conditions. A systematic approach to imaging findings, combined with good integration of all clinical data, is needed to avoid delay in diagnosis and a poor outcome.

1-P35

CEREBRAL CAVERNOUS MALFORMATIONS : SOLITARY , SPORADIC AND MULTIPLE FAMILIAL CAVERNOMATOSIS – HAEMORRHAGE AS FIRST CAUSE OF SEIZURES

*M. Karlovic-Vidakovic*¹, I. Klupke-Saric², N. Pejanovic-Skobic², I. Soldo¹

¹ University Hospital Mostar, Mostar, BOSNIA AND HERZEGOVINA,

² University Hospital Mostar, Mostar, BOSNIA AND HERZEGOVINA,

³ University Hospital Mostar, Mostar, BOSNIA AND HERZEGOVINA,

⁴ University Hospital Mostar, Mostar, BOSNIA AND HERZEGOVINA

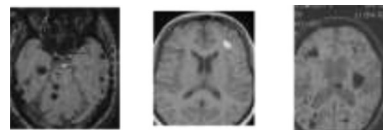
Introduction

Cerebral cavernous malformation (CCM) is the most common vascular abnormality, making up 10–25% of all vascular malformations, with the incidence ranges from 0.4% to 0.8% in the general population.

They can be solitary or multiple, sporadic or familial. Familial cases are associated with a high frequency of multiple lesions. They cause seizures and cerebral hemorrhages. Approximately 20% of patients with CCM have the familial form, inherited in an autosomal dominant pattern.

The annual risk of hemorrhage is 0.7%–1.1% per lesion in patients with no history of hemorrhage, but rises to 4.5% in patients with a previous intracerebral hemorrhage.

According to Zabramski et al, they are classified in four types.



Methods

We present twenty patients - ten patients with multiple cavernomas, of which four patients are from two families and represent cases of familial form of cavernomatosis (FCCM). Six others are sporadic multiple cavernomatosis cases. From ten cases of solitary CCM, one patient is with spinal cavernoma and nine with cerebral, three located infratentorial and six supratentorial. Four were with haemorrhage.

Most of the cerebral cavernomas are incidental findings in imaging studies performed for other nonspecific disorders. Seven patient underwent surgical treatment.

Result

3T MRI is established as the gold standard for CCM detection. T2-weighted images most often reveal the characteristic mulberry or popcorn-like appearance with a dark rim due to hemosiderin deposition after repeated bleedings. But increased sensitivity is at first achieved with susceptibility-weighted images (SWI), especially for the detection of small Zabramski type IV cerebral cavernomas. SWI is a three dimensional, high resolution technique highly susceptible to the venous vasculature, blood products and vascular malformations and therefore very sensitive for the detection of CCM.

Discussion & Conclusion

Patients with CCM, especially those with hemorrhage complications, must be considered for surgical treatment in accessible lesions that have produced symptoms. In other patients, control MRI should be performed yearly and should be suggested to other family members.

The identification of the type of lesions is important to evaluate the risk of bleeding.

The present of a single cavernous malformation in a patient, even without a history of familial multiple cavernous malformations, does not exclude this diagnosis.

1-P36

CURVILINEAR COURSE OD C1 SEGMENT OF THE RIGHT ACI AS A POTENTIAL PREDICTIVE FACTOR OF PRESENCE OF ANEURYSM AT C4 SEGMENT OF THE CONTRALATERAL ACI: A RETROSPECTIVE STUDY

*S. Jefić*¹, *D. Kozić*², *B. Georgievski-Brkić*³, *D. Marić*⁴, *D. Vranješ*⁴

¹ Polyclinic Dr Al-Tawil - Department of Radiology, Sarajevo, BOSNIA AND HERZEGOVINA, ² University of Novi Sad - Department of Radiology, Novi Sad, SERBIA, ³ St. Sava Hospital - Department of Radiology, Belgrade, SERBIA, ⁴ University Clinical Centre of the Republic of Srpska - Department of Radiology, Banja Luka, BOSNIA AND HERZEGOVINA, ⁵ University Clinical Centre of the Republic of Srpska - Ear, Throat and Nose Department, Banja Luka, BOSNIA AND HERZEGOVINA

Introduction

A very close relation between intracranial aneurysms (IAs) and variations of Circle of Willis (CoW) is conditioned by theory of hemodynamic stress explaining development of IAs. The aim of the study was an evaluation of relationship between IAs and anatomic variations of not only anatomic structures of CoW, but all of the segments of cerebral arteries.

Methods

The study included 111 patients, both sexes, hospitalized between January 2013 and May 2018 with suspicion of cerebral vascular accident (CVA) and diagnosed with IA based on 3D TOF MRA, 1.5T.

Result

Assesment of the prognostic value of kinking or angulation of C1 segment of the right ACI - as an anatomic variation - to C4 segment of the left ACI - as localization of IA - by using binary logistic regression has indicated that whole model with all of the predictors shows statistical significance $X^2(2, N=111)=9,91$ $p < 0,01$. The overall model explains between 8,5% and 13,5% of variance and precisely classifies 80,2% of cases. Other anatomic variations matched with other localizations of aneurysms did not demonstrate statistically significant results.

Discussion & Conclusion

We may suggest that compromised flow through the C1 segment of the right ACI may cause hemodynamic changes within contralateral ACI resulting with an aneurysm of the C4 segment. This potential relationship emphasizes the theory of hemodynamic stress in development of IAs and should be ascertained by further investigation of higher number of series, but also combined with results of neurophysiological quantitative measurements of endoluminal pressure and diameter as well as flow through particular segments. Our results indicate the value of the further assesment focused on that relationship.

Approach in assesment of morphological fundament for hemodynamic changes responsible for IAs that respects not only the variations of CoW, but variations of all hemodynamically relevant segments of cerebral arteries can reveal additional associations between certain vascular variations and aneurysmal localizations and improve predictive possibilities in management of IAs.

1-P37

MAGNETIC RESONANCE IMAGING FINDINGS IN NEUROSARCOIDOSIS BEFORE AND AFTER TREATMENT. LONG TERM FOLLOW-UP OF 23 PATIENTS

*L. Jaunozolina*¹, *G. Krumina*¹, *J. Khan*²

¹ Riga East Clinical University Hospital, Department of Radiology, Riga, LATVIA, ² Riga Stradins University, Faculty of Medicine, Department of Radiology, Riga, LATVIA

Introduction

Neurosarcoidosis is examined with magnetic resonance imaging (MRI) in both diagnostic and in dynamic purposes, however, the specificity to detect the disease is low and the treatment is often symptomatic. A study to evaluate the MRI findings in dynamic before and after treatment of neurosarcoidosis and multi-systemic distribution could be useful for diagnostic evaluation.

Methods

In a retrospective study, 23 patients (83% females) with the median age of 39 years met the criteria for probable neurosarcoidosis described by Zajicek et al. between 2012 – 2019 in Riga Eastern Clinical University Hospital. MRI findings were grouped according to the locations of involvement. All patients received specific treatment and had follow-up

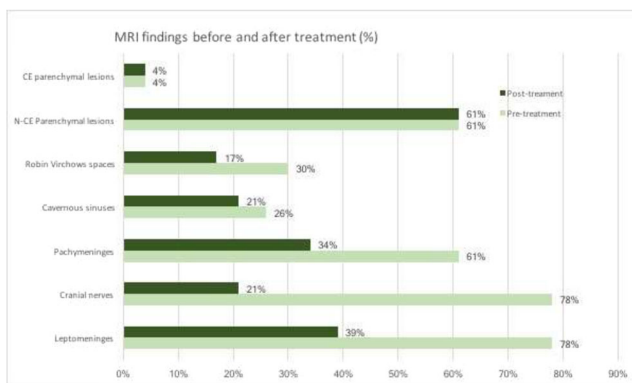
MRI. Pearson's correlation coefficient was used to determine strength of associations.

Result

The findings on MRI included leptomeningeal (78%, n=18) and perivascular (PVS) enhancement (30%, n=7), pachymeningeal thickening and enhancement (61%, n=14), cranial nerve enhancement (78%, n=18), contrast non-enhancing (61%, n=14) and enhancing (4%, n=1) parenchymal lesions. In 61% the treatment consisted of steroids, whereas in 39% immunosuppressive drugs were added. During follow-up 22% (n=5) showed complete resolution of their imaging abnormalities whereas 9% (n=2) of patients had new specific MRI findings. Reduction of granulomatous inflammation was found in 70% (n=16).

Cranial nerve enhancement (13/18, 72%) and leptomeningeal spread (9/18, 50%) were more likely to resolve with therapy than others such as pachymeningeal (4/10, 40%) and cavernous sinus involvement (1/6, 17%).

Lung and skin involvements accounted for 96% and 26% respectively. There was a correlation between lung involvement and post-treatment perivascular space (PVS) enhancement, and skin involvement and post-treatment PVS enhancement with r-values of -0.47 and 0.51, respectively ($p < 0.05$).



Discussion & Conclusion

Lung and skin are the most common multi-systemic distributions of sarcoidosis, whereas leptomeningeal and cranial nerve enhancement is the most common intracranial manifestation.

During follow-up, leptomeningeal and cranial nerves enhancement are more likely to resolve with treatment than others, thus are important to evaluate for dynamic purposes. This study also suggests a negative association between lung involvement and post-treatment PVS enhancement, but a positive association between skin involvement and post-treatment PVS enhancement which indicates that multi-systemic distribution of the disease might affect MRI findings.

1-P38

NEUROSHAPE: A NOVEL SOFTWARE INTERFACE IMPLEMENTING STATE-OF-THE ART IMAGE-BASED TARGETING FOR MRI-GUIDED TRANSCRANIAL FOCUSED ULTRASOUND NEUROSURGERY

A. Jakab¹, Z. Goey², G. Szekely², O. Goksel², B. Werner¹, R. Tuura¹

¹ Center for MR-Research, University Children's Hospital, Zurich, SWITZERLAND, ² Computer Vision Laboratory, ETH Zurich, Zurich, SWITZERLAND

Introduction

The current standard for targeting subcortical structures during functional neurosurgical interventions relies on transferring stereotactic 3D coordinates from an anatomical atlas onto the patient's brain MR or CT images. Our purpose is to utilize statistical shape models (SSM) to overcome the limitations of the atlas based targeting approaches, such as the lack of information on inter-patient variability, and to develop a user-friendly interface for neuroradiologists involved in the planning of MRI-guided neurosurgical interventions.

Methods

We demonstrate the use of a prototype targeting pipeline through five exemplary MRgFUS interventions that have been performed between January 2016 and December 2017 at the University Children's Hospital in Zurich. The method uses the pre- or intraoperatively acquired 3DT1 and T2 MR images of the patients, on which the visible outlines of the thalamus are delineated manually. Based on the anatomical correspondence between the visible thalamus outlines and the individual thalamic nuclei stored within the SSM, individualized targets maps and confidence interval maps are generated.

Result

The outlines of the thalamus could be delineated on the patient's intraoperative MRI, and the predicted volumes of the ventrolateralis-posteroventralis (VLpv or Vim) nucleus and the cerebello-thalamic tracts were in close proximity to the actual imaging targets (targeting distance < 5 mm).

By fusing the resulting target and confidence interval maps with the patient's MRI, a feasible visual guidance was provided for the operating neurosurgeon.



Discussion & Conclusion

The efficiency and safety of functional neurosurgical interventions, such as high intensity focused ultrasound ablation, depend on the accuracy by which the target structures are reached. Using patient-specific, imaging based markers of the individual thalamic anatomy has the potential to improve accuracy.

1-P39

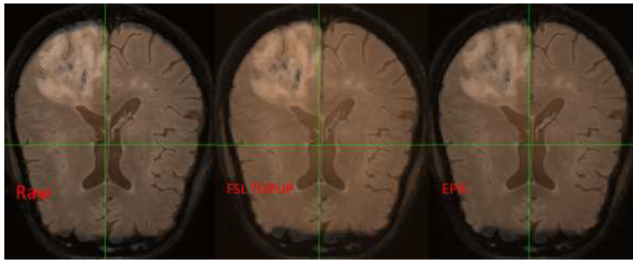
HOW DO MAGNETIC SUSCEPTIBILITY DISTORTION IMPACT EPI-BASED PERFUSION MRI?

*I.T. Hovden*¹, I. Digernes¹, G. Loevland¹, K.E. Emblem¹

¹ Department for Diagnostic Physics, Oslo University Hospital, Oslo, NORWAY, ² Department for Diagnostic Physics, Oslo University Hospital, Oslo, NORWAY, ³ The Intervention Centre, Oslo University Hospital, Oslo, NORWAY, ⁴ Department for Diagnostic Physics, Oslo University Hospital, Oslo, NORWAY

Introduction

Geometric and intensity distortions associated with Echo Planar Images (EPIs) are neglected problems in functional MRI. Among others, dynamic susceptibility contrast (DSC) perfusion MRI rely on EPIs that may produce severe image distortions typically along the phase encoding direction. A few available methods use pairs of opposite phase encoded EPIs to correct for such magnetic susceptibility distortions. In this work, we compare how the two most common distortion correction methods, FSL TOPUP(1) and EPIC(2), affect values and spatial location of Cerebral Blood Volume (CBV) maps from a dataset of 46 glioblastoma patients.



Methods

From both corrected and uncorrected EPIs, CBV maps were created using nordicICE. SPM normalization to MNI space was then performed based on 3D FLAIR MRIs. Maximum probability tissue labels in Neuromorphometrics was used to perform logrank histogram comparisons of the CBV distributions between the correction methods in multiple brain areas. ROIs of tumors were excluded from the analysis.

Result

Although preliminary NMI similarity measures show that EPIC preserves the highest whole-head similarity, visual comparison with raw EPIs indicates that TOPUP is better to preserve similarity in the brain. Rigid head movement between pos. and neg. phase encoded EPI can cause TOPUP to fail, while this was not the case for EPIC. Geometric distortions and signal loss were most pronounced in the prefrontal cortex, see Figure 1. Opposed to spin-echo EPIs, gradient-echo EPIs introduce more signal loss resulting in erroneous normalized values in the prefrontal cortex. A complete histogram comparison of all brain areas remains as further work.

Discussion & Conclusion

EPI distortion correction will likely provide more spatially accurate perfusion MRIs, especially in the prefrontal cortex. Work remains to assess changes in intensity distributions in all brain areas and their impact on the diagnosis of glioblastomas.

REFERENCES

1. Andersson, J. L. R., Skare, S. & Ashburner, J. How to correct susceptibility distortions in spin-echo echo-planar images:

application to diffusion tensor imaging. *NeuroImage* 20, 870–888 (2003).

2. Holland, D., Kuperman, J. M., & Dale, A. M. (2010). Efficient Correction of Inhomogeneous Static Magnetic Field-Induced Distortion in Echo Planar Imaging. *NeuroImage*, 50(1), 175. <https://doi.org/10.1016/j.neuroimage.2009.11.044>

1-P40

FIXEL-BASED ANALYSIS OF VISUAL PATHWAY WHITE MATTER IN PRIMARY OPEN-ANGLE GLAUCOMA

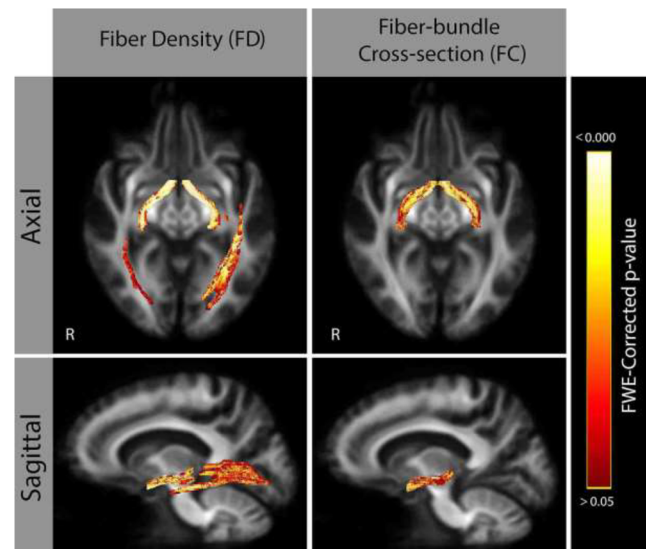
*S. Haykal*¹, B. Ćurčić-Blake², N. Jansonius¹, F. Cornelissen¹

¹ Department of Ophthalmology, University Medical Center Groningen, Groningen, THE NETHERLANDS, ² Department of Biomedical Sciences of Cells & Systems, University Medical Center Groningen, Groningen, THE NETHERLANDS

Introduction

White matter (WM) degeneration of the visual pathways in primary open-angle glaucoma (POAG) is well documented, but it remains unclear whether antero- or retrograde trans-synaptic propagation is primarily responsible for this degeneration. We address this question by exploiting the fact that in WM degeneration, microstructural axonal loss precedes macrostructural fiber bundle atrophy. Consequently, the visual pathway track where degeneration originates should exhibit more substantial macrostructural changes compared to the trans-synaptically affected one.

Fixel-based analysis (FBA) is a novel framework for analyzing diffusion-weighted images (DWIs), capable of measuring fiber density (FD), representing WM microstructure, and fiber-bundle cross-section (FC), representing WM macrostructure. To determine the directionality of glaucomatous spread along the visual pathways, we applied FBA to the optic tracts (OTs) and optic radiations (ORs) of POAG patients.



Fixel-based analysis of fiber density (FD) along the visual pathways. Fixels exhibiting statistically significant FD loss in POAG group compared to controls are color-coded by their assigned FWE-corrected p-value, while non-significant fixels are shown in black. Results are shown for a single axial slice displayed in radiological convention. Zoomed-in regions show a closer view of the fixels in the right optic tract and left optic radiation

Methods

Cross-sectional case-control study with 12 POAG patients and 16 controls. Multi-shell DWIs were acquired. FBA was utilized to produce a population template, and probabilistic tractography was then used to track the OTs and ORs in the template space. Finally, FD and FC of the tracts of interest were compared between the two groups.

Result

Compared to the controls, the OTs of the patients exhibited a significant (FWE-corrected p -value < 0.05) decrease in FD and FC, while their ORs exhibited a significant decrease in FD but not in FC.

Discussion & Conclusion

Our findings suggest that glaucomatous degeneration of the OTs precedes degeneration of the ORs, implicating anterograde trans-synaptic propagation as the primary cause of glaucomatous visual pathways degeneration.

1-P41

CRANIAL NERVE ENHANCEMENT IN MULTIPLE SCLEROSIS IS ASSOCIATED WITH YOUNGER AGE AT ONSET AND MORE SEVERE DISEASE

*L. Haider*¹, W.S.E. Chan², E. Olbert³, S. Mangesius⁴, A. Dal-Bianco⁵, F. Leutmezer⁵, D. Prayer², M. Thurnher²

¹ NMR Research Unit, Queen Square MS Centre, Institute of Neurology, Faculty of Brain Science, University College London, London, UNITED KINGDOM, ² Department of Biomedical Imaging and Image-Guided Therapy, Medical University Vienna, Vienna, AUSTRIA, ³ Department of Neurology, University Hospital Tulln, Tulln, AUSTRIA, ⁴ Univ.-Klinik für Neuroradiologie, Medical University Innsbruck, Innsbruck, AUSTRIA, ⁵ Universitätsklinik für Neurologie, Medical University Vienna, Vienna, AUSTRIA

Introduction

The overall frequency of cranial nerve pathology and its relation to brainstem lesion formation on magnetic resonance imaging (MRI) in multiple sclerosis (MS) is unknown. We aimed to determine the frequency of cranial nerve enhancement on MRI, and its association with structural imaging findings and clinical outcomes.

Methods

We retrospectively analysed 651 MRIs from 183 MS patients. Frequencies of cranial nerve enhancement on post contrast T1-weighted MRIs were compared to lesion counts and the MS-severity-score.

Result

Cranial nerve enhancement was present in 8.2% of the analysed MS patients (oculomotor-nerve: 1.1%, trigeminal-nerve: 2.7%, abducens-nerve: 2.2%, facial-/vestibulocochlear nerve: 1.6%, vagal-nerve: 0.5%). Of those, 13% suffered from repeated episodes and 27% exhibited a cranial nerve enhancement duration of >12 months. Age at MS onset

was lower in patients with cranial nerve enhancement, 23 vs. 28 years, $p=0.049$. The MS-severity-score, 5.15 vs. 0.88 ($p=0.019$), the T2 brainstem-, 1 vs. 0 ($p=0.041$), and the total intracranial contrast-enhancing lesion counts, 2 vs. 0 ($p=0.000$), were higher in patients with cranial nerve enhancement, compared to age-, disease duration-, and gender- matched MS patients.

Discussion & Conclusion

Cranial nerve enhancement, present in 8.2% of our patients, was associated with a younger age at MS onset, brainstem lesions, and a more severe disease course.

1-P42

VADEMECUM FOR THE NEURORADIOLOGIST: DIFFUSE MIDLINE GLIOMA H3 K27M-MUTANT

*P. Guadalupi*¹, *G. Marziali*¹, *C. Giordano*¹, *A. Ramaglia*¹, *E. Leone*¹, *S. Gaudino*¹, *C. Colosimo*¹

¹ Fondazione Policlinico Universitario Agostino Gemelli IRCCS Università Cattolica del Sacro Cuore, Roma, ITALY

Introduction

Our purpose is to provide a vademecum concerning the diffused midline glioma (DMG) H3K27M-mutant, a new entity added to the 2016 update of the World Health Organization (WHO) classification of Central Nervous System (CNS) tumours, including the morphological and non-morphological MRI features and the epidemiological, prognostic and anatomopathological characteristics.

Methods

Starting from the new 2016 WHO classification, that integrated histological features with molecular data, we want to underline the impact of the H3K27M mutation and to define the radiological semiology of DMG.

Result

DMG H3K27M-mutant can be found throughout the midline structures of the CNS (thalamus, brainstem, spinal cord). H3K27M mutation was first described in pediatric diffuse intrinsic pontine gliomas, but has been recently found in adults, as well as in midline tumours with other morphologies and also in non-midline sites (cerebellar peduncles, cerebello-pontine angle).

The K27M mutation occurs in either of two genes that encode the histone H3 variants leading to altered DNA methylation, which drive gliomagenesis via epigenetic regulation.

Symptoms depend on the location of the tumour, including cranial nerve palsies, signs of increased intracranial pressure, ataxia.

CT usually shows a hypointense mass without contrast-enhancement (CE).

On MRI, DMG appears as an infiltrative lesion, hypointense on T1-weighted images (WI), inhomogeneously hyperintense on T2-WI, with poor perilesional oedema and mild or absent CE.

It often shows low-grade tumour characteristics: no necrosis areas and no restricted-diffusion components.

Dynamic Susceptibility Contrast perfusion shows variable values of relative cerebral blood volume, higher if anaplastic areas are present. Spectroscopy shows reduced N-Acetyl-Aspartate, increased choline levels and possible lipid lactate peaks.

In pontine lesions (the most frequent) the pons is enlarged, the tumour can show exophytic appearance with possible encasement of the basilar artery, the floor of the fourth ventricle is flattened and obstructive hydrocephalus may be present.

The DMGs H3K27M-mutant are associated with poor prognosis and poor therapeutic response regardless of histologic grade or MRI semiology and were thus designated as a grade IV entity.

Discussion & Conclusion

A neuroradiologist who comes across a mass involving midline structures, especially in a pediatric patient, without CE, necrosis areas or intralesional hemorrhages, must consider the hypothesis of a DMG H3K27M-mutant.

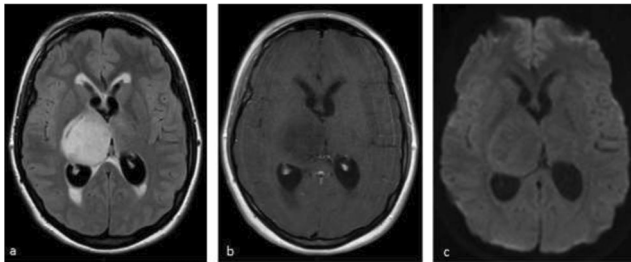


Fig. 1 Thalamus lesion, Female patient, 15 years old. a) Axial FLAIR MRI image, b) Contrast-enhanced axial T1-weighted MRI image, c) Axial Diffusion-Weighted Image

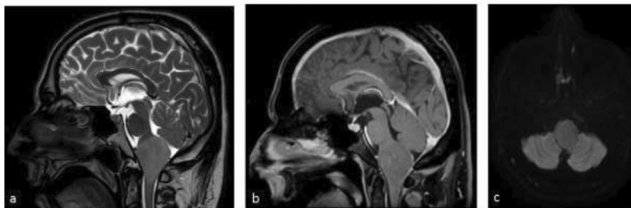


Fig. 2 Bulbar lesion, Male patient, 27 years old. a) Sagittal T2-weighted MRI image, b) Contrast-enhanced sagittal T1-weighted MRI image, c) Axial Diffusion-Weighted Image

1-P43

DEEP LEARNING SEGMENTATION OF BRAIN METASTASES ON MRI: DOES THE SIZE AND QUANTITY OF METASTASES AFFECT THE SEGMENTATION PERFORMANCE?

*E. Grøvik*¹, D. Yi², M. Iv¹, E. Tong¹, K.E. Emblem³, A. Bjørnerud³, D. Rubin², G. Zaharchuk¹

¹ Department of Radiology, Stanford University, Stanford, USA, ² Department of Biomedical Data Science, Stanford University, Stanford, USA, ³ Department for Diagnostic Physics, Oslo University Hospital, Oslo, NORWAY

Introduction

Advances in AI are suggesting the possibility of new paradigms in healthcare and are particularly well-suited for radiology. There has been

significant effort in developing the next-generation AI technology, deep learning, to learn from labeled MRI. One key advantages of AI-based radiology is the automatization of time-consuming tasks such as detection and segmentation. Today, a few studies have applied AI-approaches on patients with brain metastasis (1-3), however, little is known about their generalizability. In this work, we apply a deep learning approach using multi-sequence MRI and investigate how the size distribution and quantity of metastases affects the segmentation performance.

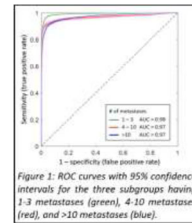


Figure 1: ROC curves with 95% confidence intervals for the three subgroups having 1-3 metastases (green), 4-10 metastases (red), and >10 metastases (blue).

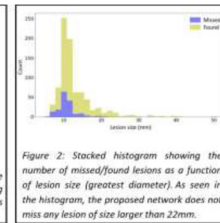


Figure 2: Stacked histogram showing the number of missed/found lesions as a function of lesion size (greatest diameter). As seen in the histogram, the proposed network does not miss any lesion of size larger than 22mm.

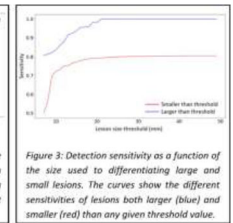


Figure 3: Detection sensitivity as a function of the size used to differentiating large and small lesions. The curves show the different sensitivities of lesions both larger (blue) and smaller (red) than any given threshold value.

Methods: A total of 156 patients with brain metastases from several primary cancers were included. Pre-surgical MRI included pre- and post-gadolinium T1-weighted 3D fast spin echo, post-gadolinium T1-weighted 3D IR-prepped FSPGR, and 3D FLAIR. The ground truth was established by two experienced neuroradiologists, manually delineating the enhancing lesions. Training was performed using a 2.5D fully convolution network based on a GoogLeNet architecture (4), which was modified to optimize segmentation. The dataset was split into 100/5/51 patients for training/validation/testing. The test set was equally and randomly selected within three different patient subgroups presenting with 1-3, 4-10, and >10 metastasis. The results were evaluated using ROC-curve statistics.

Result: The network's ability to detect and segment brain metastases was reduced in patients with higher quantity (Fig 1). The area under the ROC-curve was 0.99 ± 0.01 for patients having 1-3 metastases, 0.97 ± 0.05 for 4-10 metastases, and 0.97 ± 0.03 for >10 metastases, respectively. The segmentation performance was also associated with the lesion size (Fig. 2). Figure 3 show the network's sensitivity as a function of size-threshold for differentiating large and small lesions. If the size-threshold is set to 22mm, the network's sensitivity was 80% for detecting <22mm lesions and ~100% for detecting >22mm lesions.

Discussion & Conclusion: This work show that a deep learning network can detect and segment brain metastases on MRI with high accuracy and thus demonstrating the potential use of this method in a clinically relevant setting. However, our result indicates that the segmentation performance may be associated with metastases size and quantity.

REFERENCES

- 1.Liu;PLoSOne,2017;12:e0185844
- 2.Charron;ComputBiolMed,2018;95:43–54.
- 3.Grøvik;arXiv,2019;1903.07988.
- 4.Szegedy;IEEEComput,2015;1-9

1-P44**TEMPORAL VIRCHOW-ROBIN SPACES, A NEW AND LESSER KNOWN ENTITY**

*E. Grive Isern*¹, T. Salaya Diaz¹, A. Marin Suarez¹, E. Serrano Alcala¹, C. Simon Olive¹, S. Grossi¹, M. Rovira Cañellas¹

¹ Hospital Universitari Sagrat Cor - Department of Radiology, Barcelona, SPAIN

Introduction

Perivascular spaces (PVS) of Virchow-Robin are pial-lined, interstitial fluid-filled parenchymal structures that surround cerebral vessels. In healthy patients, a diameter <2 mm is normal and can be identified within the brain parenchyma on MRI. They are considered benign lesions associated with age, other risk factors or unknown causes.

When dilated they can mimic cystic parenchymal benign lesions or cystic neoplasms. They are usually known to occur in the inferior basal ganglia (type I), in the topography of the perforating medullary arteries of the cerebral convexity (type II) and in the pontomesencephalic junction (type III). Nevertheless, there has been recently described an atypical localization within the subcortical white matter of the anterior superior temporal lobe.

Methods

Temporal perivascular spaces of Virchow-Robin present special MRI characteristics, such as: middle size lesions (0.5 - 1.5 cm of diameter); proximity to a middle cerebral artery branch; signal variability of the adjacent white matter, generally stable over time; proximity to small size PVS.

A case series of 7 patients (6 women, 1 man) with incidental small cystic lesions within the subcortical white matter of the anterior superior temporal lobe were identified at our institution between December 2015 and March 2019. The almost identical location and imaging features of the cystic lesions suggested the diagnosis of dilated perivascular spaces.

Result

In all of our patients the temporal PVS of Virchow-Robin followed a cerebrospinal fluid (CSF) signal; were located adjacent to a subarachnoid space; demonstrated variable surrounding signal change; showed no contrast enhancement and some of them that were followed up, showed stability. 6 of them were right sided and 1 left sided.

Discussion & Conclusion

Dilated PVS in the subcortical white matter of the anterior superior temporal lobe can mimic a cystic lesion. Knowing this entity, its imaging characteristics and localization help us to diagnose and differentiate it from other pathologic lesions, thus to avoid invasive procedures.

1-P45**CT PERFUSION PATTERNS OF ANGIOSPASM AFTER NON-TRAUMATIC SUBARACHNOID HEMORRHAGE**

*E. Grigorieva*¹, N. Polunina², V. Lukyanchikov², V. Krylov¹

¹ Moscow State University of Medicine and Dentistry name after A.I.Evdokimov, Moscow, RUSSIA, ² Sklifosovsky Research Institute of Emergency Care, Moscow, RUSSIA

Introduction

Delayed ischemia is the main cause of postoperative mortality and neurologic deficits in patient with non-traumatic subarachnoid hemorrhage (SAH) due to cerebral angiospasm. We estimated different patterns of perfusion disturbances before and after surgery to reveal its influence on the outcome

Methods

Between 2014-2017 we analyzed the data of 45 patients (31-74y.o.) with the rupture of 43 aneurysms during first 8 days after rupture, following up postoperatively. All the patients underwent transcranial dopplerography twice a day and CT perfusion on the entrance and 2 times after surgery. CT perfusion was performed on the level of basal ganglia., frontal and temporal lobes using 45ml of contrast injection on 5ml/s. 3240 symmetric ROIs were analyzed. The regressive analysis was used to reveal the influence of perfusion disturbances on the outcome

Result

71% of the patients has shown Fisher 3-4 SAH on the entrance. In 1st group (13,3% of patients) neither spasm, no ischemia was diagnosed with 5p Glasgow outcome. In the 2nd group (24,4% of patients) on the entrance the slight perfusion deficits were revealed with follow up normalization in spite of Lindengaard 3-4 after surgery. The ischemic changes didn't overwhelm 20sm3 with 5p Glasgow outcome in 90,9% in group. In the 3rd group (15,6% of patients) only postoperative perfusion deficits were diagnosed with ischemic changes up to 300sm3 and 4-5p Glasgow outcome in 28,6% in group. In the 4th group (46,7% of patients) the severe perfusion deficits and peripheral angiospasm both in pre- and postoperative period were found. Maximum ischemic volume reached 350 sm3 with 4-5p Glasgow outcome in 21,4% in group.

In 3-4th groups the signs of dopplerographic spasm were found pre- and postoperatively and didn't correlate with the volume of ischemia and outcome (p>0,001)

Discussion & Conclusion

The stable and progressive perfusion deficits in patients with cerebral angiospasm on the entrance and after surgery as well as the peripheral type of the spasm have the significant influence on the outcome in patients with non-traumatic SAH

1-P46**HIGHLY ACCELERATED TIME-OF-FLIGHT MAGNETIC RESONANCE ANGIOGRAPHY USING SPIRAL IMAGING AT 3 TESLA**

*T. Greve*¹, N. Sollmann¹, A. Hock², V. Gnanaprakasam², M. Nijenhuis², C. Zimmer¹, J. Kirschke¹

¹ Department of Diagnostic and Interventional Neuroradiology, School of Medicine, Technical University Munich, Munich,

GERMANY, ² Health Systems Philips Switzerland, Horgen, SWITZERLAND

Introduction

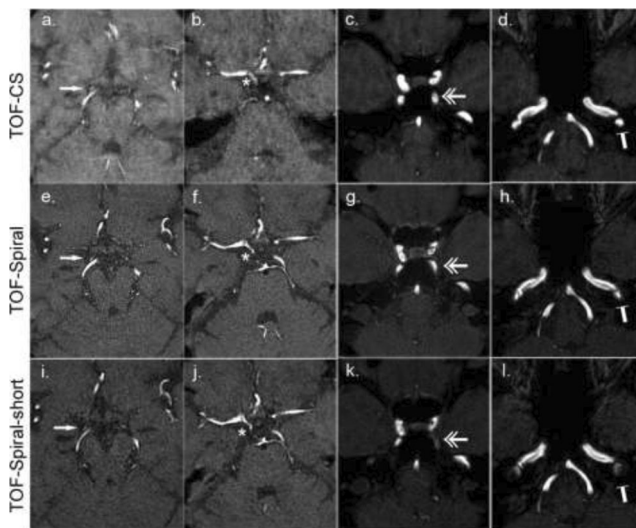
To systematically evaluate the image quality of intracranial and extracranial large and small brain-feeding arteries and assess the diagnostic confidence of vessel pathologies between time-of-flight magnetic resonance angiography (TOF-MRA) acquired with Compressed SENSE (TOF-CS), spiral image acquisition (TOF-Spiral) and an ultra-short spiral acquisition (TOF-Spiral-short) with reduced spatial resolution.

Methods

Patients who underwent 3 Tesla MRI including imaging of cranial vessels in the first 8 weeks after implementation of a new MRI software enabling spiral imaging were included in this retrospective study. TOF-MRA was performed via 3 sequences: TOF-CS (4 min), TOF-Spiral (3 min), TOF-Spiral-short (1 min). Blinded qualitative image evaluation (overall image quality, artifacts, vessel contrast, detection of vessel pathology, and diagnostic confidence) was performed by two readers [R1] and [R2] blinded to patient and sequence.

Result

TOF-CS acquired higher quality images than TOF-Spiral for extracranial (Fig 1., panel d, h, l, marked with flat head arrow) and intraosseous (Fig 1., panel c, g, k, marked with double arrow head) arteries of the anterior circulation whereas TOF-Spiral was able to better detect anterior choroidal artery (Fig 1., panel a, e, i, marked with arrow) and posterior communicating arteries (Fig 1., panel b, f, j, marked with asterisks). The diagnostic confidence to rule out or detect vessel pathology was equal in TOF-Spiral and TOF-CS. TOF-Spiral-short showed reduced image quality while still being able to sufficiently depict pathologies. All vessel pathologies were correctly identified in all sequences, despite the differences in image quality. Interobserver rating showed no significant discord.



Depiction of transversal slices of raw TOF-MRA images acquired with TOF-CS, TOF-Spiral and TOF-Spiral-short. Panels a., e., i. show slices at the level of the anterior choroidal arteries. Panels b., f., j. show slices at the level of the circle of Willis. Panels c., g., k. show slices at the level of the cavernous segment of the internal carotid artery. Panels d., h., l. show slices at the level of the entrance to the carotid canal.

Discussion & Conclusion

Both TOF-CS and TOF-Spiral resulted in high diagnostic confidence. TOF-CS performed better at the skull base whereas TOF-Spiral yields higher quality images intracranially while being 25% faster than TOF-CS. TOF-Spiral-short performed 75% faster but showed reduced image quality compared to the other sequences. It remains a promising candidate for fast screening. A combination of Spiral and Compressed SENSE may help to overcome shortcomings of both sequences alone and further reduce acquisition time.

1-P47

ADVANCED BRAIN MRI HELP DIAGNOSIS AND GIVE INSIGHT INTO THE PATHOPHYSIOLOGY OF NEURODEGENERATION IN MELAS (MITOCHONDRIAL ENCEPHALOMYOPATHY, LACTIC ACIDOSIS, AND STROKE-LIKE EPISODES) SYNDROME

*L.L. Gramegna*¹, *S. Evangelisti*², *L. Di Vito*², *C. Testa*³, *C. La Morgia*⁴, *V. Carelli*⁴, *C. Tonon*¹, *R. Lodi*¹

¹ IRCCS Istituto delle Scienze Neurologiche di Bologna, Diagnostica Funzionale Neuroradiologica, Bologna, ITALY, ² Department of Biomedical and NeuroMotor Sciences, Functional MR Unit, University of Bologna, Bologna, Bologna, ITALY, ³ Department of Physics and Astronomy, University of Bologna, Bologna, ITALY, ⁴ IRCCS Istituto delle Scienze Neurologiche di Bologna, UOC Clinica Neurologica, Bologna, Italy, Bologna, ITALY

Introduction

MELAS is a rare genetic disorder with broad manifestations commonly associated with MT-TL1 gene mutations. There are no imaging diagnostic criteria of MELAS. The pathogenesis of brain manifestation in MELAS is not yet fully understood and the proposed mechanism includes both neuronal mitochondrial dysfunction and nitric oxide (NO) deficiency. L-arginine, a NO-precursor, is reduced in patients and his administration decreases the frequency and severity of stroke-like episodes.

Methods

Twenty-three consecutive MELAS patients (age: 42.2±12.1 years, 13M) and matched healthy controls (HC) were enrolled. The MR protocol (1.5T, GE) included single voxel 1H-MRS (PRESS, TR/TE=4000/35ms) in regions without signal alterations such as the medial parieto-occipital gray matter (POGM, 18 ml), parieto-occipital white matter (POWM, 8ml), cerebellar hemisphere (6 ml), and a volumetric T1-w images (TR/TE/TI=12.5/5.1/600ms, 1mm³ isotropic).

NAA content relative to Cr was evaluated with LCMoDel 6.3 and a receiver operator characteristic (ROC) curve was configured to calculate the accuracy to distinguish between patients and

controls. Serum concentrations of lactate and arginine were evaluated in patients.

Statistical significance was set to $p < 0.05$ (after correction).

Voxel-based morphometry (VBM) analyses were performed on T1-w images (excluding patients with stroke-like) using SPM 12.0 and SUI.

Result

Six patients presented multiple stroke-like lesions. Compared to HC, MELAS patients showed lower NAA/Cr in the POGM (1.24 ± 0.16 vs 1.39 ± 0.11 , $p = 0.006$), in the POWM (1.62 ± 0.23 vs 1.80 ± 0.14 , $p = 0.007$) and in the cerebellum (0.96 ± 0.15 vs 1.29 ± 0.20 , $p < 0.001$). Lower NAA/Cr in the POGM negatively correlates with lactate acidemia ($r = 0.542$, $p = 0.024$). NAA/Cr reduction in the cerebellum was the best discriminator between patients and controls (accuracy 94%, sensitivity 83%, specificity 92%).

VBM showed a widespread mild GM loss over the whole cortex ($p < 0.05$) and a severe GM loss ($p < 0.001$) in the bilateral calcarine cortex, insular region (right > left) and auditory cortex. The GM loss negatively correlates with lactate acidemia ($r = -0.562$, $p = 0.045$) and positively with decreased serum L-arginine ($r = 0.692$, $p = 0.018$).

Discussion & Conclusion

Cerebellar NAA/Cr reduction detected by using 1H-MRS may be a valuable supplemental tool to help neuroradiologists in making the diagnosis of MELAS in clinical practice. The correlation between brain GM loss and lactate acidemia and arginine level suggest in vivo an interplay between mitochondrial and nitric oxide (NO) pathways in the mechanism leading to neurodegeneration.

1-P48

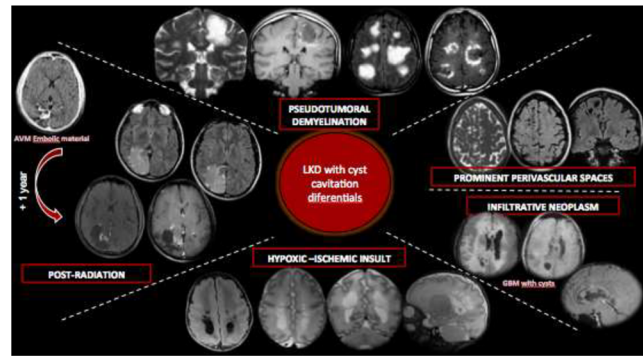
WHAT WE SHOULD LEARN ABOUT LEUKODYSTROPHIES WITH CYSTS OR CAVITATION

*I. Gomes Padilha*¹, A. Paula Alves Fonseca¹, A. Iuno Araujo¹, F. Torres Pacheco¹, R. Hoffmann Nunes¹, A. Carlos Martins Maia Jr.¹, A. Jose da Rocha¹

¹ Irmandade da Santa Casa de Sao Paulo, Sao Paulo, BRAZIL

Introduction

There are many different metabolic leukodystrophies (LKD) with distinctive specific features and, some of them, with the genetic and molecular identity established. A small subset is associated to cavitory or cystic lesions that are radiologically defined by the association of a diffuse LKD and hypointensities within large areas of dysmyelination. Our purpose is to review and discuss typical and atypical metabolic LKD with cysts and/or cavitation as well as mimicking disorders on magnetic resonance imaging (MRI) in order to scrutinize a practical approach for the differential diagnosis.



Methods

After reviewing our institution teaching files, we selected cases demonstrating metabolic LKD with cavitation and/or cysts. Disorders were presented according to specific findings highlighting the contribution of cavitation/cyst occurrences and distribution for specific diagnosis. Patient selection and data collection were performed using the electronic patient's database.

Result

The progressive improvement of magnetic resonance imaging into clinical practice contributed to advances in white matter diseases comprehension. Some metabolic LKDs with cavitation and/or cysts were found to have a relative specific pattern that could predict differential diagnosis, including lysosomal storage, amino and organic acids, muscle and mitochondrial dysfunction. In this subset, there are some disorders already well recognized such as galactosemia and others that have been more recently described: megalencephalic leukoencephalopathy with and without subcortical cysts, vanishing white matter disease and leukoencephalopathy, cerebral calcification and cysts disease (Labrune Syndrome). Furthermore, the main mimicking disorders were also reviewed, including dilated perivascular spaces related to white matter abnormalities, cytomegalovirus congenital infection and periventricular leukomalacia.

Discussion & Conclusion

The approach of metabolic LKD with cavitation and/or cysts requires an extensive understanding of specific imaging findings associating to its genetic/molecular identity, distinguishing real cystic/cavitation features and its main pitfalls in order to prevent misinterpretation and to facilitate the correct diagnosis.

1-P49

MICROSTRUCTURAL CHANGES OF THE BRAIN UNDER ANTI-TNFA TREATMENT FOR RHEUMATOID ARTHRITIS: HISTOGRAM ANALYSIS OF GREY AND WHITE MATTER DTI METRICS

*C. Gkizas*¹, L. Astrakas², A. Zikou¹, E. Kaltsonoudis³, P. Voulgari³, M. Argyropoulou¹

¹ University Hospital Department of Clinical Radiology, Ioannina, GREECE, ² Medical School Department of Medical Physics, Ioannina, GREECE, ³ University Hospital Department of Clinical Radiology, Ioannina, GREECE, ⁴ University Hospital Department of Rheumatology, Ioannina, GREECE, ⁵ University Hospital Department of Rheumatology, Ioannina, GREECE, ⁶ University Hospital Department of Clinical Radiology, Ioannina, GREECE

Introduction

The use of TNF α antagonists in rheumatoid arthritis (RA) has been associated with various neurologic adverse effects. This DTI study aims to evaluate the potential microstructural changes of the brain in RA patients receiving anti-TNF α treatment.

Methods

Nineteen patients with newly diagnosed RA (10 female and 9 male; mean age \pm SD; 53 \pm 6.6 years) were included in this study. All patients had detailed physical examination and completed a short period of therapy with methotrexate and/or corticosteroids. A baseline brain MRI including FLAIR, T1, T2 and DTI was performed and a follow up after 12 months of treatment with anti-TNF α . MRI scans revealed no obvious changes in follow up examinations. During this period all patients were immunoneurologic free. Histogram metrics of mean diffusivity (MD) and fractional anisotropy (FA) of gray matter and white matter compared before and after treatment.

Result

Mean, median, mode, and 75th percentile of the FA distribution for both grey (GM) and white matter (WM) decreased after treatment. Standard deviation of GMs FA distribution also decreased after treatment. Histogram metrics of the MD distribution of WM and GM did not reveal significant changes.

Discussion & Conclusion

Histogram analysis reveals microstructural changes in patients with RA under antiTNF α treatment. Hypomyelination with relative axonal preservation might be the anatomical substrate of decreased FA in WM. Activation of TNF α in RA is considered an important factor for GM atrophy. AntiTNF α treatment waives TNF α activity and leads to increased cellularity expressed as decreased FA.

1-P50

THE ROLE OF NEURO-RADIOLOGIST IN MULTIDISCIPLINARY TUMOR BOARD : IMPACT ON CLINICAL COURSE AND EXAMINATIONS

*C. Giordano*¹, *G. Pezzullo*², *G. La Rocca*¹, *G. Sabatino*¹, *A. Olivi*¹, *G. Marziali*¹, *A. Ramaglia*¹, *S. Cottonaro*¹, *S. Gaudino*¹, *C. Colosimo*¹

¹ Fondazione Policlinico Universitario Agostino Gemelli IRCCS, Roma, ITALY, ² Università di Napoli Federico II, Napoli, ITALY

Introduction

The aim of this study is to evaluate the impact of the multidisciplinary tumor board (MTB) on brain tumor patient's management and the role of

the neuroradiologist in this commission. The recent molecular discoveries and the therapeutic advances in neuro-oncology have determined a growing interest for MTBs, which nowadays are a fundamental component of clinical neuro-oncological management. MTBs are frequented by neurosurgeons, oncologists, radiotherapists, radiologists, pathologists, in order to collaborate in the management of complex cases. During the MTB the role of the neuroradiologist consists not only in defining the nature of the tumor, but also in specifying its location and its functional site, and in evaluating the appropriate treatment, while in the follow-up it is to evaluate signs of progression/recurrence disease or response/non-response to treatment.

Methods

One hundred seventy-seven patients were discussed in MTB of our institute, between March 2017 and March 2018. We focused on the changing treatment plan (COTP) which means cases in which the pre-MTB plan has been significantly modified, or a new treatment plan has been implemented. The COTP must be accepted by all colleagues.

Result

Across 12 months, 21 MTB were done in our Institution, a total of 177 cases (corresponding to 148 patients) were discussed. The characteristics of the enrolled patients are reported by single case in Table 1. 42.3% of the patients presented were in the post-operative phase of treatment. The most frequent question on MTB, recorded in 81 cases (49.6%), concerned treatment planning. About 10% of cases had COTP. In 107 cases (65.5%) no exams were requested after tumor board.

Table 1

Characteristics of the cases	
Total cases with available information n (%)	163 (92)
Age mean at diagnosis (SD)	55.1 (14.5)
Gender n (%)	
Male	81 (49.7)
Female	82 (50.3)
KPS n (%)	
missing	40 (24.5)
50	4 (2.5)
60	11 (6.7)
70	20 (12.3)
80	20 (12.3)
90	40 (24.5)
100	28 (17.2)
Histopathology n (%)	
Missing	14 (8.6)
Glioblastoma Multiforme (GBM)	52 (31.9)
Anaplastic Astrocytoma	14 (8.5)
Oligodendroglioma	9 (5.5)
Low grade	6 (3.7)
Meningioma	19 (11.7)
Single metastasis	23 (14.1)
Multiple metastasis	14 (8.6)
Other	12 (7.4)
Focal deficit n (%)	
Present	72 (44.2)
	91 (55.8)
Type of deficit n (%)	
Missing	11 (6.7)
Motor deficit	38 (23.4)
Language deficit	11 (6.7)
Cranial nerves deficit	8 (4.9)
Other	4 (2.5)
Care phase n (%)	
Missing	13 (8.0)
Pre surgery	16 (9.8)
Post surgery	69 (42.3)
Post radiotherapy	9 (5.5)
Post chemotherapy	37 (22.7)
Follow-up	19 (11.7)

Discussion & Conclusion

Optimal brain cancer care requires a multidisciplinary approach and MTB is focused on finding the most efficient solution from the diagnostic to therapeutic point of view, and also economically advantageous for the structure, limiting the demand for inappropriate investigations and therapies.

In this context, the neuroradiologist has the role of support for the other specialists in diagnostic purposes, in follow-up, and also establishing the most correct therapeutic approach.

1-P51

ADVANCED MRI SHAPE ANALYSIS AS A PREDICTOR OF HISTOLOGICALLY AGGRESSIVE SUPRATENTORIAL MENINGIOMA

*G. Friconet*¹, V.H. Espindola ALA¹, K. Janot², W. Brinjikji³, C. Bogey¹, L. Lemnos¹, H. Salle¹, S. Saleme¹, C. Mounayer¹, A. Rouchaud¹

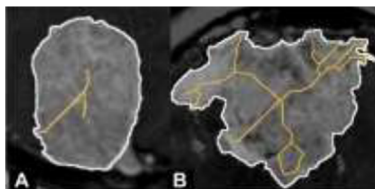
¹ Centre Hospitalier et Universitaire Dupuytren, Limoges, FRANCE, ² Fondation Adolphe-de-Rothschild, Paris, FRANCE, ³ Mayo Clinic, Rochester, USA

Introduction

A subset of aggressive meningioma is associated with higher morbidity and requires a different therapeutic management. This subset consists of World Health Organization (WHO) grade II and III meningioma, characterized particularly with microscopic brain invasion. Numerous studies tried to screen aggressive meningioma on pre-operative MRI. The objective of the study was to determine if an advanced shape analysis of supratentorial meningioma outlines could reliably predict WHO II-III grade and histological brain invasion.

Methods

We performed a retrospective analysis of our prospective database for all consecutive patients who underwent surgery for supratentorial histologically-proven meningioma from 2010 to 2018. Pre-operative MRI contrast enhanced axial, coronal and sagittal slices were collected. Advanced shape analysis including fractal analysis and topological skeleton analysis was performed (Figure 1). Shape analysis parameters were correlated with histopathological WHO grading and brain invasion on surgical pieces.



Result

A low circularity ($P = .046$), a low solidity ($P = .02$), a high number of skeleton's branches ($P = .03$) and high relative skeleton's length ($P =$

$.045$) were significantly correlated with histological brain invasion. No significant correlation was identified between shape analysis and WHO grading. With an appropriate diagnostic threshold these four parameters could help to exclude histopathological brain invasion with negative predictive values > 0.90 .

Discussion & Conclusion

MRI shape analysis is a potentially informative tool to predict histological brain invasion in case of supratentorial meningioma.

1-P52

MR IMAGING FINDINGS AFTER GAMMA KNIFE RADIOSURGERY FOR VESTIBULAR SCHWANNOMAS: A SINGLE-CENTER STUDY

*T. Freddi*¹, F. Dantas¹, L. Arteaga², A. Ferreira¹, N. Ferreira¹, J. Salvajoli²

¹ Hcor Neuroradiology Department, São Paulo, BRAZIL, ² Hcor Radiosurgery Department, São Paulo, BRAZIL

Introduction

Vestibular schwannomas (VS) are benign intracranial tumors arising from the vestibular division of the VIII cranial nerve. Several treatment options are currently used, such as, observation, stereotactic radiosurgery (SRS), conventional fractionated radiotherapy (CFRT), and microsurgery (MS). Due the complex anatomy of the cerebellopontine angle, surgical treatment of the VSs may cause significant morbidity (1). Large series reported excellent control rates and significantly lower complication rate with SRS than with MS (2).

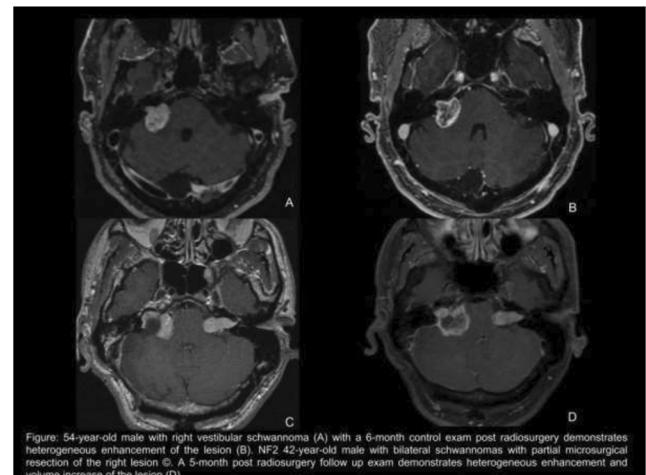


Figure: 54-year-old male with right vestibular schwannoma (A) with a 6-month control exam post radiosurgery demonstrates heterogeneous enhancement of the lesion (B). NF2 42-year-old male with bilateral schwannomas with partial microsurgical resection of the right lesion (C). A 5-month post radiosurgery follow up exam demonstrates heterogeneous enhancement and volume increase of the lesion (D).

Methods

In this study, we present a retrospective analysis of our institution patients diagnosed with VS and treated with SRS, between 2014 and 2018.

All patients were submitted to magnetic resonance imaging (MRI) pre and post surgical treatment and tumors were evaluated by their dimensions, volume and presence or absence of necrosis.

Result

A total of 77 patients, 26 (33%) have done MRI follow-up in our institution. Thus, 26 patients were included in our retrospective analysis. 19 (73%) patients were treated exclusively with SRS, other 7 (27%) were treated with combined modality, microsurgery followed by SRS. 04 (15%) were diagnosed with neurofibromatosis type 2 (NF2). The target and the ipsilateral cochlea were defined on T1, T2 and fiesta series and adapted to bone window CT scans. The mean prescribed dose with GK was 12Gy and mainly, we targeted the isodose line of 50%. The mean maximum cochlear dose was 7,03Gy and the used constraints were, 08 Gy as maximum dose and 04Gy as median dose. The mean interval follow up was 448 days with 04 (15%) patients demonstrating stable imaging findings in the control exam. 15 (57%) patients demonstrated tumor growth and 06 (23%) exhibited lesion reduction volume. All lesions that increased demonstrated necrotic areas in the follow up exam. Tumors that were stable or had volume reduction demonstrated variable imaging pattern in the follow up exam.

Discussion & Conclusion

The purpose of this study is to describe the main MRI findings related to SRS of VS. Radiologists should be aware that tumor growth in control exam is not always related to tumor progression, specially if necrotic areas appear in the follow up exam.

1-P53

CT FINDINGS OF CENTENARIANS IN EMERGENCY ROOM: A RETROSPECTIVE STUDY

*A. Fischetti*¹, N. Romano¹, V. Cozzolino², M. Federici², S. Parodi², M. Pensa², U. Ruffinengo², A. Castaldi²

¹ Departement of Health Sciences (DISSAL), University of Genoa, Genoa, ITALY, ² Departement of Diagnostic and Interventional Neuroradiology, E.O. Ospedali Galliera, Genoa, ITALY

Introduction

The continuous growth of the prospect of life leads us to face, more and more frequently, with a new generation of patients: the centenarians. In 2018 in Italy lived 15647 people 100 years old and more (17% males, 83% females).

The study retrospectively evaluates the findings of brain Computed Tomography (CT) in evaluation of centenary patients presented in the Neuroradiology Department of our Institute in emergency conditions. To the best of our knowledge, this is the first study that evaluate neuroradiological findings exclusively in centenary patient.

Methods

We retrospectively recruited all consecutive patients with 100 or more years who underwent brain-CT in emergency room who underwent brain-CT in emergency room in the last 10 years (2009-2018). All clinical and neuroradiological data were stored in the local database; all CT examinations were reviewed by two experienced observers.

For all patients, we collected the followings data: sex, age, previous neuroradiological examinations, reasons of examination, CT diagnosis and incidental CT findings.

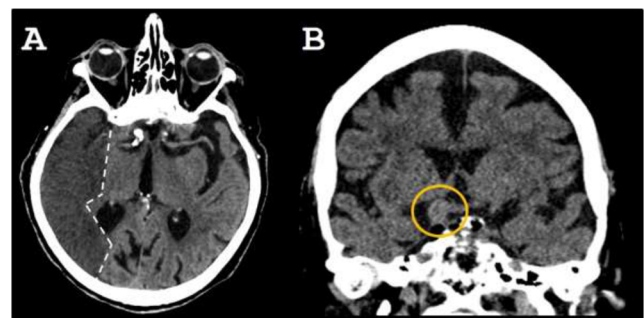
Result

We enrolled 55 patients, with 48 females (87%) and 7 males (13%). Patient age was between 100-105 years old. Number of examinations for year was 5.5 (± 2.37). Mean age was 101 ($\pm 1,36$).

In 42 cases it was the first brain CT examination (76,3%).

Reason of examination was: trauma (38), suspected stroke (13), coma (2), headache (1), dementia (1). In 42 cases (76,3%) it was the first brain CT examination.

CT diagnosis was: 6 cases of findings compatible with stroke (Fig 1.A), 4 cases of haemorrhages, 1 case of C2 fracture. Incidental findings were: 2 aneurysms of internal carotid artery (Fig 1.B), 3 meningiomas.



Discussion & Conclusion

In traumatic cases, only 10,5% of CTs were positive for intra- and/or extra-axial traumatic haemorrhages. As regards suspected stroke, there is a higher concordance between clinical suspicion and CT findings (46%). Data suggest that centenary patients rarely have a history of neurological disorders and their clinical risk in emergency is often overestimated.

1-P54

REVISITING IDIOPATHIC NORMAL PRESSURE HYDROCEPHALUS AND IMAGING DIAGNOSTIC APPROACHES

*L. Fajardo Ramin*¹, S.F. Ferracioli¹, W.R. Fernandes JR¹, L. Tavares Lucato¹, C. Costa Leite¹

¹ Instituto De Radiologia - Hospital Das Clinicas Da Fmusp, São Paulo, BRAZIL

Introduction

Normal pressure hydrocephalus (NPH) is a syndrome identified in 1957 by Hakim. NPH is considered a treatable cause of dementia and is characterized by the clinical triad of gait disturbance, mental deterioration and urinary incontinence in association with enlargement of the ventricular system and normal cerebrospinal fluid (CSF) pressure. Although idiopathic NPH (iHPN) is considered a CSF circulation disorder, chronic

hypertension, white matter disease and also the glymphatic system seems to play a role in iNPH. The estimated number of undetected cases of iNPH is high, specially due to the the non specific nature of the symptoms.

Methods

Here we will review several cases of iNPH from a teaching institution. Pertinent atual literature will also be reviewed, including MRI emerging techniques.

Our purpose is to show the diagnostic imaging approach to iNPH including a simple way to establish the diagnosis of ventriculomegaly, assessment to the signal loss of CSF flow and aqueductal CSF stroke volume, measurement of the callosal angle and evaluation of disproportionately enlarged subarachnoid space hydrocephalus (DESH). We will discuss the improved accuracy when combining these imaging findings as well as their clinical correlation and prognostic considerations.

We will also propose a protocol for MRI in suspected iNPH.

Result

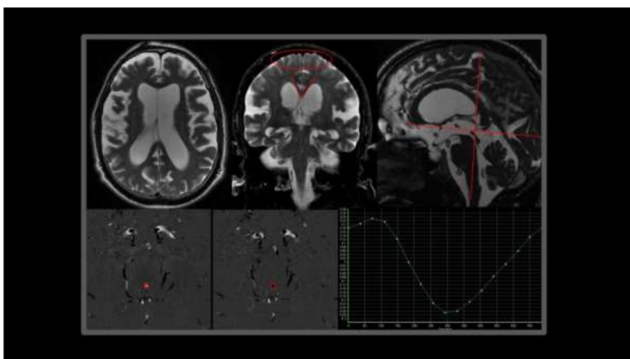
Neuroimaging is extremely important in establishing the diagnosis of iNPH, as one of the diagnostic requisites is the presence of a ventriculomegaly not attributable to central atrophy or to a non-communicating hydrocephalus.

The analysis of flow dynamics and aqueductal patency can be established by cardiac-gated phase contrast MRI, which is extremely sensitive to CSF motion and provides CSF hydrodynamic quantification but can also be assessed by a combination of heavily 3D T2W sequences (that provides anatomical information of the aqueduct) and 3D T2W TSE sequences (which offers an easy evaluation of the presence of CSF flow).

MRI may also be effective in identifying patients who will respond to shunting treatment.

Discussion & Conclusion

The diagnosis of iNPH and the decision to treat a patient is typically a multistage and challenging process, suspected on the basis of the history, neurological examination and interpretation of CT/MRI scans.



1-P55

GABA LEVELS IN PATIENTS RECEIVING ELECTROCONVULSIVE THERAPY

V.J. Erchinger¹, C. Abbott², T.R. Jones², U. Kessler^{1,3}, K.J. Oedegaard^{1,3,4}, L. Ersland^{5,6,7}, L. Oltedal^{1,8}

¹ Department of Clinical Medicine, University of Bergen, Bergen, NORWAY, ² Department of Psychiatry, University of New Mexico School of Medicine, Albuquerque, USA, ³ Division of Psychiatry, Haukeland University Hospital, Bergen, NORWAY, ⁴ K.G. Jebsen Centre for Research on Neuropsychiatric Disorders, Bergen, NORWAY, ⁵ Department of Clinical Engineering, Haukeland University Hospital, Bergen, NORWAY, ⁶ NORMENT Center of Excellence, University of Bergen, Bergen, NORWAY, ⁷ Department of Biological and Medical Psychology, University of Bergen, Bergen, NORWAY, ⁸ Mohn Medical Imaging and Visualization Centre, Department of Radiology, Haukeland University Hospital, Bergen, NORWAY

Introduction

Electroconvulsive therapy (ECT) is regarded as a safe and effective acute treatment of major depressive episodes. ECT has been used for ~ 80 years, but we still lack knowledge about how the therapy works. It has been suggested that gamma-aminobutyric acid (GABA) plays an important role for the effects of ECT. Magnetic resonance spectroscopy (MRS) allows non-invasive in vivo measurements of GABA in the brain. So far two studies have compared brain GABA-levels before and after ECT, reaching opposite conclusions.

Methods

GABA levels were investigated in 45 Patients (P) that were accepted for ECT-treatment at Haukeland University Hospital or University of New Mexico Mental Health Center, and 37 age-matched Healthy Controls (HC) from the same geographical areas. Spectroscopic Imaging was performed on a 3 Tesla GE Discovery 750 scanner system and a 3-Tesla Siemens Trio scanner. MEGA-PRESS was used for 1H-MRS single-voxel point resolved spectroscopy. Measurements were performed in the anterior cingulate cortex (ACC) before and after ECT. The R software was used for statistical analysis. For difference in GABA between timepoints at each site, the paired t-test was used. General linear models (GLM) were used for exploring relationships between change in GABA and clinical outcome (MADRS change) as well as the relationship between number of ECTs and change in GABA. Analyses were controlled for age, sex and site.

Result

Mean GABA values at baseline for the two sites were 2.80 (P) and 2.83 (HC) $p=0.83$, and 2.84(P) and 2.93 (HC) $p=0.48$ (Figure 1). Paired samples t-test (patients from both sites combined) showed a mean difference of -0.007 for GABA concentration before and after ECT, $p=0.92$ (Figure 2). The linear model testing the association between number of ECTs and percentage change in GABA was not statistically significant (Estimated slope= 0.14 , $p=0.13$). We did not find a difference for

percentage change in GABA when comparing remitters and non-remitters ($p=0.61$).

Discussion & Conclusion

Our findings do not support GABA being a main factor for the effect of ECT, but further studies are warranted to determine the role of GABA in the ECT treatment.

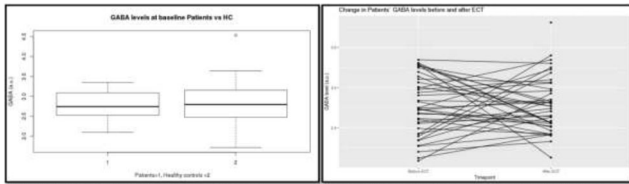


Figure 1: Boxplot of baseline GABA levels in HC and P

Figure 2: Change in GABA levels before and after ECT in P

1-P56

POST STEREOTACTIC RADIOSURGERY MRI SIGNAL INTENSITY DISTRIBUTIONS PREDICT SURVIVAL IN INTRACRANIAL METASTASES

A. Dudek¹, E. Lim¹, S. Thust², N. Fersht³, N. Kitchen⁴, C. Tancu⁴, M. Sokolska⁵, H. Hyare¹

¹ University College London Hospital - Department of Imaging, London, UNITED KINGDOM, ² National Hospital for Neurology and Neurosurgery - Department of Neuroradiology, London, UNITED KINGDOM, ³ University College London Hospital - Department of Radiotherapy, London, UNITED KINGDOM, ⁴ National Hospital for Neurology and Neurosurgery - Department of Neurosurgery, London, UNITED KINGDOM, ⁵ University College London Hospital - Medical Physics and Biomedical Engineering, London, UNITED KINGDOM

Introduction

Conventional MRI is insufficient to accurately differentiate between local tumour recurrence and radiation-induced necrosis post stereotactic radiosurgery (SRS) of intracranial brain metastases. We investigated whether pre and post SRS tumour signal intensity (SI) distributions could aid radiological assessment.

Methods

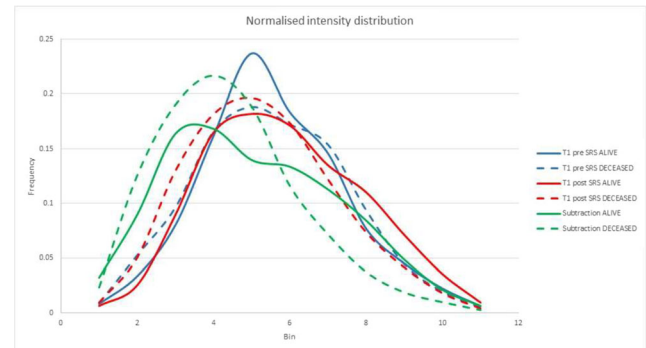
Subjects: 43 patients (21 female) with intracranial metastases (primary: 16 breast, 20 lung, 6 melanoma, 1 renal) who underwent SRS between 03/2015 and 11/2016. MRI: 3D T1 weighted sequences with contrast (T1Wc) pre SRS (n=43) and T1Wc and T1 subtraction images (T1Ws) at 3 months post SRS (n=16) were analysed for voxel volume and SI distribution by drawing regions of interest (ROI) encompassing the total tumour volume using ITK-Snap and histogram parameters generated in Matlab. Sub-analysis was stratified by survival at 1-year (Alive n=27, Deceased n=16) and 2-years (Alive n=20, Deceased n=23).

Result

Overall, a decrease in tumour volume on T1Wc post SRS (mean -37.49%, p-value 0.4) was seen irrespective of survival at 1 or 2 years. Across the

whole group, there was no significant difference in any histogram parameters between pre and post SRS T1Wc but a significant difference in SI skewness between post SRS T1Wc and post-SRS T1Ws (0.236 versus 0.481, $p=0.008$) was observed.

For Alive versus Deceased at 2 years, a significant difference in SI kurtosis on post-SRS T1Wc (-0.12 versus 0.69, $p=0.02$) and a significant difference in post-SRS T1Ws p50 (0.485 versus 0.422, $p=0.031$; see Graph) was seen. For Deceased at 2 years, a significant difference in kurtosis for T1Wc pre vs post treatment (-0.077 versus 0.694, $p=0.006$) was observed. No significant differences were observed for Alive versus Deceased at 1 year.



Discussion & Conclusion

Post SRS p50 of the T1Ws SI distribution and kurtosis of the T1Wc SI distribution were able to differentiate patients alive versus deceased at 2 years. The shift towards lower SI distribution on T1Ws compared to T1Wc post SRS is likely due to subtraction of high T1W SI intralésional blood products which is associated with survival at 2 years.

Conclusion: T1Wc and T1Ws SI distributions demonstrate detectable difference in tumour SI that may help to predict survival following SRS.

1-P57

FAST SUSCEPTIBILITY WEIGHTED IMAGING USING T2* ECHO PLANAR IMAGING

N. Campeau¹, N. Meyer¹, J. Trzasko¹

¹ Mayo Clinic, Rochester, MN, USA

Introduction

SWI and SWAN have the drawback of long acquisition times, typically in the 5–7 minute range depending on desired resolution. Despite suboptimal detection of subtle susceptibility abnormalities, conventional T2* GRE (2 minutes) and EPIGRE (15–20 seconds) techniques have now become the accepted default for susceptibility imaging at many centers, primarily because of imaging time constraints. The purpose of this work was to implement SWI postprocessing for single echo T2* echo planar imaging (EPIGRE-SWI), and then compare the diagnostic sensitivity of EPIGRE-SWI to standard EPI-GRE using conventional SWI images as the “gold standard”.

Methods

Phase-based SWI postprocessing was developed for EPIGRE imaging using MATLAB based Orchestra SDK 1.7-1 software package (GE Medical Systems). Phase information from raw complex EPIGRE data was combined in a meaningful manner to preserve phase information, accounting for echo-planar acquisition and individual coils. The resultant complex post-processed image was further filtered and post-processed into a phase mask that was applied exponentially to the magnitude images to create EPIGRE-SWI images. EPIGRE-SWI, EPIGRE, and conventional SWI images obtained in 10 patients were then evaluated for detection of susceptibility abnormalities. Imaging was reviewed by a neuroradiologist in non-blinded manner. The number and size of susceptibility abnormalities were recorded. Motion artifact was also graded.

Result

Acquisition times for EPIGRE was 15 seconds, compared to 5:40 for SWI on both 1.5T and 3.0T MRI scanners. Punctate <1mm susceptibility foci were not routinely detected using either EPIGRE or EPIGRE-SWI. Large susceptibility foci were identified on all techniques. Intermediate size lesions (primarily 1-5mm) were better detected on EPIGRE-SWI versus routine EPIGRE. The EPI-based techniques were more susceptible to false positive results, usually from partial-volume effects of a small vessel. Motion artifact severely limited diagnostic sensitivity of SWI in three studies.

Discussion & Conclusion

EPIGRE-SWI post-processing improves detection sensitivity of susceptibility abnormalities over conventional EPIGRE, and requires zero additional scan time. Compared to routine EPIGRE images, EPIGRE-SWI provided improved detection of small lesions (1-5mm range). Both EPIGRE and EPIGRE-SWI performed poorly for detection of punctate susceptibility foci measuring < 1mm. EPIGRE-SWI was particularly useful in uncooperative patients, where increased motion artifacts from lengthy SWI acquisition time can negate its advantages.

1-P58

MICRO-CT AND DUAL-SOURCE CT OF THE RETRIEVED CLOT IN ACUTE STROKE

*D. Botta*¹, *P. Machi*¹, *M. Muster*¹, *M. Vargas Gomez*¹, *D. Rufenacht*², *I. Wanke*², *K. Lovblad*¹

¹ Hôpitaux universitaires de Genève- Service de Neuroradiologie diagnostique et interventionnelle- Département Diagnostique, Genève, SWITZERLAND, ² Hirslanden Private Hospital Group - Zentrum für Neuroradiologie, Zurich, SWITZERLAND

Introduction

Mechanical thrombectomy has allowed to improve outcome of patients with acute ischemic stroke. Selection of patients is based on brain tissue CT and IRM imaging. Little is known about the composition of the clot before intervention. Characterization of clot composition in acute ischemic stroke patients is becoming increasingly important given the fact that

many studies have demonstrated that thrombus composition can predict recanalization success following mechanical thrombectomy.

Our aim is to evaluate the capacity of dual-source CT to determine clot composition and to compare it to micro-CT images.

Methods

14 patients (10 male, 4 female, ages: 34-90) with acute ischemic stroke were included in this study. All patients underwent mechanical thrombectomy after dual-source CT (Siemens Force, Erlangen). A stroke CT protocol was performed with pre-contrast images as well as angio-CT, perfusion CT and post-contrast images. After thrombectomy (Thromboaspiration +/- Stent retriever), the clot was imaged on a micro-CT (CT Lab GX series, Rigaku). Images were loaded up to OsiriX, regions of interest were defined on the clot and density values were measured in Hounsfield units.

Result

Recanalization by mechanical thrombectomy was obtained in all patients of our series. Clinical Hounsfield units of the clot were between 54 and 66, whereas the Hounsfield values measured to micro CT were between 57 and 60.

Discussion & Conclusion

Clinical CT as measured by dual-energy CT reflects clot composition and clot density seen on micro-CT.

1-P59

IMAGING FINDINGS OF UNCOMMON SELLAR AND PARASELLAR LESIONS

*C. Altintas Taslicay*¹, *E. Dervisoglu*¹, *I. Anik*², *Y. Anik*¹

¹ Kocaeli University Faculty of Medicine /Radiology, Kocaeli, TURKEY,

² Kocaeli University Faculty of Medicine /Neurosurgery, Kocaeli, TURKEY

Introduction

The sellar and parasellar region is a complex region and contains many vascular and neural structures of different anatomical structure. Although pituitary adenomas are seen often, many neoplastic, infectious, inflammatory, developmental and vascular lesions can also be located in the sellar and parasellar region. Knowledge of relevant neuroimaging features may assist in characterization of these lesions, delineation of their extent, and awareness of potential mimics prior to diagnostic biopsy or resection. We aim to show the imaging characteristics of uncommon lesions arising from the sellar-parasellar region and narrow the differential diagnosis.

Methods

One hundred and ninety seven patients undergoing pituitary MRI with the pituitary symptoms were retrospectively reviewed. Lesions involving sellar and parasellar region were evaluated.

Radiological findings of various pathologies are demonstrated and discussed thoroughly.

Result

We retrospectively reviewed patients with pathologically confirmed clival chordoma (n=30), intradural clival chordoma (n=1), chondrosarcoma (n=9), spindle cell oncocytoma (n=1), giant cell bone tumor (n=1), ATRT (n=1), craniopharyngioma (n=33), teratoma (n=1), schwannoma (n=1), hypothalamic hamartoma (n=4), astrocytoma (n=6), germinoma (n=2), lipoma (n=1), meningioma (n=17), pituitary tumor (n=1), dermoid (n=1), epidermoid (n=2), pituitary metastases (n=4), primary CNS lymphoma (n=1), benign notochordal cell tumor (n=2), lymphocytic hypophysitis (n=1), langerhans cell histiocytosis (n=3), granulomatous hypophysitis (n=7), granulomatosis with polyangiitis (n=1), amyloidosis (n=1), pituitary abscess (n=1), cavernous hemangioma (n=1), sellar aneurysm (n=1), parasellar aneurysm (n=1), ectopic neurohypophysis (n=3), rathke cleft cyst (n=57), clival fibrous dysplasia (n=5), arachnoid cyst (n=1), clival aneurysmal bone cyst + meningioma (n=1) and echordosis physaliphora (n=4). We grouped these diseases as neoplastic, inflammatory-granulomatous, infectious, vascular, congenital and others.

Discussion & Conclusion

The sellar and parasellar regions are relatively small areas of the skull base that harbor important neurovascular structures. A variety of neoplastic and non-neoplastic lesions that are difficult to distinguish from each other can occur in there. The diagnosis of these lesions requires endocrine, ophthalmic and neurological examination together with advanced imaging methods. MRI is the mainstay for the diagnosis and follow-up of sellar and parasellar lesions. The information obtained from such examinations may aid in the distinction of these disease processes and in the accurate delineation of their extent prior to biopsy or treatment planning.

1-P60

HISTOGRAM TEXTURE ANALYSIS OF ARTERIAL SPIN LABELLING (ASL) AND DYNAMIC SUSCEPTIBILITY CONTRAST (DSC) PERFUSION IMAGING IN GLIOMAS PHENOTYPING

A. Alsaedi¹, J. Panovska-Griffiths², X. Golay³, S. Bisdas³

¹ Department of Radiology Technology, Taibah University, Medina, SAUDI ARABIA, ² Department of Applied Health Research, UCL, London, UNITED KINGDOM, ³ Department of Brain Repair & Rehabilitation, UCL Queen Square Institute of Neurology, London, UNITED KINGDOM

Introduction: This study assesses the value of ASL and DSC using histogram indicators in glioma phenotyping according to WHO-2016 classification that includes stratification by the involved mutation status.

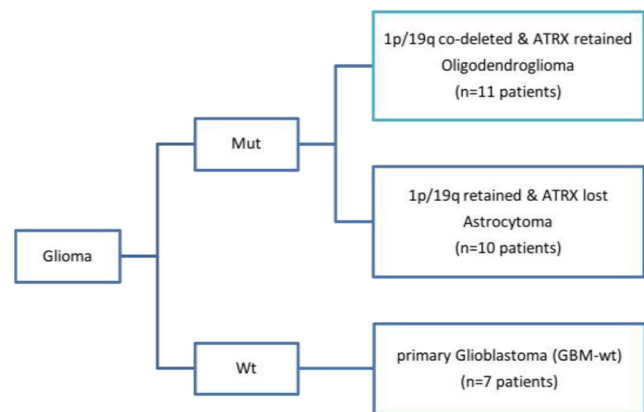


FIG 1: flowchart showing the patient number in each of the classified groups.

Methods

Data from 28 adult glioma patients, using both Pseudo-Continuous-ASL (PCASL) and DSC, were stratified into primary glioblastoma (GBM-WT), astrocytoma and oligodendrogliomas (Figure 1). Histogram indicators considered included: mean, standard deviation (SD), variance, 95-percentile (95tile), median, interquartile-range (IQR), kurtosis, skewness, median Z-score, mode, slope, entropy, min and max. One-way-ANOVA identified the statistically significant indicators and, multinomial-logistic-regression was used to assess the ability of these indicators to predict the three glioma classes depicted in Figure 1. The accuracy of the prediction was projected by confusion matrices for each perfusion map. Pearson-correlation coefficient (r) was used to quantify the relationship between the ASL and DSC.

Result

The most significant histogram indicators from ASL were relative tumour blood flow (rTBF) mean, skewness, median, mode and median-Z-score, from DSC the relative tumour blood flow (rCBF) mean, 95tile, median, IQR, skewness, median Z-score, mode, and tumour blood volume (rCBV) mean, SD, 95tile, median, IQR, kurtosis, skewness, median Z-score, mode, slope, entropy, min and max. Using the most significant indicators, we were able to correctly classify the three classes of gliomas with an average respective accuracy of 57% and 28% for GMB-WT, 80% and 70% for astrocytoma and 64% and 64% for oligodendrogliomas. The rCBV-entropy from DSC possess the highest prediction precision 71% for GMB-wt, 70% for astrocytoma and 72% for oligodendroglioma. The correlation analysis suggests that the ASL histogram indicators were significantly correlated with DSC indicators: with rCBF, r-range=[0.5,0.66] and with rCBV, r-range=[0.5,0.84].

Discussion & Conclusion

Our results suggest that ASL (via rTBF) is better than DSC (via rCBF/rCBV) in classifying gliomas (F1={72%,51%/62%} across the three glioma groups), respectively. However if we use only rCBV-entropy the accuracy of DSC improves (F1=71%). Both methods classify astrocytoma with highest accuracy (80% and 70% for ASL and DSC,

respectively). Further studies, on larger data sets are required to indicate whether ASL should be used clinically instead of DSC for glioma phenotyping.

1-P61

SINGLE SLICE MAGNETIC RESONANCE TEXTURE ANALYSIS FOR THE DISTINCTION OF PRIMARY CENTRAL NERVOUS SYSTEM LYMPHOMA AND GLIOBLASTOMA

C. Maciver¹, A. Al Busaidi², B. Ganesan³, J.A. Maynard^{1,2}, S. Wastling^{1,2}, H. Hyare⁴, S. Brandner⁵, M. Lewis¹, K. Cwynarski⁶, S.C. Thust^{1,2,4}

¹ Neuroradiological Academic Unit, Department of Brain, Repair and Rehabilitation, UCL Institute of Neurology, London, UNITED KINGDOM, ² Lysholm Department of Neuroradiology, National Hospital for Neurology and Neurosurgery, London, UNITED KINGDOM, ³ Department of Nuclear Medicine, University College London Foundation Hospital, London, UNITED KINGDOM, ⁴ Imaging Department and Department of Nuclear Medicine, University College London Foundation Hospital, London, UNITED KINGDOM, ⁵ Department of Neurodegenerative Disease, UCL Institute of Neurology and Division of Neuropathology, London, UNITED KINGDOM, ⁶ Haematology and Oncology Department, University College London Foundation Hospital, London, UNITED KINGDOM

Introduction

Primary central nervous system lymphoma (PCNSL) is a rare, highly malignant form of brain tumour. The current best available therapy is non-surgical consisting of combination chemotherapy, but mandates tissue diagnosis because of a high risk of bone marrow toxicity. The distinction of PCNSL from differentials, specifically glioblastoma, can be challenging and is not reliably achieved by conventional MR imaging. We tested if single slice MR texture analysis (MRTA) could contribute to discriminating between the two entities.

Methods

Post Gadolinium T1-weighted (T1+Gad) images, T2-weighted (T2) images and apparent diffusion coefficient (ADC) maps of 90 patients (PCNSL = 48, GBM= 42) were studied. Largest tumor cross-section segmentations were performed on a proprietary texture analysis research platform (TexRAD, Cambridge, UK) using the software's freehand drawing tool. MRTA commences with a filtration step to extract and enhance features of different sizes, followed by quantification of texture using statistical and histogram texture parameters (mean, standard deviation, entropy, mean positive pixels (MPP), skewness, kurtosis). Results were correlated using non-parametric statistics, with Holmes correction for multiple comparisons. For texture metrics that significantly differed in PCNSL versus glioblastoma, a receiver operating characteristic (ROC) analysis was performed.

Result

ADC performed best for the distinction of the two tumour types with PCNSL exhibiting lower ADC values ($p < 0.05$). Unfiltered ADC mean

and MPP achieved a sensitivity of 83.8% and specificity of 78.9% (AUC 0.88). For tumours featuring greater than 1/3 necrosis, the ADC based distinction was highly accurate with a sensitivity of 96.9% and specificity of 100%. Using T1+Gad, the algorithm was able to distinguish PCNSL from glioblastoma with moderate accuracy (sensitivity 71.4%, specificity 77.1% and AUC 0.779) using coarse filtered kurtosis. T2 produced less accurate results overall with a sensitivity of 66.7% and specificity of 82.8% for identifying PCNSL (AUC 0.82).

Discussion & Conclusion

MR texture analysis may support the identification of PCNSL on imaging. Although the single slice method is not a substitute for biopsy as the reference standard, the ADC based distinction appears promising especially for necrotic tumours.

1-P62

ROLE OF DIFFUSIONAL KURTOSIS IMAGING IN GRADING OF BRAIN GLIOMAS: A DIAGNOSTIC TEST ACCURACY SYSTEMATIC REVIEW AND META-ANALYSIS

G. Abdalla¹, E. Sanverdi¹, P. Machado², J. Kwong³, J. Panovska-Griffiths^{4,5}, A. Rojas-Garcia⁴, D. Yoneoka⁶, J. Veraart^{7,8}, S. Van-Cauter⁹, T. Yousry¹, S. Bisdas¹

¹ The National Hospital for Neurology and Neurosurgery UCL Hospitals NHS Trust, London, UNITED KINGDOM, ² MRC Centre for Neuromuscular Diseases & Centre for Rheumatology, University College London, London, UNITED KINGDOM, ³ Jockey Club School of Public Health and Primary Care, Faculty of Medicine, The Chinese University of Hong Kong, Hong Kong, CHINA, ⁴ NIHR CLAHRC North Thames, Department of Applied Health Research, University College London, London, UNITED KINGDOM, ⁵ Department of Global Health and Development, London School of Hygiene and Tropical Medicine, London, UNITED KINGDOM, ⁶ Department of Global Health Policy, Graduate School of Medicine, University of Tokyo, Tokyo, JAPAN, ⁷ Champalimaud Research, Champalimaud Centre for the Unknown, Lisbon, PORTUGAL, ⁸ imec-Vision Lab, Department of Physics, University of Antwerp, Antwerp, BELGIUM, ⁹ University Hospitals Leuven, Leuven, BELGIUM

Introduction

We aim to illustrate the diagnostic performance of diffusional kurtosis imaging (DKI) in the diagnosis of gliomas.

Methods

A review protocol was developed according to the Preferred Reporting Items for Systematic Review and Meta-analysis Protocols (PRISMA-P), registered in the international prospective register of systematic reviews, PROSPERO and published. A literature search in 4 databases was performed using the keywords "glioma" and "diffusional kurtosis". After applying a robust inclusion/exclusion criteria, included articles were independently evaluated according to the QUADAS-2 tool (revised tool of quality assessment of diagnostic accuracy studies). Data extraction was

done in a pre-designed pro forma. Reported sensitivities and specificities were used to construct 2x2 tables and paired forest plots using the Review Manager (RevMan®) software. A random-effect model was pursued using the hierarchical summary receiver operator characteristics.

Result

Initially, 216 hits were retrieved. Considering duplicates and inclusion criteria; 23 articles were eligible for full-text reading. Ultimately, 19 studies were deemed to be eligible for final inclusion. Quality assessment revealed 9 studies with low risk of bias in the 4 domains. Using a bivariate random-effect model for data synthesis; summary ROC curve showed pooled area under the curve (AUC) of 0.92 and estimated sensitivity and specificity of 0.87 (95% CI: 0.78 - 0.92) and 0.85 (95% CI: 0.76 - 0.91) respectively, in high/low grade gliomas' differentiation. A mean difference in Mean Kurtosis (MK) value between HGG and LGG of 0.22 [95% CI: 0.25 - 0.19] was illustrated (p-value = 0.0014) and a moderate degree of heterogeneity ($I^2=73.8\%$).

Discussion & Conclusion

DKI shows good diagnostic accuracy in high/low-grade gliomas' differentiation; which might qualify it to be part of the routine clinical practice, however; further evidence is deemed for technique standardization.

1-P63

MORPHOLOGICAL CHARACTERISTICS OF RUPTURED INTRACRANIAL ANEURYSMS: A COMPARATIVE STUDY BETWEEN CTA AND DSA

*E. Kapsalaki*¹, A. Brotis², M.K. Kyparissi¹, G. Karagiorgas¹, C. Rountas¹, A. Tasiou², A. Mitsos³, K. Fountas²

¹ Radiology Department, Univ of Thessaly, Larissa, GREECE, ² NEUROSURGERY Department, Univ of Thessaly, Larissa, GREECE, ³ Neurosurgery Department, 401 Gen Military Hospital, Athens, GREECE

Introduction

The agreement between digital subtraction angiography (DSA) and computerized tomographic angiography (CTA) on the main morphological characteristics of the intracranial aneurysms remains controversial. Our primary goal was to study the correlation and agreement between DSA and CTA measurements on the aneurysmal neck and dome.

Methods

We performed a retrospective agreement analysis on all consecutive patients who reached our Hospital with aneurysmal subarachnoid hemorrhage. We included patients who underwent both CTA and DSA in the period between 2012 and 2018. The analysis focused on the maximal neck and dome diameters, and the neck-to-dome ratio. It was realized using intra-class correlation for the intra-observer agreement, Lin's concordance correlation for between study agreement, and Bland-Altman analysis to estimate the between-study bias and the mean normalized detectable difference.

Result

The minimally required study patient recruitment was twenty-seven individuals. Thirty-two patients with an equal number of IAs fulfilled our eligibility criteria and formed the study sample of the current analysis. There were 15 males (47%) and 17 females (53%) with a mean age of 55 years. In 28 cases (87.5%) the aneurysm was located at the anterior circulation. In more than half of the cases (53%), the aneurysmal rupture was associated with severe subarachnoid hemorrhage and in two thirds the aneurysm was located at the anterior circulation. The inter-observer agreement of CTA was "weak" for the neck, and ranged from "strong" (2D-CTA) to "very-strong" (3D-CTA) regarding the dome diameters, respectively. The maximal neck and maximal sac diameter bias of 3D-CTA was -0.94mm and -0.51mm, respectively, and the mean normalized smallest detectable differences (MNSDD) of 2D-CTA were 0.92mm and 0.41mm intended for the neck and sac, respectively. Likewise, the MNSDD regarding 3D-CTA were 0.92mm and 0.36mm for the neck and sac, respectively.

Discussion & Conclusion

Concluding, CTA is an imaging study that describes the size of a ruptured IA dome accurately, but fails to delineate the morphology of the aneurysmal neck. CTA seems to overestimate the aneurysm neck and its relationship to the surrounding brain arteries and thus, be inferior to DSA in the decision making process for the management of ruptured IAs of the anterior circulation with SAH.

2. INTERVENTIONAL

2-P1

SELECTIVE INTRAARTERIAL CHEMOTHERAPY IN TREATMENT OF RETINOBLASTOMA – SINGLE-CENTER COHORT

*M. Szaniawska*¹, E. Jurkiewicz¹, K. Nowak¹, P. Rago¹, J. Bartuszek¹, U. Zienkiewicz¹, B. Dembowska-Baginska², O. Rutynowska², W. Hautz³, K. Cieslik³, A. Olechowski³

¹ Children's Memorial Health Institute Department of Radiology, Warsaw, POLAND, ² Children's Memorial Health Institute Department of Oncology, Warsaw, POLAND, ³ Children's Memorial Health Institute Department of Ophthalmology, Warsaw, POLAND

Introduction

Retinoblastoma (RB) is an embryonic malignant neoplasm of retinal origin. It almost always emerges in early childhood (median age at diagnosis is 2 years) and is often bilateral. Standard treatment involves enucleation, multiagent systemic chemotherapy, cryotherapy and laser therapy, radiation and selective intraarterial chemotherapy (IAC). IAC is a novel method for precise delivery of a small dose of chemotherapy into the ophthalmic artery, minimizing systemic chemotherapy toxic effects. Side effects of IAC include swelling of the eyelid, bleeding into the

eye, eye muscle dysfunctions, drooping of the upper eyelid, damaging the artery, and stroke (very rare).

We have described our experience with treatment of retinoblastoma using the IAC.

Methods

The IAC has been performed using anticoagulation means - with intravenous heparin. Chemotherapeutic agents diluted in saline are delivered to retina using a pulsatile, non-laminated technique. The selected chemotherapy drugs are melphalan combined with topotecan. Carboplatin is used as well.

During procedure an arteriogram is taken to confirm patency of the ophthalmic artery.

Children under 5 months, and under 7 kg are excluded from this procedure

Result

We have retrospectively analyzed thirty-five patients undergoing 94 IAC procedures between May 2017 and March 2019. An average patient's age at IAC is 26 months (range: 8 months -7 years). Each of the patients has been given from 1 to 6 doses (range: 2.75) of chemotherapy. One patient has suffered from an MRI-confirmed stroke and one has had TIA.

2 patients had a vessels spasm during cannulation.

8 times the procedure has been interrupted because of the anatomical anomalies of carotid or meningal artery.

No patients have developed internal carotid artery or femoral artery occlusion.

Discussion & Conclusion

As the priorities in treatment children with retinoblastoma are saving life, eyes, and vision, IAC allows to deliver chemotherapy locally to the eye while minimizing systemic exposure

2-P2

AN INTRODUCTION OF THE RAPID SOFTWARE INCREASED THE NUMBER OF MECHANICAL THROMBECTOMY WITH FAVORABLE OUTCOME IN STROKE PATIENTS

*K. Seo*¹, G.S. Kim¹, P.H. Yun², S.H. Suh³

¹ Department of Neurology, National Health Insurance Service Ilsan Hospital, Goyang, SOUTH KOREA, ² Department of Radiology, National Health Insurance Service Ilsan Hospital, Goyang, SOUTH KOREA, ³ Department of Radiology, Gangnam Severance Hospital, Yonsei University College of Medicine, Seoul, SOUTH KOREA

Introduction

The revised guideline in 2018 recommends mechanical thrombectomy for selected patients even after 6 hours of symptom onset. In order to select the patients to be treated, it is necessary to measure the volume of ischemic core by the RAPID software (iSchemaView Inc, Menlo Park, CA). However, there are only three hospitals in the Republic of Korea

where the software is available. We report the results of mechanical thrombectomy in patients using the software for the first time in Korea.

Methods

Our hospital had established a critical pathway for patients with hyperacute stroke, and since we adopted the RAPID software in May 2018, we extended the time window to select the eligible patient to be treated with mechanical thrombectomy. Brain CT perfusion images performed in emergency room were analyzed by software automatically. The decision whether to perform thrombectomy was made by a single stroke specialist. We analyzed all cases who received mechanical thrombectomy after the introduction of software.

Result

Thirty patients had received mechanical thrombectomy for eleven months after introduction of the RAPID software. Compared to the same period of time, the number of thrombectomy was increased by 10 cases. Six patients were not subject to mechanical thrombectomy beyond the conventional time window, and these patients were not clear regard to the stroke onset. Five patients had a large proximal artery occlusion in the anterior circulation. Mean time from last normal to the puncture was 15hours (range: 9hours 50minutes ~ 21hours 20minutes). Mean volume of ischemic core (CBF<30%) was 18.2ml, and mismatch volume was 98.8ml. Range of mismatch ratio was 3.1~20.5. Mean initial NIHSS was 16.2. All patients achieved successful recanalization. Two patients had good outcomes (mRS 1) and one had a poor outcome (mRS 5) due to a parenchymal hemorrhage.

Discussion & Conclusion

The introduction of a new software had increased the number of patients being treated by mechanical thrombectomy, and the prognosis was also favorable. We assume that more stroke patients can get the benefit of thrombectomy in the future by the establishment of the software.

2-P3

COMBINED SURGICAL AND ENDOVASCULAR CAROTID ACCESS FOR ENDOVASCULAR THROMBECTOMY IN ACUTE ISCHEMIC STROKE

*O. Nikoubashman*¹, J. Kalder², A. Reich³, S. Dekeyzer^{1,4}, A. Riabikin¹, A. Mpotsaris¹, M. Wiesmann¹

¹ University Hospital RWTH Aachen, Departement of Neuroradiology, Aachen, GERMANY, ² University Hospital RWTH Aachen, Departement of Vascular Surgery, Aachen, GERMANY, ³ University Hospital RWTH Aachen, Departement of Neurology, Aachen, GERMANY, ⁴ University Hospital Antwerp, Department of Radiology, Antwerp, BELGIUM

Introduction

Conventional access to the occlusion site via femoral catheterization is impossible in 2-5% of acute stroke cases. Surgical carotid cutdown may be a necessary bailout strategy to allow for carotid access, if percutaneous

femoral, radial/brachial, or carotid access fails. We assessed the effectiveness and safety of surgical carotid cutdown for vascular access in interventional acute stroke treatment.

Methods

We compare imaging and clinical data of 15 consecutive patients, in whom we performed a carotid cutdown for acute stroke treatment with 10 consecutive patients, in whom treatment was discontinued because trans-femoral access to the occlusion site was not possible.

Result

Baseline characteristics of both groups were comparable ($p > .065$). Cutdown patients had significantly smaller infarctions ($p = .031$), significantly more often favorable clinical outcome (38% vs. 0% mRS 0–2, $p = .046$), and a lower mortality (31% vs. 60%, $p = .222$) at three months. Other than a small hematoma at the operation site, there were no procedure-related complications.

Discussion & Conclusion

Carotid cutdown is an effective bailout strategy for acute stroke patients, in whom conventional catheterization is not possible.

2-P4

DETECTION OF PLAQUE PENETRATION IN CAROTID ARTERY STENTING (CAS) BY DIGITAL VOLUME TOMOGRAPHY (DVT)

*T. Mayer*¹, *L. Schneider*¹

¹ Friedrich-Schiller-Universität, Jena, GERMANY

Introduction

Ultrasound (US) is the gold standard for the indication prior and monitoring after CAS. CT-A and MR-A are also used, but after stenting its value is limited due to metal artifacts. To get an objective image after CAS, we investigated the use of DVT with systemic contrast enhancement.

Methods

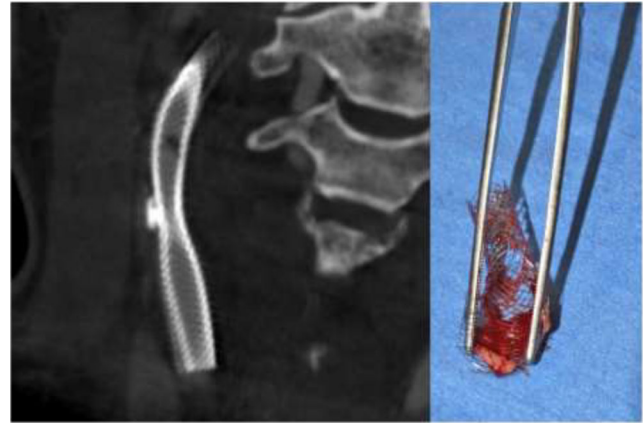
All patients were treated with Wall stents and filter protection. For the DVT 60 ml contrast were injected i.v. during a 5 second rotation of a Zeego Q angiography machine. MPR were done. US controls were performed at the time of the DVT.

Result

62 patients received a DVT 1–3 days and 6 months after CAS. Quality of the DVT depended of streak artifacts and lumen contrast, 83% of the examinations had sufficient quality. The only restenosis greater 50% as seen in US was also detected by DVT. DVT also clearly showed the intimal overgrowth in the 6 month follow-up. In the early control DVT detected plaque penetration through the stent which was not seen by US.

Discussion & Conclusion

Contrast enhanced DVT is widely used for intracranial stents. In CAS the pulsations of the carotid artery during DVT causes artifacts, limiting the image quality. Nevertheless it seems to be a means to document the stent and the artery after treatment. Surprisingly plaque penetration through the quite dense Wall stent could be observed, confirmed by subsequent surgery. This may be the reason for microembolie after CAS as seen by MRI.



2-P5

COMPUTED TOMOGRAPHY (CT) GUIDED CORE-NEEDLE BIOPSY OF ORBITAL LESIONS: A CASE SERIES

*A. Martin*¹, *B. Bata*², *N. Hersey*¹, *S. Salvi*², *D. Connolly*¹

¹ Department of Neuroradiology, Sheffield Teaching Hospitals NHS Foundation Trust, Sheffield, UNITED KINGDOM, ² Department of Ophthalmology, Sheffield Teaching Hospitals NHS Foundation Trust, Sheffield, UNITED KINGDOM

Introduction

Obtaining tissue diagnosis of orbital lesions is important in establishing an accurate diagnosis and appropriate treatment. It usually involves major surgery, the recovery from which can take six to eight weeks, which can subsequently delay chemotherapy and radiotherapy. Image-guided fine needle aspiration (FNA) provides a less invasive alternative but this only produces a small volume of cells suitable for cytological smears only. There is limited literature on the use of CT guided core needle biopsy in obtaining tissue to allow histological diagnosis.

Methods

This case series describes our experiences of performing 5 CT-guided core needle biopsy (CNB) performed on patients with retro-orbital mass lesions. We describe the technical aspects of performing this procedure and review the medical records, imaging appearances and histopathological diagnoses of these patients.

Result

Five patients underwent this procedure in our department in a 4 month period. They were all deemed to be poor grade patients with several co-

morbidities that rendered orbitotomy and general anesthesia risky. The core needle biopsy was successful in 4 patients in whom it revealed: metastatic prostate adenocarcinoma, diffuse large B cell lymphoma, metastatic neuroendocrine tumour, and small vessel vasculitis. In 1 case we were unsuccessful due to failure to advance the biopsy needle into the tumour despite good localization on CT. This mass was subsequently diagnosed as a fibrous meningioma. There were no serious complications.

Discussion & Conclusion

CT-guided core needle biopsy of orbital mass lesions appears safe and effective in obtaining tissue to allow diagnosis. It is less successful in calcified and fibrous tumours. It avoids major surgery meaning that chemotherapy and radiotherapy can be commenced earlier when compared with orbitotomy. Its use would also free up valuable theatre time and bed space. We also believe it has cost saving benefits compared with surgery.

2-P6

THROMBECTOMY WITH PRESET LITE IN ISOLATED M2 OCCLUSIONS

*J. Madjidyar*¹, J. Hensler¹, N. Larsen¹, O. Jansen¹

¹ Department of Radiology and Neuroradiology, UKSH, Kiel, GERMANY

Introduction

Mechanical thrombectomy is very effective in large vessel occlusions, though limited data are available for recanalization of peripheral occlusions. The outcomes of isolated M2 recanalizations with the pREset LITE stent retriever were reviewed in a single center study.

Methods

A retrospective review of all patients treated for isolated M2 occlusions between November 2017 and February 2019 with the pREset LITE 3/20 mm and 4/20 mm was performed. Technical aspects of the recanalization procedure, recanalization rate, and complication rate were analyzed.

Result

Thrombectomy with pREset LITE 3/20 mm and 4/20 mm was performed in 23 patients with an isolated M2 occlusion (median age 80 years). The median National Institute of Health Stroke Scale was 10, the median ASPECT-Score was 10. Successful reperfusion modified Thrombolysis in Cerebral Infarction (mTICI 2b or 3) was achieved in 16 patients (70%), with additional rescue strategy (ADAPT via 5F Aspiration Catheter (4 patients) or Trevo XP Provue Retriever 3/20 mm (1 patient)) in 21 patients (91%). First pass mTICI 3 was achieved in 9 patients (39%). Symptomatic subarachnoid hemorrhage occurred in 1 patient (4%) due to M2 perforation. Asymptomatic subarachnoid hemorrhage occurred in 3 patients (13%).

Discussion & Conclusion

The pREset LITE stent retriever is an effective thrombectomy device for isolated M2 occlusions. An advantage is that both the 3/20 mm and 4/20 mm device fit through a 0.0165" microcatheter. Nevertheless, additional techniques like ADAPT and other stent retrievers should be available to achieve a favorable recanalization in refractory occlusions.

2-P7

ANGIOPLASTY AND STENTING OF POST-IRRADIATED STENOSIS OF SUBCLAVIAN ARTERY

Z.Y. Zhou^{1,2,3}, C.C. Huang^{1,2}, W.M. Huang^{1,2,3}, J.H. Chen⁴, C.Y. Huang^{1,2,3}, C.H. Chen^{1,2,3}, C.B. Luo^{4,5}, F.C. Chang^{4,5}

¹ Department of Radiology, MacKay Memorial Hospital, TAIPEI, TAIWAN, ² Department of Medicine, MacKay Medical College, TAIPEI, TAIWAN, ³ Mackay Junior College of Medicine, Nursing, and Management, TAIPEI, TAIWAN, ⁴ Department of Radiology, Taipei Veterans General Hospital, TAIPEI, TAIWAN, ⁵ National Yang Ming University, School of Medicine, TAIPEI, TAIWAN

Introduction

The technical safety and outcome of percutaneous transluminal angioplasty and stenting (PTAS) of severe symptomatic stenosis of the subclavian artery in the patients of head, neck, and thoracic cancer accepted irradiation was not clarified. This retrospective study was designed to evaluate the technical safety and outcome of the patients of post-irradiated stenosis of subclavian artery (PSSA) accepted PTAS.

Methods

We retrospectively evaluated the 169 patients of severe symptomatic stenosis of subclavian artery accepted PTAS between 1999 and 2017 in our institute. Of them, 8 cases of PSSA were noted. We evaluate their clinical and imaging findings before and after PTAS. The mean age of the 8 patients was 67.5±11.9 (50-85) years old. The mean interval between radiotherapy and PTAS was 118.1±75.9 (44-251) months. Their cancers included 2 tonsillar cancers, 2 nasopharyngeal cancers, 1 hypopharyngeal cancer, 1 laryngeal cancer, 1 breast cancer and 1 malignant thymoma.

Result

All patients were successfully treated with PTAS without any neurological complications. Their symptoms included dizziness (7/8 [87.5%]) and upper limb weakness ipsilateral to the diseased SA (2/8 [25%]). These symptoms relieved after PTAS. The mean length of the stenotic lesions were 18.6±11.0 (6-35) mm. The severity of the stenotic lesions were 82.5±12.5 (70-100%). Post-procedural MRI of brain was done in the next day which showed tiny asymptomatic acute embolic infarcts on DWI in 4 patients (50%). In a 29.9±34.2 (6-94) months follow-up, no significant restenosis was noted.

Discussion & Conclusion

PTAS of the patients of PSSA was associated high technical safety and favorable long-term outcome, including the long-term stent patency.

2-P8**CAROTID NEAR-OCCLUSION: IS IT REALLY A LOW RISK CONDITION? IPSILATERAL LARGE VESSEL STROKE IN A CAROTID NEAR-OCCLUSION AFTER CONTRALATERAL CAROTID ARTERY STENTING. CASE REPORT AND REVIEW OF THE LITERATURE**

*N. Cavinin*¹, *M. Cazzagon*¹, *A. Critelli*¹

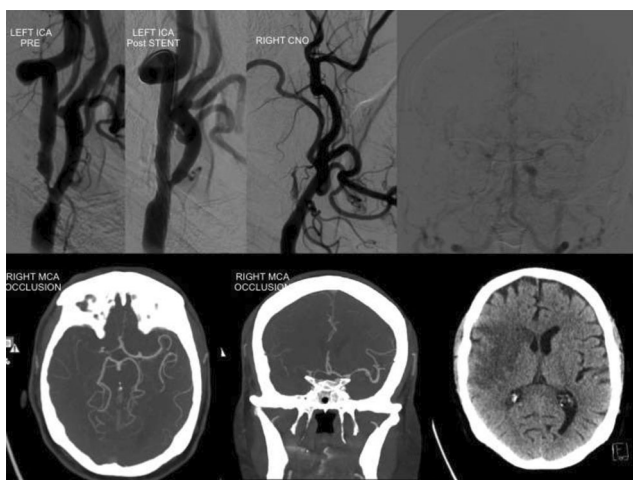
¹ Ospedale dell'Angelo, Department of Neuroradiology, Mestre-Venezia, ITALY, ² Ospedale dell'Angelo, Department of Neuroradiology, Mestre-Venezia, ITALY, ³ Ospedale dell'Angelo, Department of Neurology, Mestre-Venezia, ITALY

Introduction

We define carotid near-occlusion (CNO) a critical stenosis of the bulb with minimal residual flow through the internal carotid artery and distal luminal narrowing with or without full collapse. The risk of ipsilateral stroke seems to be low compared to severe carotid stenosis cases but the natural history of this disease is not well understood and no clear recommendations on the best treatment option are available so far

Methods

We present the case of a 67 yo male who presented at our institution for a single dysarthria episode. US Color Doppler and CT angio revealed right internal CNO and severe stenosis of the left internal carotid artery. We postulated the symptom to be related to a left hemisphere TIA and considered functionally occluded the right carotid artery. The patient underwent a left internal carotid artery stenting and angioplasty. The procedure was uneventful. The morning after he woke up with left limbs weakness and dysarthria. A CT scan and CT angio revealed right middle cerebral artery occlusion and initial signs of right hemisphere ischemia. We attempted a new endovascular procedure in order to recanalise the right internal carotid artery and perform right middle cerebral artery thrombectomy but we failed and the patient developed a right hemisphere stroke

**Result**

This case shows that, even if rare, ipsilateral ischemic complications in a CNO are not negligible. The patient's dysarthria was referred to the left carotid artery stenosis whereas the symptom is aspecific and could have been related to the right CNO. Patients with CNO and contralateral stenosis need a thorough clinical examination and a full imaging workout to better understand the nature of the disease. Furthermore we hypothesize that the left internal carotid stenting could have decompensate the right side further lowering the antegrade flow through the CNO and eventually stimulating blood stagnation and clot formation.

We review the current recommendations and the published literature on CNO

Discussion & Conclusion

Although the CNO best treatment strategy remains unknown we must revise current recommendations and further stratify the risk profile of CNO patients

2 – P9**LONG TERM OUTCOME OF WEB TREATED INTRACRANIAL ANEURYSMS - SINGLE CENTRE EXPERIENCE**

*H. Hameed*¹, *A. Siddiqui*¹, *S. Jenkins*¹

¹ Institute of Neurosciences and Spinal Unit, Glasgow, UNITED KINGDOM

Introduction

Purpose of the study was to evaluate the long-term efficiency, stability of occlusion and complications related to WEB treatment of intracranial aneurysms (IAs) at a tertiary referral centre.

Methods

Patients with ruptured and unruptured intracranial aneurysms initially treated with WEB devices were included. Data was collected retrospectively from medical records, imaging and interventional reports about patient demographics and aneurysm characteristics. Angiographic assessments at baseline, short term (0-6 months), mid-term (12-18 months), long (>24 months) and extended long term (>36 months) time points were analyzed by two independent interventional neuroradiologists under blinded conditions. Outcomes assessed included adequate angiographic occlusion as per web occlusion scale, stability of occlusion and safety. Latter was evaluated by the mortality rate, associated complications and rate of patients with interval increase in modified Rankin Scale score

Result

44 patients were included. 10 of the 44 (23%) IAs were ruptured. Predominant aneurysm locations were MCA (44%), basilar artery (20%) bifurcation and ACOM complex (16%).

31 patients (70%) had very long-term imaging follow up with median follow-up in this cohort of 48 months, range 36-66 months.

No device related procedural complications or intra-operative ruptures were encountered. 5 patients experienced complications consisting of groin pseudoaneurysm (1) and thromboembolic events (4/44, 9%). Of latter, in two cases despite favorable outcome after treatment there was morbidity at 6 months (mRS score of more than 2).

Despite 75% of the IAs being adequately occluded at short-term follow up, retreatment was eventually planned in 9/44 (20%). Aneurysm occlusion was stable between midterm and long-term follow-up in 70% of patients with increasing neck remnants and recurrences mainly observed past this time point. Rate of neck remnants was not negligible with almost a third of treated aneurysms having residual neck at at very long term angiographic assessment, presumably secondary to device compaction in several cases.

TABLE 2. Anatomical Results at different follow-up time points

Status, WOS grade	Short term FU (<6 mo), n/N (%)	Mid term FU (12–18 mo), ^a n/N (%)	Long term FU (≥24 mo), ^b n/N (%)	Extended Long term FU (≥36 mo), ^c n/N (%)
Complete, A/B	21/44(47%)	16/40 (40%)	13/34 (38%)	11/28 (39%)
Neck remnant, C	13/44 (30%)	12/40 (30%)	10/34 (30%)	9/28 (32%)
Sac remnant, D	10/44 (23%)	12/40 (30%)	11/34 (32%)	8/28 (29%)
Adequate occlusion	34/44 (77%)	28/40 (70%)	23/34 (68%)	20/28 (71%)

^a Midterm results not evaluated in 3 patients lost to follow up and 1 patient retreated

^b Long term results not evaluated in 8 patients lost to follow-up and 2 patients retreated

^c Extended long term results not evaluated in 13 patients lost to follow-up and 3 patients retreated

Discussion & Conclusion

This series is currently the largest retrospective analysis of extended long term (>36 months) outcome of patients with WEB treated aneurysms. With almost a third of cases having residual neck and 20% requiring re-treatment, long-term anatomic data on larger prospective cohorts is needed to more accurately evaluate the efficacy of the WEB device.

2-P10

THE UTILITY OF PREPROCEDURAL PLATELET FUNCTION TESTING(PFT) TO COUNTER CLOPIDOGREL RESISTANCE IN RELATION TO INCIDENCE OF THROMBOEMBOLIC INFARCTION DURING STENT-ASSISTED ANEURYSM COIL EMBOLIZATION

J. Walsh¹, D. Bhattacharya², P. Burns³, P. Flynn⁴, I. Rennie⁵, G. Smyth¹

¹ Queens University, Belfast, UNITED KINGDOM, ² Royal Victoria Hospital, Belfast, UNITED KINGDOM, ³ Royal Victoria Hospital, Belfast, UNITED KINGDOM, ⁴ Royal Victoria Hospital, Belfast, UNITED KINGDOM, ⁵ ROYAL Victoria Hospital, Belfast, UNITED KINGDOM, ⁶ Royal Victoria Hospital, Belfast, UNITED KINGDOM

Introduction

The purpose of this study was to assess incidence of thromboembolism in patients treated by stent-assisted coil embolization for aneurysms, with no preprocedural PFT and standardised anticoagulation (aspirin/clopidogrel) vs those with PFT and modified anticoagulation regimen (aspirin/prasugrel).

Methods

68 patients who had coiling of intracerebral aneurysms were included, equally divided into pre PFT(PFA100®) group 1(n=34) and post PFT group 2(n=34)

MR imaging was reviewed by 2 Neuroradiologists, with calculation of infarction volume/nos. Data was collected regarding procedural complications and need for intraprocedural anticoagulation.

Result

In group 1, MR imaging available in 24 patients showed acute infarcts in 12(50%) cases with an average infarct volume of 0.61 cc(median 0.095 cc), and 19(79%) less than/equal to 5 infarcts; 4 patients required iv abciximab, 2 also receiving iv aspirin, with 2 patients having clinical strokes. Other complications included acute intraprocedural rupture of aneurysm(1) and retroperitoneal haematoma(1).

In group 2, MR imaging available in 30 patients showed acute infarcts in 18(60%) cases with an mean infarct volume of 0.87 cc(median 0.19), and 23(68%) patients having less than/equal to 5 infarcts; 1 patient required IV abciximab, with 1 patient having a clinical stroke and 2 cases of intraprocedural SAH.

Discussion & Conclusion

Dual antiplatelet therapy with aspirin and clopidogrel is a standard requirement while coiling aneurysms requiring adjunctive stent placement. Up to 30% of the population demonstrate resistance to clopidogrel - in identifying these patients prior to their procedure, steps can be taken to potentially decrease the risk of stroke, typically by changing clopidogrel for an alternative agent, such as prasugrel.

We wished to assess if this change resulted in improved rates of stroke, infarct volume or use of intra-procedural rescue strategies such as aspirin (intravenously) or abciximab (a platelet IIb/IIIa inhibitor).

In our experience, there was reduced incidence of clinical strokes, reduction in number of infarcts on MR and need for intraprocedural rescue with abciximab, in patients with preprocedural PFT as opposed to those without.

2-P11

MECHANICAL THROMBECTOMY (MT) PERFORMED WITH EMBOTRAP: THE VERONA HOSPITAL EXPERIENCE

R. Augelli¹, A. Agnello¹, N. Mandrizzato¹, M. Conte¹, M. Plebani¹, G.K. Ricciardi¹, P.G. Zampieri¹, A. Bucci¹, E. Ciceri¹

¹ Neuroradiology Department, University Hospital of Verona, Verona, ITALY

Introduction

To evaluate feasibility and safety of EmboTrap revascularization device in acute ischemic stroke treatment.

Methods

We examined all patients data with acute stroke treated with the EmboTrap device from April 2018 and April 2019 in our center undergone to MT. We analyzed clot localization, length, number of passages in a single vessel and number of passages in different vessels in the same patient, evaluating rate of complication device-related, recanalization rate (using Thrombolysis In Cerebral Infarction – TICI score) and clinical outcomes at 3 months (modified Rankin Scale (mRS) 0–2).

Result

We used EmboTrap in 15 patients (4 with posterior stroke and 8 with Middle Cerebral Artery (MCA) occlusion and 3 with Internal Carotid Artery and MCA tandem lesions). Clot length was estimated between 2–5 mm. As first-line, we treated 8 patients (in 1 used in two different branches of MCA, with a total of 9 vessels treated); in 4 cases EmboTrap-retriever was the lone procedure performed in one pass, in 2 cases we performed 2 passes, and in other 2 cases EmboTrap was followed by thrombo-aspiration (TA). In only 2 cases the device was unsuccessful (both of them on fronto-opercular M2-M3 branches). As second-line approach after TA, in all cases we obtained complete recanalization both in Large Vessels Occlusion (LVO) partially reopened with aspiration, than in distal branches occlusion. We never observed distal fragmentation after EmboTrap use; we observed one case of subarachnoid hemorrhage device-related, asymptomatic. In 4 cases at first-line treatment we obtained a TICI 3; in all the other cases we observed a significant improvement of TICI score. With regard to clinical outcome, 5 patient are still waiting for the 3 month FU, (treated from January to April 2019), while among the other 10 patients, mRS was < 3 in 6 patients, between 3–5 in 3 patient. One patient died after 10 days for causes not related with ischemic stroke nor MT/EmboTrap (pulmonary embolism).

Discussion & Conclusion

Based on our experience in LVO cases as in selected cases of distal occlusion (dominant straight artery), EmboTrap seems to be effective and safe. More data need in order to reach a statistical analysis value.

2-P12

NEUROFORM ATLAS STENT IN THE TREATMENT OF WIDE-NECKED INTRACRANIAL ANEURYSMS. SINGLE CENTER EXPERIENCE

*A. Alexandre*¹, F. Giubolini¹, G. Garignano¹, I. Valente¹, E. Lozupone¹, F. D'Argento¹, C. Colosimo¹, A. Pedicelli¹

¹ Fondazione Policlinico Universitario A. Gemelli IRCCS, Roma, Italia. UOC Radiologia e Neuroradiologia., Roma, ITALY

Introduction

Wide-necked intracranial aneurysms therapy remains a challenge for neurointerventionalists, mainly for the high recurrence rate. In our series

we report clinical and angiographic results of Neuroform Atlas stent-assisted coiling.

Methods

A retrospective single center evaluation of patient treated from November 2015 to April 2018 for wide-necked intracranial aneurysms using the low profile Neuroform Atlas stent. We treated 31 patients with 32 aneurysms.

The Atlas stent-assisted coiling procedures were performed under general anesthesia with stent-through or jailing techniques.

In 8 cases an Y stent technique was used, in 1 case a telescopic technique, and in 22 a single stenting technique. Patients were followed with a three and six months MR/angio-MR, and with a 12 months DSA, performed to assess the recurrence rate through the modified Raymond-Roy occlusion scale (RROC). Moreover, patients were evaluated clinically to analyse the degree of disability according to the mRS.

Result

In all the procedures it was feasible to navigate the Neuroform Atlas to the goal vessel and deploy the stent across the aneurysmal neck.

The immediate occlusion rate was RROC 1 in 27 patients (87,5%), RROC 2 in 3 patients (9,5%) and RROC 3 in 1 patient (3%)

The 12 months follow-up showed RROC of 1 in 28 patients (90%), RROC 2 in 2 patients (6%). No aneurysm has been retreated.

Intra-procedural complications were 3 out of 31 treatments: in 2 cases a small intrastent aggregate was immediately solved with a glycoprotein IIb/IIIa receptor antagonist, while in 1 case there was a small sac perforation with the second coil. These complications had no clinical consequences.

Late complications were 4: 1 patient had a retroperitoneal hematoma for femoral access, requiring surgery, 2 patients had a minor ischemic stroke in the 15 days following the treatment due to poor adherence to antiaggregant therapy, and 1 patient died for a subarachnoid hemorrhage 2 months after the treatment.

Discussion & Conclusion

In our single center experience the Neuroform Atlas stent assisted-coiling has shown to be a safe and effective technique for the treatment of wide-necked intracranial aneurysms with encouraging clinical and angiographic results.

3. HEAD & NECK

3-P1

COMPARISON OF CONTRAST ENHANCED NECK MRI BETWEEN THE SPINE-ECHO AND BLADE TECHNIQUE

*J.H. Yoo*¹

¹ Mokdong Hospital, Seoul, SOUTH KOREA

Introduction

The purpose of study is to assess the artifacts, image qualities, and delineation of lesions in contrast enhanced neck MRI between spine-echo and BLADE technique.

Methods

Consecutive 53 contrast-enhanced neck MRIs were included with SE and BLADE technique. Two radiologists compared both sequences for qualitative assessment of motion, pulsation, and streak artifacts; image qualities of vessel, spinal cord, neck muscle; and delineation of lesions. Artifacts were graded on a 4 point scale (0, no artifact; 1, mild artifact; 2, moderate artifact; or 3, severe artifact). Image quality of vessels was assessed based on luminal area of signal void (0, 100% signal void; 1, >50% signal void; 2, <50% signal void; 3, 0% signal void). The Wilcoxon signed rank test was used to compare MRI images with and without BLADE technique. We selected preferred MR sequences based on image quality of spinal cord, neck muscle, and delineation of lesions (1, SE superior; 2, sequences equal; 3, BLADE superior). The Chi-square test and Fisher's exact test were used to compare artifacts, image quality, and lesion delineation between SE and BLADE sequences with a p-value of 0.05.

Result

Forty-seven lesions were detected in 53 patients (mean age, 52.3 years, age range, 18–81 years). Mean grade of motion and pulsation artifacts were 0.06 and 0.00 in BLADE, 1.23 and 2.50 in SE, respectively. In contrast, mean grade of streak artifacts were 2.43 in BLADE and 0 in SE. In the evaluation of vessel image quality, vessels showed as signal void in nearly 100% of arterial luminal area and more than 50% of venous luminal area on BLADE with significant difference from SE (p-value, 0.009 in artery and 0.045 in vein). In the MR sequence preference, BLADE was preferred to SE, based on the image quality of neck muscle and delineation of lesions (2.77 and 2.79, respectively), while there is no preference, based on the image quality of spinal cord. Overall, BLADE was a preferred sequence in 94% and 81% by reader 1 and 2, respectively.

Discussion & Conclusion

Contrast-enhanced neck MRI with BLADE technique is superior to SE technique for reduction of motion or pulsation artifacts and delineation of lesions.

3-P2

A CLASSIFICATION OF THE ZYGOMATIC ROOT FOR PRESURGICAL PLANNING FOR CHOLESTEATOMA REMOVAL

*J. Thiessen*¹, G. B.¹, S. G.¹, B. H.¹

¹ Oregon Health and Science University - Department of Diagnostic Radiology, Portland, USA

Introduction

Preoperative temporal bone CT is useful for assessing extent of cholesteatoma and identifying related complications, but can improve

selection of surgical approach for surgeons. A zygomatic root approach may be preferred in some cases due to lower complication rates, but the success of surgery depends upon native anatomy. We propose an anatomically-based classification system that could improve pre-operative planning.

Methods

100 consecutive patients from 1/9/2018 to 31/12/2018 with a dedicated CT temporal bone study were retrospectively reviewed to determine zygomatic root height and pneumatization. Patients with prior tympanic or mastoid surgeries altering the normal relevant landmarks were excluded. Temporal bone CT were acquired at 0.5 mm thickness, and images were reformatted into a coronal plane paralleling the long axis of the external auditory canal on each side. Three measurements of zygomatic root height were obtained and rounded to the nearest tenth millimeter: one medially at the level of the scutum, one laterally at the junction of the zygomatic root and squamous temporal bone, and one at the mid point between these two. Zygomatic root heights were graded: less than 5 mm scored as grade 1, 5 to 10 mm scored as grade 2, greater than 10 mm scored as grade 3. The lowest score was used as the overall grade. The degree of pneumatization of the zygomatic root was visually scored: none present scored as A, less than 50% pneumatization scored as B, and greater than 50% pneumatization scored as C.



Result

Following exclusions, a total of 152 ears in 45 female and 33 male patients ranging in age from 14 months to 95 years old had temporal bone CT exams sufficient for grading. Preliminary results show zygomatic root heights between 0.2 mm and 14.3 mm. Zygomatic height grades are 42 grade 1, 103 grade 2, and 11 grade 3. Pneumatization scores are 12 score A, 113 score B, and 27 score C.

Discussion & Conclusion

Zygomatic root height and pneumatization varies among patients. This classification system could improve selection of the appropriate use of

endoscopic, zygomatic root, or middle cranial fossa surgical approach based on temporal bone CT anatomical grading.

3-P3

PEDIATRIC AND ADULT SKULL BASE LESIONS: A MULTIMODALITY IMAGING APPROACH

I. Lloret ¹, A. Server Alonso ²

¹ Department of Radiology and Nuclear Medicine, Oncology Section Radiumhospitalet, Oslo University Hospital, Oslo, NORWAY,

² Department of Radiology and Nuclear Medicine, Neuroradiology Section Rikshospitalet, Oslo University Hospital, Oslo, NORWAY

Introduction

There are a wide variety of lesions that can involve the skull base, either arise from or secondarily invade this region. These lesions are often challenging to diagnose and it is sometimes not possible to distinguish them. The first purpose of this work is to provide an update on the role of high-resolution skull base imaging in the evaluation of tumors; the second is to establish a diagnostic algorithm based on tumors arising from the bone and cartilage, and adjacent compartments, and third to emphasize the critical role of the radiologist to define the extent of the tumor, its relationship with vital neurovascular structures both for preoperative purposes and in planning focused high-energy radiation approaches.

Methods

We reviewed CT and MRI findings in patients with skull base lesions referred to the National Resource Center for Sarcomas at the Norwegian Radium Hospital during the last 20 years, from 1998 to 2018. These cases include benign and malignant lesions arising from the bone and cartilage, neoplasms arising from adjacent compartments. The diagnosis was based on CT and MRI findings, clinical records, and pathologic features including the molecular profiling.

Result

We propose an imaging-guided algorithm to aid in the preoperative diagnosis of these skull base lesions. The lesions will be classified based on localization: anterior, middle and posterior skull base and anywhere in the skull base. Further differentiation will be based on: 1) the radiological characterization; 2) definitions of the extent of the disease; 3) features of pediatric skull base tumors versus adult tumors.

Discussion & Conclusion

There are a wide range of neoplasms and non-neoplastic lesions that involve the skull base and can overlap. By utilizing a methodical approach that includes tumor epicenter, specific imaging patterns of these lesions and knowledge of clinical issues, we aim to provide the radiologist a framework for the strategic role of radiology in the diagnosis, in concert with clinicians to optimize clinical management and therapy.

3-P4

THE SMALL X-RAY TUBE FOCAL SPOT CAN IMPROVE THE RESOLUTION OF HEAD AND NECK CTA

J. Roskopf ¹, M. Braun ², M. Beer ¹, B. Schmitz ^{1,2}

¹ Department of Radiology, University of Ulm, Ulm, GERMANY, ² Department of Neuroradiology, University of Ulm, Günzburg, GERMANY

Introduction

The spatial resolution of a CT system depends on the focal spot size of the X-ray tube. In the present study we investigated the effect of reducing the tube focal spot size on the vessel wall clarity of head and neck vessels in CTA. We hypothesized that Hounsfield density increase at vessel borders would be sharper by reducing focal spot size of the tube focus.

Methods

CTA data were acquired at a 40-row multi-detector CT with large and small focal spot size (1.0 x 1.0 mm vs. 1.0 x 0.5 mm), respectively. In 544 sections of head and neck vessels (including A1, M1, P1, V1, V4, tip of basilar artery, and proximal ACI) the density increase at vessel borders was quantified by using a semi-automatic analysis process performed on the software package ImageJ.

Result

Comparing large with small tube focal spot size, density increase at vessel borders was significantly sharper using the small tube focus, on average an increase from 75° to 82° angle degrees ($p < 0.05$). As expected, group comparisons showed significant effects ($p < 0.05$) for all investigated segment arteries.

Discussion & Conclusion

In conclusion, spatial resolution of CTA of head and neck vessels can be improved by using the small x-ray tube focal spot.

3-P5

EVALUATION OF SUBSPECIALTY-SPECIFIC PROTOCOL EDUCATION TO ENHANCE APPROPRIATE ORDERING

M. Maher ¹, P. Utukuri ¹

¹ Columbia University Medical Center Department of Radiology, New York, USA

Introduction

The rising cost of healthcare and prevalence of over-imaging in the United States of America have demanded initiatives for responsible imaging on a local and national level. In response, the American Academy of Radiology Appropriateness Criteria (ACRAC) were issued to guide protocolling. There is no documentation of subspecialty-resident education benefit or feedback in the literature to date. The purpose of this study was to assess the impact of subspecialty-specific protocol education for ophthalmology residents.

Methods

The study was submitted to the Institutional Review Board who deemed no approval was necessary. Three lectures introduced the concept of protocoling, how to use the ACRAC, indications for different modalities and the basics of contrast use. The residents were invited to attend the lectures, complete a pretest and posttest survey and provide feedback. The ACRAC was taught by case-based learning with a clinical history, order discussion and explanation for each case.

Result

The pretest was completed by 91.6% ophthalmology residents. Results suggested that protocols appropriateness lectures would benefit both residents and their patients. For example, 72.7% would give pregnant patients MRI contrast. The posttest was completed by 17% after attending all lectures. No resident would give a pregnant patient MRI contrast on the posttest.

Feedback was given by 53.8% of residents; 100% reported the ACRAC would change their ordering pattern. Before the lectures, no one felt very confident, 75% felt somewhat confident and 25% felt not so confident. After, 75% felt very confident and 25% felt somewhat confident.

Discussion & Conclusion

Subspecialty residents showed improved understanding of protocoling after education. Though the study is limited by sample size, great enthusiasm was demonstrated with a request for recurring lectures of this kind on an annual. Furthermore, an additional lecture was created which American Academy of Ophthalmology requested to publish as Continuing Medical Education. In summary, increased sub-specialty protocol education by radiology improves diagnostic efficiency and is met with great interest by referring clinicians.

3-P6

CLINICAL APPLICATIONS OF MR NEUROGRAPHY: A CASE BASED APPROACH

*M. Kumar*¹, *R. Samant*¹, *T. Pandey*¹, *K. Jambhekar*¹, *R. Ram*¹, *G. Bajaj*¹, *A. Gunasekaran*², *H. Newhart*², *N. Kazemi*², *R. Ramakrishnaiah*¹, *R. Vanhemert*¹

¹ University of Arkansas for Medical Sciences- Department of Radiology, Little Rock, USA, ² University of Arkansas for Medical Sciences - Department of Neurosurgery, Little Rock, USA

Introduction

MR Neurography (MRN) is a relatively newer MRI technique in the study of neural structures. Based on our experience, and review of literature, it is proving to be a very helpful technique in the direct visualization of nerves, with good sensitivity and potential to provide much more additional information compared to conventional imaging. The purpose of our study is to discuss the advantages and utility of MRN in various pathological conditions, using case studies from our clinical practice.

Methods

MRN studies performed at a single tertiary care institute from November 2015 to March 2019 were analyzed. All studies were performed on a single 1.5 Tesla magnet. MRN was performed by acquiring high resolution STIR weighted sequences in the coronal plane, with reconstructions performed in the coronal and oblique coronal planes. DWIBS images were acquired in the axial plane with reconstructions performed in the coronal and oblique coronal planes. Images were inverted for viewing. Conventional imaging which included T1 and T2 axial and sagittal images were obtained either at the time of MRN or previously as dedicated exams.

Result

Utility of MRN was studied in a spectrum of clinical and pathological conditions. These included -

1. Trauma
2. Neoplasms including Neurofibromatosis and Schwannomatosis.
3. Degenerative Spine Diseases.
4. Inflammatory Diseases.
5. Extrinsic Compressive Etiologies.
6. Post Surgical and Post Radiation Complications.
7. Miscellaneous

Discussion & Conclusion: Discussion:

MRN has many practical advantages over conventional imaging in clinical practice. Some of these include -

1. Direct visualization of nerves.
2. Determining the level of pain generation with multilevel abnormalities, typically seen in multilevel degenerative spine disease.
3. potential to grade injuries in trauma cases.
4. determine the relation of a nerve root with a neoplasm, and by extension differentiate between neurofibroma and schwannoma in some cases.
5. increased sensitivity to nerve pathologies.
6. better appreciation of images by non radiology physicians which helps in management like surgical planning.

Conclusion:

1. MRN adds value and helps in better management of patients with varying clinical conditions, and in some cases changes management drastically.
2. The addition of time in performing MRN is more than offset by the additional information obtained.

3-P7

BRACHIAL PLEXOPATHY: TRAUMATIC AND NONTRAUMATIC CAUSES

*M. Karlovic-Vidakovic*¹, *D. Batinic*², *I. Soldo*¹, *N. Pejanovic-Skobic*²

¹ University Hospital Mostar, Mostar, BOSNIA AND HERZEGOVINA,

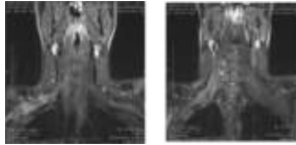
² University Hospital Mostar, Mostar, BOSNIA AND HERZEGOVINA,

³ University Hospital Mostar, Mostar, BOSNIA AND HERZEGOVINA,

⁴ University Hospital Mostar, Mostar, BOSNIA AND HERZEGOVINA

Introduction

Brachial plexopathy is a neurological condition that cause pain and/or functional impairment of the ipsilateral upper extremities. Brachial plexus lesion can be classified according to their relation to the clavicle, as supraclavicular, retroclavicular and infraclavicular lesions. Supraclavicular lesions are the most common. The leading cause of brachial plexopathy is trauma, found in more than 50% of cases, in the first row after motor vehicle crashes, followed by sports and rucksack injury. Non-traumatic causes are tumors and other space occupying lesions, radiation plexopathy, brachial plexitis.



Methods

We present fifteen patients with brachial plexopathy. Pathology of brachial plexus requires clinical assessment, electrophysiologic tests, and diagnostic imaging techniques. Magnetic resonance imaging (MRI) is the imaging modality of choice for the evaluation of the brachial plexus due to its superior soft tissue resolution and multiplanar capabilities. We performed MRI with 3T system, coronal, axial and sagittal plane, T1 and T2-weighted sequence, T2-weighted with fat suppression, T1-weighted contrast enhanced with and without fat suppression.

Result

Most of our patients suffered traumatic injuries with nerve root avulsions with or without pseudomeningoceles. Two were with Erb-Duchenne palsy as a result of obstetric brachial plexus injury.

One patient has a radiation injury after radiotherapy for breast cancer, one has brachial plexitis (Parsonage-Turner syndrome) and one has extrinsic tumor with compression of brachial plexus.

Discussion & Conclusion

MR imaging plays an essential role in diagnosis of brachial plexopathy, especially in differentiating preganglionic injuries from postganglionic lesions, which is crucial for the management of brachial plexus injury, predominantly in the setting of trauma. Clinically, lesions of the brachial plexus represents a diagnostic challenge, however imaging assessment of the brachial plexus is especially challenging due to the complexity of its anatomy, its distribution in space and due to technical factors such as long scanning time.

3-P8

THE CHALICE SIGN: CHARACTERISTIC MORPHOLOGY OF THE CERVICAL CAROTID BIFURCATION IN PATIENTS WITH LOEYS-DIETZ SYNDROME

J. Benson¹, G. Lanzino¹, W. Brinjikji¹

¹ Mayo Clinic, Rochester, USA

Introduction

Loeys-Dietz syndrome (LDS) is a connective tissue disorder characterized by arterial aneurysms and dissections. This study sought to assess and describe the arterial changes of the cervical arterial vasculature of such patients, with an emphasis on the carotid bifurcation.



Methods

A retrospective review was completed of patients with a known diagnosis of LDS. Maximum diameters of the ECA and ICA origins, CCA terminus, maximum transverse and cranio-caudal dimensions of the carotid bifurcation, and bifurcation angle were obtained. The presence of a “Chalice sign” (see discussion, below) was defined as a carotid bifurcation angle of equal to or greater than 80°. A semi-quantified analysis of vertebral artery tortuosity was completed by comparing intraluminal vascular length to a straight-lined vertebral artery course. All measurements were compared to a cohort of age-matched controls.

Result

The presence of a Chalice sign had 61.9% sensitivity and 100.0% specificity for LDS if present bilaterally; the sensitivity and specificity of a unilateral Chalice sign were 66.7% and 82.3%, respectively. LDS had significantly greater diameters of the ICA and ECA origins and larger carotid bifurcation dimensions of both the right and left carotid arteries compared to controls. LDS patients also had significantly greater tortuosity of the left vertebral artery ($p=0.0047$); no difference was seen between the tortuosity of vertebral arteries on the right side ($p=0.1334$).

Discussion & Conclusion

LDS patients have characteristic findings within their cervical arterial vasculature, most notably including marked widening of the

carotid bifurcation angle in what we propose to be referred to as the “Chalice sign.”

3-P9

THE ROLE OF FIESTA SEQUENCE IN INVESTIGATION OF VASCULAR COMPRESSION OF COCHLEAR NERVE AND DISTORTIONS

A.O. Balik ¹, S. Nacar Dogan ²

¹ Haydarpasa Numune Training and Research Hospital - Department of Radiology, Istanbul, TURKEY, ² Gaziosmanpasa Training and Research Hospital - Department of Radiology, Istanbul, TURKEY

Introduction

The purpose of the present study was to examine whether radiologic evidence of neurovascular compression of the vestibulocochlear nerve was pathognomonic in tinnitus and hearing loss by using 3D fast imaging employing steady-state acquisition (FIESTA) magnetic resonance imaging (MRI).

Results of evaluating the occurrence of symptoms with the presence of vascular loops and the Chavda classification.

		Chavda classification				
		No vascular loop	Chavda 1	Chavda 2	Chavda 3	
		n (%)	n (%)	n (%)	n (%)	
Tinnitus	Absent	13 (37,1)	19 (54,3)	2 (5,7)	1 (2,9)	$\chi^2: 2,588$
	Present	23 (46,0)	22 (44,0)	5 (10,0)	0 (0)	$p: 0,476$
Hearing Loss	Absent	26 (48,1)	24 (44,4)	4 (7,4)	0 (0)	$\chi^2: 3,475$
	Present	10 (32,3)	17 (54,8)	3 (9,7)	1 (3,2)	$p: 0,298$

Fisher-Freeman-Halton Exact Test

Methods

The study was conducted on eighty-five patients (170 temporal bones) measurements, including the right and left sides. Noninvasive evaluation of the anatomic relation between the classified vascular variations (Chavda classification) of the anterior inferior cerebellar artery (AICA) and the presence of AICA, superior cerebellar artery (SCA), vertebral artery (VA) compression or distortion of the vestibulocochlear nerve in the orifice of internal acoustic canal (IAC) was performed by using 1.5-Tesla MRI. The Pearson chi-squared test and Fisher-Freeman-Halton Exact Test was used for statistical analysis.

Result

Tinnitus and hearing loss were observed in 50 (58.8 %) and 31 (36,4 %) cases (n=85), respectively. Of the 85 patients evaluated, 36 (42,4%) presented no vascular loop, 41(48,2%) presented a grade 1 vascular loop, 7 (8,2%) presented grade 2 and 1(1,2%) presented grade 3 vascular loop according the Chavda classification. Also VA compression 6 (7,1%) and SCA compression 3(3,5%) were visualized in the patient group. IAC distortion was observed in 16(32%) patients of complaint with tinnitus.

Vascular loop also demonstrated a high incidence in cases without tinnitus (25,8 %) and healthy hearing (32,9 %) respectively.

No statistically significant differences were found between the presence and absence of the AICA loop types, VA or SCA and IAC distortion for the tinnitus or hearing loss of patients ($P>0.05$).

Discussion & Conclusion

Neurovascular contact is not a rare finding and it does not appear to cause tinnitus. Nonetheless using FIESTA, the vestibulocochlear nerve and adjacent vascular variations are well identified especially by determining the relationship of the AICA variations and contribute to case selection for microvascular operations.

3-P10

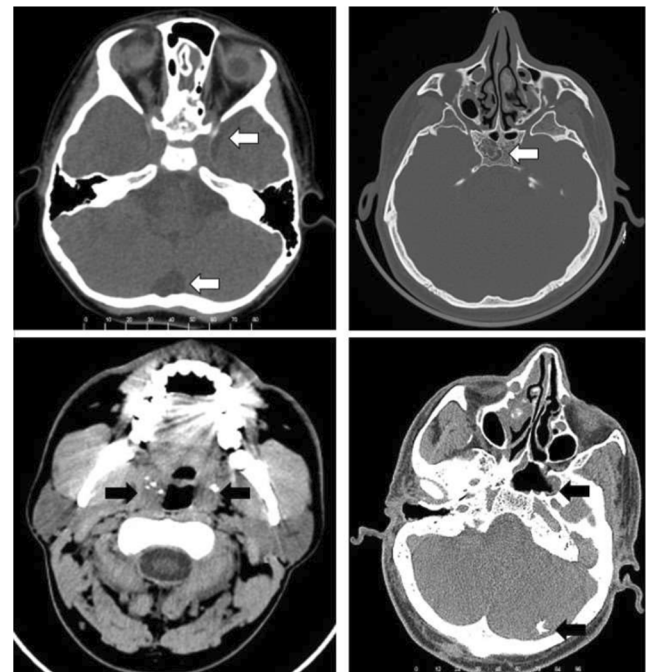
HOW FREQUENT ARE INCIDENTAL FINDINGS ON TEMPORAL BONE CT?

Z. Tekin ¹, M. Eser ¹, M. Kalcioğlu ²

¹ Medeniyet University Göztepe Training and Research Hospital- Department of Radiology, Istanbul, TURKEY, ² Medeniyet University Göztepe Training and Research Hospital- Department of Otorhinolaryngology, Istanbul, TURKEY, ³ TURKEY

Introduction

The aim of this study was to describe the prevalence of incidental findings in temporal bone CT images.



Methods

The temporal bone CT scans of 130 patients (69 female and 61 male) were re-evaluated retrospectively. All of the cases had undergone

temporal bone CT because of possible temporal disease, after a clinical indication. The ages were between 1 and 80 years old with the mean age of 38.20.

The CT was performed by using a 64-detector CT scanner including temporal CT parameters standardized as 120 kVp and 300 mAs with 0.625 mm axial, and coronal image reconstructions. Regardless of temporal findings, re-evaluation of the CT scans in bone and brain windows was retrospectively done by two radiologists.

Result

A total of 780 incidental extratemporal findings were noted in 129 of 130 patients (99.2%). In 128 patients (98.5 %), more than one incidental findings were noted. Incidental extratemporal findings were classified into 9 groups; intracranial intraaxial, vascular, intracranial extraaxial, bone, lymph node, sinus, nasal cavity, nasopharynx and tonsillar pathologies.

Any nasal cavity pathology was the most frequent incidental finding with a rate of 68.5% (89 cases). Among the patients with the nasal cavity pathology, the most common findings were 85 nasal septum deviation (65.4%) and 72 inferior concha hypertrophy (55.4%).

Discussion & Conclusion

High-resolution temporal bone CT is widespread used especially in the diagnosis of the diseases and detection of temporal bone anatomic variations.

The high rate of incidental extratemporal pathologies reveals the necessity of evaluating images as a whole, even if they were performed for different reasons. In particular, this is necessary to prevent misdiagnosis and to avoid malpractices by radiologists, which is important medicolegally.

4. PEDIATRICS

4-P1

KLEEFSTRA SYNDROME: NEW MOLAR TOOTH SIGN OF MID- BRAIN?

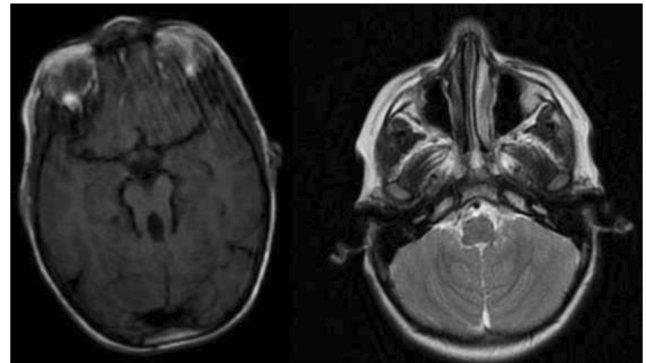
*M. Yazol*¹, Ç. Oztunali¹, E. Gumus³, H. Ozer⁴

¹ Sanliurfa Education And Research Hospital, Department of Radiology, Sanliurfa, Sanliurfa, TURKEY, ² Sanliurfa Education And Research Hospital, Department of Radiology, Sanliurfa, Sanliurfa, TURKEY, ³ Harran University Medicine Faculty, Medical Genetics Department, Sanliurfa, Sanliurfa, TURKEY, ⁴ Ankara City Hospital , Department of Radiology,Bilkent, Ankara, TURKEY

Introduction

Kleefstra syndrome (KS) is a rare genetic condition with autosomal dominant inheritance characterized by intellectual disability (ID), autistic-like features, childhood hypotonia, and distinctive

facial features. The diagnosis of KS is established on by either a mutation in the (EHMT1) gene (rarely) or by a microdeletion in the 9q34.3. Currently, brain abnormalities are reported in half of KS subjects and include white matter abnormalities, cortical atrophy, corpus callosum(CC) hypoplasia. To date, approximately 114 cases have been described. We herein report 3 novel cases from a single family that presented with severe ID and speech delay, aggressive behavioral problems and discuss the differences and similarities in their neuroimaging features. Furthermore, we determine a novel radiological finding for this condition “Molar Tooth Sign” that considered as a pathognomonic sign in Joubert Syndrome and Related Disorders (JSRD).



Methods

Patient 1 is a 4-year-old male and Patient 2 is a 6-year-old male child born to parents who are second cousins and referred to for severe intellectual disability, severe speech delay and similar facial phenotype. Patient 3 is a 30-year-old male is the father of sons. Central nervous system and clinical evaluation revealed that severe (ID), severe speech delay, aggressive behavioral problems in both children. Patient 3 Chromosomal microarray analysis was used and all patients underwent Cranial MRI and CT.

Result

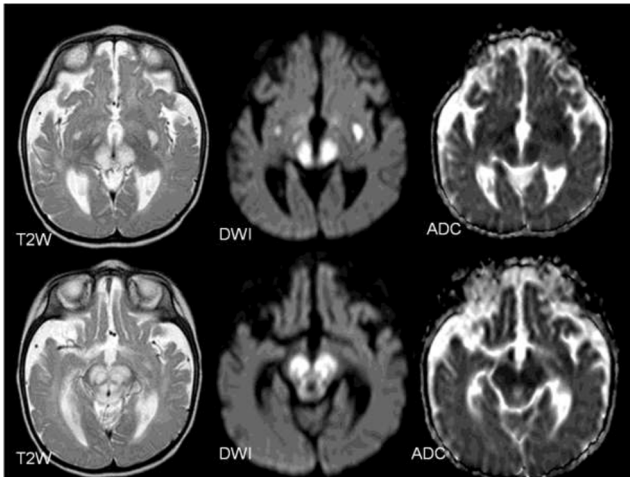
The patients had normal head circumference and typical facial appearance: a broad forehead, short nose. Both cases had enlargements of CSF spaces in the posterior fossa. Patient 1 and 2 revealed deep interpeduncular fossa, elongated superior cerebellar peduncles, hypoplasia of inferior cerebellar vermis with midline clefting, cerebellar disorganized foliation. Molar tooth sign was distinctive in patient 1. Patient 3 had mild inferior vermian hypoplasia and molar tooth sign was not detected in MRI. CC and white matter myelination patterns were normal/ age-related in all cases.

Discussion & Conclusion

Cortical atrophy, white matter defects have been described as brain imaging findings before in KS. In this study, we demonstrated KS with severe psychomotor retardation and novel brain MRI – CT findings, including hypoplasia of inferior cerebellar vermis, “Molar Tooth Sign”, cerebellar disorganized foliation that are important for differential diagnosis of JSRD.

4-P2**LEIGH SYNDROME: CRANIAL CT AND MRI FINDINGS OF AN INFANT***O. Yapici Ugurlar*¹, H. Onder¹¹ Okmeydani Training and Research Hospital - Department of Radiology, Istanbul, TURKEY**Introduction**

Leigh syndrome (LS) is a progressive neurodegenerative and mitochondrial disorder with onset usually in infancy or early childhood with an estimated incidence of 1:40000 births. Clinically, it is characterized by psychomotor retardation, muscular hypotonia, feeding difficulties, intermittent abnormalities of the respiratory rhythm, cranial palsies, ataxia, lactic acidosis, deterioration after acute infection. Hereby we present cranial computerized tomography (CT) and magnetic resonance imaging (MRI) findings of a 11-months-old male patient having intractable seizures, respiratory distress and hypotonia.

**Methods**

Unenhanced cranial CT and MRI of the patient were performed and evaluated in our pediatric radiology department.

Result

Unenhanced cranial CT of the patient showed bilateral symmetrical hypodense areas at putamen, thalamus, mesencephalon. Cranial MRI showed symmetrical lesions at putamen, thalamus, mesencephalon, medulla oblongata, corticospinal tracts, hyperintense in T2-weighted and hypointense in T1-weighted images, and also restricted diffusion in the affected areas on diffusion weighted images (Figure 1). Moderate cerebral atrophy was also present. Hypertrophic cardiomyopathy and optic nerve pathology were diagnosed during his hospitalization. Metabolic tests of the patient supported the diagnosis of Leigh syndrome. After completing the treatment of sepsis and lung infection, he was discharged with home ventilator (+ tracheostomy), antiepileptic and multivitamin treatments.

Discussion & Conclusion

LS is a mitochondrial disease characterized by progressive neurodegeneration which usually results in death during childhood. The onset of symptoms is usually before 2 years of age. Affected children often become symptomatic with nutritional difficulties, vomiting and developmental retardation in the first year of life. A few years after the onset of symptoms, death is typically caused by progressive respiratory distress. Cranial imaging plays an important role in diagnosis. Bilateral, symmetric focal hyperintensities in T2-weighted images of basal ganglion, thalamus, substantia nigra and brain stem nuclei are the most common neuroradiological findings. In the basal ganglia, especially putamen is affected. High T2 signals on MRI reflect spongiform changes and vacuolization in affected brain structures. Putaminal low attenuation was evaluated as characteristic in terms of disease. In conclusion, LS should be considered in patients with clinical features of a neurometabolic disease, with bilateral symmetric involvement pattern in basal ganglia and multiple brain stem nuclei.

4-P3**SEPTO-OPTIC DYSPLASIA REVIEW OF MRI BRAIN FINDINGS***D. Ward*¹, D.J.A. Connolly¹, P.D. Griffiths²¹ Sheffield Childrens Hospital NHS Foundation Trust - Department of Radiology, Sheffield, UNITED KINGDOM, ² Academic Unit of Radiology, University of Sheffield, Sheffield, UNITED KINGDOM**Introduction**

Septo-optic dysplasia (SOD) is a rare congenital disorder characterised by any combination of midline brain defects, optic nerve hypoplasia and hypothalamic-pituitary dysfunction.

In this paper we report the magnetic resonance imaging (MR) findings from a retrospective case analysis of children with SOD from a single centre in the United Kingdom (UK).

Methods

For the purposes of this review SOD was defined in radiological terms as an absence of the septum pellucidum (complete or partial) associated with hypoplasia of the optic nerves and/or optic chiasm.

The local MR databases were searched for cases of SOD reported on MR studies in children over an 18-year period (2001-2018 inclusive).

Those MR studies were reviewed by two consultant paediatric neuroradiologists. The septum pellucidum was determined to be either absent or partially absent, and the extent of involvement of the optic nerve(s)/chiasm was recorded. Involvement of the hypothalamus/pituitary gland was also recorded, along with any other coexisting brain abnormalities.

Result

49 cases of confirmed SOD were found and 44/49 (90%) demonstrated complete absence of the septum pellucidum while 5/49 (10%) had partial absence.

In 9/49 cases (18%) there was unilateral hypoplasia of the optic nerve. 24/49 cases (49%) had a structural abnormality of the pituitary, which included an ectopic posterior pituitary bright spot in 4/49 cases (8%). The olfactory nerves were hypoplastic in 5/49 cases (10%). 28/49 cases (57%) had another associated brain abnormality, which resulted from some form of cortical formation abnormality and/or schizencephaly in 24/49 (49%).

Discussion & Conclusion

We found a high rate of associated brain abnormalities in our cohort of children with SOD including pituitary abnormalities in 49% and cortical formation abnormalities or schizencephaly in 49%. The wide range of intracranial abnormalities found in this cohort suggests that there is not a single cause for SOD, rather SOD is the phenotypic end point from multiple aetiological events. An individual child with SOD may have several other coexisting intracranial abnormalities, hence high quality MR imaging is required in all cases.

4-P4

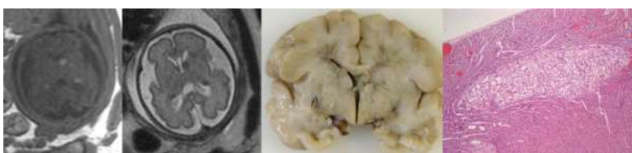
TUBEROUS SCLEROSIS COMPLEX: PRENATAL CNS MRI FINDINGS

*E. Vazquez*¹, L. Rianza², I. Delgado³, A. Sánchez-Montañez⁴, A. Macaya⁵, S. Arévalo⁶

¹ University Hospital Vall d'Hebron, Barcelona, SPAIN, ² University Hospital Vall d'Hebron, Barcelona, SPAIN, ³ University Hospital Vall d'Hebron, Barcelona, SPAIN, ⁴ University Hospital Vall d'Hebron, Barcelona, SPAIN, ⁵ University Hospital Vall d'Hebron, Barcelona, SPAIN, ⁶ University Hospital Vall d'Hebron, Barcelona, SPAIN

Introduction

Fetal MRI is valuable in diagnosing TSC in fetuses with intracardiac rhabdomyomas seen on US, even the importance of being aware that a negative fetal MRI exam does not exclude TSC.



Methods

Twelve fetuses with cardiac rhabdomyomas (22–36 weeks' gestation) underwent cerebral MRI in our tertiary center. The study was approved by the local ethics committee, and written informed consent was obtained from all participants. MRI examinations were performed on an Avanto scanner (Siemens, Erlangen, Germany) using a body phased-array coil. Images were read by two pediatric neuroradiologists experienced in neurofetal imaging. MR imaging results were correlated with postnatal imaging, genetic data, and/or histology.

Result

In 10 cases, fetal MRI demonstrated typical characteristics of TSC, which were confirmed by postnatal MRI in pregnancies that continued gestation, or histology in those that were interrupted. There was one false-negative case, whilst one early case was a false-positive.

Discussion & Conclusion

Our results indicate that fetal MRI is a sensitive modality for detecting cerebral lesions in TSC and should become a component of the early interdisciplinary diagnostic workup in suspected fetal TSC. Diagnosis was more difficult before 28 weeks' gestation. Presence of multiple lesions increases the diagnostic confidence.

4-P5

PITUITARY CYSTS IN CHILDREN AND ADOLESCENTS: MRI FEATURES AND CLINICAL IMPLICATIONS

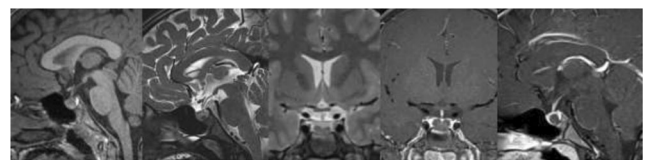
*E. Vazquez*¹, I. Delgado², A. Sánchez-Montañez³, J. Escudero⁴, D. Yeste⁵, A. Carrascosa⁶

¹ University Hospital Vall d'Hebron, Barcelona, SPAIN, ² University Hospital Vall d'Hebron, Barcelona, SPAIN, ³ University Hospital Vall d'Hebron, Barcelona, SPAIN, ⁴ University Hospital Vall d'Hebron, Barcelona, SPAIN, ⁵ University Hospital Vall d'Hebron, Barcelona, SPAIN, ⁶ University Hospital Vall d'Hebron, Barcelona, SPAIN

Introduction

Pituitary cysts are often seen in pediatric MRI examinations performed for related or unrelated symptoms. These lesions are often misinterpreted as microadenomas, but their typical location and certain imaging features enable their recognition and differentiation.

There is limited information regarding the proper management of these pituitary cysts in the pediatric age. We provide practical data on this condition, useful for radiologists and pediatricians.



Methods

A retrospective review was performed of 25 consecutive pediatric cases of pituitary cyst seen in a tertiary center over the last ten years. All patients were examined using our MRI protocol for the hypothalamic-hypophyseal region. The patients' clinical and hormonal data were also reviewed and correlated with the imaging findings.

MRI protocol included sagittal 3D MPGR, 3D CISS, axial FLAIR, coronal T2 FSE, axial GRE T2, postcontrast sagittal MPR GRE, and postcontrast fat-sat sagittal T1 sequences.

We retrospectively analyzed the imaging characteristics of the cysts (eg, size, location, and signal intensity). Two experienced pediatric

neuroradiologists who were unaware of the patients' clinical features, read the images and collected the findings.

Result

The reviewed cases included 25 patients (14 boys, 11 girls), mean age 4.6 years (range 2–17). no follow-up performed in 8 patients, 17 patients had follow-up, with a mean period 4.3 years (6 months to 10 years).

Five patients showed hypointense content of the cyst on T1WI and hyperintense on T2, 11/25 had iso-hypointense cysts on T1 and hypointense on T2, whilst a total of 9 showed hyper-signal on T1 and hypointensity on T2, attributable to higher protein content.

Maximum size diameter was 11 mm. All cysts remained stable, although some evolved to a higher hyperintensity on T1WI. In two cases, the cyst caused deviation of the pituitary stalk. Other two cases showed diffusion restriction.

All patients who received medical treatment for GH deficiency or CPP responded adequately to therapy.

All our patients were managed conservatively

Discussion & Conclusion

Pituitary cysts in childhood are fairly common and should be recognised by radiologists and adequately managed by pediatricians. Based on our experience and on the literature reviewed, an imaging algorithm is proposed, including several criteria for proper assessment and suitable follow-up.

4-P6

NEUROCHEMISTRY EVALUATED BY MR SPECTROSCOPY IN TWO PATIENTS WITH ANTI-NMDA RECEPTOR ENCEPHALITIS

*J. Takanashi*¹, *Y. Murofushi*¹, *K. Sano*¹, *H. Sakuma*², *H. Terada*³

¹ Tokyo Women's Medical University Yachiyo Medical Center, Department of Pediatrics, Yachiyo, JAPAN, ² Tokyo Metropolitan Institute of Medical Science, Department of Brain Development and Neural Regeneration, Tokyo, JAPAN, ³ Toho University Sakura Medical Center, Department of Radiology, Sakura, JAPAN

Introduction

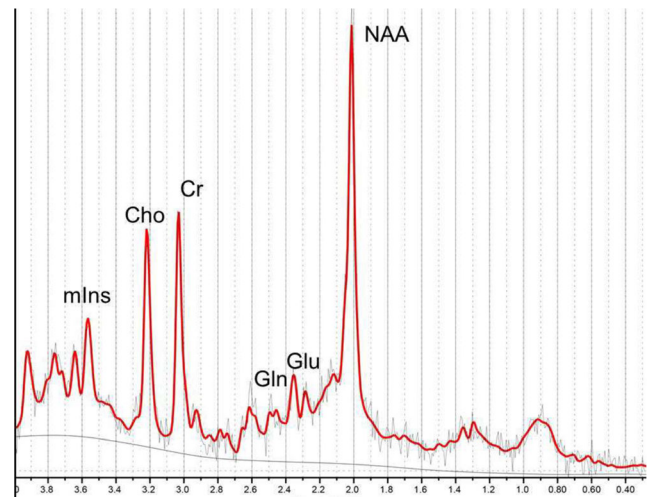
Anti-N-methyl-D-aspartate receptor (NMDAR) encephalitis is an autoimmune disorder associated with CSF IgG antibodies against the GluN1 subunit of NMDAR, predominantly affecting young females with ovarian teratomas. There has been no specific laboratory or imaging marker except for the antibody. We examined whether MRS could detect the neurochemical abnormalities characteristic of NMDAR encephalitis.

Methods

Two teenage patients with anti-NMDAR encephalitis (pt. 1, 12 year-old female, pt. 2, 15 year-old male) were enrolled in this study. They clinically showed psychiatric symptoms, disturbed consciousness, involuntary movements, and hypoventilation, and recovered almost completely after the first and second line therapies. Quantitative MR spectroscopy

(3T Philips, PRESS, TR=5,000 msec, TE=31 msec) analyzed by LCModel were performed multiple times (four times for patient 1, and twice for patient 2) in the frontal white matter,

Result: MRS (Figure) showed a good S/N ratio (>17 on LCModel), and normal concentrations of metabolites, including N-acetylaspartate, myo-Inositol, creatine, choline, and glutamate (Glu) and glutamine (Gln), except for decreased Glu in the 3rd MRS study on patient 1. MR imaging scanned at the same time as the MRS showed no parenchymal lesion except for mild cerebral atrophy after methylprednisolone pulse therapies.



Discussion & Conclusion

Neuropathology of anti-NMDAR encephalitis has been reported that neuronal degeneration seems to be largely absent. The prognosis of anti-NMDAR encephalitis is good in about 80% of patients, especially when responded to first-line immunotherapy, 97% had a good prognosis. The normal NAA observed on MRS in anti-NMDAR encephalitis is considered to be consistent with these neuropathological findings and clinical course. Anti-NMDA destabilizes GluN2A-NMDAR, which causes a rapid dispersal of GluN2A-NMDAR out of synapses. The surface GluN2-NMDAR changes possibly lead to NMDAR dysfunction, completely blocked synaptic plasticity, and neuropsychological manifestations. Glutamatergic neurons may release Glu in quantities into the synaptic clefts to compensate NMDAR dysfunction, however, it would be mild compared to the release in the condition of excitotoxicity. As intrasynaptic Glu in anti-NMDAR encephalitis will be promptly taken up and processed to Gln by surrounding astrocytes, it may be difficult to detect intrasynaptic Glu derangement on MRS in anti-NMDAR encephalitis.

4-P7

A CASE REPORT OF PHELAN-MCDERMID SYNDROME: MRI FINDINGS.

*K. Suzuki*¹, *M. Hori*¹, *H. Watanabe*¹, *M. Kobayashi*¹, *J. Kodera*¹, *K. Tamura*¹, *N. Shiraga*¹, *Y. Takahashi*¹

¹ Toho University Omori Medical center, Tokyo, JAPAN

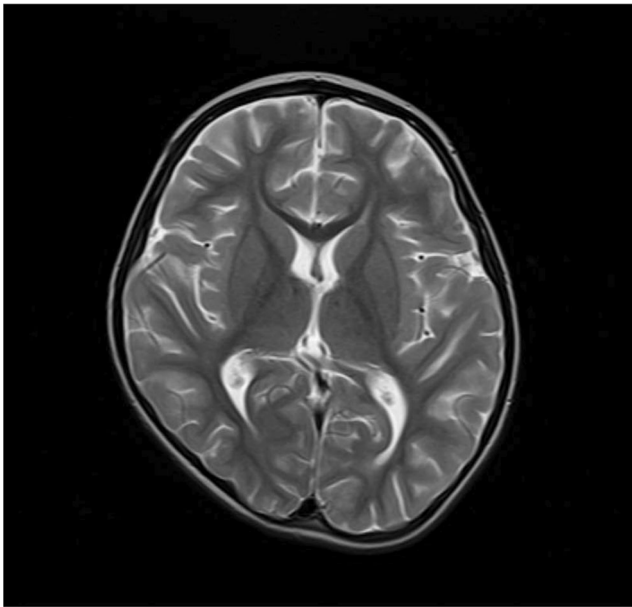
Introduction

We report a case of Phelan-McDermid syndrome with magnetic resonance imaging (MRI) findings.

Phelan-McDermid syndrome (PMS) is characterized by neonatal hypotonia, absent to severely delayed speech, developmental delay, and minor dysmorphic facial features. Most patients have moderate to severe intellectual disability.

Cause of PMS is a heterozygous deletion of chromosome 22q13.3 with disfunction of SHANK3.

Characteristic MRI findings are thinning or hypoplasia of the corpus, generalized white matter atrophy, nonspecific white matter hyperintensities in T2WI, ventricular dilatation, interventricular, cerebellar, or temporal sylvian arachnoid cysts, and cerebellar vermis hypoplasia.



Methods

Case report

A 4-years-old female presented a severely delayed speech. She was diagnosed PMS by genetic diagnosis.

Result

Imaging findings

MRI demonstrated cerebral ventricular transformation caused by the corpus callosum hypoplasia and the white matter atrophy. Hyperintense area was seen in white matter of bilateral frontal lobe, on T2-weighted image.

The atrophy and the abnormal signal were not found in pons and cerebellum.

Discussion & Conclusion

Summary

We report a case of Phelan-McDermid syndrome. Characteristic white matter atrophy and signal change have been demonstrated by MRI.

4-P8

MR IMAGING FEATURES OF RETINOBLASTOMA – ONE CENTER EXPERIENCE

*K. Nowak*¹, B. Dembowska-Baginska², O. Rutynowska², W. Hautz³, K. Cieslik³, M. Szaniawska¹, A. Olechowski³, E. Jurkiewicz¹

¹ Department of Diagnostic Imaging, The Children's Memorial Healthy Instytut, Warsaw, POLAND, ² Department of Pediatric Oncology, The Children's Memorial Healthy Instytut, Warsaw, POLAND, ³ Department of Ophthalmology, The Children's Memorial Healthy Instytut, Warsaw, POLAND

Introduction

Retinoblastoma (RBL) is the most common primary intraocular tumor in children, usually diagnosed under 3 years old. It is a highly malignant tumor of the primitive neural retina detected by ophthalmologists during ophthalmoscopy and ultrasound examination. MRI is important tool for precise initial diagnosis, monitoring focal response to the therapy and complications of the treatment. It can detect intra-, extra-ocular and intracranial extension of the tumor.

We present a variety of tumors MR images before/during and after the treatment.

Methods

MR examinations were performed with a 1.5T scanner, using multichannel head and neck coil and 4 channels small surface coils (circular polarizing coil). The imaging protocol for orbits and optic nerve consist of: T2-space (0,7mm), axial T2-dark fluid (2.5mm), axial (2,5mm) and sagittal oblique (1mm) T1-fatsat pre- and post- contrast injection. Standard brain imaging (with DWI and T1-post contrast) were performed in all patients.

The extent of the tumor (infiltration of the globe, optic nerve, retrobulbar space, orbital fat), retinal detachment, the presence of leptomeningeal spread, and associated brain abnormalities were estimated in the initial and follow-up examinations. Region of pineal gland was assessed in all cases.

Result

We analysed the group of 179 children: 124 patients had unilateral (72 pts right, 52 pts left), 52 patients - bilateral, and 3 patients presented trilateral RBLs. An average patient's age at moment of diagnosis is 2.2 years (range: 2 weeks - 6 years). A large tumor with infiltration of the tissues or/and leptomeningeal dissemination at the moment of recognition was recognized in 15pts.

NF1, NF2, TSC were diagnosed respectively in 3 pts.

Discussion & Conclusion

MR imaging is the accurate method for the initial diagnosis of RBL and follow-up given possibility of detection of intraocular tumor infiltration, optic nerve invasion, extraocular extension and metastatic lesions.

4-P9

BILATERAL CONGENITAL ABSENCE OF INTERNAL CAROTID ARTERIES - CASE REPORT

*I. Markovic*¹, S.Y. Al Ghailani², A. Kakaria¹

¹ Sultan Qaboos University Hospital, Muscat, OMAN, ² Oman Medical Speciality Board, Muscat, OMAN

Introduction

Congenital absence of bilateral internal carotid arteries is a rare entity and occurs in less than 0.01% of the population.

Methods

We are presenting a case of a 5 years old boy known to have sickle cell disease running a severe course of the disease who presented with sudden onset left hemiparesis. Magnetic resonance imaging with MR Angiography was performed initially and revealed acute watershed infarcts of the anterior circulation and absence of flow in both internal carotid arteries.

Result

Further evaluation with CT Angiography was obtained to evaluate intracranial vessels and confirmed diagnosis of bilateral agenesis of internal carotid arteries.

Discussion & Conclusion

Although, congenital absence of bilateral internal carotid arteries is usually asymptomatic but it is considered this condition increases risk of stroke at areas of collateral flow and developing of aneurysms in brain circulation.

4-P10

SURVEY OF BRAIN MATURATION IN PREMATURE NEONATES AT TERM USING DIFFUSION WEIGHTED AND MULTI-ECHO T2 IMAGING

O. Geier¹, H.C.V. Pfeiffer², B. Nguyen¹, A.A. Hagen-Kersten¹, T. Stiris^{3,5}, S.J. Moltu³, I. Maximov⁴

¹ Department of Radiology, Oslo University Hospital, Oslo, NORWAY, ² Department Paediatric Neurology, Oslo University Hospital, Oslo, NORWAY, ³ Department of Neonatal Intensive Care, Oslo University Hospital, Oslo, NORWAY, ⁴ Faculty of Psychology, University of Oslo, Oslo, NORWAY, ⁵ Faculty of Medicine, University of Oslo, Oslo, NORWAY

Introduction

Several MRI methods are sensitive to myelination, an essential brain maturation process, but few approaches survey myelination state quantitatively. We present the potential of myelin water fraction (MWF) imaging for the estimation of the brain maturation in neonates. We use the different relaxation properties of water dedicated to the myelin compartment and water localized in the intra- and extra-axonal spaces recalling DWI and multi echo T2 techniques (MET2).

Methods

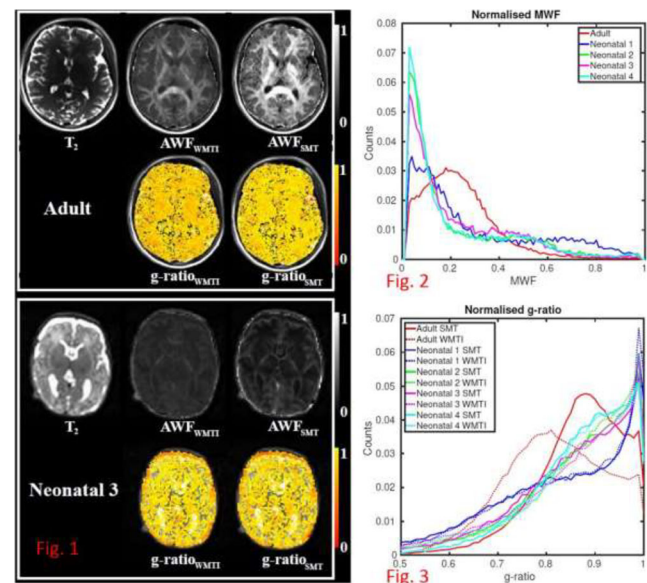
Four neonates born prematurely (GA 27+1, 28+2, 28+2, and 29+0 at birth) were scanned at term equivalent age (GA 40+5, 40+5, 42+1, and 42+6) using a 3 T MR scanner (Magnetom Prisma, Siemens Medical Solutions) and a 32 channel head coil. Gender ratio was 1:1.

All patients had morphologically normal MRI scans at term, normal brain ultrasonographies during hospitalization, and no medical history of intraventricular haemorrhages, other CNS disease or chromosomal defects. Additionally a healthy adult subject was examined with a comparable protocol.

DWI data were processed in accordance with optimized pipeline (Maximov et al., 2019). White matter tract integrity (WMTI) (Fieremans et al., 2011) and spherical mean technique (SMT) (Kaden et al., 2016) models were used to estimate axonal water fraction. MET2 data were estimated using multi-echo T2 TSE. T2 data were corrected for noise (Does et al., 2019) and Gibbs ringing artefacts (Kellner et al., 2016). MWF was estimated using the MERA package (Does, Github). G-ratio (ratio of inner to outer diameter of the myelin sheath) for adult and neonatal brains was estimated using the approach developed by Stikov et al., 2015.

Result

Figure 1 shows G-ratio maps using the WMTI and SMT approaches for a neonate and an adult. The neonatal brain shows less and more inhomogeneous myelination. Figure 2 and figure 3 show the histogram distribution of the normalized MWF and the normalized G-ratio, respectively. As expected, neonates exhibit overall lower normalised MWF and higher normalised G-ratios, in accordance with less maturation.



Discussion & Conclusion

This pilot study demonstrates a method of quantifying brain maturation and has a great practical impact.

4-P11

THE SPECTRUM OF NEUROIMAGING FINDINGS IN FEBRILE INFECTION RELATED EPILEPSY SYNDROME (FIRES)

*G. Talenti*¹, S. Culleton¹, M. Kaliakatsos¹, S. Pujar¹, F. D'Arco¹

¹ Great Ormond Street Hospital for Children, London, UNITED KINGDOM

Introduction

Febrile infection related epilepsy syndrome (FIRES) is a rare severe epileptic syndrome occurring in previously healthy children and characterised by refractory status epilepticus (SE) following a febrile illness.

Brain imaging findings in affected patients have been reported in few case series and some case reports.

Methods

We performed a comprehensive, systematic review of the magnetic resonance imaging (MRI) characteristics in patient with clinical diagnosis of FIRES in our institution and in all reported patients in literature, describing the findings in the acute and chronic phases of the disease, and discussing possible pathogenesis and radiologic differential diagnoses.

Result

Most of the patients had normal brain scans in the acute phase and about 1/4 of the patients reported in literature had abnormalities in the temporal lobes. Changes in the basal ganglia and rarely in thalami or brainstem have also been described, as well as diffuse cerebral edema in a minority of patients during the acute phase. The chronic phase of the disease was characterised by atrophic changes and evidence of mesiotemporal sclerosis.

Discussion & Conclusion

An understanding of these MRI abnormalities is necessary to support the diagnosis of FIRES and exclude mimics.

There are several different MRI imaging patterns all compatible with FIRES, they need to be recognised and do not misdiagnosed for infections or inflammations.

Imaging abnormalities in this clinico-electroencephalographic entity can also help in interpreting the still poorly understood mechanism of so-called seizure-related MRI changes.

4-P12

WHITE MATTER TRACT ORGANIZATION IN POLYMICROGYRIA AND LISSENCEPHALY: A MULTI-FIBER DIFFUSION MRI TRACTOGRAPHY STUDY

*F. Arrigoni*¹, D. Peruzzo¹, S. Mandelstam^{2,3,4,5}, G. Amorosino¹, D. Redaelli¹, R. Romaniello¹, R. Leventer^{2,3,4}, R. Borgatti¹, M. Seal^{2,4}, J.Y.M. Yang^{2,3}

¹ Scientific Institute IRCCS E. Medea, Bosisio Parini, ITALY, ² Murdoch Children's Research Institute, Melbourne, AUSTRALIA, ³ Royal Children's Hospital, Melbourne, AUSTRALIA, ⁴ The University of

Melbourne, Melbourne, AUSTRALIA, ⁵ The Florey Institute of Neuroscience and Mental Health, Melbourne, AUSTRALIA

Introduction

Malformations of cortical development (MCD) may be associated with abnormal organization of the underlying white matter tracts (WMTs) that have been rarely investigated so far.

The aim of this study is to assess WMT organization in a cohort of children and young adults with severe MCD using a high-order diffusion MRI model (Constraint Spherical Deconvolution – CSD) and tractography.

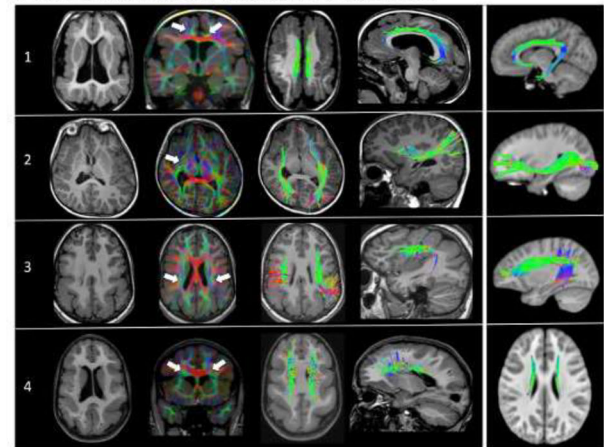
A) WM tracts appearance in each MCD subgroup

For each bundle, the number of tracts classified as normal/irregular/thick/absent is reported

MCD	No. of patients	SLF	CG	SFOF	IFOF	PCR-OR	ILF
Perisylvian PMG	16	9/15/0/8	27/5/0/0	31/1/0/0	27/5/0/0	20/12/0/0	21/11/0/0
Fronto-parietal PMG	7	4/6/0/4	13/1/0/0	12/2/0/0	12/2/0/0	6/8/0/0	7/7/0/0
Frontal PMG	7	3/10/0/1	5/9/0/0	12/1/0/1	12/2/0/0	10/4/0/0	11/3/0/0
Generalized PMG	4	0/2/0/6	1/5/0/2	2/2/0/4	2/6/0/0	0/8/0/0	0/8/0/0
Multifocal PMG	6	9/3/0/0	7/5/0/0	10/0/0/2	12/0/0/0	9/3/0/0	11/1/0/0
Parieto-Occipital PMG	1	2/0/0/0	2/0/0/0	2/0/0/0	2/0/0/0	1/1/0/0	2/0/0/0
PMG - Schizencephaly	1	0/0/0/2	0/2/0/0	0/0/1/1	0/2/0/0	0/2/0/0	0/2/0/0
Pachygyria - SBH	5	0/6/0/4	2/8/0/0	2/4/4/0	2/8/0/0	0/10/0/0	0/10/0/0
SBH	2	0/4/0/0	2/2/0/0	4/0/0/0	2/2/0/0	0/4/0/0	0/4/0/0
Pachygyria	1	0/2/0/0	0/2/0/0	2/0/0/0	0/2/0/0	2/0/0/0	2/0/0/0
All PMG	42	27/36/0/21	55/27/0/2	69/6/1/8	67/17/0/0	46/38/0/0	52/32/0/0
All LIS	8	0/12/0/4	4/12/0/0	8/4/4/0	4/12/0/0	2/14/0/0	2/14/0/0

MCD: malformation of cortical development; PMG: polymicrogyria, SBH: subcortical band heterotopia, LIS: lissencephaly, SLF: Superior longitudinal fasciculus, CG: cingulum, SFOF: superior fronto-occipital fasciculus, IFOF: inferior fronto-occipital fasciculus, PCR-OR: posterior corona radiata – optic radiation; ILF: inferior longitudinal fasciculus

B) MRI findings, DEC maps and tractography in selected patients



T1w images, DEC maps and tractography reconstructions in 4 different patients are shown (1,2,3,4). For each abnormal tract, the tractography reconstruction obtained by the age-matched healthy-controls template is shown in the last column for comparison. 1) Thin and irregular CG (arrows on DEC map) in a patient with generalized PMG. 2) Abnormal right IFOF (arrow on DEC map) in a patient with unilateral right perisylvian PMG. 3) Abnormal SLF (arrows on DEC map) in a patient with posterior predominant pachygyria and thick SBH. 4) Bilaterally thick SFOF (arrows on DEC map) in a patient with pachygyria and SBH.

Methods

We retrospectively included 42 subjects with polymicrogyria (PMG) and 8 subjects with lissencephaly (LIS) (mean age: 8.3 ± 5.4; range: 1.4 - 21.2; 27 males). The CSD technique was used to estimate the local fiber orientation distribution, generate fiber direction-encoded color (DEC) maps and reconstruct tractography of the major association WMTs for each patient. Patients data were visually compared to DEC maps and tractography reconstructed from seven age-matched, healthy control WM templates. Each WMT appearance was assessed by two experienced pediatric

neuroradiologists, and scored in consensus, based on degrees of structural abnormalities as normal, irregular, thick or absent. The results were summarized by different PMG and LIS subgroups.

Result

Overall, more LIS patients demonstrated abnormal appearing WMTs compared to PMG patients (79.2% versus 37.3%). Majority of the tract abnormalities in PMG patients were observed in superior longitudinal fasciculus (SLF), cingulum, posterior corona radiata/optic radiations and inferior longitudinal fasciculus while in LIS all WMT were equally affected (Fig1a).

The extents of WMT abnormalities in PMG were associated with the severity and the distribution/location of the MCD. As an example, generalized PMG demonstrated more tracts abnormalities than frontal or front-parietal PMG. The SLF was absent in case of diffuse peri-sylvian PMG and normal in case of focal peri-sylvian PMG. The involvement of the SLF was less severe in case of PMG caused by prenatal CMV infection. Thickened superior fronto-occipital fasciculus was demonstrated in three patients.

Discussion & Conclusion

We demonstrated a range of WMT structural abnormalities in PMG and LIS patients. The patterns of WMT involvement are related to the PMG and LIS subtypes, distribution and possibly their underlying aetiologies.

4-P13

OBSERVATIONAL STUDY: AN OVERVIEW OF NEUROIMAGING FINDINGS IN PATIENTS WITH MUCOPOLYSACCHARIDOSIS ON MR IMAGING

*M. Almuntashri*¹, *A. Albukhari*², *F. Almohideb*³

¹ King Abdulaziz Medical city, NGH, Riyadh, SAUDI ARABIA, ² King Abdulaziz University, Jeddah, SAUDI ARABIA, ³ King Saud University, Riyadh, SAUDI ARABIA

Introduction

Mucopolysaccharidosis (MPS) are a group of inherited lysosomal storage disorders result from the deficiency of one of the enzymes required for the breakdown of glycosaminoglycans (GAGs). This enzyme deficiency results in progressive accumulation of GAGs in cells and tissues, which progressively and permanently affects tissues and organs leading to multi-organ dysfunction.

There are seven distinct types of MPS, which are divided into subtypes according to the affected enzyme and the severity of the clinical picture. The aim of this study is to illustrate the CNS signs seen by imaging of the different types of MPS. with emphasis is on the posterior fossa features seen by MRI



Methods

This is a retrospective study from 2009 up to 2015 in two tertiary centers in KSA.

It included 13 patients representing all children under the age of 14 with MPS.

The diagnosis was made on the basis of abnormal enzyme assays and/or DNA analysis.

Only 7 diagnosed patients were available to be included in the study.

The images were collected from the PACS and retrospectively evaluated by a pediatric neuro-radiologist.

Result

The craniocervical junction stenosis found in 5/7 of patients.

4/7 of the patients had frontal bossing and increased antero-posterior diameter.

4/7 patients had a mega cistern magna.

VRS was most common in cerebral white matter in 4/7 patients, in comparison to only 3 in corpus callosum, one in brainstem and none in the cerebellum.

3 patients also were noted to have white matter changes.

Cerebral atrophy was seen in only two patients while cerebellar atrophy was in one.

During examining the infratentorial images, we found that mega cisterna magna is the most common finding, where we found it in (4/7)patients with type I, III, and IV.

Cerebellar atrophy seen only in one MPS patient with type I and the dilated PVS involving the brainstem seen also in one patient with MPS type II.

Discussion & Conclusion

Knowledge of radiological and neuroradiological appearances of MPS is essential for radiologists. MRI brain may show specific features in MPS patients, although it is not possible to accurately differentiate between MPS types based on neuroradiological characteristics.

4-P14

NEUROIMAGING MANIFESTATIONS AND GENETIC VARIABILITY OF WALKER-WARBURG SYNDROME IN SAUDI PATIENTS, CASE SERIES

S. Alharbi¹, K. Tlili-Graïess¹, A. Alhashem²

¹ Prince Sultan Military Medical City, Radiology department, Neuroradiology section, Riyadh, SAUDI ARABIA, ² Prince Sultan Military Medical City, Pediatric department, Genetic section, Riyadh, SAUDI ARABIA

Introduction

Saudi Arabia has the highest rate of consanguinity among Middle Eastern countries, which lead to an increased risk of genetic disorders. Walker-Warburg syndrome (WWS), an autosomal recessive disease, is the most severe phenotype of congenital muscular dystrophies. Its diagnosis still relies heavily on neuroimaging. Identification of its causative mutations will assist premarital and prenatal genetic counseling.

We aim to describe neuroimaging and genetic findings and investigate the correlation between them in 12 cases of Saudi neonates with WWS.

Methods

We retrospectively reviewed clinical and genetic findings of 12 Saudi neonates diagnosed with WWS between April 2012 and December 2018 in a single tertiary care center. Brain imaging studies including the orbits were reevaluated. Correlation between neuroimaging and genetic findings was investigated.

Result

Female to male ratio was 2:1. Macrocephaly and microcephaly was found in 7 and 3 patients, respectively. Dysmorphic features included micrognathia, low set ears and depressed nasal bridge in only 20% of cases. Creatine kinase results were available and elevated in 9/12.

Variable genetic mutations were noted. POMT1, TMEM5, POMT2 mutations identified in 4, 3 and 2 cases, respectively. ISPD was implicated in 2 cases with additional PGAP2 mutation in 1 case. The last case showed genetic mutation known to cause Cockayne syndrome.

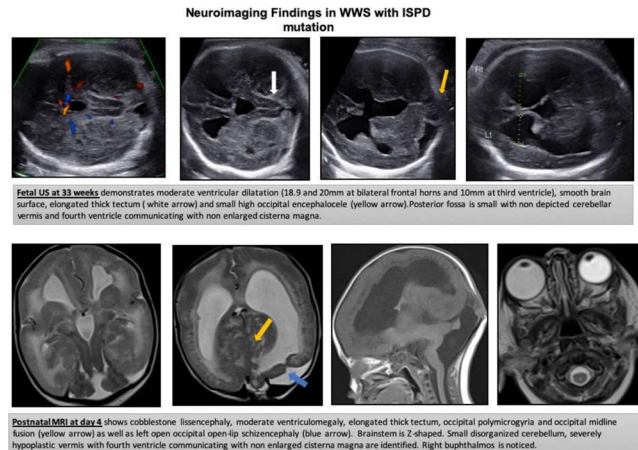
All patients showed cobblestone cortex with severe overmigration resulting in midline fusion in 3 cases. Five patients had subependymal heterotopia. One case with ISPD mutation had occipital polymicrogyria and open-lip schizencephaly.

All cases showed classical infratentorial findings including small posterior fossa, hypoplastic Z-shaped brainstem, thick tectum with fused

colliculi, anterior pontine cleft, hypoplastic and dysplastic vermis and cerebellum with cysts.

Hydrocephalus was noted in 11 cases with large supraoccipital encephalocele (1 case) and meningocele (1 case).

Buphthalmos, microphthalmia, and persistent hyperplastic primary vitreous were the most frequent eye abnormalities found in 8, 7, and 6 cases, respectively.



Discussion & Conclusion

WWS is genetically heterogeneous among Saudis. Associated mutations in PGAP2 and Cockayne- related genes emphasize on increased risk of autosomal recessive disorders expression in consanguineous marriages. MRI is excellent in demonstrating spectrum of WWS brain and orbit malformations; however, no correlation could be noted between the MRI appearance and the mutated gene.

4-P15

EARLY ANTIRETROVIRAL THERAPY IN HIV-INFECTED CHILDREN IS ASSOCIATED WITH DIFFUSE WHITE MATTER STRUCTURAL ABNORMALITY AND CORPUS CALLOSUM SPARING

C. Ackemann¹, S. Androniko², M.G. Saleh³, B. Laughton⁴, A.A. Alhamud³, A. van der Kouwe⁵, M. Kidd⁶, M. F. Cotton⁴, E.M. Meintjes³

¹ Department of Radiodiagnosis, Stellenbosch University, Faculty of Medicine and Health Sciences, Stellenbosch, South Africa, ² Department of Pediatric Radiology, Children's Hospital Philadelphia and the University of Pennsylvania, Philadelphia, USA, ³ MRC/UCT Medical Imaging Research Unit, Department of Human Biology, University of Cape Town, Cape Town, South Africa, ⁴ Family Clinical Research Unit, Department of Paediatrics and Child Health, Faculty of Medicine and Health Sciences, Univ, Stellenbosch, South Africa, ⁵ Athinoula A. Martinos Center for Biomedical Imaging, Massachusetts General Hospital, Charlestown, USA, ⁶ Centre for Statistical Consultation, University of Stellenbosch, Stellenbosch, South Africa

Introduction

Background, purpose:

Fractional anisotropy in the frontal white matter, corpus callosum and internal capsule are abnormal in HIV+ adults. The distribution and nature of white matter abnormalities in a cohort of children who started ART within the first year of life and benefit of early treatment are described using DTI measures.

Materials, methods:

DTI was performed on children in a neurodevelopmental sub study from the Children with HIV Early Antiretroviral (CHER) trial. Voxel-based group comparisons were done to determine regions where fractional anisotropy and mean diffusion differed between HIV+ and uninfected children. Associations of DTI parameters with timing of ART initiation were examined.

Results:

39 HIV+ children (15 male, mean age 5.4 years) and 13 controls (5 male, mean age 5.7 years) were imaged. 2 Clusters with lower fractional anisotropy and 7 clusters with increased mean diffusion were identified in the HIV+ group with symmetrical distribution predominantly due to increased radial diffusion, suggestive of decreased myelination. Corticospinal tracts rather than the corpus callosum were predominantly involved. Children on early interrupted ART had lower fractional anisotropy compared to those receiving continuous treatment.

Conclusion:

HIV+ children at 5 years have white matter abnormalities measured by fractional anisotropy, despite early ART, suggesting that early ART does not fully protect the white matter either from peripartum or in utero infection. In contrast to adults, the corticospinal tracts are predominantly involved rather than the corpus callosum, possibly due to early ART. Continuous early ART can limit white matter damage.

5. SPINE

5-P1

HUGE MULTIFOCAL EXTRAMEDULLARY MYXOPAPILLARY EPENDYMOMA WITH SYNCHRONOUS EXTENSIVE INTRACRANIAL IMPLANTS IN A YOUNG ADULT AT INITIAL PRESENTATION. CASE REPORT

A. Petrou¹, S. Papathanassiou¹, A.D. Papathanassiou¹

¹ Radiologie im Silberturm, St. Gallen, SWITZERLAND

Introduction

Ependymoma is a rare neuroepithelial tumor with different histopathological entities. Myxopapillary ependymoma (MPE) is a benign variant (WHO grade I) occurring mostly in the caudal spinal canal; metastases are very rare, while multifocality has been occasionally mentioned due to CSF-dissemination. We report an unusual case of a MPE in a young adult

with simultaneous extensive intracranial and spinal tumor manifestations on initial admission.

Methods

23-years-old male presented with back pain and gait disturbances; he reported neither headaches, nor seizures. After clinical examination a MRI of the entire neuroaxis was performed and a spinal microscopical biopsy was carried out with histopathological examination of the surgical specimen.

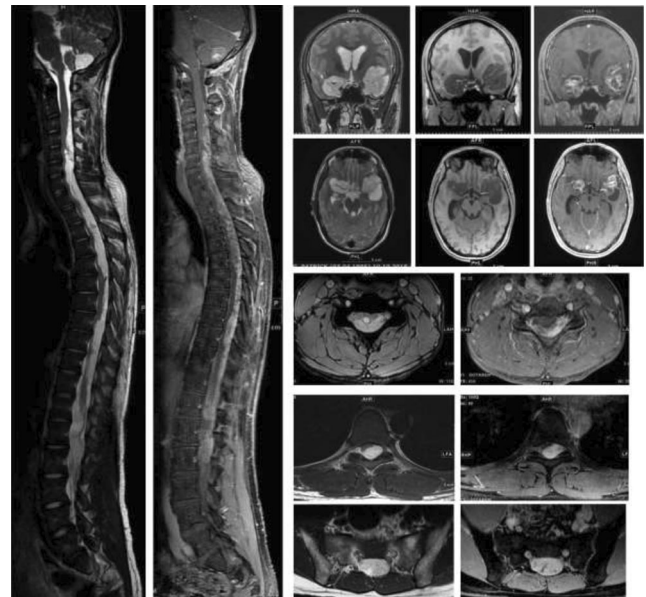
Result

The physical examination revealed gait ataxia and hypaesthesia sub TH11/12 while motor activity and the function of bladder/endgut were preserved.

On incipient cranial MRI five extraaxial masses (supra- and infratentorial) were found with features of ependymomas.

Immediate subsequent spinal MRI demonstrated extensive multifocal intradural extramedullary masses within almost the whole spinal canal. The tumors showed inhomogenous enhancement after gadolinium administration and had associated cystic changes to a variable extent. In addition there was also secondary syringohydromyelia and signs of compromised CSF-circulation. Furthermore multisegmental cord compression was depicted.

After laminectomy TH8/9 a grayish glassy mass was found and tissue was removed for histological examination; final diagnosis: myxopapillary ependymoma WHO grade I.



Discussion & Conclusion

The presented case showed a diffuse multifocal extramedullary MPE WHO grade I with concurrently several cranial extraaxial tumors. Though there was no biopsy of the intracranial lesions we believe - due to identical MR imaging characteristics - that these are rostral implants of the primary huge spinal masses developed via retrograde CSF-dissemination; nevertheless the alternative hypothesis of true multicentric

primary tumor foci has to be considered as well. The differential diagnosis includes i.a. meningioma, schwannoma, and metastases; the previous healthy young patient had neither known malignancy, nor neurofibromatosis. In such an extensive dissemination of the disease the adjuvant radiotherapy seems to be the favorable starting option of treatment. MRI-Examination of the entire neuroaxis is mandatory if an intracranial lesion is found with features of an ependymoma to detect/exclude associated simultaneous spinal masses.

5-P2

AUTOMATED DETECTION OF OSTEOPOROTIC VERTEBRAL FRACTURES USING A CONDITIONED VARIATIONAL AUTO-ENCODER AND PROBABILISTIC POINT CLOUD RECONSTRUCTIONS

*J. Kirschke*¹, M. Löffler¹, M. El-Husseini^{1,2}, A. Jacob¹, A. Valentinitsh¹, B. Menze², A. Sekuboyina^{1,2}

¹ Neuroradiology, TUM, Munich, GERMANY, ² Informatics, TUM, Munich, GERMANY

Introduction

Recent work showed that fracture detection in CT scans works on a global level. In this work, we aim to automatically detect osteoporotic vertebral fractures in MDCT scans on a single vertebra level.

Methods

With an automated deep-learning based pipeline we labeled and segmented 631 individual thoracolumbar vertebrae in 75 patients. Osteoporotic fractures were graded according to the Genant classification by two experienced neuro-radiologists in consensus; clinically relevant fractures were defined as grade 2 or 3. The dataset was divided in 2/3 training and 1/3 testing data. Using two different deep-learning approaches, we aimed to distinguish between vertebrae without vs. with clinically relevant fractures. Specifically, we used (1) a conditioned variational auto-encoder with a multilayer perceptron and (2) probabilistic point cloud reconstructions (fig.1) to create a healthy version of the respective vertebra. Fractures were classified by assessing the mismatch between original and reconstructed vertebra.

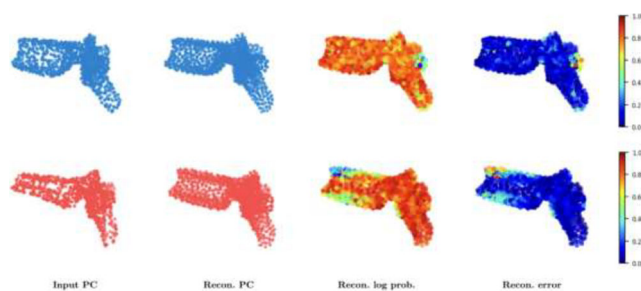


Figure: Probabilistic reconstruction of a healthy (top) and a fractured (bottom) vertebral point cloud. Observe that the pAE reconstruct a ‘healthy’ representation of the fractured vertebrae, consequently

enabling spatial localisation of the error based on the reconstruction error and log likelihood (both normalised between 0 and 1 within the PC).

Result

Using the variational auto-encoder, we were able to achieve an area under the curve of 0.85, with the probabilistic point cloud reconstructions an area under the curve of 0.78; using a combination of both approaches we were able to increase the area under the curve to 0.92. In this setting, all grade 3 fractures were detected.

Discussion & Conclusion

A combination of different deep-learning approaches allows for an accurate assessment of vertebral fractures based on the individual shape of each vertebrae. However, more training data is needed to further improve the results.

5-P3

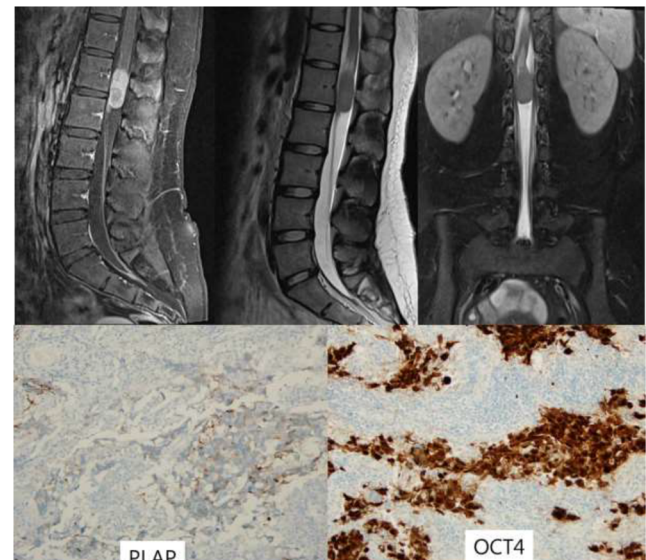
PRIMARY INTRAMEDULLARY SPINAL CORD GERMINOMA: CASE REPORT AND DISCUSSION

*Y.K. Ihn*¹, I.S. Kim¹, C.Y. Yoo¹, J.H. Shin¹

¹ St. Vincent's hospital, Suwon, SOUTH KOREA

Introduction

Germ cell tumors account for 1-3 % of intracranial neoplasm and are associated with spinal metastases in 10-20% of cases of intracranial germinoma. Primary intramedullary spinal cord germinoma is rarely reported, but many of the reported cases occur in Asian population. Spinal germinomas are difficult to identify based on the neuroimaging findings because of the similarity with spinal astrocytoma and ependymoma. We report a rare case of primary spinal germinoma which occurred in conus medullaris without intracranial lesion



Methods

A twenty years-old female came to our institution with a gait disturbance and paresthesia. She had suffered from intermittent lower back pain for 1 months. Neurological examination revealed right leg numbness and bilateral paresthesia. Laboratory workup was not remarkable. Magnetic resonance imaging on admission demonstrated the fusiform, heterogeneously enhanced, intramedullary mass at conus medullaris.

Result

Hemilaminectomy was performed with total removal of the mass. The tumor appeared after midline myelotomy, was slightly solid, and had well-defined borders, unlike astrocytoma. Histologic examination revealed that the tumor was typical germinoma, without syncytiotrophoblastic giant cells. Immunohistochemical stainings for placental alkaline phosphatase (PLAP) and OCT3/4 were positive. Chemotherapy was administered concurrently with local spine radiation after total resection of tumor. Follow-up MR imaging showed no recurrence without any distant metastasis.

Discussion & Conclusion

Primary spinal germinoma is very rare disease. MR image findings of spinal germinoma are similar to spinal astrocytoma. Hence, spinal germ cell tumors are difficult to distinguish from spinal astrocytoma based on neuroimaging findings. Previous treatments with either radiotherapy or chemotherapy have resulted in relatively high recurrence, so we expected that combination therapy would be effective for intraspinal lesion.

5-P4

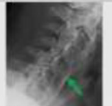
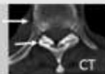


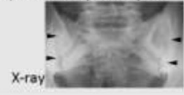
ACUTE SPINAL FRACTURES IN AN ANKYLOSED SPINE. WHAT LIES BEHIND A CARROT STICK FRACTURE?

*M.E. Capilla*¹, L. Ibanez Sanz², A. Paniagua³, M. Ibanez Moya¹, Y. Herrero⁴, V. Artiles⁴

¹ Unidad Central de Radiodiagnóstico- Department of Radiology, San Sebastián de los Reyes, Madrid, SPAIN, ² Hospital 12 de Octubre-Department of Radiology, Madrid, SPAIN, ³ Hospital Gregorio Marañón- Department of Radiology, Madrid, SPAIN, ⁴ Complejo Hospitalario de Toledo-Department of Radiology, Toledo, SPAIN

Introduction

Carrot stick fracture is a non-metastatic acute transverse fracture, often unstable, that can be found in two pathologies in its advanced stage: ankylosing spondylitis (AS) and diffuse idiopathic skeletal hyperostosis (DISH). Much less common in the latter.

IMAGING DIFFERENTIAL DIAGNOSIS		
Ankylosed spine	DISH	AS
Bone mineralization	Normal bone density (except advanced stage)	Diffuse osteopenia
	Anterior flowing ossification of anterior longitudinal ligament of at least four contiguous vertebral bodies (green arrow)	Syndesmophytes (Thin, vertical, forming in annulus, orange arrows).
Facet joints costovertebral joints	Not fused 	Fused (also sternoclavicular, costochondral and pubis) 
Sacrum and sacroiliac (SI) joints	No true sacroiliitis; ossification of nonsynovial fibrous superior portion of SI joint asymmetric 	Sacroiliitis: Usually bilaterally symmetric, synovial part 

Methods

After two cases with carrot stick fractures that caused spinal cord compression in old patients with no known previous history, a retrospective search for more cases and review of the literature was done. The 2 cases showed signs of DISH in an advanced stage on imaging. A comparison with other 2 cases of carrot stick fracture with AS was done.

Result

No more cases were found in our institution. Both cases with DISH were thoracic, mixed transdiscal and transvertebral fractures with spinal cord compression in old patients with minor trauma who were treated with surgical posterior fixation. The first case with AS was on old male who was not diagnosed of this condition who presented with a thoracic transvertebral non-displaced fracture who was treated conservatively. The other AS case was a 55 year-old patient with a long-standing disease who presented with a cervical transdiscal displaced fracture who was treated with surgical anterior fixation.

Discussion & Conclusion

Discussion

Review of the literature revealed few articles dealing with this pathology, especially acute fractures in patients with DISH.

Indications of the imaging diagnostic modalities: X-ray, CT and MRI in a carrot stick fracture will be discussed, with a description of the radiological signs using our cases.

Differential diagnosis between AS and DISH will be done based on clinical background, pathomechanics and radiological signs.

Conclusion

Ankylosed spine and minor trauma or acute pain is a condition to which radiologists must be alert. Diagnostic delay of a fracture in a rigid spine is common. CT or MRI should be performed (ideally both). MRI is highly recommended as there is a high incidence of neurologic complications.

MRI is mandatory if neurologic symptoms are present and treatment with transpedicular screws should be performed without delay.

5-P5

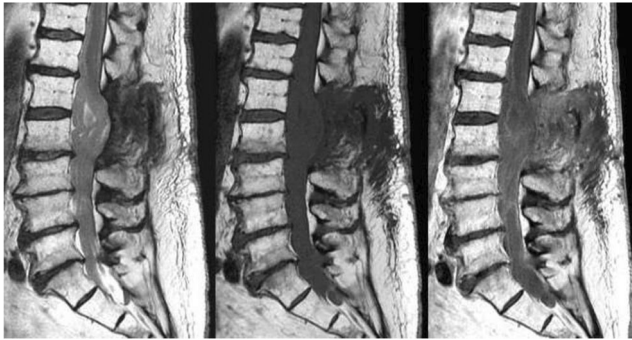
POLYCLONAL LYMPHOCYTIC INFILTRATE WITH ARACHNOIDITIS: A COMPLICATION OF INTRATHECAL STEM CELL TRANSPLANTATION

*J. Benson*¹, L. Eckel¹, G. Liebo¹, N. Campeau¹, G. Miller¹, F. Diehn¹, S. Messina¹

¹ Mayo Clinic, Rochester, USA

Introduction

Complications arising from intrathecal administration of stem cells have been scantily reported. This abstract will present such a case in the context of a comprehensive review of the available literature.



Methods

A review was completed of the relevant imaging and historical data of a patient with a pathologically proven complication to a prior intrathecal stem cell injection.

Result

The patient is a 74-year-old male who had fatigue and decreased exercise tolerance 3 years prior to presentation at our institution. To treat these symptoms, he underwent a combination of intravenous and intrathecal stem cell injections in Moscow, Russia. Subsequently, he began to have progressive symmetrical lower extremity weakness. The patient underwent L1-2 laminectomies and a diagnostic micro-dissection of the underlying tissue, which demonstrated fibrotic arachnoid with gliosis and polyclonal lymphocytic infiltrates. Pathologically, the cells were composed of two cell populations: one “self” and one “non-self.” The patient’s symptoms continued to progress despite treatment efforts with IVIG, high-dose Methotrexate, and radiation. Imaging at the time of presentation to our institution showed massively thickened cauda equina nerve roots, some of which appeared adhered to a prior L1-2 laminectomy decompression site. Abnormal signal was seen throughout the thecal sac from the upper thoracic spine to the sacrum.

Discussion & Conclusion

The presented case has similarities to prior reports of complications arising from so-called “stem-cell tourism,” in which patients travel to undergo treatment at clinics that sometimes operate with minimal or no regulation. Intrathecal stem-cell injections administered at such facilities have been reported to cause a proliferative neoplastic-type response that may be partly composed of non-host tissue. These examples underscore the need to further explore the risks and benefits of intra-thecal stem cell therapy in regulated environments.

AUTHORS INDEX

Lastname	Firstname	Abstract number			
Abbott	C.	1-O15, 1-P55	Bakulin	I.	1-P12
Abdalla	G.	1-P62	Balakrishna	S.	4-O6
Ackemann	C.	4-P15	Balik	A.O.	3-P9
Afridi	S.	1-O42	Baltacioglu	F.	2-O8
Agnello	A.	1-O21, 2-P11	Barbato	C.	1-O30
Aguilera	C.	1-O7	Barber De La Torre	I.	4-O9
Ahn	M.J.	1-O6	Bargallo	N.	1-O31
Aixut	S.	2-O4	Barile	A.	5-O3
Aja	L.	1-O7, 2-O4	Barkhof	F.	1-O12, 1-O31, 1-O44
Akande	Y.	1-O42	Baroncini	M.	1-O22, 1-O23, 1-P31
Al Busaidi	A.	1-O18, 1-P61	Barranco	R.	2-O4
Al Ghailani	S.Y.	4-P9	Barrett	R.	1-O12
Al Mansoori	T.	1-P10	Barros	A.	1-P16
Al Qatami	H.	5-O11, 5-O12	Bartlett	P.	1-O31
Alberalar	N.D.	2-O8	Bartmann	P.	4-O8
Alberich	M.	1-O45	Bartsch	H.	1-O15
Albukhari	A.	4-P13	Bartuszek	J.	2-P1
Alexandre	A.	2-O7, 1-P6, 2-P12	Bata	B.	2-P5
Alhamud	A.A.	4-P15	Batalov	A.	1-O41
Alharbi	S.	4-P14	Batinic	D.	3-P7
Alhashem	A.	4-P14	Battocchio	M.	1-O14
Almohideb	F.	4-P13	Batty	R.	5-O9
Almossawi	O.	1-O18	Baum	T.	5-O7, 1-P11
Almuntashri	M.	4-P13	Baylis	G.C.	1-P10
Alsaedi	A.	1-P60	Bednarik	J.	1-P9
Altintas Taslicay	C.	1-P59	Beer	M.	3-P4
Altmann	D.	1-O44	Beltramello	A.	1-O21
Amorosino	G.	4-P12	Benesova	Y.	1-P9
Androniko	S.	4-P15	Benson	J.	3-P8, 5-P5
Anik	I.	1-P59	Bhattacharya	D.	2-P10
Anik	Y.	1-P59	Bhullar	K.	1-O34
Anzalone	N.	1-O43	Bianchi	G.	5-O3
Apine	I.	4-O4	Biandzetskaya	M.E.	1-P10
Arévalo	S.	4-P4	Biermayr	M.	4-O7
Argyelan	M.	1-O15	Birch	G.	1-O44
Argyropoulou	M.	1-P49	Biswas	S.	1-O12, 1-O31, 1-O40, 1-P60, 1-P62
Arikan	F.	1-O35	Biswas	S.	5-O4
Arrambide	G.	1-O45	Björkman-Burtscher	I.	1-P5
Arrigoni	F.	2-O6, 4-P12	Bjørnerud	A.	1-P43
Arteaga	L.	1-P52	Bladowska	J.	1-P3
Artiles	V.	5-P4	Boecker	H.	4-O8
Asif	M.	1-O42	Boffa	G.	1-P17, 1-P31
Astrakas	L.	1-P49	Bogey	C.	1-P51
Augelli	R.	1-O21, 2-P11	Borgatti	R.	4-P12
Auger	C.	1-O45, 5-O2, 1-P16, 1-P23	Botta	D.	1-P58
Azuar	C.	1-O11	Bouillot	P.	1-O10
Baev	A.	3-O2	Bozzao	A.	1-O37, 1-P25, 1-P26
Bajaj	G.	3-P6	Brandner	S.	1-O4, 1-O18, 1-O40, 1-P61
			Braun	M.	3-P4
			Breivik	B.	1-O17
			Brescia Morra	V.	1-O36, 1-O38
			Brina	O.	1-O10
			Brinjikji	W.	1-P51, 3-P8
			Brogna	C.	4-O11
			Brotis	A.	1-P63
			Browning	S.	1-O30
			Brunetti	A.	1-O14, 1-O36, 1-O38
			Bruno	F.	2-O6, 5-O3
			Bryukhov	V.	1-P32
			Bucci	A.	1-O21, 2-P11
			Burd	C.	1-O12

Bürger	M.	4-O3	Cottonaro	S.	1-P50
Burns	P.	2-P10	Cozzolino	V.	1-P53
Byun	J.S.	1-P29	Crescenzo	F.	1-O45
Callegari	I.	1-P31	Cristiano	L.	4-O11
Camins	A.	1-O7	Critelli	A.	2-P8
Campeau	N.	1-P57, 5-P5	Culleton	S.	4-P11
Campion	T.	1-O31, 4-O12	Cuocolo	R.	1-O38
Capellades	J.	1-O32	Ćurčić-Blake	B.	1-P40
Capilla	M.E.	5-P4	Cwynarski	K.	1-P61
Cardona	P.	2-O4	Daamen	M.	4-O8
Cardoso	M.	1-O12, 1-O31	Daducci	A.	1-O14
Carelli	V.	1-P47	Dagniaux	R.	1-O22, 1-O23
Carletti	F.	1-O40	Dal-Bianco	A.	1-P41
Carlos Martins Maia Jr.	A.	1-P48	Dale	A.M.	1-O15
Carotenuto	A.	1-O36	D'Amico	A.	4-O10
Carrascosa	A.	4-P5	Dantas	F.	1-P52
Castaldi	A.	1-P53	D'Arco	F.	4-O10, 4-P11
Castillo	J.	1-P23	D'Argento	F.	2-O7, 1-P6, 2-P12
Catalucci	A.	2-O6, 5-O3	Darwish	O.	1-P8
Caulo	M.	1-P22	Das	K.M.	1-P10
Cavasin	N.	2-P8	Das	R.	1-O12, 1-O31
Cazzagon	M.	2-P8	Davidovic	K.	5-O10
Cellerino	M.	1-P31	De Arcos	J.R.	1-P8
Chan	L.L.	1-P4	De Blasi	B.	1-O31
Chan	W.S.E.	1-P41	De Miquel	M.A.	2-O4
Chandra	S.P.	1-O34	De Sèze	J.	1-P23
Chang	F.C.	2-P7	De Tiege	X.	1-O20
Chard	D.	1-O44	De Vivo	A.E.	5-O11, 5-O12
Charnchaowanish	P.	1-O39	Degos	V.	1-O11
Charykova	I.A.	1-P10	Dekeyzer	S.	2-P3
Chauhan	R.	5-O4	Del Casale	A.	1-P26
Chawalparit	O.	1-O39, 1-P21	Del Ferraro	G.	1-O13, 1-P24
Chen	C.H.	2-P7	Delattre	B.	1-O10
Chen	J.H.	2-P7	Delgado	I.	4-P4, 4-P5
Chen	M.	1-O27, 5-O8, 1-P20	Delle Piane	F.	1-P26
Chia	N.	1-P4	Dellepiane	F.	1-O37, 1-P24, 1-P25
Chirife	O.	2-O4	Dembowska-Baginska	B.	2-P1, 4-P8
Choi	X.	1-P4	Dervisoglu	E.	1-P59
Chung	K.	1-O44	Dezi	T.	1-P25
Chung	M.S.	1-P29	Di Cesare	E.	5-O3
Chung	W.	2-O3	Di Sibio	A.	5-O3
Cicala	D.	4-O10	Di Stasi	M.	1-O36
Ciccarelli	O.	1-O44	Di Vita	A.	1-P25
Ciceri	E.	1-O21, 2-P11	Di Vito	L.	1-P47
Cieslik	K.	2-P1, 4-P8	Diehn	F.	5-P5
Cinnante	C.	4-O11	Digernes	I.	1-O17, 1-P39
Cipullo	M.B.	1-O36	Dinia	L.	1-O35
Cirak	M.	1-P1	Dobrynina	L.	1-O25
Clarencon	F.	1-O11	Doniselli	F.	5-O2
Clarke	M.	1-O45	Dormont	D.	1-O11
Clavel	P.	2-O5	Dostal	M.	1-P9
Coath	W.	1-O12	Dotsenko	T.	1-P10
Cocozza	S.	1-O14, 1-O36, 1-O38	Dudek	A.	1-P56
Colafati	G.S.	4-O10	Duncan	J.	1-O31
Colosimo	C.	2-O7, 1-P6, 1-P42, 1-P50, 2-P12	Ebden	S.	1-P15
Conesa	G.	1-O32	Eckel	L.	5-P5
Connolly	D.	5-O9, 2-P5, 4-P3	Edwards	M.	1-P15
Connor	S.	3-O3	Eide	P.K.	1-O8
Conte	M.	2-P11	Elefante	A.	1-O36, 1-O38
Cooper	J.	4-O12	El-Husseini	M.	5-P2
Cornelissen	F.	1-P40	Elke Hattingen	E.	4-O3
Corridore	A.	2-O6	Emblem	K.E.	1-O17, 1-P8, 1-P39, 1-P43
Cos	M.	1-O7	Erchinger	V.J.	1-P55
Coscojuela	P.	1-O35	Ersland	L.	1-P55
Costa Leite	C.	1-P54	Escudero	J.	4-P5
Cotton	F.	4-P15	Eser	M.	3-P10

Eshaghi	A.	1-O44	Grossi	S.	1-P44
Espindola Ala	V.H.	1-P51	Grøvig	E.	1-O17
Evangelisti	S.	1-P47	Grøvik	E.	1-P43
Evangelou	N.	1-O45	Gruschkus	S.	1-P20
Fadeeva	L.	1-O3, 3-O2	Guadalupi	P.	1-P42
Fajardo Ramin	L.	1-P54	Guarnera	A.	1-O30
Farhat	M.	1-O10	Güclü	G.	1-P1
Federici	M.	1-P53	Gule-Monroe	M.	1-O27, 5-O8, 1-P13, 1-P20
Fernandes Jr	W.R.	1-P54	Gumus	E.	4-P1
Fernández	M.	1-O7	Gunasekaran	A.	3-P6
Fernandez-Taranilla	M.	1-P18	Guo	W.	2-O3
Ferraciolli	S.F.	1-P54	Gurses	M. A.	1-P14
Ferraz Meyer	M.I.	1-O5	Guthrie	L.	1-P15
Ferreira	A.	1-P52	Gyebnár	G.	1-P33
Ferreira	N.	1-P52	Hagen-Kersten	A.A.	4-P10
Fersht	N.	1-P56	Hahm	M.H.	1-O29
Fischetti	A.	1-P53	Haider	L.	1-O31, 1-O44, 1-P13, 1-P41
Flynn	P.	2-P10	Håkansson	C.	1-P5
Fountas	K.	1-P63	Haller	S.	1-O12
Fox	N.	1-O12	Hameed	H.	2-P9
Freddi	T.	1-P52	Hammam	A.	1-O16
Friconnet	G.	1-P51	Han	M.	3-O5
Fuller	G.	1-P20	Han	S.	1-O1
Fuller	G.N.	1-P13	Hansson	O.	1-P5
Gagliardi	A.	2-O6	Hara	S.	4-O5
Galanaud	D.	1-O11	Harper	L.	1-O12
Ganesan	B.	1-P61	Hartono	S.	1-P4
Garcia Vidal	A.	1-O45	Hautz	W.	2-P1, 4-P8
Garg	A.	1-O34	Haykal	S.	1-P40
Garignano	G.	2-P12	Hebert	S.	2-O5
Gaser	C.	4-O8	Hedderich	D.	4-O8
Gasparini	A.	1-O21	Helland	A.	1-O17
Gaudino	S.	1-P6, 1-P42, 1-P50	Hellebust	T.	1-O17
Geier	O.	1-O17, 1-O22, 4-P10	Heng	D.	1-P4
Gemic	F.	1-O15	Hensler	J.	2-P6
Gene	M.	1-O13	Hernandez	D.	1-O35
Gentile	L.	1-P22	Hernandez-Lain	A.	1-P19
Georgievski-Brkic	B.	1-O33, 1-P36	Herrero	Y.	5-P4
Ghezzi	A.	1-P31	Hersey	N.	2-P5
Gil	I.	5-O12	Hilario	A.	1-P18
Giordano	C.	1-P42, 1-P50	Hilario	A.	1-P19
Giove	G.	1-P25	Hiraka	T.	1-O28
Giubolini	F.	2-O7, 2-P12	Hiura	M.	3-O4
Gizewski	E.R.	1-O19, 4-O7	Hock	A.	1-P46
Gkizas	C.	1-P49	Hodel	J.	1-O22, 1-O23
Glebova	I.V.	1-P10	Hoffmann Nunes	R.	1-P48
Gnanaprakasam	V.	1-P46	Holm	S.	1-P8
Goey	Z.	1-P38	Holodny	A.	1-O13, 1-P24
Goh	V.	1-O42	Hope	T.	1-O22
Goksel	O.	1-P38	Hori	M.	4-P7
Golay	X.	1-O16, 1-P60	Hovden	I.T.	1-P39
Goldman	S.	1-O20	Hu	Y.	2-O3
Gomes Padilha	I.	1-P48	Huang	C.C.	2-P7
Gómez-Chiari	M.	4-O9	Huang	C.Y.	2-P7
González-Ortiz	S.	1-O32	Huang	W.M.	2-P7
Goodkin	O.	1-O12, 1-O31	Hulova	M.	1-P9
Gordon	E.	1-O12	Hussl	A.	1-O19
Goriaynov	S.	1-O41	Hyare	H.	1-P56, 1-P61
Gorkom	K.N.	1-P10	Iannucci	G.	5-O6
Govind	V.	1-O2	Iazeva	E.	1-P12
Gramegna	L.L.	1-O35, 1-P47	Ibanez Moya	M.	5-P4
Grams	A.E.	4-O7	Ibanez Sanz	L.	5-P4
Greve	T.	1-P46	Ihn	Y.K.	5-P3
Griffiths	P.D.	4-P3	Inarejos	E.J.	4-O9
Grigorieva	E.	1-P45	Inci	E.	1-P1
Grive Isern	E.	1-P44	Inglese	M.	1-P17, 1-P31

Ingram	G.	1-P15	Kodera	J.	4-P7
Ishibashi	K.	3-O4	Kokurcan	A.	1-P1
Ishii	K.	3-O4	Konno	Y.	1-O28
Ishii	Y.	4-O5	Kopp	F.K.	1-P11
Iuno Araujo	A.	1-P48	Koren	L.	1-P18, 1-P19
Iv	M.	1-P43	Kornienko	V.	1-O3
Jabeen	S.	5-O4	Kostic	D.	1-O33
Jaber	H.	1-P15	Kostic	I.	5-O10
Jacob	A.	5-O7, 5-P2	Kostic	J.	5-O10
Jacobsen	K.	1-O17	Kozák	L.R.	1-P33
Jacquiez	C.	1-O22, 1-O23	Kozić	D.	1-P36
Jager	R.	1-O4, 1-O18, 1-O30	Kremer	S.	1-P23
Jakab	A.	1-P38	Kremneva	E.	1-O24, 1-O25, 1-P12
Jambhekar	K.	3-P6	Krismer	F.	1-O19
Janjic	T.	4-O7	Krotenkova	I.	1-P32
Janot	K.	1-P51	Krotenkova	M.	1-O25, 1-P32
Jansen	O.	2-P6	Krumina	G.	4-O4, 1-P37
Jansonius	N.	1-P40	Krylov	V.	1-P45
Jaramaz-Ducic	T.	1-O33	Kuchcinski	G.	1-O22, 1-O23
Jaunmuktane	Z.	1-O18	Kuhn	M.	1-P9
Jaunozolina	L.	1-P37	Kulagin	A.S.	1-P10
Jefic	S.	5-O5, 1-P36	Kumar	M.	1-O2, 3-P6
Jenabi	M.	1-O13	Kumar	S.	1-P2
Jenaby	M.	1-P24	Kumar	A.	1-O4
Jenkins	S.	2-P9	Kupta	R.K.	1-P21
Jhou	Z.Y.	2-P7	Kutniakhova	L.V.	1-P10
Johnson	J.	1-O27, 5-O8, 1-P20	Kwong	J.	1-P62
Jones	T.R.	1-P55	Kyparissi	M.K.	1-P63
Jose Da Rocha	A.	1-P48	La Morgia	C.	1-P47
Jousmäki	V.	1-O20	La Rocca	G.	1-P50
Jung	Y.	3-O5	Lagares	A.	1-P19
Jurcoane	A.	4-O3	Lain-Hernandez	A.	1-P18
Jurkiewicz	E.	2-P1, 4-P8	Lamplmayr	L.	4-O7
Kafiabadi	S.	3-O3	Lanzillo	R.	1-O36, 1-O38
Kakaria	A.	4-P9	Lanzino	G.	3-P8
Kalashnikova	L.	1-O25	Lapucci	C.	1-P17, 1-P31
Kalcioglu	M.	3-P10	Lara	B.	2-O4
Kalder	J.	2-O1, 2-P3	Larsen	N.	2-P6
Kaliakatsos	M.	4-P11	Larsson	E.	1-O26
Kaltsonoudis	E.	1-P49	Latysheva	A.	1-O17, 1-O22
Kanoto	M.	1-O28	Laughton	B.	4-P15
Kao	Y.	2-O3	Laurell	K.	1-O26
Kapsalaki	E.	1-P63	Leclerc	X.	1-O22, 1-O23
Karlovic-Vidakovic	M.	1-P35, 3-P7	Lee	A.	1-P30
Katayama	Y.	3-O4	Lee	C.	2-O3
Kazemi	N.	3-P6	Lee	E.J.	1-P29
Kecman	B.	5-O5	Lee	H.J.	1-O29
Kerkovsky	M.	1-P9	Lee	H.S.	1-O29
Kessler	U.	1-O15, 1-P55	Lefranc	F.	1-O20
Khan	I.	1-P34	Legostaeva	L.	1-O24, 1-P12
Khan	J.	1-P37	Lemnos	L.	1-P51
Kidd	M.	4-P15	Lenck	S.	1-O11
Kiechl-Kohlendorfer	U.	4-O7	Leone	E.	1-P42
Kim	G.S.	2-P2	Leutmezer	F.	1-P41
Kim	I.S.	5-P3	Leventer	R.	4-P12
Kim	J.	3-O1	Lewis	M.	1-P61
Kim	M.	1-O16	Lhermitte	B.	1-P23
Kim	S.T.	1-O6	Li	Q.	1-P24
Kirii	K.	1-O28	Liebo	G.	5-P5
Kirschke	J.S.	1-O9, 5-O7, 1-P11, 1-P46, 5-P2	Lim	E.	1-P56
Kitapci	M.T.	1-P14	Lim	J.K.	1-O29
Kitchen	N.	1-P56	Lin	C.	2-O3
Klupke-Saric	I.	1-P35	Lin	K.	1-P27
Kobayashi	M.	4-P7	Lin	T.	2-O3
Koc	M.	1-O18	Lisi	S.	1-P25
Kockum	K.	1-O26	Ljubisabljevic	M.	1-P10

Lloret	I.	3-P3	Mestre	T.	1-O32
Lodi	R.	1-P47	Meyer	N.	1-P57
Loevland	G.	1-P39	Micallef	C.	1-O4
Löffler	M.	5-O7, 1-P11, 5-P2	Micelli	M.V.M.	2-O6
Lolli	V.	1-O20	Mikic	D.	5-O5
Londos	E.	1-P5	Milatovic	B.	1-P28
Losak	J.	1-P9	Mileusnic	V.	1-O33
Lovblad	K.	1-O10, 1-P58	Miller	G.	5-P5
Løvland	G.	1-P8	Milonia	L.	1-P6
Lozupone	E.	2-O7, 1-P6, 2-P12	Milosevic	S.	1-P28
Lucic	M.	1-O33	Miserocchi	A.	1-O40
Lucignani	M.	1-P26	Mitsos	A.	1-P63
Lukyanchikov	V.	1-P45	Moggridge	J.	1-O12, 1-O31
Luo	C.B.	2-O3, 2-P7	Molina-Garcia	D.	1-P18
Luthman	A.S.	1-O10	Moltu	S.J.	4-P10
Luzi	M.	1-O35	Moon	W.	1-O1
Macaya	A.	4-P4	Moon	Y.	1-O1
Machado	P.	1-P62	Mora	P.	1-O7
Machi	P.	1-O10, 1-P58	Moraschi	M.	1-P25
Maciag	E.	5-O2, 1-P23	Morozova	S.	1-P12
Maciver	C.	1-P61	Mounayer	C.	2-O5, 1-P51
Madjidyar	J.	2-P6	Mpotsaris	A.	2-O1, 2-O2, 2-P3
Maehara	T.	4-O5	Muangpaisan	W.	1-O39
Maher	M.	3-P5	Muchart	J.	4-O9
Mahlknecht	P.	1-O19	Mühlau	M.	1-O9
Majós	C.	1-O7	Müller	C.	1-O19
Makse	H.	1-O13, 1-P24	Munuera Del Cerro	J.	4-O9
Mancardi	G.	1-P31	Murofushi	Y.	4-P6
Mancini	L.	1-O4, 1-O18, 1-O40	Murumkar	V.	5-O4
Mandelstam	S.	4-P12	Muster	M.	1-P58
Mandruzzato	N.	1-O21, 2-P11	Muta	A.	3-O4
Manfre	L.	5-O11, 5-O12	Nacar Dogan	S.	3-P9
Mangesius	S.	1-O19, 1-O44, 1-P41	Nanda	B.	1-P27
Mankad	K.	1-O4, 4-O12	Napolitano	A.	1-O37, 1-P26
Mansour	M.	5-O6	Narayana Vamyanmane	D.K.	4-O6
Margariti	C.	1-O42	Nariai	T.	3-O4, 4-O5
Margiotta	R.	1-P25	Narr	K.L.	1-O15
Maric	D.	5-O5, 1-P36	Naval	P.	1-O7
Marin	B.	2-O5	Neubauer	V.	4-O7
Marin Suarez	A.	1-P44	Newhart	H.	3-P6
Maristany Daunert	T.	4-O9	Ng	S.	1-P4
Markovic	I.	4-P9	Ngamsombat	C.	1-O39, 1-P21
Martin	A.	5-O9, 2-P5	Nguyen	B.	4-P10
Martinez	E.	1-O35	Nicolato	A.	1-O21
Martin-Medina	P.	1-P18, 1-P19	Nidhi	L.	4-O6
Martino	M.	2-O6	Nijenhuis	M.	1-P46
Marziali	G.	1-P42, 1-P50	Nikolic	I.	1-P28
Mascali	D.	1-P25	Nikoubashman	O.	2-O1, 2-O2, 2-P3
Masciocchi	C.	2-O6, 5-O3, 1-P7	Nilsen	L.B.	1-O17
Masullo	M.	1-O36	Ningunha	K.	1-O39
Masulovic	D.	5-O10	Noel	P.B.	1-P11
Mattei	P.A.	1-P22	Nordhøy	W.	1-P8
Mawlawi	O.	1-O27, 5-O8	Novi	G.	1-P31
Maximov	I.	4-P10	Nowak	K.	2-P1, 4-P8
Mayer	T.	2-P4	Oedegaard	K.J.	1-O15, 1-P55
Maynard	J.	1-O18, 1-P61	Okuchi	S.	1-O4, 1-O16, 1-O18
Mbatha	W.	1-O18	Olbert	E.	1-P41
Mccrone	P.	1-O42	Olechowski	A.	2-P1, 4-P8
Mcevoy	A.	1-O40	Olivi	A.	1-P50
Mechl	M.	1-P9	Oltedal	L.	1-O15, 1-P55
Medrano	R.	1-O32	Onder	H.	4-O1, 4-P2
Mei	K.	1-P11	Ooi	L.	1-P4
Meintjes	E.M.	4-P15	Örs Kukurcan	S.	1-P1
Menze	B.	5-P2	Othman	A.E.	2-O1, 2-O2
Mercuri	E.M.	4-O11	Ourselin	S.	1-O12, 1-O31
Messina	S.	5-P5	Ousdal	O.T.	1-O15

Ozer	H.	4-P1	Porto	L.	4-O3
Oztunali	Ç.	4-P1	Potapov	A.	1-O41
Paccanaro	M.	5-O6	Pottecher	J.	1-P23
Paipa	A.	2-O4	Poydasheva	A.	1-P12
Panara	V.	1-P22	Prabhu	S.	1-O27
Pandey	T.	3-P6	Prados	F.	1-O12, 1-O31, 1-O44
Panebianco	L.	2-O6	Praksova	P.	1-P9
Paniagua	A.	5-P4	Prayer	D.	1-P41
Panovska-Griffiths	J.	1-P60, 1-P62	Premat	K.	1-O11
Paolella	C.	1-O14, 1-O36	Pronin	I.	1-O3, 1-O41, 3-O2
Papathanassiou	A.D.	5-P1	Pruvo	J.	1-O22, 1-O23
Papathanassiou	S.	5-P1	Pujar	S.	4-P11
Pardini	M.	1-P17	Puyalto	P.	1-O7
Pardini	M.	1-P31	Quarantelli	M.	1-O36
Pareto	D.	1-O45	Quesada	H.	2-O4
Park	S.	1-O6, 3-O1	Quirk	B.	3-O3, 4-O12
Parodi	S.	1-P53	Rago	P.	2-P1
Pasquini	L.	1-O13, 1-O37, 1-P24, 1-P25, 1-P26	Rajput	K.	4-O10
Paula Alves Fonseca	A.	1-P48	Ram	R.	3-P6
Peacock	J.	1-O42	Ramaglia	A.	1-P42, 1-P50
Pearce	K.	1-O31	Ramakrishnaiah	R.	3-P6
Pearson	O.	1-P15	Ramette	G.	1-O22, 1-O23
Peck	K.	1-O13, 1-P24	Ramos	A.	1-P18, 1-P19
Pedicelli	A.	2-O7, 1-P6, 2-P12	Razavi	R.	1-O42
Pejanovic-Skobic	N.	1-P35, 3-P7	Rebollo	M.	4-O9
Pemberton	H.	1-O12, 1-O31	Redaelli	D.	4-P12
Pendharkar	H.	5-O4	Rees	J.	1-O40
Pensa	M.	1-P53	Reich	A.	2-O1, 2-O2, 2-P3
Pereira	V.	1-O10	Rennie	I.	2-P10
Pereverzyev Jr.	S.	4-O7	Reymond	P.	1-O10
Perez-Beteta	J.	1-P18	Rhim	J.H.	3-O1
Perez-Garcia	V.	1-P18	Riabikin	A.	2-O1, 2-O2, 2-P3
Perez-Nuñez	A.	1-P18, 1-P19	Riaza	L.	4-P4
Perri	M.	5-O3	Ribbens	A.	1-O5
Peruzzo	D.	4-P12	Ricciardi	G.K.	1-O21, 2-P11
Pessini Ferreira	L.	1-O45, 5-O2, 1-P16, 1-P23	Ridwan	H.	2-O1, 2-O2
Petracca	M.	1-O36, 1-O38	Riederer	I.	1-O9, 1-P11
Petrillo	T.	1-O36	Riklund	K.	1-O26
Petrou	A.	5-P1	Ringsby	J.O.	1-O8
Petsuksiri	J.	1-P21	Ringstad	G.A.	1-O8
Pezzullo	G.	1-P50	Rivera	A.	4-O9
Pfeiffer	H.C.V.	4-P10	Rocamora	R.	1-O32
Phipps	K.	4-O12	Roccatagliata	L.	1-P17, 1-P31
Piccirilli	E.	1-P22	Rojas-Garcia	A.	1-P62
Pichiecchio	A.	4-O11	Romaniello	R.	4-P12
Pilatus	U.	4-O3	Romano	A.	1-O37, 1-P25, 1-P26
Pinelli	L.	4-O10	Romano	N.	1-P17, 1-P53
Pinna	G.	1-O21	Rossi Espagnet	M.	1-O37, 1-P25, 1-P26
Pinna	V.	5-O6	Roskopf	J.	3-P4
Piradov	M.	1-O24, 1-P12	Rouchaud	A.	2-O5, 1-P51
Pisani	A.	1-O14	Rountas	C.	1-P63
Pitura	R.	4-O4	Rovai	A.	1-O20
Piyapittayanan	S.	1-P21	Rovira	A.	1-O35, 1-O45, 5-O2, 1-P16, 1-P23
Pizzini	F. B.	1-O21	Rovira Cañellas	M.	1-P44
Placidi	G.	1-P7	Rua	T.	1-O42
Plans	G.	1-O7	Rubin	D.	1-P43
Plebani	M.	2-P11	Rubio-Palau	J.	4-O9
Poewe	W.	1-O19	Rufenacht	D.	1-P58
Pogosbekian	E.	3-O2, 1-O41	Ruffinengo	U.	1-P53
Poidasheva	A.	1-O24	Rummeny	E.J.	1-P11
Pokhylevych	H.	1-P20	Russo	C.	1-O14, 1-O36, 1-O38
Pokryszko-Dragan	A.	1-P3	Rutynowska	O.	2-P1, 4-P8
Polsinelli	M.	1-P7	Ryabinkina	Y.	1-O24, 1-P12
Polunina	N.	1-P45	Ryang	Y.	5-O7
Pons	A.	1-O7	Sabatino	G.	1-P50
Pontillo	G.	1-O14, 1-O36, 1-O38	Sadeghi	N.	1-O20

Sadiq	S.	1-P15	Smeets	D.	1-O5
Sætre	D.	1-O17	Smyth	G.	2-P10
Saitta	L.	1-P17	Söderström	L.	1-O26
Sakata	M.	3-O4	Soke Miang	C.	1-P34
Sakinis	T.	1-O8	Sokolska	M.	1-P56
Sakuma	H.	4-P6	Soldo	I.	1-P35, 3-P7
Salan	T.	1-O2	Sollmann	N.	1-O9, 1-P11, 1-P46
Salaya Diaz	T.	1-P44	Sorg	C.	4-O8
Saleh	M.G.	4-P15	Sormani	M.	1-P17, 1-P31
Saleme	S.	1-P51	Sosars	D.	4-O4
Salerno	A.	1-P16	Soteriades	E.	1-P10
Salle	H.	1-P51	Sourour	N.	1-O11
Salvador	E.	1-P18, 1-P19	Splendiani	A.	2-O6, 5-O3, 1-P7
Salvajoli	J.	1-P52	Sprlakova-Pukova	A.	1-P9
Salvi	S.	2-P5	Stankovic	A.	5-O10
Samandouras	G.	1-O40	Statsenko	Y.	1-P10
Samant	R.	3-P6	Steiger	R.	4-O7
Sanchez	E.	1-O31	Stiris	T.	4-P10
Sánchez	J.J.	1-O7	Stulik	J.	1-P9
Sánchez-Montanez	A.	4-P4, 4-P5	Sugai	Y.	1-O28
Sanmillan	J.L.	1-O7	Suh	S.H.	2-P2
Sano	K.	4-P6	Suponeva	N.	1-O24, 1-P12
Santarosa	C.	1-O10	Suzuki	K.	4-P7
Sanverdi	E.	1-O40, 1-P14, 1-P62	Svensson	S.F.	1-P8
Sasiadek	M.	1-P3	Szaniawska	M.	2-P1, 4-P8
Sathornsumetee	S.	1-P21	Szekely	G.	1-P38
Savic	M.	1-O33	Szolics	M.	1-P10
Sawangthap	T.	1-P21	Tago	T.	3-O4
Sawaya	R.	1-P13	Takahashi	Y.	4-P7
Saxhaug	C.	1-O17	Takanashi	J.	4-P6
Scheef	L.	4-O8	Talenti	G.	1-O21, 4-O10, 4-P11
Schiavi	S.	1-O14, 1-P17	Tamura	K.	4-P7
Schmitt	A.	1-O12	Tan	A.P.	4-O2
Schmitz	B.	3-P4	Tan	E.K.	1-P4
Schmitz-Koep	B.	5-O7	Tan	L.	1-P4
Schneider	L.	2-P4	Tanaka	Y.	4-O5
Schocke	M.	1-O19	Tancu	C.	1-P56
Schomer	D.	5-O8, 1-P13	Tartaglione	T.	4-O11
Schön	S.	1-P11	Tasiou	A.	1-P63
Seal	M.	4-P12	Tatsui	C.	5-O8
Sekuboyina	A.	5-P2	Taurino	M.	1-P25
Seo	K.	2-P2	Tavares Lucato	L.	1-P54
Seong	M.	1-O6	Tekin	Z.	3-P10
Seppi	K.	1-O19	Terada	H.	4-P6
Sepulveda	J.	1-P18, 1-P19	Testa	C.	1-P47
Sergeev	D.	1-O24, 1-P12	Thientunyakit	T.	1-O39
Sergeeva	A.	1-O24, 1-P12	Thiessen	J.	3-P2
Serrano Alcalá	E.	1-P44	Thorne	L.	1-O40
Server	A.	1-O22, 3-P3	Thornton	J.	1-O31
Shamtieva	K.	1-O25	Thumher	M.	1-P41
Shankar	A.	1-O4	Thust	S.	1-O4, 1-O16, 1-O18, 1-O40, 1-P56, 1-P61
Shearer	J.	1-O42	Tintore	M.	1-O45
Shin	J.H.	5-P3	Tlili-Graïess	K.	4-P14
Shiraga	N.	4-P7	Tomasello	A.	1-O35
Shotar	E.	1-O11	Tommasino	E.	2-O6, 5-O3, 1-P7
Siddiqui	A.	4-O10, 5-O4, 2-P9	Tong	E.	1-P43
Signori	A.	1-P17	Tonon	C.	1-P47
Sima	D.M.	1-O5	Torisson	G.	1-P5
Simister	R.	1-O30	Torlone	S.	2-O6
Simon Olive	C.	1-P44	Torres	A.	1-O7
Sindu	G.	4-O6	Torres Pacheco	F.	1-P48
Singh	P.	1-O2	Toyoguchi	Y.	1-O28
Singh	R.	2-O1, 2-O2	Toyohara	J.	3-O4
Sinitsyn	D.	1-O24, 1-P12	Tripathi	M.	1-O34
Sinkus	R.	1-P8	Trombatore	P.	1-P6
Slettebø	H.	1-O8			

Trotta	N.	1-O20	Watarai	F.	1-O28
Trzasko	J.	1-P57	Wattjes	M.	1-O12
Tse	G.	5-O9	Weinberg	J.	1-O27, 5-O8
Tuggia	M.	5-O6	Werner	B.	1-P38
Türelı	D.	2-O8	Werring	D.	1-O30
Turkin	A.	3-O2	White	M.	1-O12, 1-O31
Turville	J.	1-O42	Whiteley-Jones	H.	1-O12
Tuura	R.	1-P38	Wiesmann	M.	2-O1, 2-O2, 2-P3
Tyurina	A.	1-O3	Williams	E.	1-O31
Uccelli	A.	1-P17, 1-P31	Winston	G.	1-O31
Ugga	L.	1-O38	Wolke	D.	4-O8
Ulivi	L.	1-O30	Wu	H.	2-O3
Umapathi	T.	1-P2	Yadav	N.	5-O4
Utukuri	P.	3-P5	Yang	H.	2-O3
Valente	I.	2-O7, 1-P6, 2-P12	Yang	J.Y.M.	4-P12
Valentinitsch	A.	5-O7, 5-P2	Yapici Ugurlar	O.	4-O1, 4-P2
van der Kouwe	A.	4-P15	Yazeva	E.	1-O24
van Hecke	W.	1-O5	Yazol	M.	4-P1
van Westen	D.	1-P5	Yeong	K.	1-P27
van-Cauter	S.	1-P62	Yeste	D.	4-P5
Vanhemert	R.	3-P6	Yi	D.	1-P43
Vargas	M.I.	1-O10	Yim	Y.	1-O1
Vargas Gomez	M.	1-P58	Yoneoka	D.	1-P62
Varrassi	M.	2-O6, 5-O3	Yong	A.	1-P4
Vazquez	E.	4-P4, 4-P5	Yoo	C.Y.	5-P3
Veraart	J.	1-P62	Yoo	J.H.	3-P1, 5-O1
Verdolotti	T.	4-O11	Yousry	T.	1-O12, 1-O31, 1-P62
Vernooij	M.	1-O12	Yun	P.H.	2-P2
Vert	C.	1-O35	Zacharzewska-Gondek	A.	1-P3
Vichianin	Y.	1-O39	Zaffaroni	M.	1-P31
Vik-Mo	E.	1-P8	Zaharchuk	G.	1-P43
Virhammar	J.	1-O26	Zakharova	M.	1-P32
Vitale	V.	5-O6	Zakharova	N.	1-O41
Vojvodic	N.	1-P28	Zampieri	P.G.	2-P11
Vola	E.A.	1-O36	Zhang	H.	1-P2
Vos	S.	1-O12, 1-O31	Zienkiewicz	U.	2-P1
Voulgari	P.	1-P49	Zikou	A.	1-P49
Vranješ	D.	1-P36	Zimmer	C.	1-O9, 4-O8, 5-O7, 1-P11, 1-P46
Vukicevic	M.	1-O33	Zimmermann	M.	4-O7
Vukomancic	B.	1-O33	Zoccatelli	G.	1-O21
Vyas	S.	1-O2			
Wagatsuma	K.	3-O4			
Wallner	V.	4-O7			
Walsh	J.	2-P10			
Wanke	I.	1-P58			
Ward	D.	4-P3			
Wastling	S.	1-O4, 1-O18, 1-P61			
Watanabe	H.	4-P7			

Publisher's note Springer Nature remains neutral with regard to jurisdictional claims in published maps and institutional affiliations.